Molecular and cellular analysis of the membrane binding C2 domain of Notch ligands in health and disease



Yao Meng

Department of Biochemistry and St Catherine's College

University of Oxford

Trinity Term 2021

A Thesis submitted for the degree of Doctor of Philosophy, University of Oxford

Molecular and cellular analysis of the membrane binding C2 domain of Notch ligands in health and disease

Yao Meng, Department of Biochemistry and St Catherine's College, University of Oxford

A thesis submitted for the degree of Doctor of Philosophy, Trinity Term 2021

Abstract

The Notch signalling pathway is evolutionarily conserved across metazoan species and plays key roles in many physiological processes. Aberrant Notch signalling causes a wide variety of diseases including various cancers and developmental disorders. Both Notch ligands and receptors are single-pass transmembrane proteins with large extracellular domains that mediate signal transduction in adjacent cells. Several domains within Notch ligands and receptors have been identified as important for Notch activation. In particular, the N-terminal C2 domain, with distinct lipid-binding and Notch-binding faces, present in all canonical mammalian Notch ligands, has been suggested to modulate activation through its membrane-binding capacity.

The focus of this project was to further characterise the role of the C2 domain in Notch activation modulation and gain mechanistic insight, using *in vitro* biochemical and cell biological assays. A series of somatic missense mutations affecting the C2 domain of human Jagged1, obtained from the COSMIC cancer database, were expressed as Fc-His tag fusion proteins containing the N-terminal region (C2-EGF3) of the ligand using HEK293T cells. Out of 13 COSMIC variants, all but one showed loss of function, predominantly through effects on Notch activation measured in two reporter cell lines.

One of the variants T145N, which altered an N-glycosylation consensus sequence on the β5-6 lipid binding loop, showed dramatically low Notch activation capability. The role of the C2 N-glycan was therefore further studied using additional site-directed variants designed to remove the consensus asparagine within the NXT/S N-glycan recognition sequence. The C2 N-glycan, but not a DSL N-glycan, was shown to be essential for Jagged1's ability to activate Notch. These data were recapitulated using a primary vascular smooth muscle cell differentiation assay emphasising the likely physiological importance of the Jagged1 C2 N-glycan. Further mechanistic insight was provided by development of a novel FACS-based liposome binding assay, and loss of the C2 N-glycan was shown to impair both lipid and Notch binding, suggesting global effects on C2 domain structure. Additional insight into loss of function mechanisms associated with other COSMIC variants was also obtained, with all but three variants explained by effects on protein folding, Notch- or lipid binding. In parallel, a new high expression system for DLL4 constructs was established using HEK293F cells. This facilitated study of C2 variants of DLL4, also identified from cancer databases. Variants which had altered C2 lipid-binding loops showed equivalent or enhanced Notch activation capability, in contrast to the loss of function associated with Jagged1 variants with lipid-binding loop changes. These data suggest different roles for membrane-binding loops in the two ligand families, with the Jagged C2 N-glycan facilitating formation of a ternary complex necessary for Notch cleavage at the membrane.

Acknowledgements

First and foremost, I would like to express my sincere gratitude to my supervisor Prof. Penny Handford for giving me the opportunity to work in the lab on such an exciting project. I appreciate the continuous support and guidance she has given me all the time in the lab, especially during the difficult COVID pandemic situation, and prompt reply to my emails even in evenings and weekends, no matter how trivial they are. Her consistent encouragement throughout my DPhil gave me the motivation to overcome challenges of this project and relieved my stress. Additionally, I would like to thank her for critical, but extremely helpful, suggestions during the writing of this thesis.

Second, many thanks must go out to past and present members of Handford lab. In particular, I would like to express my sincere thanks to Dr Sacha Jensen. He guided me on experimental technique through the early days of my DPhil. Thanks for his invaluable advice and support every time, teaching me native English speaking and proofreading my thesis. I am also very thankful to Dr Thomas Rowntree, Dr Pat Whiteman and Dr Shruti Mittal for their help and advice with my research skills. Many thanks also go to Oliver Webb, Xinyi Feng, Zhihan Bo, Ondine Atwa, Sophie Wicken, who made my time in the lab enjoyable and memorable.

I would like to thank our collaborators Prof Cecilia Sahlgren and Sami Sanlidag for kindly providing help with the vascular smooth muscle differentiation assay and Dr Weston Struwe for helping with glycoproteomic analysis. A sincere thank you to the flow lab in the Sir William Dunn School of Pathology for the flow cytometry support in this project. I would like to extend my appreciation to members of the Biochemistry

department, St Catherine's College and New College for fostering a helpful, cooperative, and welcoming environment. Additionally, I would also like to gratefully acknowledge the financial support from St Catherine's College.

I am forever grateful to make a lot of friends during these four years of DPhil study, all of you made my time in Oxford meaningful and memorable. Thank you for all the good times we spent together. I would especially like to thank Guangyu Liu, the first friend I met in Oxford, who gave me lots of valuable suggestions for my DPhil study. A heartfelt thank you to my friends from China for their moral support and encouragement across the lands.

I would also like to express my deep appreciation to my family for constant support and encouragement. Special thanks to my parents for their endless love and support through all my ups and downs, for always being there when I needed it most, and without whom I could not have kept going. I am so lucky to be your daughter. Last, but not least, I would like to thank my boyfriend, Jiaao Wei, for his continuous company, support, understanding and encouragement during my DPhil study, for his advice on my project, and without whom my life at Oxford would not be the same.

Table of Contents

List of Abbreviations ..... **xi**

Chapter 1. Introduction **1**

1.1 General background to the Notch signalling pathway 2
1.1.1 Discovery of Notch Signalling 2
1.1.2 Distinct Modes of Notch Signalling 3
1.1.3 Molecular mechanism of canonical Notch Signalling 5
1.1.4 Non-canonical Notch signalling 9

1.2 Medical relevance of Notch Signalling 10
1.2.1 Physiological roles of Notch signalling 10
1.2.1.1 Angiogenesis 10
1.2.1.2 Somitogenesis 13
1.2.1.3 Blood cell development 14
1.2.1.4 Neurogenesis 16
1.2.2 Notch signalling in human disease 17
1.2.2.1 Notch and cancer 17
1.2.2.2 Alagille syndrome 19
1.2.2.3 Adams-Oliver syndrome 20
1.2.2.4 CADASIL 21
1.2.2.5 Bicuspid aortic valve disease 21

1.3 Regulation of Notch activation 23
1.3.1 Trans and cis interactions 23
1.3.2 Endocytosis and trafficking 25
1.3.3 Notch signalling cross-talk 26
1.3.4 Ligand proteolysis 27

1.4 Notch ligands and receptors 27
1.4.1 Notch ligands 27
1.4.2 Notch receptors 29
1.4.3 Post-translational modifications of Notch receptor 32

1.4.3.1 O-Glycosylation 32
1.4.3.2 Ubiquitinylation of Notch receptors 39
1.4.4 Post-translational modifications of Notch ligands 39
1.4.4.1 O-glycosylation of Notch ligands 39
1.4.4.2 Ubiquitinylation modifications of Notch ligands 40
1.5 C2 domain 41
1.5.1 General introduction 41
1.5.2 Calcium ion binding by C2 domains 44
1.5.3 C2 domains in Notch ligands 46
1.6 Project Aims 51
Chapter 2. Materials and methods 53
2.1. Mutagenesis 54
2.1.1. Primer sequences 54
2.1.2. Site-directed mutagenesis using overlap extension PCR 54
2.1.3. PCR reactions 54
2.1.4. Restriction enzyme digestions 56
2.1.5. DNA gel electrophoresis 57
2.1.6. DNA ligation 57
2.1.7. Transformation 58
2.1.8. Isolation of plasmids and DNA sequencing 58
2.2. Protein purification 58
2.2.1. HEK293T cell maintenance and protein expression 59
2.2.1.1. HEK293T cell maintenance 59
2.2.1.2. Freeze and thaw HEK293T cells 59
2.2.1.3. Large scale transfection of HEK293T 60
2.2.1.4. HEK293T culture medium collection 60
2.2.2. HEK293F cell maintenance and protein expression 61
2.2.2.1. HEK293F cell maintenance 61
2.2.2.2. Freezing and thawing of HEK293F cells 61
2.2.2.3. Large scale transfection of HEK293F 61
2.2.2.4. HEK293F culture medium collection 62
2.2.3. S2 cell maintenance and protein expression 62

2.2.3.1. S2 cell maintenance 62
2.2.3.2. S2 cell freezing and thawing 63
2.2.3.3. S2 stable cell lines generation 63
2.2.3.4. S2 cell protein expression and medium collection 64
2.2.4. Affinity and size exclusion chromatography 65
2.2.4.1. Immobilised metal affinity chromatography (IMAC) using a nickel column 65
2.2.4.2. Size exclusion chromatography (SEC) 67
2.2.5. Protein concentration measurements 67
2.2.6. SDS-PAGE 68
2.2.7. Western blot 69
2.3. Notch activation assays 69
2.3.1. Notch activation assay of HEK mN1-NLuc/CLuc-RBPjk and mN2-NLuc/CLuc-RBPjk reporter cells 70
2.3.1.1. HEK mN1-NLuc/CLuc-RBPjk and mN2-NLuc/CLuc-RBPjk cell culture 70
2.3.1.2. Setting up of the activation assay by HEK reporter cells 70
2.3.2. Notch activation assay of CHO hN1G4^{esn} reporter cells 71
2.3.2.1. CHO hN1G4^{esn} reporter cells maintenance 71
2.3.2.2. Setting up of the activation assay by CHO hN1G4^{esn} reporter cells 72
2.4. Notch binding assays 72
2.4.1. Notch binding assay using MaxiSorp^{TM} plates 72
2.4.2. Notch binding assay by nickel-coated plates 73
2.5. Liposome binding assays 74
2.5.1. Lipid stock preparation 74
2.5.2. Liposome extrusion and characterisation 75
2.5.3. Protein G bead coating 75
2.5.4. FACS-based liposome turbidity assay 76
Chapter 3. Study of the C2 domain of human Jagged1 using COSMIC variants 78
3.1 Introduction 79
3.2 COSMIC missense mutation selection 81

3.3 Mutagenesis of Jagged1$_{N\text{-}EGF3\text{-}Fc\text{-}His}$ COSMIC variants 87

3.4 Secretion tests of Jagged1 COSMIC mutants 89

3.5 Production and purification of recombinant Jagged1 91

3.6 Testing the effect of Jagged1 COSMIC variants on Notch activation by two different reporter systems 94

3.7 Summary of COSMIC variants (expression and activity) 107

Chapter 4. Study of the functional importance of N-glycosylation in the C2 domain of Jagged1 109

4.1 Introduction 110

4.2 Conservation of the C2 N-glycosylation site in Jagged ligands 111

4.3 Target sites for mutagenesis and secretion tests 115

4.4 Protein purification and PNGase F digestion of Jagged1 N-glycan variants 117

4.4.1. Purification of N-glycan variants 117

4.4.2. PNGase F digestion of Jagged1 N217A monomer 119

4.5 Mass spectrometry based glycoproteomic analysis of Jagged1 N-glycan 122

4.6 Testing the effect of Jagged1 N-glycan related variants on Notch activation 126

4.6.1. Notch1 activation measurement 126

4.6.2. Notch2 activation measurement 130

4.6.3. Deglycosylated Jagged1$_{N\text{-}EGF3\text{-}Fc\text{-}His}$ Notch activation measurement 131

4.7 Physiological importance of the Jagged1-C2 N-glycan complex 133

4.8 Conclusions 139

Chapter 5. Investigation of Notch- and lipid-binding properties of Jagged1 variants 142

5.1 Introduction 143

5.2 Production and purification of recombinant Notch receptors 144

5.3 Notch binding ability of COSMIC variants 149

5.4 Notch binding ability of N-glycan variants 154
5.5 Development of a novel lipid binding assay 160
5.6 Lipid binding property of COSMIC variants 168
5.7 Lipid binding property of N-glycan variants 171
5.8 Conclusion 174

Chapter 6. Study of the C2 domain of human DLL4 using cancer databases. 180

6.1. Introduction 181
6.2. Designing constructs for production of $DLL4_{N\text{-}EGF3\text{-}Fc\text{-}His}$ 182
6.3. Production and purification of $DLL4_{N\text{-}EGF3\text{-}Fc\text{-}His}$ 185
6.3.1. Preliminary expression trials of DLL4 constructs 185
6.3.2. Protein purification of recombinant DLL4 187
6.4. Testing Notch activation of DLL4 cancer variants 191
6.4.1. Selection and expression of DLL4 cancer variants 191
6.4.2. Testing the effect of DLL4 cancer variants on Notch1 activation 193
6.5. Conclusion 196

Chapter 7. Discussion and future work 198

7.1. Thesis objective 199
7.2. Expression and secretion of cancer-associated variants 199
7.3. The effect of cancer-associated variants on Notch activation 201
7.4. Significance of opposing effects on Notch activation by Jagged1 and DLL4 cancer substitutions 203
7.5. Functional assessment of Jagged1 cancer-associated variants in lipid-binding and Notch-binding 203
7.6. Implications of Jagged1 COSMIC variants in Notch signalling 205
7.7. The role of Jagged1-C2 highly conserved N-glycan in Notch signalling ... 207
7.7.1. Conservation and the presence of the N-glycan in Jagged1-C2 207
7.7.2. Regulation of Notch activation by the N-glycan in Jagged1-C2 208
7.7.3. Physiological importance of the N-glycan in Jagged1 210

7.7.4. Possible implications of the effect of the N-glycan 210

7.8. Future directions 212

References 216

Appendix A – Primers 238

Appendix B – Peptide sequences 240

Appendix C – DLL4 cancer variants expression 242

List of Abbreviations

ADAM	A disintegrin and metalloprotease-containing protein
ANK	Ankyrin repeat
ATP	Adenosine triphosphate
A_{xnm}	Absorbance at wavelength x nm
bp	Base pairs
BSA	Bovine serum albumin
CADASIL	Cerebral autosomal dominant arteriopathy with subcortical infarcts and leukoencephalopathy
cbEGF	Ca^{2+}-binding epidermal growth factor-like
CMV	Cytomegalovirus
CHO	Chinese hamster ovarian
CSL	CBF-1/Suppressor of Hairless/LAG-2 transcription factor
Da	Dalton
DAPI	4′,6-diamidino-2-phenylindole
DAPT	N-[N-(3,5-Difluorophenacetyl)-L-alanyl]-S-phenylglycine t-butyl ester
DLL1	Delta like 1 ligand
DLL3	Delta like 3 ligand
DLL4	Delta like 4 ligand
DNA	Deoxyribonucleic acid
dNTPs	Deoxynucleotide triphosphates
DMEM	Dulbecco's modified Eagle medium
DMSO	Dimethyl sulfoxide
DSL	Delta/Serrate/Lag-2
DTT	Dithiothreitol
EC	Endothelial cell
EDTA	Ethylenediaminetetraacetic acid
EGF	Epidermal growth factor-like
EHBA	Extrahepatic biliary atresia
EMT	Epithelial-mesenchymal transitions
ER	Endoplasmic reticulum

FBS	Fetal bovine serum
FPLC	Fast protein liquid chromatography
Fuc	Fucose
GFP	Green fluorescent protein
GlcNAc	N-acetylglucosamine
Gluc	Glucose
h	Human
HPLC	High pressure liquid chromatography
HD	Heterodimerization
HEK	Human embryonic kidney
HES	Hairy/enhancer of split
HEY	Hairy/enhancer of split related with YRPW motif
HEPES	4-(2-hydroxyethyl)-1-piperazineethanesulfonic acid
HRP	Horseradish peroxidase
HUVEC	Human umbilical vein endothelial cell
IMAC	Immobilized metal affinity chromatography
L	Litre
LNR	Lin12/Notch repeat
Luc	Luciferase
m	Mouse
mg	Milligram
mL	Millilitre
μL	Microlitre
mAb	Monoclonal antibody
M	Moles / dm^3
MAML	Mastermind-like protein
MW	Molecular weight
NEDD4	Neural precursor cell-expressed developmentally downregulated gene 4
NICD	Notch intracellular region
NRR	Negative regulatory region
Ofut1	O-fucosyltransferase-1
PBS	Phosphate buffered saline
PCR	Polymerase chain reaction

PDB	Protein Data Bank
PEST	Proline, glutamic acid, serine, threonine-rich sequence
rpm	Revolutions per minute
RAM	RBPjk-associated module
RBPjk	Recombination signal binding protein for immunoglobulin kappa J region
RNA	Ribonucleic acid
SDS-PAGE	Sodium dodecyl sulfate–polyacrylamide gel electrophoresis
SEC	Size exclusion chromatography
SEL	Suppressor and/or enhancer of lin-12
SuDX	Suppressor of Deltex
S2	Schneider 2
T-ALL	T-cell acute lymphoblastic leukaemia
TAE	tris/acetate/EDTA
TBE	Tris/borate/EDTA
TE	Tris/EDTA
TEMED	N,N,N',N'-tetramethylethylenediamine
T_m	Melting temperature
Tris	Tris (hydroxymethyl) aminomethane
UV	Ultraviolet
V	Volts
VSMC	Vascular smooth muscle cell
WT	Wild type
YT	Yeast tryptone medium
YFP	Yellow fluorescent protein

List of amino acid abbreviations used

A	Ala	Alanine
C	Cys	Cysteine
D	Asp	Aspartic acid
E	Glu	Glutamic acid
F	Phe	Phenylalanine
G	Gly	Glycine
H	His	Histidine

I	Ile	Isoleucine
K	Lys	Lysine
L	Leu	Leucine
M	Met	Methionine
N	Asn	Asparagine
P	Pro	Proline
Q	Gln	Glutamine
R	Arg	Arginine
S	Ser	Serine
T	Thr	Threonine
V	Val	Valine
W	Trp	Tryptophan
Y	Tyr	Tyrosine

List of lipid abbreviations used

PC	Phosphatidylcholine
PS	Phosphatidylserine
PE-CF	Phosphatidylethanolamine-carboxyfluorescein
SM	Sphingomyelin

Metric prefixes

n	10^{-9}
μ	10^{-6}
m	10^{-3}
k	10^{3}

Chapter 1. Introduction

1.1 General background to the Notch signalling pathway

1.1.1 Discovery of Notch Signalling

The Notch mutation in *Drosophila* was first recorded over 100 years ago, and its name comes from the distinctive pattern of notches that appear on the mutant fly's wings (Dexter, 1914). Later work showed that this mutation is sex-linked in *Drosophila*, and the genotype of Notch is dominant regarding the wing character and recessive in the lethal effect (Morgan, 1917). In addition, the eggs of *Drosophila* Notch mutants failed to develop segmentation showing the important role of Notch in embryonic development (Poulson, 1937). Further mutant alleles of the Notch locus were subsequently produced by X-ray mutagenesis of *Drosophila* (W. J. Welshons, 1962). Studies of the effects of *Notch* mutations on *Drosophila* embryonic development also resulted in *Notch* being recognised as an important neurogenetic locus since some *Notch* mutations caused defects in the central nervous system (Lehmann et al., 1983) (Xu et al., 1990).

The *Notch* gene encodes a protein which has a transmembrane domain and large extracellular domain. The first characterization of the Notch extracellular domain was in 1985 in *Drosophila*, and it showed homology to epidermal growth factor by amino acid sequence (Wharton et al., 1985). Notch homologues were subsequently identified in other organisms such as *C. elegans* (Yochem et al., 1988) (Austin and Kimble, 1989), *Xenopus* (Coffman et al., 1990), human (Ellisen et al., 1991a), rat (Weinmaster and Roberts, 1991), mouse (Del Amo et al., 1992), zebrafish (Bierkamp and Campos-Ortega, 1993), chicken (Lardelli et al., 1995) and Sea Urchin (Sherwood and McClay, 1997). After a decade, it became clear that Notch signalling is evolutionarily conserved in metazoan species and plays a fundamental role in cell fate determination

(Artavanis-Tsakonas, 1999). Its role in human disease was first recognized with the association between *Notch1* and T lymphoblastic neoplasms (Ellisen et al., 1991b). The link between Notch and human congenital disease was first made with the association of *Notch3*, on chromosome 19, to CADASIL, a stroke disorder (Joutel et al., 1996). Subsequently, many other acquired and genetic diseases have been linked to the Notch pathway (see section 1.2.2).

1.1.2 Distinct Modes of Notch Signalling

Notch signalling is a short-range signalling system and is activated by the interaction between neighbouring cells which express transmembrane ligands and receptors on the cell surface. The interaction between ligands and receptors results in proteolysis of the receptor within its transmembrane domain, release of an intracellular fragment and expression of target genes. The Notch signalling pathway plays three main roles in cell fate decision: lateral inhibition, inductive signalling and asymmetric cell division (Artavanis-Tsakonas et al., 1995) (Figure 1-1). Activation of Notch has opposing effects on Notch receptor and Notch ligand expression, which allows equivalent precursor cells to adopt different cell fates resulting from amplifications of feedback loops, contributing to lateral inhibition (Figure 1-1). The lateral inhibition model has been proved by tracing the lineage commitment of the anchor cell and the ventral uterine precursor cell in *C. elegans* and the development of the sensory bristles in *Drosophila* (Wilkinson et al., 1994) (Simpson, 1997). In these examples, all cells in the same group are equivalent and initially express both Notch ligands and receptors. A random cell fate decision between these cells, caused by subtle differences arising from stochastic fluctuations, is then expanded by a feedback loop (Figure 1-1). In contrast to lateral inhibition, inductive signalling happens between non-equivalent cells, which are usually located at the boundary of two distinct cell populations, with cells

that are located at the interface adopting a new cell fate (Figure 1-1). The inductive signalling role of Notch has been well studied in the dorsal-ventral boundary of *Drosophila* wing and eye development (Kim et al., 1995) (Papayannopoulos et al., 1998). In addition, Notch is required in asymmetric development processes. It arises from the asymmetric distribution of cytoplasmic regulators, such as Numb, between daughter cells, which results in Notch being activated in one daughter cell but not the other, further controlling daughter cell fate. A well-studied example of asymmetric division is the generation of different types of sensory organ cells from sensory organ precursors in *Drosophila* (Guo et al., 1996).

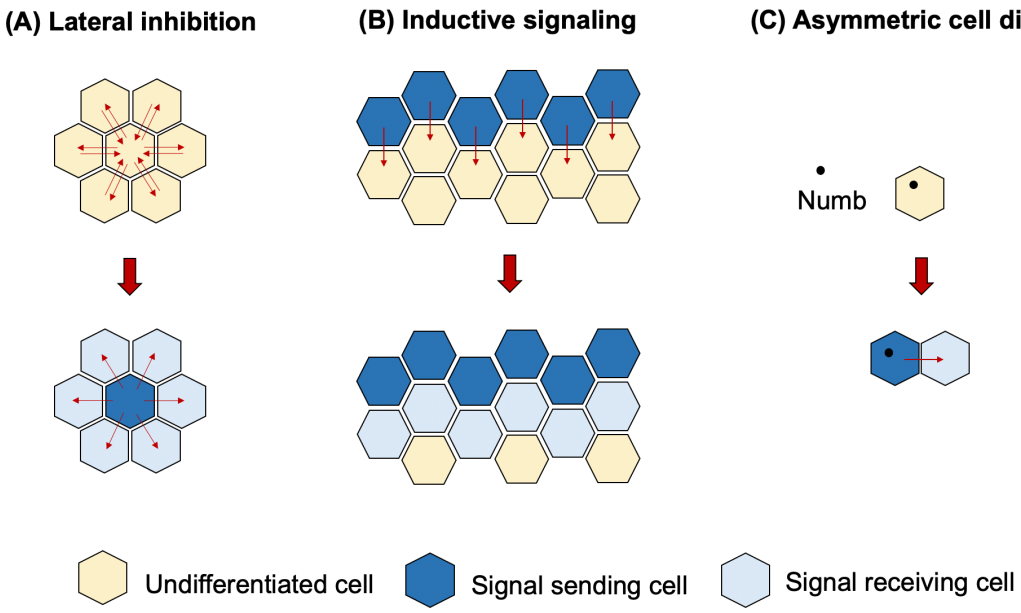


Figure 1-1. Distinct modes of Notch signalling

The Notch signalling pathway contributes to cell fate decisions by three distinct modes: lateral inhibition, inductive signalling and asymmetric cell division shown schematically. (A) Lateral inhibition. Light yellow hexagons indicate equivalent undifferentiated precursor cells that inhibit each other's ability to adopt a distinct cell fate. After feedback loop amplifications (shown by red arrows), one cell in the population adopts a different cell fate (dark blue) by lacking Notch activation, and other cells develop an alternative cell fate (light blue) caused by the activation of Notch signalling within that cell. (B) Inductive signalling. One group of cells (dark blue) induces (arrows between hexagons) a different group of cells (light yellow) to a new cell fate (light blue) along the interface. (C) Asymmetric cell division. Asymmetrical inheritance of certain factors such as Numb that promote or inhibit Notch signalling can cause Notch activated in one daughter cell (light blue) but not in the other daughter cell (dark blue), which contributes to different cell fates between daughter cells.

1.1.3 Molecular mechanism of canonical Notch Signalling

Compared to other highly conserved signalling pathways, the core Notch-transduction pathway only includes a small number of components without amplification by secondary messenger cascades (Figure 1-2). The Notch signalling pathway plays critical roles in a wide variety of cell types in metazoan species (Artavanis-Tsakonas et al., 1999). As both its ligands and receptors are transmembrane proteins, the Notch

signalling pathway dictates its multiple functions mostly through local cell-cell interactions between neighbouring cells, although long-range Notch signal transduction has been found to occur by extension of filopodia (De Joussineau et al., 2003). Multiple factors at each step, including ligands, receptors, signal transducers and effectors, play important roles in regulation of signalling.

Both ligands and receptors are single-pass transmembrane proteins with tandem epidermal growth factor (EGF)-like repeats. There are four Notch receptors (Notch1-4) in mammals, while there is only one *Drosophila* Notch homologue (most similar to mammalian Notch1) (Table 1-1). Most Notch receptors are cleaved by furin-like convertases within the secretory pathway at site1 (S1). This cleavage results in the Notch extracellular-transmembrane domain and Notch intracellular domain being held together to form a heterodimer by non-covalent interactions (Kopan and Ilagan, 2009). In mammals, there are 2 classes of canonical Notch ligands, Jagged (Jagged1, Jagged2) and Delta (DLL1, DLL4), which are homologues of their *Drosophila* counterparts Serrate and Delta, respectively (Table 1-1). However, unlike other Notch ligands, DLL3 in mammals can only inhibit signalling activated by other ligands rather than activate Notch by itself, and instead of being located on the cell surface, is present within the trans-Golgi network (Ladi et al., 2005a).

Canonical ligands interact via their C2 and DSL domains to bind to EGF11-12 of Notch. When the Notch ligand binds to the Notch receptor extracellularly in trans, it causes the release of the Notch intracellular domain (NICD) by initiating two proteolytic cleavage events by ADAM family metalloproteases (site2 (S2) cleavage) and γ-secretase (site3 (S3)/ site4 (S4) cleavage) subsequently (Figure 1-2). After site2

cleavage, Notch is still a transmembrane molecule, and γ-secretase cleaves at the intramembrane site3 which liberates the NICD. The NICD then translocates into the nucleus to form a complex with DNA-binding proteins of the RBPjk family (also known as CSL or CBF1/Su(H)/Lag-1), which bind to specific DNA binding sites ((C/T)GTGGAA). The RBP-jk family of proteins act as nuclear mediators of the canonical Notch pathway, functioning as transcriptional repressors and histone deacetylases. The binding of the NICD to RBPjk family proteins displaces the corepressors and causes the recruitment of co-activators such as Mastermind proteins (MAML1-3). This in turn converts RBPjk from a transcriptional repressor to a transcriptional activator and the expression of primary target genes such as *HES* and *HEY* is initiated (Kopan and Ilagan, 2009). HES is a helix-loop-helix transcriptional repressor and suppresses the expression of downstream target genes such as tissue-specific transcriptional activators (Iso et al., 2003). Notch ligands and receptors can also interact in cis when they are expressed in the same cell. This process, known as cis-inhibition, is important in regulating the Notch signal during development.

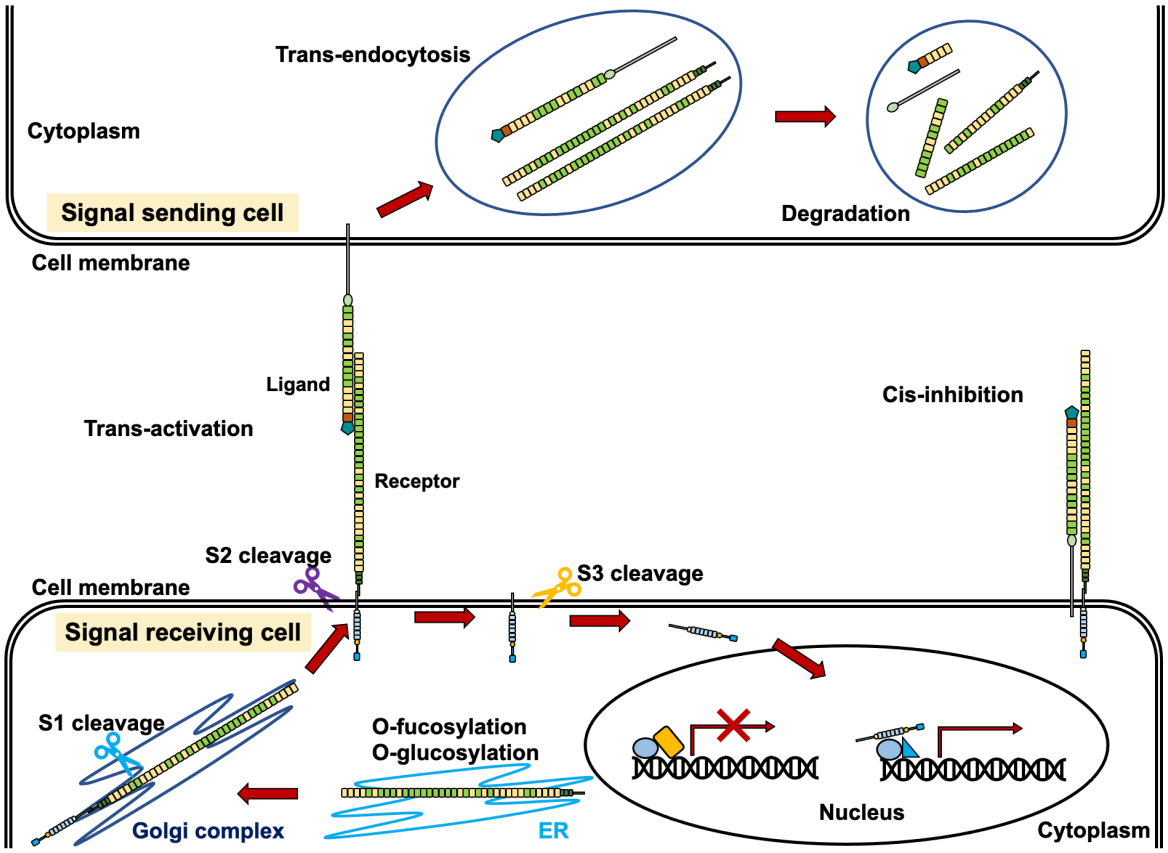


Figure 1-2. The core canonical Notch signalling pathway

Essential steps of the core Notch signalling pathway are shown in the schematic. Yellow boxes indicate EGF repeats, green boxes represent cbEGF domains. Orange boxes indicate DSL domains and teal pentagons represent C2 domains in Notch ligands. Further details of domain organisation are given in Figure 1-4 and Figure 1-5. The mature receptor is produced after it is modified by glycosylation steps in the ER and undergoes proteolytic cleavage at site 1 (S1) in the Golgi complex. After S2 and S3 cleavage events triggered by ligand binding in trans, the Notch intracellular domain (NICD) is released, and Notch ligand bound to the Notch extracellular domain (NECD) is degraded. In the nucleus, NICD interacts with RBPjk family (blue oval). Corepressors (yellow rectangle) are displaced, and coactivators are recruited (blue triangle) subsequently to initiate gene expression. The ubiquitination and degradation of NICD is vital for Notch signalling regulation. A cis-inhibiting complex of ligand and receptor expressed in the same cell is also shown.

Component type	*Drosophila melanogaster*	*Caenorhabditis elegans*	Mammals
Ligand	Delta, Serrate	APX-1, LAG-2, ARG-1, DSL-1*	Jagged1 and 2, DLL1 and 4
Receptor	Notch	LIN-12, GLP-1	Notch1-4
Glycosyl transferase	OFUT-1, RUMI, Fringe	OFUT-1	POFUT-1, Lunatic Fringe, Radical Fringe, Manic Fringe
S1 cleavage			PC5/6, Furin
S2 cleavage	Kuzbanian, Kuzbanian-like, TACE	SUP-17/Kuzbanian, ADM-4/TACE	ADAM10/Kuzbanian, ADAM17/TACE
S3 cleavage	Presenilin, Nicastrin, APH-1, PEN-2	SEL-12, APH-1, APH-2, PEN-2	Presenilin1 and 2, Nicastrin, APH-1a-c, PEN-2
CSL DNA-binding protein	Su(H)	LAG-1	CBF1/RBPjk
Co-activator	Mastermind	LAG-3	Mastermind1-3
Co-repressor	Hairless, SMRTR		SMRT
Target bHLH Repressor Genes	*E(spl)*	*REF-1*	*HES/ESR/HEY*

Table 1-1. Comparison of Notch components among species

*Only transmembrane ligands are shown, *C. elegans* has a number of soluble DSL ligands.

1.1.4 Non-canonical Notch signalling

Non-canonical Notch signalling is activated by a diverse group of structurally unrelated proteins (either secreted or membrane-tethered) without a critical receptor-binding domain (DSL domain), which contribute to pleiotropic effects of Notch pathway (D'souza et al., 2010). Some non-canonical Notch ligands can active non-canonical downstream Notch signalling components, like Deltex, which regulate transcription independently of CSL (Yamamoto et al., 2001).

Transmembrane non-canonical ligands include Delta-like1 (also known as Dlk-1, Pref-1 or FA-1), Delta/Notch-like EGF-related receptor (DNER), F3/contactin, NB3/contactin, Jagged and Delta (Jedi). Dlk-1 was one of first identified non-canonical ligands and shares homology, through a series of EGF-repeats, with the Notch-Delta family. Although Dlk-1 lacks a Notch binding DSL domain and has a shorter intracellular domain, it has the capability of altering Notch signalling and has a role in

preventing adipogenesis (Smas and Sul, 1993) (Bray et al., 2008). DNER, which also contains EGF repeats, activates Notch/Deltex signalling and participates in Bergmann glial development (Eiraku et al., 2005). Another non-canonical ligand that actives Notch/Deltex signalling is F3/contactin, which is important for oligodendrocyte maturation (Hu et al., 2003).

In addition to transmembrane Notch ligands, secreted non-canonical Notch ligands have also been identified in both *Drosophila* (Scabrous (Sca) and wingless (Wg)) and mammals (such as CCN3, MAGP-1, MAGP-2, thrombospondin2 (TSP2), Y-*box* (YB) and EGFL7). EGFL7 is secreted by endothelial cells and neurons and acts as an antagonist of Notch signalling, affecting cell migration, blood vessel formation, neural stem cell proliferation and differentiation (Parker et al., 2004)(Schmidt et al., 2009). Interestingly, another secreted non-canonical ligand, MAGP-2, is the only ligand so far that has been identified to activate Notch without an ADAM cleavage event (Miyamoto et al., 2006).

1.2 Medical relevance of Notch Signalling

1.2.1 Physiological roles of Notch signalling

Each Notch ligand may associate with a specific cell population to regulate particular physiological processes. For example, Jagged1 and DLL4 are required for angiogenesis; DLL4 and Jagged2 have essential functions in the thymus; Jagged1 is important for hepatic and biliary cell development, while DLL1 and Jagged2 play essential roles in somite formation and skeletal development.

1.2.1.1 Angiogenesis

The blood vessel mainly consists of endothelial cells (ECs) and vascular smooth muscle cells (VSMCs). Normal angiogenesis requires a high degree of coordination between the maintenance of existing vessels and EC sprouting that relies on tip cell migration and stalk cell proliferation. ECs located at the inner surface of the vessel have high plasticity and can be quiescent for years before they receive signals to initiate sprouting. After receiving proangiogenic signals, ECs will differentiate into tip cells with filopodia located at the tips of vascular sprouts (Figure 1-3). Following tip cell specialization, stalk cells with fewer filopodia proliferate to support sprout elongation (Figure 1-3) (Potente et al., 2011). These processes can be modulated by proangiogenic growth factors (such as vascular endothelial growth factor (VEGF)) and proinflammatory cytokines (such as tumour necrosis factor (TNF)) (Kang et al., 2019). Studies from a human umbilical vein endothelial cell (HUVEC) 3D model indicates that Notch signalling contributes to the regulation of tip cell formation, thereby regulating the diameter and branching of blood vessel (Sainson et al., 2005).

Jagged1 and DLL4 are two Notch ligands prominently expressed in the vasculature. In embryonic vascular development, Jagged1 has been reported to have an essential role as mice with homozygous null mutations of *Jag1* die at E10 due to vascular defects in both the embryo and the yolk sac (Xue et al., 1999). Endothelial specific *JAG1* knock out mice showed that Jagged1 is critical for VSMCs differentiation during the embryonic angiogenesis process, which is consistent with *in vitro* experiments (High et al., 2008) (Doi et al., 2006). DLL4 is also a requisite ligand in embryonic angiogenesis, as heterozygous DLL4 deletion mice die at E10.5 with profound vascular defects (Gale et al., 2004). *In vitro* experiments showed that DLL4 stimulate adjacent ECs to arterial cell fate (Iso et al., 2006).

In postnatal life, DLL4 is highly expressed in tip cells and can suppress sprouting in its neighbouring cells (stalk cells). Accordingly, low DLL4 expression in mouse retina was shown to increase the number of tip cells and branches (Hellström et al., 2007). In contrast, Jagged1 levels in the mouse adult are high in stalk cells and act as an antagonist of DLL4 by blocking DLL4/Notch interactions. *JAG1* deletion mice have a decreased number of blood vessel branches. In addition, reduced Jagged1 expression in ECs leads to a decrease in the number of tip cells and filopodia (Benedito et al., 2009a). Recently, it has been reported that suppression of Notch1 and DLL4 in human endothelial cells and murine bone leads to impaired growth of vessels in adult bone (Fu et al., 2020).

Angiogenesis is also required for the maintenance, growth and metabolism of tumours. Notch signalling is a pivotal regulator during tumour angiogenesis and will further affect tumour development. Decreased DLL4 expression in tumour vessels contributes to increased, but non-productive, tumour vascular density, thereby slowing tumour growth (Noguera-Troise et al., 2006). Furthermore, ECs in blood vessels can promote tumour progression in different ways, and Notch signalling has been shown to participate in these processes. For example, during lymphomagenesis, Jagged1 expressed by ECs accelerated the aggressive features of the tumour (Cao et al., 2014). In addition to canonical Notch ligands, a soluble form of truncated Jagged1 secreted by ECs has been found to promote the formation of colorectal cancer (Lu et al., 2013). In addition to Notch ligands, Notch3 has been proved to be highly expressed in tumour ECs and can regulate tumour angiogenesis through non-canonical Notch pathway downstream regulators (Lin et al., 2017). As the Notch pathway is important for tumour

angiogenesis, components of Notch signalling can provide potential drug targets for tumour treatment.

Notch signalling in blood vessel cells can also be accompanied by effect on metabolic regulation. Recently, it was shown that Notch activation levels in ECs of blood vessels can regulate insulin transport to muscle, and higher levels of Notch signalling in ECs increases blood glucose levels due to lower insulin sensitivity. This was accompanied by increased micro vessel density. (Hasan et al., 2020).

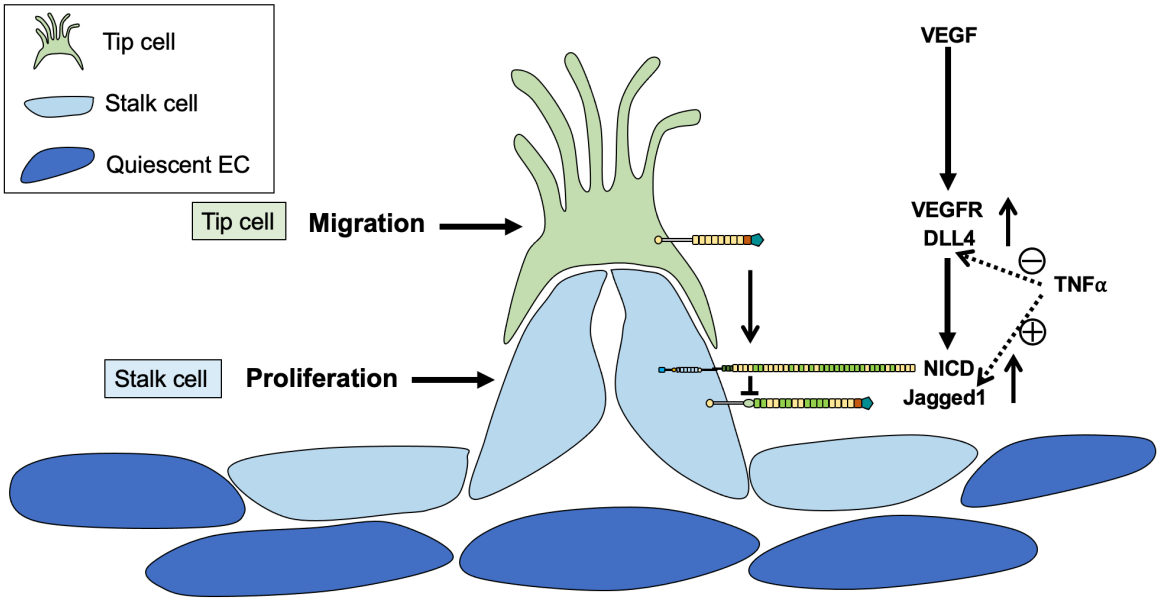


Figure 1-3. Tip and stalk cell formation

In response to VEGF stimulation, VEGF signalling in ECs increases VEGF receptor (VEGFR) and DLL4 levels. These ECs develop filopodia and migrate toward VEGF leading the formation of the new branch and are called tip cells (green). DLL4 from tip cells activates Notch signalling in the neighbouring cells which then adopt the stalk fate (light blue) with high Jagged1 expression level. Jagged1 also counteracts DLL4 signalling through cis-inhibition by direct binding to the Notch in the signal receiving cell. TNFα, a proangiogenic growth factor, induces Jagged1 expression but reduces DLL4 to modulate angiogenesis.

1.2.1.2 Somitogenesis

Somitogenesis is the process of transient blocks of epithelial cells giving rise to the segmented ribs, skeletal muscle and skin of vertebrates. Abnormal Notch signalling results in segmentation defects in zebrafish, chick and mouse models (Gibb et al., 2010). Recently, an *in vitro* study in human cells indicated that segmentation oscillations are conserved from fish to human (Diaz-Cuadros et al., 2020). Altering NICD levels affects both the segmentation clock period and somite size (Carrieri et al., 2019). Among Notch ligands, Delta ligands play major roles in somitogenesis. The oscillated expression of DLL1 in presomitic mesoderm cells is essential to drive the segmentation clock, and steady DLL1 expression in these cells causes disorganized and diffused somites in mouse models (Shimojo et al., 2016). The non-canonical Notch ligand DLL3 is also essential for normal somite formation and patterning, and homozygous mutations of DLL3 are associated with an axial skeletal disease termed spondylocostal dysostosis (Bulman et al., 2000).

1.2.1.3 Blood cell development

Hematopoietic stem cells (HSCs) are derived from endothelial cells during embryonic development and function as a foundation of the components of the bloodstream. Normally, HSCs need to be able to maintain a stem cell reservoir but also differentiate into various cell type such as lymphoid, myeloid and erythroid lineages. HSC specification is modulated by multiple Notch signalling events, from either hematopoietic precursors or neighbouring somites. The first mammalian homologue of *Drosophila Notch* was identified in humans suffering from a blood cancer, T cell acute lymphoblastic leukaemia (T-ALL) (see section 1.2.2.1), which was also the first evidence of Notch involvement in the hematopoietic compartment (Ellisen et al., 1991a).

During embryonic development, Notch signalling functions to maintain HSCs. Reduced Notch expression levels contributes to a decreased number of HSC and vice versa (Lee et al., 2009). Components of the Notch signalling have shown to be essential for HSC emergence. For instance, Notch1 and Jagged1 are essential for the generation of HSCs from endothelial cells in mice (Kumano et al., 2003) (Robert-Moreno et al., 2008). Notch3 was shown to be required for somite HSC emergence in zebrafish embryos (Kim et al., 2014). In addition, in embryos, Notch signalling contributes to T and B cell lineage development. From experiments in mouse embryos, Notch signalling plays a vital role in maintaining erythroid homeostasis by inducing apoptosis, as Notch loss-of-function contributed to an increased number of erythroid cells and the opposite is also true (Robert-Moreno et al., 2007). In addition, Notch signalling also contributes to different types of innate lymphoid cell development in mouse embryo (Lee et al., 2012) (Wong et al., 2012).

In addition to embryonic development, Notch signalling is also important for B cell maturation in postnatal life. Notch2 expression, rather than the expression of Notch1 receptors, increases during the B cell maturation process, and Notch2 deficient mice have fewer mature B cells (Saito et al., 2003). Consistent with the data from Notch2 targeted mice, DLL1 deficient mice showed a similar loss of mature B cells, suggesting a potential interaction with the ligand during B cell maturation (Pajcini et al., 2011).

In adult haematopoiesis, the Notch pathway plays important roles in development of T (Radtke et al., 1999) and B cells (Tanigaki et al., 2002). Notch1 has been shown to increase HSC self-renewal and promote lymphoid lineage commitment over myeloid

choice (Stier et al., 2002). Without Notch1 in bone marrow, bone marrow progenitors enter the thymus and develop into B cells instead of T cells in mouse models. Mouse models, where Notch2 or Notch3 are inactivated, have not shown hematopoietic phenotypes (Pajcini et al., 2011). Consist with Notch1 mutagenesis data, Notch1 or DLL4 overexpression in bone marrow impairs B cell development and lead to lymphoproliferative disease (Dorsch et al., 2002). In addition to T cell development, Notch signalling also plays a role in inducing regulatory T cells. Jagged1 overexpressed in the presence of antigen contributes to induction of human regulatory T cells, which is consistent with mouse experiments (Pajcini et al., 2011).

1.2.1.4 Neurogenesis

The crucial role of Notch in nervous system development was indicated by the embryonic phenotype of a *Drosophila* homozygous *Notch* null mutant (Poulson, 1940). Later on, studies from rats and zebrafish showed that activation of Notch signalling in retina blocks neuronal differentiation but promotes glial cell (astrocytes, radial glia and Müller cells) fate determination (Furukawa et al., 2000) (Scheer et al., 2001) except oligodendrocytes (Wang et al., 1998). In particular, Delta/Notch signalling is required for specifying neurons and glia during spinal cord development (Kang et al., 2012). Jagged1 plays an important role in neural stem cell maintenance and proliferation in postnatal life, which contributes to the generation of new neurons and learning processes (Lavado and Oliver, 2014). In addition, Notch modulation has also been reported to affect morphology (Major and Irvine, 2005), plasticity (Wang et al., 2004) and neurogenesis (Santopolo et al., 2020) of neuron cells, which suggest Notch signalling is a potential therapeutic target for neurodegenerative diseases, such as Alzheimer’s disease and Parkinson’s disease.

1.2.2 Notch signalling in human disease

As a wide range of physiological processes are regulated by Notch signalling, abnormalities in the Notch pathway contribute to many human diseases (Table 1-2).

1.2.2.1 Notch and cancer

Tumorigenesis is thought to be initiated by the accumulation of a number of mutations in uncommitted cells. These cells then reach a point where they cannot respond properly to the developmental signals and are unable to differentiate correctly. As the Notch pathway participates in cell proliferation, differentiation and migration/sprouting, all of which are involved in tumour formation, Notch signalling can potentially affect tumorigenesis in multiple ways.

Notch was identified as a key gene involved in tumorigenesis when a *Notch* transcript, *TAN-1*, was found to contribute to the development of T-cell acute lymphoblastic leukaemia (T-ALL) (Table 1-2) (Ellisen et al., 1991b). T-ALL was initially identified as being caused by chromosomal translocation. Analysis of neoplasms showed that breakpoints on human chromosome 9 occur within *Notch1* and resulted in the T-cell receptor-β promoter region being located at the 3' region of *Notch1* in the resulting allele. This generates a Notch1 fusion protein with ligand-independent activity and leads to a gain of function. This molecular mechanism of leukaemia was later replicated in a mouse model that showed that the progress of leukaemia in tumour-prone mice is accelerated of by this type of *Notch1* allele (Pear et al., 1996). Later studies found that the most frequent mutations of T-ALL cases affect the heterodimerization domain of the Notch1 receptor (section 1.4.2). These mutations

enhance Notch activation in two ways. One class of mutation enhances Notch1 transmembrane domain and Notch extracellular domain dissociation, which exposes the S2 cleavage site to the ADAM metalloproteases. The other class of mutation increases Notch activation by exposing the S2 cleavage site without changing the stability of the heterodimer (Malecki et al., 2006). The second hot spot of T-ALL mutations on *Notch1* affect the intracellular PEST domain. These mutations affect the ubiquitination and degradation of NICD, which leads to increased levels of NICD and constitutive Notch activation (Pagliaro et al., 2020).

Head and neck squamous cell carcinoma (HNSCC) is one of the most common cancers with a poor survival rate in the world. Recently, it has been reported that 67% of HNSCC patient samples showed an inactivation of the Notch signalling pathway, such that this feature is regarded as a hall mark of HNSCC (Loganathan et al., 2020). Exome Sequencing of HNSCC suggests that *Notch1* may act as a tumour suppressor gene rather than oncogene in HNSCC as most mutations identified in *Notch1* contributed to truncated gene products (Agrawal et al., 2011). Moreover, *JAG1* and *JAG2* gene expression levels in HNSCC were increased suggested their potential role in oncogenesis (Sun et al., 2014). These data are in contrast to the T-ALL “story” where Notch mutations in the T-cell lineage are activating or gain of function and oncogenic.

Aberrant Notch activity has also been identified in other types of cancers such as small-cell lung cancer (SCLC), neuroblastoma and epithelial cancer. Increased Notch1 and Notch2 NICD levels have been shown to contribute to dramatically decreased expression of human achaete-scute homologue-1 (hASH1), a helix-loop-

helix transcription factor expressed in normal foetal pulmonary neuroendocrine cells and also in lung cancer cells, which appears to decrease the SCLC potential (Sriuranpong et al., 2001). Another tumour associated with hASH1 and Notch is neuroblastoma. This childhood tumour is also affected by increased Notch activation resulting in decreasing expression of hASH1 (Grynfeld et al., 2000). In addition, abnormal Notch signalling, including mutations in receptors and abnormal downstream transcription factor levels, was identified in squamous cell carcinomas (Wang et al., 2011) (Labban et al., 2018). Recently, by an integrative pathway and network analysis, cancer-related mutations from 27 tumour types, such as breast cancers and lung cancers, have been found to alter the activity of the Notch signalling pathway by both coding and non-coding mutations (Reyna et al., 2020).

1.2.2.2 Alagille syndrome

Alagille syndrome is an inherited autosomal dominant disease caused by mutations in *JAG1* or *Notch2* (Table 1-2). Patients with Alagille syndrome usually have a variety of developmental disorders, such as bile duct paucity, heart defects, skeletal abnormalities, liver diseases, renal insufficiency and distinct facial features. These phenotypes show inter- and intra-familial variation. It is a rare disease, affecting only 1 in 30,000 to 1 in 50,000 individuals (Fabris et al., 2019). Alagille syndrome is caused by Jagged1 and Notch2 haploinsufficiency (Maya Kamath et al., 2012). In 94% of identified cases it is caused by mutations in *JAG1*, while only 6% of cases are caused by *Notch2* (Kamath et al., 2013). Frameshift, non-sense and splice site mutations have all been observed, demonstrating haploinsufficiency is a mechanism of dominance. In addition, missense mutations and gene deletions have also been found in patients, but at a lower frequency. Most of missense mutations affect the C2 domain of Jagged1

and cause misfolding (Chillakuri et al., 2013). By studying Alagille syndrome, it has been found that Notch signalling not only participates in liver development and repair response, biliary and bile duct development, but is also involved in cardiac, pulmonary and kidney development (Fabris et al., 2007) (Meester et al., 2019).

Another Jagged1 associated disease relate to bile duct development is Extrahepatic biliary atresia (EHBA). EHBA is a neonatal liver disease with partial or total absence of bile duct between porta hepatis and the duodenum. It is a rare disease with an incidence of 1 in 8,000 to 1 in 18,000 living births (Rakheja et al., 2006). In 102 EHBA cases, 9 missense mutations were reported related to *JAG1* (Kohsaka et al., 2002). A subset of these result in the production of Jagged1 but have a reduced ability to activate Notch (Suckling et al., 2017). Two main hypotheses of the pathogenesis have been proposed: perinatal inflammatory process and early embryonic malformation (Kohsaka et al., 2002).

1.2.2.3 Adams-Oliver syndrome

Adams-Oliver syndrome is a rare genetic condition that can be inherited in an autosomal dominant or autosomal recessive manner and is caused by mutations in the Notch pathway (Notch1, Notch3, DLL4, RBP-jk family) or GTPase signalling pathway. These mutations include nonsense mutations, and missense mutations which alter the number of cysteine residues in EGF domains in DLL4 without any obvious mutational hotspots (Table 1-2) (Meester et al., 2015). Diagnosis is based on the presence of terminal limb-reduction defects, an absence or scarred skin, a partial absence or thin skull and cardiovascular anomalies (Adams and Oliver, 1945). It has been reported that most of these symptoms are caused by impaired circulation, for

example vascular obstruction by thromboses, during embryonic development (Stittrich et al., 2014). Another pathophysiological mechanism of Adams-Oliver syndrome that has been proposed is the dysfunction of endothelial cells causing defective smooth muscle coverage in blood vessels (Patel et al., 2004).

1.2.2.4 CADASIL

Cerebral Autosomal Dominant Arteriopathy with Subcortical Infarcts and Leukoencephalopathy, usually called CADASIL, is an inherited autosomal dominant developmental brain disorder caused by mutations in *Notch3* (Table 1-2). Patients with CADASIL present with at least four disorders: defects in small cerebral arteries lead to subcortical infarcts and white matter damage, small arteries in all organs are affected, lateral meningocele syndrome, and infantile myofibromatosis (Maš and Andersson, 2017). The vast majority of CADASIL-related *Notch3* mutations are missense mutations, and most of them result in addition or deletion of a cysteine residue in EGF domains. However, the precise mechanism for the disorder still needs to be discovered. The arteriopathy of CADASIL is characterized by abnormal function of vascular smooth muscle cells (Joutel et al., 2000). In particular, biochemical fractions of brain and artery samples suggested that Notch3 extracellular domain aggregated into granular osmiophilic material in the matrix of brain small vessels, which would promote the abnormal recruitment of functionally important matrix proteins and cause toxicity (Monet-Leprêtre et al., 2013).

1.2.2.5 Bicuspid aortic valve disease

Bicuspid aortic valve disease, also mentioned as BAV, is the most common congenital cardiac disorder in humans resulting in only two aortic valve leaflets instead of the normal three (Table 1-2) (Harrison et al., 2019). BAV patients have abnormal aorta in

strength and size, which contributes to high risk of developing thoracic aortic aneurysms and acute aortic dissection. *Notch1* is identified as one of a few genetic anomalies in BAV disease, and mutations in *Notch1* are found in both familial and sporadic BAV disease (Garg et al., 2005) (McKellar et al., 2007). In inherited BAV disease, *Notch1* mutations cause an early developmental defect in the aortic valve and a later calcium deposition, which shows autosomal-dominant transmission in human pedigrees (Garg et al., 2005). In BAV patients, mRNA levels of Notch signalling components including Notch receptors and downstream transcriptional regulators are found to decrease (Sciacca et al., 2013). These data suggest that Notch signalling plays an important role in the development of BAV aortopathy.

Disease	Related genes	Mutations	Phenotypes
Alagille EHBA	*JAG1, Notch2*	Missense/frameshift/splice site leading to decay/retention of Jagged1	Hepatic, skeletal, cardiac, renal developmental disorders.
Adams-Oliver	*Notch1, Notch3, DLL4, RBP J*	Addition/deletion of a cysteine residue in EGF domains	Terminal limb-reduction defects, skin/skull absence and cardiovascular anomalies.
CADASIL	*Notch3*	Addition/deletion of a cysteine residue in EGF domains	Subcortical infarcts and white matter damage, small arteries defective, lateral meningocele syndrome, infantile myofibromatosis.
T-ALL	*Notch1*	Mutations at HD domain/PEST domain	Hyperproliferation of T cells.
BAV	*Notch1*	Missense/frameshift mutation	Abnormal aortic valve leaflets and aorta.
Tetralogy of Fallot	*JAG1*	Missense/frameshift mutation, most reported missense mutations cluster at the extreme N-terminus	Hole in septum of heart.
Spondylothoracic dysostosis	*DLL3, LFNG, MESP2, HES7*	*DLL3*: most occur in the extracellular domain and truncate the protein *LFNG:* mutations result in leucine substitution and no enzymatic activity *MESP2*: frameshift/null mutations *HES7:* missense mutations	Fused/deleted/uneven/severe curvature spine, truncal shortening.

Table 1-2. A summary of main genetic and acquired diseases related to the Notch signalling pathway

1.3 Regulation of Notch activation

Notch signalling is a juxtacrine system based on cell-cell contact. However, three types of interaction between receptor and ligand have been described trans-activation, cis-activation and cis-inhibition. The physiological significance of trans-activation and cis-inhibition in development is well known.

1.3.1 Trans and cis interactions

Ligands and receptors of Notch pathway can interact either on the same cell (cis-interaction) or between neighbouring cells (trans-interaction) in a calcium-dependent manner. Transactivation has been described in 1.1.3. Each type of interaction has a different outcome on signalling activity. Cis-inhibition of Notch signalling was first shown during normal growth patterning (without over-expression or non-physiological levels of ligands) by experiments on *Drosophila* wing development (de Celis and Bray, 1997). Another instance of cis-inhibition in a physiological role came from *Drosophila* eye development, showing that cis-inhibition within the neuron precursor cell contributes to a Notch lateral inhibition effect (Miller et al., 2009) (Figure 1-1). In vertebrates, studies on cis-inhibition of Notch receptors by ligands were mostly based on overexpression experiments. For example, knowledge that DLL1 promotes human epidermal stem cell maintenance by cis-inhibition was gained by overexpressing full-length DLL1 in keratinocytes (Lowell et al., 2000). In mammals, DLL3 was shown to perform its function by cis-inhibition only, in contrast to other canonical ligands that can alter Notch activation through both cis and trans interactions (Ladi et al., 2005b). Recently, cis-activation has been observed in multiple cell lines using both engineered and endogenous Notch components, and it appears to have a role in neural stem cell maintenance (Nandagopal et al., 2019).

In terms of molecular mechanisms, cis-inhibition plays an important role in maintaining the signalling polarity from signal-sending to signal receiving cells (Becam et al., 2010). Available data indicate that cis-inhibition requires a physical interaction between ligands and receptors to limit trans-interactions through EGF repeats of Notch and N-terminal/DSL domain of ligands (Sakamoto et al., 2001). Unlike cis-inhibition, which appears to depend on both EGF 11-12 and the *Abrupt*ex region (EGF 24-29) of *Drosophila* Notch, trans-activation only requires domains EGF 11-12 (de Celis and Bray, 2000) (Fiuza et al., 2010). Thus, it suggests a competitive mechanism between cis and trans for Notch ligand-receptor interactions. Structural analysis of receptor ligand interacting regions show an antiparallel interaction, but it is unclear whether or not this is the only conformation that can occur at the cell surface (Luca et al., 2015). Studies from *Drosophila* cells further indicated that the conformation of the Notch-ligand complex in cis-inhibition prevents proteolytic cleavage events and Notch extracellular domain shedding, which inhibits Notch activation (Fiuza et al., 2010).

The ratio between the ligand and the receptor concentrations is known to influence trans and cis interaction responses and this subsequently affects the signalling outcome (Sprinzak et al., 2010). Interestingly, recent work showed that cis-ligands can also activate Notch receptors by controlling cell density and ligand concentration (Nandagopal et al., 2019). Findings in *Drosophila* are consistent with a model in which accumulation of Notch extracellular domains on the cell surface promote the clearance of the surface ligand Serrate (Table 1-1), suggesting that cis-inhibition also works by removing ligands and receptors on the cell surface through endocytosis (Becam et al., 2010). Post-translational modifications are important for trans and cis interactions. The

expression of glycosyltransferase in mammalian cells could reduce both cis-inhibition and cis-activation of Notch (Sakamoto et al., 2001) (Nandagopal et al., 2019). Another post-translational modification of ligand, ubiquitination, has been reported to be essential for trans-interaction but not in cis-inhibition (Glittenberg et al., 2006)

1.3.2 Endocytosis and trafficking

Endocytosis as a mechanism to modulate Notch signalling was first suggested by a temperature-sensitive *Drosophila* mutant, termed *shibire*, which had similar neurogenic phenotypes as *Notch* mutants. Studies of *Shibire* flies indicate that membrane recycling of these flies was blocked in endocytosis (Poodry, 1990). Endocytosis has been shown to play a vital role in regulating cell surface expression levels of Notch ligands and receptors. In Notch signalling, small differences in ligand and receptor expression can be amplified by the positive and negative transcriptional feedback mechanisms. Moreover, as Notch generates a signal through a proteolytic process, one molecule can only signal once. Thus, regulating expression levels of Notch signalling components is important for modulating intensity and duration of signalling. After Notch has been transported to the membrane, if it does not interact with ligands, it will be labelled for degradation through endocytosis and ubiquitination.

In addition to Notch component levels, endocytosis is also essential for Notch activation. Ligands undergo two distinct endocytic events, before and after engagement of Notch, respectively, to activate Notch signalling. The first endocytic event happens before the engagement of Notch, contributing to the activation and recycling of ligands. It has been suggested that this recycling step may help in the concentrating, clustering and localisation of ligands, which is vital for cell polarization

(Nichols et al., 2007). Moreover, microdomains with higher Notch ligand concentrations could facilitate Notch receptor activation (Heuss et al., 2008). The second endocytosis function is the generation of a pulling force to facilitate Notch S2 cleavage events. Proteolysis of Notch is facilitated by the specific uptake of Notch extracellular domain generated by ligand endocytosis of the signal-sending cell. This uptake force changes the conformation of Notch in the NRR region and destabilizes the non-covalent interactions that keep the Notch heterodimer in an inactive state. Subsequently, the uptake event allows for proteolysis by ADAM proteases and removal of the Notch extracellular domain (Nichols et al., 2007).

1.3.3 Notch signalling cross-talk

The development and morphogenesis of metazoans relies on a handful of evolutionarily conserved signalling pathways that function as an integrated network. Other signalling systems are thought to interact with the Notch pathway including vascular endothelial growth factor (VEGF), tumour necrosis factor alpha (TNFα), fibroblast growth factor, Hedgehog, Jak/STAT, RTK, Toll-like receptors and Wnt (Hurlbut et al., 2007). Most of these pathways can upregulate the expression levels of Notch components. For example, in angiogenesis, VEGF-signalling is upstream of Notch pathway and can induce DLL4 expression (Figure 1-3), while TNFα can promote Jagged1 expression, and they work together to modulate the sprouting of blood vessels (Benedito et al., 2009a). In tumorigenesis, Notch signalling is downstream of Wnt, and Jagged1 is upregulated by Wnt (mediated by β-catenin) to promote vasculogenesis in tumours (Rodilla et al., 2009). Interestingly, CD46 can not only regulate Jagged1 expression levels in T cells but also binds directly to it, and this crosstalk is important for the immune response (Le Friec et al., 2012). This crosstalk

can potentially affect the spatio-temporal expression of Notch ligands, which allows Notch signalling to perform in a highly ordered and complex molecular network of interactions.

1.3.4 Ligand proteolysis

Notch ligands can be cleaved by ADAM family proteases and γ-secretase, like Notch receptors. ADAM-mediated cleavage first releases extracellular domains of Notch ligands, and the membrane-tethered fragment undergoes further cleavage by γ-secretase (D'souza et al., 2008). Studies in *Drosophila* showed that cleavage of Delta by ADAM protease (Kul) is vital for maintaining an asymmetric distribution of ligands between signal-sending and signal-receiving cells (Sapir et al., 2005). In mammals, DLL1 shedding mediated by ADAM12 regulates the ligand-to-receptor ratio and helps to maintain the unidirectional Notch signalling of muscle cells (Sun et al., 2008). Interestingly, natural secreted soluble ligands in *C.elegans* were demonstrated to activate Notch signalling and play a role in body wall muscle cell and gonadal sheath cell fate decision *in vivo* (Chen and Greenwald, 2004). *In vitro*, these secreted Notch ligands have been shown to activate the Notch pathway but need to be pre-clustered or immobilized, while un-clustered soluble ligands can bind to Notch receptors and block Notch activation (Hicks et al., 2002) (Shimizu et al., 2002).

1.4 Notch ligands and receptors

1.4.1 Notch ligands

The canonical Notch ligands are single pass type I transmembrane glycoproteins and comprised of two families, Delta and Jagged/Serrate. The extracellular domain of Notch ligands consists of C2, DSL, EGF (including both calcium binding and non-

calcium binding) domains and the Jagged/Serrate family have an additional cysteine-rich region (Figure 1-4) (D'Souza et al., 2008). The C2 domain (previously known as the MNNL domain) at the extreme N-terminus was identified as a lipid-binding domain that can modulate signalling through interactions with the cell membrane in addition to providing an interaction site for Notch (Chillakuri et al., 2013) (Luca et al., 2015) (Luca et al., 2017). Adjacent to the C2 domain is a disulphide-rich module termed DSL (Delta/Serrate/LAG-2) domain (Henderson et al., 1997). The DSL domain together with the C2 and EGF1-2 (also referred as DOS domains, Delta and OSM-11-like proteins） are required for the Notch binding ability (Luca et al., 2017). Following EGF1 and 2 domains, there are either 5 (DLL3), 6 (DLL1/DLL4) or 14 (Jagged1/Jagged2) EGF repeats in human Notch ligands (Figure 1-). Each EGF domain is around 40 amino acids long and has six conserved cysteine residues forming three disulphide bonds in a 1-3, 2-4, 5-6 configuration.

Following the ligand extracellular domains, the transmembrane segments connect with relatively short intracellular domains that comprise 100 to 150 amino acids. These intracellular domains have the lowest sequence homology between ligands. Apart from DLL3, all Notch ligands contain multiple lysine residues that can be ubiquitinated. In addition, at the C-terminus of Jagged1, DLL1 and DLL4 in mammals, there is a PDZ domain (PSD-95/Dlg/ZO-1) that can promote the interaction of the ligands with the actin cytoskeleton and modulate Notch signalling (Figure 1-4) (Pintar et al., 2007) (Tetzlaff et al., 2018).

Among all the DSL-containing Notch ligands, DLL3 is the most structurally divergent, having a degenerate DSL domain and lacking both the EGF1-2 and intracellular domains.

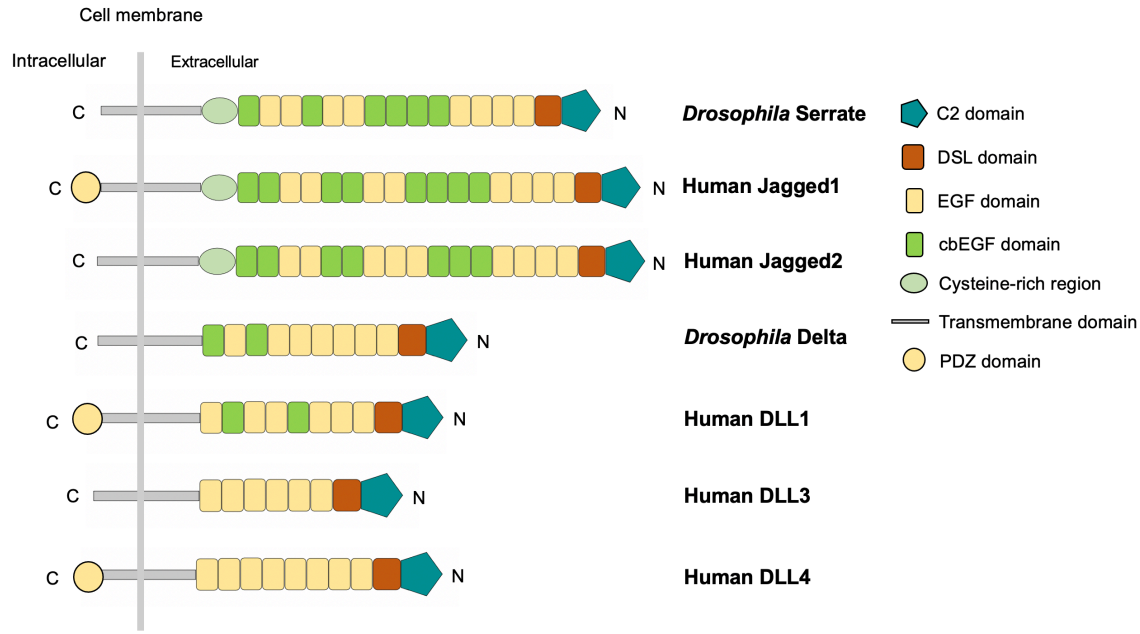


Figure 1-4. Domain organization of Notch ligands

Notch ligands from *Drosophila* and human are shown, with the extracellular region on the right. Canonical Notch ligands are single-pass membrane proteins with large extracellular regions. At the extreme N-terminus of the extracellular regions are C2 domains (teal) that interact with cell membranes. Serrate/Jagged ligand class has more EGF repeats than Delta, and they also have a cysteine-rich region (light green) that is absent in the Delta family.

1.4.2 Notch receptors

Notch receptors are 300 kDa to 350 kDa type I transmembrane heterodimers. The major part of the Notch extracellular domain (NECD) consists of 29 to 36 EGF repeats (Figure 1-5). Some of these EGF repeats have unique carboxylate or carboxyamide sequences involved in binding a single calcium ion (Rao et al., 1995)(Hambleton et al., 2004) (Cordle et al., 2008). Among these EGF repeats, EGF11-12 is known to be important for the ligand binding function of Notch receptor (Rebay et al., 1991). Following EGF repeats is a unique extracellular negative regulatory region (NRR) consisting of Lin12-Notch repeats (LNR) and a heterodimerization domain (HD). The NRR is crucial for preventing receptor activation without ligands since its conformation

protects exposure of the S2 cleavage site. It has been shown that ligand and receptor interaction in combination with endocytosis by the signal sending cell results in an NRR conformational change, which subsequently exposes the S2 cleavage site. Missense mutations affecting the NRRs of Notch receptors are known to contribute to gain-of-function phenotypes which are associated with T-ALL (Gordon et al., 2007) (see section 1.2.2.1).

The N-terminus of the NICD (Notch intracellular domain) contains a 12 amino acids sequence external to the transmembrane region, termed the Notch Extracellular Truncation (NEXT), that is non-covalently linked to the NECD at the HD. NEXT is cleaved by γ-secretase at site 3 within the transmembrane domain when Notch is activated (Figure 1-5). Next to the HD, the RAM domain in the NICD first interacts with RBP-jk family member, Su(H), after Notch NICD translocates to the nucleus (Tamura et al., 1995). Following the RAM domain and an unstructured linker, ANK domains (having seven ankyrin repeats) are found that can associate with CSL, which in turn aids in recruiting coactivators such as Deltex (Matsuno et al., 1995). Following the ANK domain is the potential phosphorylated domain (PPD), which also contains ankyin repeats and is able to enhance Su(H) binding and connect to the TAD (transactivation of transcriptional repressors) domain (Le Gall and Giniger, 2004). At the C-terminal end of the Notch receptor is the conserved PEST domain (proline/glutamic acid/serine/threonine-rich motifs), which regulates the stability of NICD and is thought to be involved in downregulation of the signal through ubiquitination (Li et al., 2001). *Drosophila* Notch has a glutamine-rich domain next to its PEST domain.

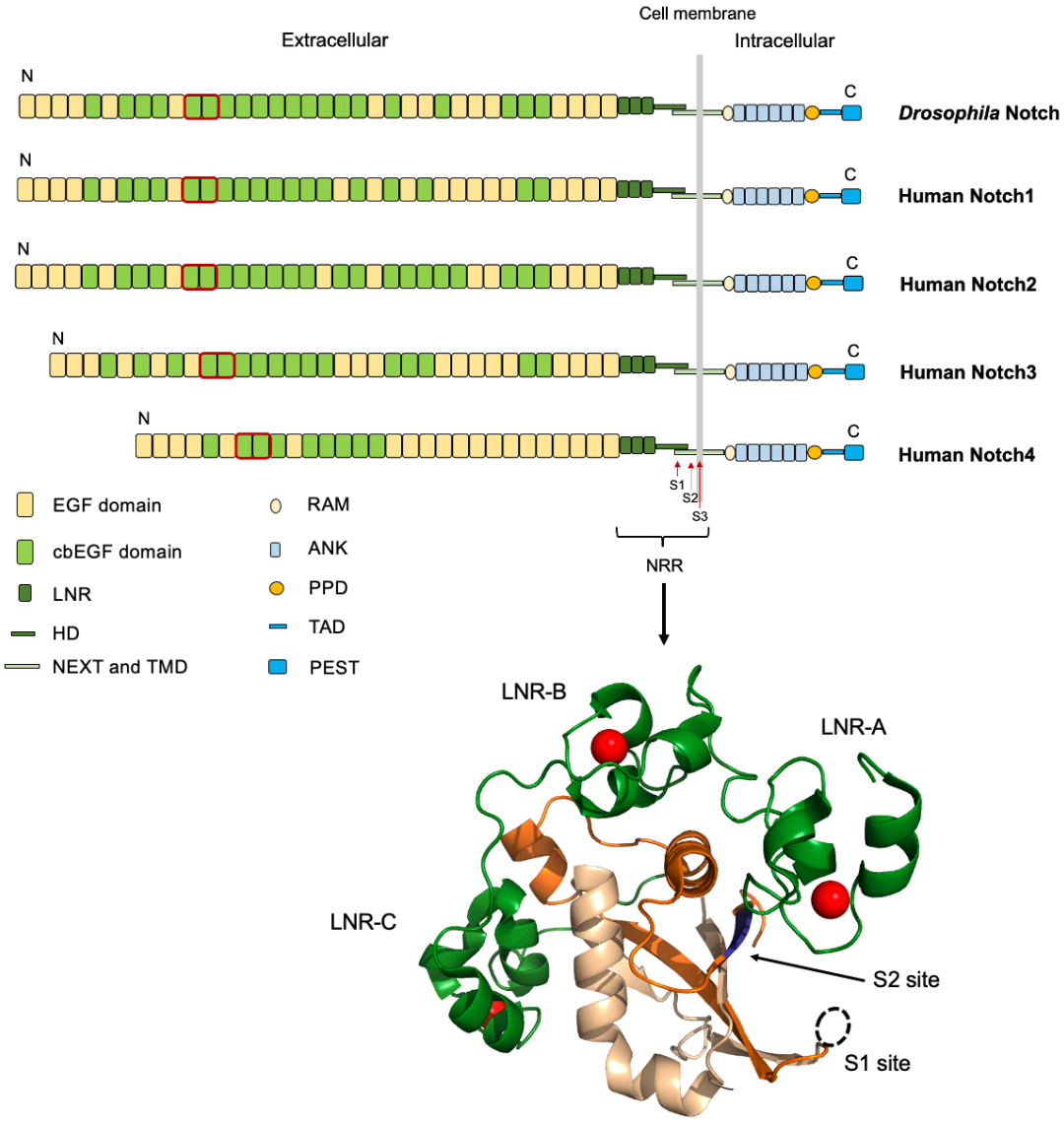


Figure 1-5. Domain organization of Notch receptors

Notch receptors are large type I single pass membrane proteins. The orientation of the receptors relative to the cell membrane is shown, with the extracellular region on the left. The NECD contains multiple extracellular EGF-like repeats, and the number of EGF repeats are the same in *Drosophila* Notch, human Notch1 and Notch2. Some EGF domains bind Ca^{2+} (green), and some do not (yellow). The ligand binding EGF domains are outline in red rectangles. The NRR region structure consists of LNRs (green) and a HD (the N-terminal HD in wheat, C-terminal HD in orange) is shown below. Calcium ions binding to LNR domains are shown as red spheres. The S2 cleavage site on the NRR structure is indicated in dark blue, and S1 site in dashed line. The HD bind to the NEXT through non-covalent interactions.

1.4.3 Post-translational modifications of Notch receptor

1.4.3.1 O-Glycosylation

There is a wide variety of modulators that can affect the Notch signalling pathway at different levels of the transduction cascade. O-Glycosylation in particular has raised a large amount of interest in recent years. In general, glycosylation can affect the signalling pathway by altering protein conformation or by modifying the recognition sites of proteins and the strength of intermolecular interactions. The EGF domains of the Notch receptor contain consensus sites for different types of O-glycan modifications that are added in the ER (Figure 1-6). Initially, glycosyltransferases add O-glycans to EGF domains by transferring fucose from GDP-fucose (POFUT1), glucose from UDP-glucose (POGLUT1) and GlcNAc from UDP-GlcNAc (EGOT1) to a serine or threonine residue (Table 1-4). Afterwards, each glycan may subsequently be elongated by the addition of one to three sugar molecules. The importance of glycosylation on Notch signalling was first identified in a study of a glycosyltransferase, Fringe, and its role in *Drosophila* wing development (Panin et al., 1997).

Before Notch is modified by Fringe, an O-fucose monosaccharide, is added by O-fucosyltransferase1 (OFUT1 in *Drosophila*, POFUT1 in human) in the ER. The OFUT1/POFUT1 enzymes in the ER have been well-studied (Figure 1-6) (Table 1-4). The transfer of fucose is most efficient when added to properly folded EGF domains (Moloney et al., 2000a). Notch receptors have several O-fucose modification consensus sites, C2-X-X-G-G-(S/T)-C3, and all of them are efficiently modified (Harvey et al., 2016) (Kakuda and Haltiwanger, 2017). Loss of O-fucosyltransferase1 in both *Drosophila* and mouse leads to Notch-null phenotypes suggesting that it is a core component required for activity associated with Fringe-dependent and Fringe-

independent processes (Okajima and Irvine, 2002) (Shi and Stanley, 2003). Moreover, aberrant Notch signalling due to POFUT1 defects affects several developmental processes such as haematopoiesis and angiogenesis (Yao et al., 2011) (Wang et al., 2017). In humans, mutations in *POFUT1* have been found in both Dowling-Degos disease and recessive limb-girdle muscular dystrophy (Duchatelet et al., 2018) (Servián-Morilla et al., 2016).

These phenotypes were initially partially explained by the fact that modifications by OFUT1/POFUT1 at the NECD affect Notch binding ability, which contributes to low levels of Delta1 and Jagged1 induced Notch signalling (Okajima et al., 2003) (Stahl et al., 2008). Co-crystals of Notch1 ligand-binding (EGF11 to EGF13) with a DLL4 fragment (from C2 to EGF2) identified precisely how O-fucose modification of domain EGF12 interacts with the C2 domain of DLL4 (Luca et al., 2015). Subsequently, co-crystals of Notch1 (EGF8 to EGF12) with Jagged1 (from C2 to EGF3) showed that it was not only O-fucose at EGF12 of Notch1 that could interact with the C2 domain of Jagged1, but also O-fucose at Notch1 EGF8 could interact with Jagged1 domain EGF3 (Luca et al., 2017). Moreover, OFUT1 has been identified as a Notch chaperone facilitating the folding and secretion of Notch on the cell surface in *Drosophila* (Okajima et al., 2008). However, whether POFUT1 acts as a chaperone in mammals is yet to be determined as both stable cell surface expression and ER accumulation of Notch receptors have been observed in POFUT1 deficient mammalian cells (Stahl et al., 2008) (Okamura and Saga, 2008).

The O-fucose modification on Notch can be further elongated to form a disaccharide, trisaccharide or tetrasaccharide (Figure 1-6). Fringe is an N-acetylglucosaminyl

(GlcNAc) transferase that is responsible for transferring GlcNAc onto fucose-O-EGF in a β1,3 bond (O-fucose monosaccharide elongation process), and it is the second step in the synthesis of the O-fucose tetrasaccharide on EGF domains (Moloney et al., 2000a) (Figure 1-6) (Table 1-4). Only a subset of the Notch signalling pathway processes are regulated by Fringe, and these Fringe-dependent processes mostly belong to inductive signalling procedures. In *Drosophila*, the function of Fringe in wing development has been well-studied. The effects of Fringe localise to a stripe of Notch activation along the border between the dorsal and ventral cells in wing imaginal disk. At these sites, Fringe plays roles in patterning, outgrowth and compartmentalization of wing formation (Irvine and Wieschaus, 1994). Recently, it was found that Fringe is important for lateral inhibition in flies. Fringe modification of EGF12 is vital for Delta-mediated lateral inhibition, while Fringe modifications of EGF8 and EGF12 work together to prevent Serrate lateral inhibition (Pandey et al., 2019). In mammals, Fringe can affect several developmental processes such as T-cell commitment (Koch et al., 2001), forebrain (Zeltser et al., 2001) and limb (Rodriguez-Esteban et al., 1997) development. Although Notch ligands have O-fucosylation sites as well, there is no evidence so far that Fringe regulates the function of Notch ligands.

In contrast to the single Fringe isoform found in *Drosophila*, 3 homologues are found in mammals: Lunatic Fringe (*Lfng*), Manic Fringe (*Mfng*) and Radical Fringe (*Rfng*) (Table 1-4). In *Drosophila*, Fringe can positively regulate Notch signalling activated by Delta and negatively regulate the signal activated by Serrate (Fleming et al., 1997) (Xu et al., 2007). However, the molecular mechanisms of Fringe in mammals are more complex with the increased number of Fringe homologues, Notch ligands and receptors. It has been showed that Lunatic and Manic Fringe in mammals inhibit

Jagged1-induced Notch1 signalling while promoting DLL1 activation of Notch1 (Table 1-3). Radical Fringe enhances Notch1 activation by both Jagged1 and DLL1 (Kakuda and Haltiwanger, 2017) (Table 1-3). Common to all of these processes is that Fringe can regulate different glycosylation forms of Notch receptors by changing the distribution of glycosyltransferases, which will alter Notch signalling regulation in cells (Haines and Irvine, 2003). As there are a number of consensus O-fucosylation sites throughout the Notch extracellular domain, different numbers and profile of O-fucose glycans on Notch may be another potential mechanism of regulating developmental processes temporally and spatially (Harvey et al., 2016). *In vivo* and *in vitro* experiments have shown that *Drosophila* Notch lacking the GlcNAc added by Fringe showed a deficiency in ligand binding (Panin et al., 1997) (Xu et al., 2007) (Table 1-3). Consistent with the *Drosophila* data, Fringe-mediated elongation of O-fucose enhances Notch binding to limited fragments of mammalian ligands Jagged1 and DLL1 but not DLL4 (Taylor et al., 2014).

In addition to O-fucose, other post-translational modifications such as O-glucose, O-GlcNAc and N-glycans have also been found on Notch receptors (Figure 1-6) (Table 1-4). O-glucose sites in Notch, with the consensus sequence of C1-X-S-X-P/A-C2, are highly conserved across species (Moloney et al., 2000b). Mass spectrometric analysis of *Drosophila* Notch NECD showed the presence of O-glucose on all predicted sites (Harvey et al., 2016). O-glucosyltransferase is widely distributed in different tissues and species suggesting that O-glucosylation might have a general role in Notch signalling. O-glucosylation sites are modified by O-glucosyltransferase1 (Rumi in *Drosophila* and POGLUT1 in mammals) and are elongated by GXYLT1, GXYLT2 and XXYL1 (Figure 1-6) (Acar et al., 2008) (MK et al., 2009) (Sethi et al., 2012)

(Fernandez-Valdivia et al., 2011). Studies in *Drosophila* showed that O-glucosylation played a role in Notch trafficking and folding, and *rumi* mutations in flies lead to a temperature-dependent Notch signalling deficiency (Acar et al., 2008) (Matsumoto et al., 2016). In mammalian cells, studies on Notch1 showed that most of O-glucose sites are elongated to the trisaccharide, Xyl-Xyl-Glc. Without the O-glucose at most of the individual sites, little or no Notch activation was observed (Rana et al., 2011). Unlike O-fucose, which has a duel role in ligand binding, O-glucose is essential for ligand-induced cleavage of Notch, potentially by changing the conformation of Notch (Ma et al., 2011). Crystal structures of Notch1 with DLL4 further found that O-glycans are also engaged in mediating ligand binding (Luca et al., 2015). More recently, studies on Notch1 indicate that an O-glycan site at EGF11 in combination with O-fucosylation site (either at EGF8 or EGF12) affects Notch1 activity and cell-surface presentation (Takeuchi et al., 2018). These results suggest that the O-glucose modifications on the Notch receptor are important for Notch signalling regulation, and O-fucosylation and O-glucosylation have different roles in modulating Notch signalling.

The third type of conserved glycosylation found on EGF domains of Notch is O-GlcNAcylation, which is mediated by O-GlcNAc transferase (EOGT in *Drosophila* and EOGT1 in mammals) (Sakaidani et al., 2011) (Sakaidani et al., 2012) (Figure 1-6) (Table 1-4). The consensus sequence for O-GlcNAc is C5-X-X-G-X-(T/S)-G-X-X-C6. Less than one third of these consensus sites are modified by O-GlcNAc in purified *Drosophila* Notch (Harvey et al., 2016). In flies, EOGT deficiency does not show a Notch typical phenotype, however the wing blister phenotypes may be contributed to by O-GlcNAc modification of Notch (Sakaidani et al., 2011) (Müller et al., 2013). In mammals, EOGT deficiency reduces the binding ability of Notch1 to DLL1 and DLL4,

but not Jagged1. Loss of EOGT also has an impact on angiogenesis due to the suppression of Delta-initiated Notch signalling (Sawaguchi et al., 2017). EOGT1 mutations in humans are linked to Adams-Oliver syndrome (section 1.2.2.3) and cause impaired O-GLcNAc modifications at EGF domains as a result of decreased O-GlcNAc transferase activity (Shaheen et al., 2013) (Ogawa et al., 2015). However, the major functions of O-GlcNAc modification of Notch remains largely unknown.

Multiple N-linked glycosylation sites, of the consensus N-X-(T/S), are known to exist in the Notch sequence, and some are known to be modified. Despite the modification of these sites by N-glycans, however, no change in Notch signalling was observed in a study using CHO cells with defects in glycosylation (Moloney et al., 2000a) (Chen et al., 2001).

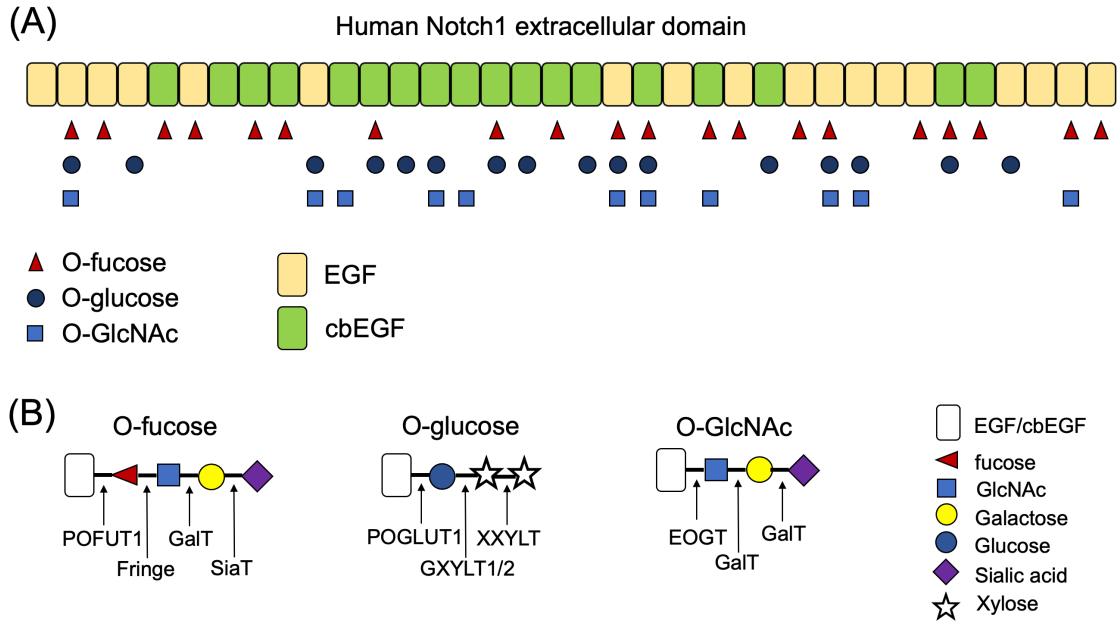


Figure 1-6. Human Notch1 with predicted glycosylation consensus sequences

(A) Representation of EGF domains with consensus sequences for glycosylation in human Notch1 are indicated. Potential sites for O-fucosylation are labelled with red triangle, O-glucosylation with dark blue circle, O-GlcNAc with blue square. “N” stands for N-terminus, and “C” for C-terminus of human Notch1. (B) The schematic diagrams of O-linked glycans on human Notch receptors. Sugar symbols are labelled according to Consortium for Functional Glycomics guidelines, and the glycosyltransferases responsible for the transfer of each sugar are shown below each schematic structure. The solid black line indicates the linkage in the O-glycan structure.

Glycosytransferases of Notch receptors		Function	Donor substrate
Drosophila	**Mammals**		
OFUT1	POFUT1	O-fucosyltransferase	GDP-fucose
Fringe	LFng, MFng, RFng	N-acetyglucosaminyl transferase	UDP-GlcNAc
Rumi	POGLUT1	O-glucosyltransferase	UDP-Glc, UDP-Xyl
EOGT	EGOT1	O-GlcNAc transferase	UDP-GlcNAc

Table 1-4. A summary of Glycosyltransferases modifying the Notch receptor

1.4.3.2 Ubiquitinylation of Notch receptors

E3 ubiquitin ligases that act on the Notch receptor have been identified in mammals include Fbw-7 (SEL-10 in *C.elegans* and Archipelago in *Drosophila*), Itch/AIP4 (Su(dx) in *Drosophila*), Nedd4 and Deltex1 (Moretti and Brou, 2013). The first ubiquitinylation event to be identified in the Notch pathway is mediated by a E3 ubiquitin ligase termed SEL-10, which regulates NICD stability and negatively regulates Notch signalling in *C. elegans* (Hubbard et al., 1997). The regulation of NICD by ubiquitination is vital for function since reduced abnormal ubiquitinylation leads to a prolonged signal and can cause severe disease such as T-ALL (mutations at ubiquitinylation domain, PEST, see section 1.2.2.1 and section 1.4.3). Monoubiquitinylation is required before activated Notch (ADAM-cleaved Notch) is cleaved by γ-secretase in mammals (Gupta-Rossi et al., 2004). In addition to affecting NICD, ubiquitinylation can also regulate the quantity and quality of Notch at the cell surface to modulate Notch activation (McGill et al., 2009). As Notch has a limited half-life at cell surface, non-activated Notch will be ubiquitinylated by E3 ligase in order to be degraded by Itch/AIP4 E3 ligase in mammals (Chastagner et al., 2008) (Moretti and Brou, 2013).

1.4.4 Post-translational modifications of Notch ligands

1.4.4.1 O-glycosylation of Notch ligands

In addition to Notch receptors, O-fucose modifications have also been found in the EGF repeats of Notch ligands, although there may be a wider range of consensus sites on the ligands than on the receptors. Compared to Notch receptors, glycosylation of Notch ligands is less well studied. Mammalian Jagged1 and DLL1 O-fucoses are substrates for Manic Fringe, while *Drosophila* Serrate and Delta can be elongated by *Drosophila* Fringe (Panin et al., 2002). DLL3 was the first example where it was shown

that O-fucosylation is necessary for its physiological functions *in vivo*. The O-fucose on DLL3 is elongated by Lunatic Fringe, and O-fucosylation-deficient mice showed abnormal embryonic somitogenesis (Serth et al., 2015). However, the lack of O-fucose on mDLL1 showed no impact on Notch activation *in vitro*, although DLL1 variants with O-fucose mutations showed some intracellular accumulation (Müller et al., 2014). In addition to O-fucose, Delta and Serrate are substrates of EOGT for O-GlcNAc modification, although the function of this still need to be investigated (Müller et al., 2013). More recently, in humans, modifications that impair O-linked glycosylation in Jagged1 EGF domains have been identified in autosomal dominant peripheral nerve disease (Sullivan et al., 2020). There are also N-linked glycan consensus sequences throughout the Notch ligand extracellular domains, however, the functions of these are still unknown.

1.4.4.2 Ubiquitinylation modifications of Notch ligands

Modification of Notch ligands (intracellular domains) by ubiquitylation regulates their expression levels and activities. Ubiquitinylation is mediated by two families of RING (Really Interesting New Gene) E3 ubiquitin ligases: Neuralized (Neur) and Mind bomb (Mib). Although these E3 ligase families are evolutionarily conserved with gene duplication, the two families share no similarities in either structure or domain architecture, and they have distinct developmental functions (Le Borgne et al., 2005). In mammals, there are four E3 ligases (Mib1, Mib2, Neur1 and Neur2), and Mib1 has a primary role in Notch ligand ubiquitination rather than other E3 ligases (Yoon et al., 2007). The RING domain at C-terminus of Mib1 could recognise ankyrin repeats in Notch ligands and conjugate to E2~ubiquitin (Guo et al., 2016). As mentioned

previously (section 1.3.2), endocytosis mediated by ubiquitination of ligands plays a vital role in Notch activation.

1.5 C2 domain

1.5.1 General introduction

Although domain organisation of Notch receptors and ligands is mostly well understood, an unexpected finding that the N-terminal domain of DSL ligands was a lipid binding module has prompted interest in its functional role. Lipid-mediated targeting through lipid-binding domains is important for cellular signalling, membrane trafficking and fusion events. To date, more than ten lipid binding domain types have been identified including the C1, C2, PH and PX (Stahelin, 2009). C2 domains are the second most common membrane binding domains behind PH domains and occur most widely in intracellular proteins involved in membrane targeting and vesicle trafficking such as synaptotagmins and Munc 13 (Corbalan-Garcia and Gómez-Fernández, 2014). They share a common structure: two sets of four stranded antiparallel β-sheets forming a β-sandwich hydrophobic core with various loops on the top and bottom (Figure 1-7) (Figure 1-8). Unlike other lipid-binding domains, such as C1 and PH, C2 domains have neither a well-defined lipid-binding pocket nor a conserved cationic patch for lipid binding specificity (Cho and Stahelin, 2006). Biophysical and biochemistry studies have shown that the C2 domain selectively binds to different lipids by two separate binding sites, the cationic β-groove and the apical loops with disparate Ca^{2+} sensitivities, neither of which is conserved in terms of amino acid sequence and tertiary structures (Cho and Stahelin, 2006).

Most of C2 domains have a cationic groove (also called a cationic β-groove or polybasic cluster) in the concave position of the β sandwich, which can have different sizes and electrostatic potentials. Several aromatic and cationic residues in this β groove have been found to be conserved in most of C2 domains and to contribute to the electrostatic potential of the C2 domain (Guerrero-Valero et al., 2009) (Figure 1-8). Some C2 domains bind Ca^{2+}, coordinated by aspartic acid residues in 3 loops, located in the apical region (also referred as CBR1-3), and some, such as the C2 domains of novel PKCs, have lost these Ca^{2+} binding residues but are still able to bind to lipids (Zhang and Aravind, 2010) (Figure 1-8). In general, the lipid selectivity is determined by a combination of different electrostatic and hydrophobic interactions. Moreover, the variation in residues located at the top of the loops allows selectivity and specificity for different phospholipids (Corbalan-Garcia and Gómez-Fernández, 2014). The lipid preference of a C2 domain may govern its subcellular location, such as PC-preferring C2 domain of cPLA2 $cPLA_{2}\alpha$, which moves from the cytoplasm to the PC-enriched perinuclear region in response to Ca^{2+} (Stahelin et al., 2003).

C2 domains have been divided into two families according to the different connectivities of the β strands: the type I topology, also termed as the synaptotagmin-like variants or S-family, and the type II topology, also termed as or the PLC-like variants or P-family (Figure 1-7) (Figure 1-8) (Corbalan-Garcia and Gómez-Fernández, 2014). However, this classification does not provide information on functional or regulatory characteristics. Proteins with C2 domains are considered to be peripheral membrane proteins, being either membrane docking forms of soluble proteins (like PKCs) or integral membrane proteins (like synaptotagmins) (Corbalan-Garcia and Gómez-Fernández, 2014). Some proteins contain multiple C2 domains, which may

increase the membrane affinity through additive effect (Earles et al., 2001). Interestingly, glycosylation of C2 domains may also affect their physiological functions. A highly conserved N-glycan in the C2 domain of an HIV-1 envelope protein was shown to play an important role in co-receptor binding (Lombardi et al., 2015). To date, C2 domains have been found that are capable of binding multiple targets, including lipids and proteins, which has raised interest in its molecular scaffold function in facilitating signal transduction and vesicle trafficking.

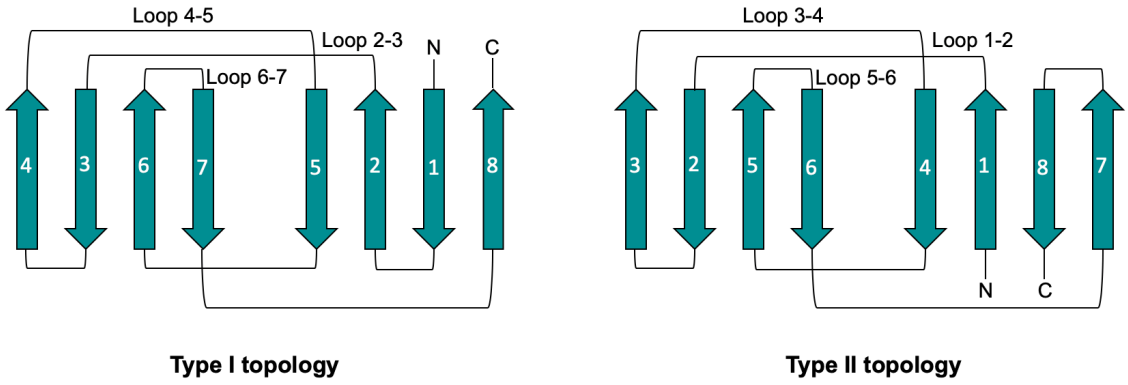


Figure 1-7. Configuration of β strands in type I and type II C2 domain

Diagram of the topography of β strands in two types of C2 domains. β strands are shown as teal arrows and loops as black lines. The N- and C- termini are on the bottom of the type II C2 domain, whereas they are on the top in the type I. Although the localization of the loops within the three-dimensional structure is same in two types of C2 domains, the connectivity of the β strands by these loops is different. Notch ligands exhibit type II topology.

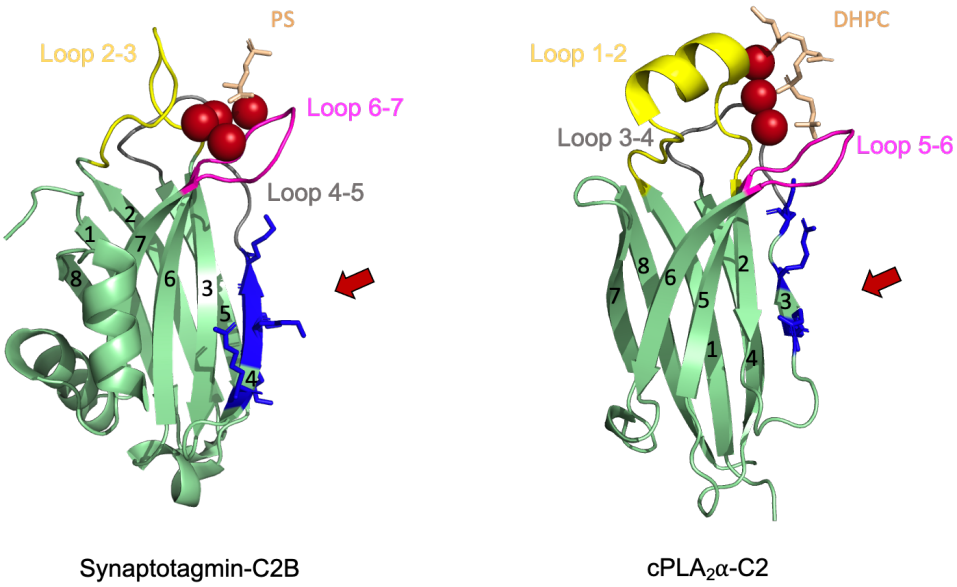


Figure 1-8. Representative structures of C2 domains

Structures of Synaptotagmin1-C2B (PDB: 2YOA) and cPLA2α-C2 (PDB: 6IEJ) containing lipid (wheat) and calcium (red) are shown. CBR1 (loop 2-3 in type I and loop 1-2 in type II C2 domain) are shown as yellow, CBR2 (loop 4-5 in type I and loop 3-4 in type II C2 domain) are coloured in grey, CBR3 (loop 6-7 in type I and loop 5-6 in type II C2 domain) are in magenta. Cationic residues on the β-groove are labelled in blue and stick models. Position of β-groove is shown by red arrows. PS = phosphatidylserine, DHPC = 1,2-diheptanoyl-sn-glycero-3-phosphocholine.

1.5.2 Calcium ion binding by C2 domains

C2 domains are the second most abundant Ca^{2+} binding domain type in the human genome and Ca^{2+} has been shown to have three major roles in the C2 domain function. Firstly, Ca^{2+} binding changes the electrostatic potential of the domain and influence its lipid binding preference (Shao et al., 1997). Most Ca^{2+}-dependent C2 domains contain positively charged residues in the Ca^{2+} binding loops and prefer negatively charged and zwitterionic lipids. Some bind to lipids through electrostatic interactions without selectivity, such as synaptotagmin C2A domain (Davletov and Sudhof, 1993). Secondly, the electrostatic neutralization of Ca^{2+} acts as a bridge between the C2 domain and lipid head groups since oxygen groups of the phospholipid serve to

complete the calcium coordination sphere. For example, in the crystal structure of the PKCα C2 domain, Ca^{2+} functions as a bridge connecting the C2 domain and phosphatidylserine, which is important for phosphatidylserine recognition (Verdaguer et al., 1999). Recently, the X-ray crystal structure of the $cPLA_2\alpha$ C2 domain with lipid showed Ca^{2+} is located at the interface between the C2 domain and the DHPC (1,2-diheptanoyl-sn-glycero-3-phosphocholine) phosphate group and plays a key role in lipid preference and selection (Hirano et al., 2019) (Figure 1-8). Thirdly, Ca^{2+} ions can affect the conformation of C2 domains so that they can stereospecifically recognize a lipid headgroup after binding Ca^{2+} ions. In PKCα, Ca^{2+} binding to the C2 domain produces subtle rearrangements of side chains that contribute to the sterospecific binding of PKCα to phosphatidylserine (Verdaguer et al., 1999).

C2 domains show widely different Ca^{2+} affinities, but little is known about the molecular mechanisms underlying these differences. Structures of C2 domains that do not contains Ca^{2+} binding sites, suggest that these conformations are incompatible with Ca^{2+} chelation due to distances between the loops that are either too wide or too narrow (Garcia et al., 2004). In some cases, binding of lipid to the C2 domain has been found to increase Ca^{2+} binding of the C2 domain. For example, binding of lipid to Synaptotagmin-1-C2 domain dramatically increases the C2 domain Ca^{2+} binding capacity to phosphatidylinositol4,5-bisphosphate (PIP2) by around 40-fold (Bogaart et al., 2012). Characterization of the differences between Ca^{2+}-bound and Ca^{2+}-free C2 domains is important for studying Ca^{2+} regulation in the C2 domain.

Due to the presence of calcium-binding sites, C2 domains have been postulated as calcium sensors in the cell. For example, the translocation of PKCα from the cytoplasm

to the plasma membrane is triggered by Ca^{2+} signals affecting the PKCα C2 domain under physiological conditions (Evans et al., 2006). In Munc13, the C2 domain acts as a Ca^{2+}-dependent modulator of synaptic plasticity by interacting with phosphatidylinositol and PIP2 (Shin et al., 2010). Another example is cPLA$_{2}\alpha$, in which Ca^{2+} occupation at the cPLA$_{2}\alpha$ C2 domain, controlled by intracellular Ca^{2+} concentration, neutralizes Asp residues and induces cPLA$_{2}\alpha$ translocation and penetration into the membrane interface in the perinuclear region (Hirano et al., 2019).

Binding of Ca^{2+} to C2 domains also affects protein stability. In perforin, an extracellular C2 domain protein, Ca^{2+} binding to the C2 domain has a vital role in its proteostasis which is necessary for perforin folding and trafficking (Brennan et al., 2018). It also plays a critical role in its cytotoxic function after it is secreted (Moreno et al., 2009).

1.5.3 C2 domains in Notch ligands

The extreme N-terminal, C2 domain of Notch ligands, is conserved in all mammalian species and is involved in the modulation of Notch signalling (Chillakuri et al., 2013) (Luca et al., 2015) (Suckling et al., 2017) (Luca et al., 2017). The C2 domain of Notch ligands has both phospholipid and receptor binding abilities (Figure 1-9) (Figure 1-10) and has strong structural homology to the Munc13 C2B domain (Chillakuri et al., 2013) (Luca et al., 2015) (Suckling et al., 2017) (Luca et al., 2017). All of them have a type II topology that is most similar to the PKC-C2 family (Figure 1-7). In mammals, Jagged family C2 domains bind Ca^{2+} (one Ca^{2+} in Jagged1 C2 and three Ca^{2+} in Jagged2), whilst the Delta-like family do not (Figure 1-11). In all of these C2 domains, the apical loop regions, regardless of whether they bind Ca^{2+} or not, have several hydrophobic

residues. However, these hydrophobic residues are not located at the tips of those loops, suggesting that these C2 domains are not deeply buried in the cell membrane (Suckling et al., 2017).

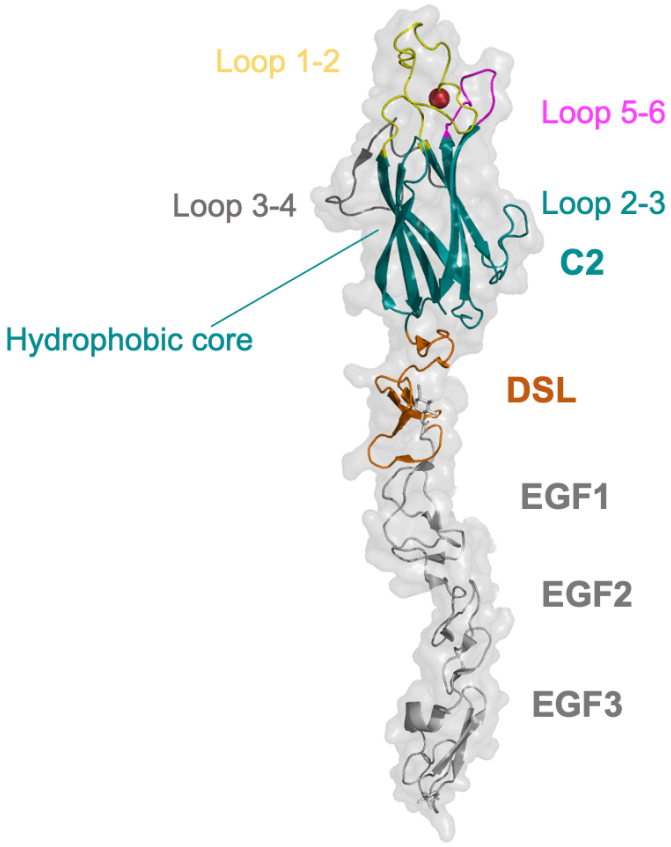


Figure 1-9. Structure of human Jagged1 N-terminus to EGF3 (J-1$_{N\text{-}EGF3}$)

The structure of J-1N-EGF3 (PDB: 4CBZ) is shown in ribbon representation, and C2 domains are coloured in teal, DSL domains in orange, EGF domains in grey. The calcium ion is drawn as a red sphere. The position of hydrophobic core of C2 domain is indicated by a teal arrow. Loop 1-2 is shown as yellow, loop 3-4 is coloured in grey and loop 5-6 is in magenta.

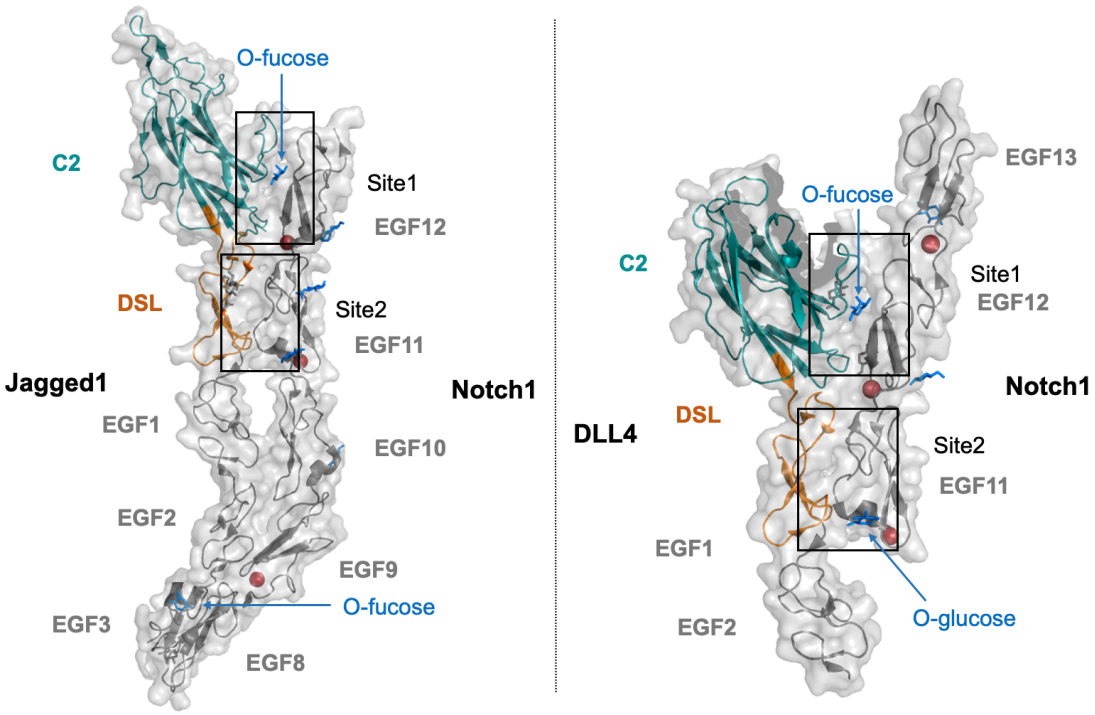


Figure 1-10. Notch receptor and ligand structure complexes

PyMOL model of Jagged1 interacting with Notch1 (PDB code: 5UK5) and DLL4 interacting with Notch1 (PDB code: 4XL1). C2 domains are coloured in teal, DSL domains in orange and EGF domains in grey. Two interacting regions, site1 and site2, in each complex are outlined in black boxes. Site1 indicates C2-EGF12 contacts and site2 is the DSL-EGF11 interacting site in each complex. All O-glycans on the Notch receptors are coloured in blue, and two glycans indicated by blue arrows in each complex engage in ligand-receptor contacts. All Ca^{2+} on Notch receptors are labelled as red spheres.

The role of the C2 domain in binding to the Notch receptor has been shown by the structure of the receptor-ligand complex. In Notch1-Jagged1 and Notch1-DLL4 complex structures, the long loop between β strands 2 and 3 of the ligand C2 domains binds to EGF12 of Notch1 (binding site 1) (Figure 1-9) (Figure 1-10) (Taylor et al., 2014). Moreover, the O-fucose modification in EGF12, also interacts with the bottom of the C2 domain of the Notch ligands directly (Figure 1-10) (Luca et al., 2015) (Luca et al., 2017). DLL4 has been shown by a domain-swapping strategy to have a stronger affinity than DLL1 for Notch due to this bottom loop (loop 2-3) of the C2 domain (Figure 1-9) (Figure 1-10) (Hirano et al., 2020). During the Notch binding process, Notch ligand

undergoes conformational changes at domain interfaces and such rearrangements are said to confer 'catch bond' properties to the interaction (Luca et al., 2017).

In addition to its Notch binding capacity, the lipid-binding property of the C2 domain has also been observed to regulate Notch signalling. *In vivo* experiments showed that glycosphingolipids, components of lipid rafts, are essential in Notch signalling in both *Drosopila* and *C.elegans* (Katic et al., 2005) (Hamel et al., 2010). Data from *in vitro* assays showed that the C2 domains of all canonical Notch ligands, except DLL3, bind lipids in a calcium-dependent manner. In addition, point mutations causing amino acid substitutions in the apical loops of the ligand C2 domains have been found to reduce Notch signalling without changing the binding ability of ligands to Notch (Chillakuri et al., 2013). These data indicate that the lipid binding ability plays an important role in modulating Notch signalling. The 3 connecting loops at the top of the C2 domains (loops between β strands 1-2, loops between β strands 3-4 and loops between β strands 5-6) (Figure 1-9) are highly variable in both length and conformation among Notch ligands, suggesting functional diversity. It is possible that this is linked to different lipid binding preferences and physiological roles of the domains. As the ligand C2 domain has both receptor and lipid binding properties, a ternary complex of Notch receptor, ligand and lipid (cell membrane) may have an important role in Notch signalling modulation (Figure 1-12).

A number of disease-associated mutations have been found in the C2 domains of Notch ligands, including mutations linked to Alagille syndrome and extrahepatic biliary atresia (section 1.2.2.2). Mutations associated with Alagille syndrome that affect the Jagged1 C2 domain alter residues in the hydrophobic core of the domain (β-sheet

strands) and lead to domain misfolding. This misfolding lead to a functional haploinsufficiency of Jagged1 on cell surface (Penton et al., 2012). Three mutations affecting the loop structures of C2 domains have been found to associate with extrahepatic biliary atresia. These variants appear to fold normally and alter Notch activation without changing the binding capacity of Notch ligands. *In vitro* assays showed that these variants have a reduced capacity for lipid binding and ternary complex formation suggesting that the lipid binding capacity of C2 domains has an impact on bile duct development (Chillakuri et al., 2013). However, a more detailed understanding of the C2 domain structure-function paradigm in Notch signalling and the role of lipid binding is required.

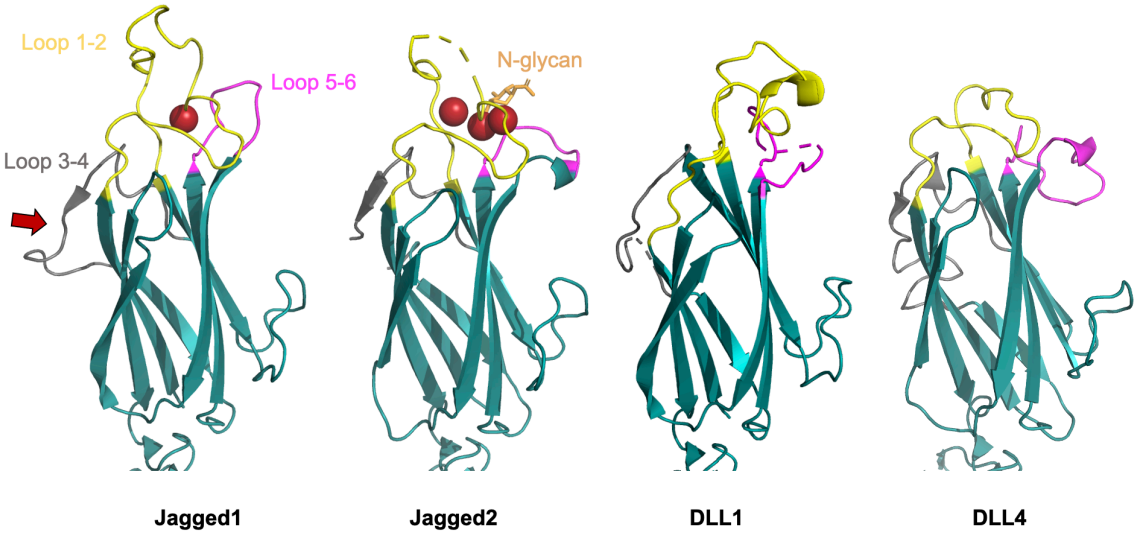


Figure 1-11. Comparison of C2 domains in different Notch ligands

The loops between β strands 1 and 2 (yellow), between 3 and 4 (grey) and between 5 and 6 (purple) of Notch ligand C2 domains differ in length and conformation (Jagged1 PDB code: 4CBZ, Jagged2 PDB code: 5MW5, DLL1 PDB code: 4XBM, DLL4 PDB code: 5MVX). The Jagged1 and Jagged2 C2 domains bind Ca^{2+} (red), whereas Delta family ligands do not. The potential position of the cationic β-groove identified in other C2 domains is shown by a red arrow. An N-glycan on the loop 5-6 of Jagged2 C2 domain is shown in orange. All of these differences at the C2 domain apex may affect Notch ligand lipid-binding preferences.

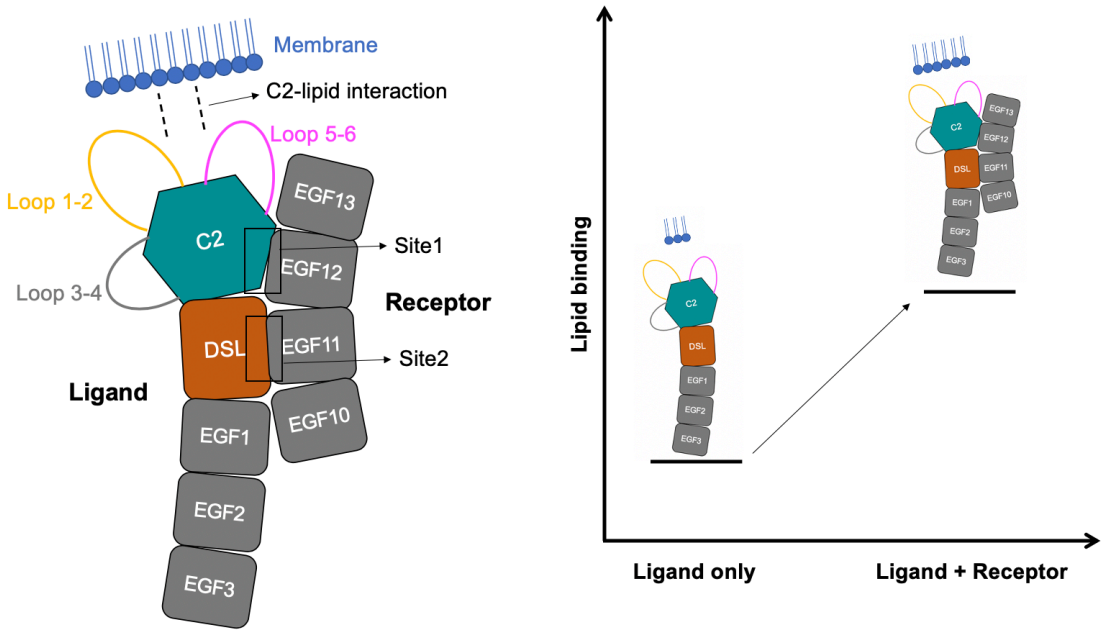


Figure 1-12. Cartoon picture of Notch signalling ternary complex

The proposed ternary complex (left) consists of Notch receptor, ligand and cell membrane (blue). The C2 domain is coloured in teal, DSL in orange and EGF domains in grey. The two receptor-ligand binding sites are labelled by black boxes and can be seen in detail in Figure 1-8. The loops on the apex of the C2 domain are labelled in different colours, and this project mainly focuses on loop 1-2 (yellow) and loop 5-6 (purple) which are implicated in C2 lipid binding. The ternary complex was proposed after it was observed that ligand binding to Notch enhances binding to lipids *in vitro* (show on the right).

1.6 Project Aims

The core Notch-transduction pathway is well understood, however, the mechanisms that regulate the formation of the extracellular receptor-ligand complex under different conditions are still not fully understood. It is still unclear how Notch/ ligand/ membrane interactions, particularly these conferred by the C2 domain, modulate the Notch signalling pathway due to the scarcity of disease mutations or *in vivo* studies using model organisms.

The aims of this thesis are therefore:

1. To select relevant Jagged1 C2 mutations from the COSMIC cancer database to examine whether or not these mutants affect Notch activation using reporter assays.
2. For those COSMIC mutations that cause changes in activity, investigate the molecular mechanisms underlying these changes using Notch and lipid binding assays.
3. To examine the C2 domain of DLL4, using a similar approach, and compare its properties with the Jagged1 C2 domain.

Chapter 2. Materials and methods

2.1. Mutagenesis

2.1.1. Primer sequences

Oligonucleotide primers for mutagenesis and sequencing were ordered from Thermo Fisher Scientific. Annealing temperature (T_m) of primers were designed around 60 °C. Primers were dissolved in MilliQ water at a 60 μM concentration. T_m of each primer was calculated according to the following formula:

$$T_m\ (°C) = 4 \times (\mathrm{G}\ + \mathrm{C}) + \ 2 \times (\mathrm{A}\ + \mathrm{T})$$

Primers used in this project are listed in the Appendix.

2.1.2. Site-directed mutagenesis using overlap extension PCR

Human Jagged1$_{\text{N-EGF3-Fc-His6}}$ (residues 1 to 335) was expressed from plasmid pHL-sec while human DLL4$_{\text{N-EGF3-Fc-His6}}$ (residues 1 to 325) was expressed from the plasmid pcDNA-3.1(+). Overlap extension PCR was used to generate Jagged1$_{\text{N-EGF3}}$ and DLL4$_{\text{N-EGF3}}$ plasmids with the desired mutations. This mutagenesis method involves two rounds of PCR, the first of which consists of two reactions to create the left arm and right arm products (Figure 2-1). These two reactions each utilise a backbone primer in combination with a mutagenesis primer that contains a mismatch corresponding to the desired substitution (Figure 2-1). After visualizing PCR products on an agarose gel, gel extraction of desired size products was performed and followed by a second round of PCR, which uses first round PCR products as templates to generate the final desired DNA sequence (Figure 2-1). All primers are listed in section 2.1.1.

2.1.3. PCR reactions

All PCR reactions in this project were performed using the KOD Hot-Start Polymerase kit (Merck), following the manufacturer's suggested protocol in a 50 μL reaction volume. The reactions contained 5 μL of 10 × KOD Buffer, 3 μL of 25 mM $MgSO_4$, 5 μL of 2 mM dNTPs, 1.5 μL of 10 μM forward primer, 1.5 μL of 10 μM reverse primer, 20 ng of template DNA, 1 μL of KOD Hot Start DNA Polymerase (stock concentration: 1U/μL), and MilliQ water to make the reaction volume up to 50 μL.

The amplification programme included an initiation step at 95 °C for 2 minutes, followed by 30 cycles of: denaturation at 95 °C for 20 seconds, annealing at 55 °C for 10 seconds, elongation at 70 °C for an appropriate time proportional to the DNA length (20 seconds/1kb). Reactions were then kept at 4 °C if they were to be used imminently, or at -20 °C if they were to be stored for longer periods of time.

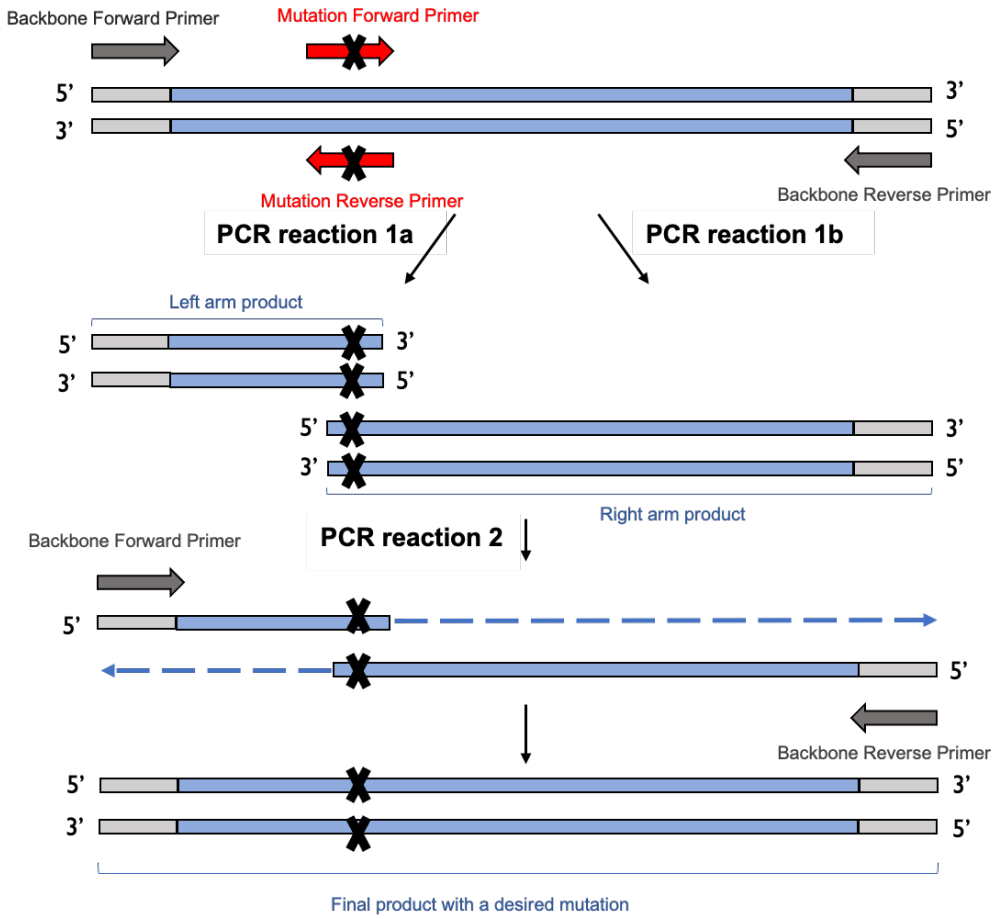


Figure 2-1. Site-directed mutagenesis using overlap extension PCR

All variants in this project were produced by site-directed mutagenesis using overlap extension PCR. The open reading frame is shown in blue, and DNA from the plasmid is shown in grey. Primers are indicated by arrows. "X" indicates the site of mutagenesis.

2.1.4. Restriction enzyme digestions

All enzymes and buffers for restriction enzyme digestions were supplied by New England Biolabs (NEB). Digestions were performed with 1 unit of restriction enzyme per 1 μg substrate DNA, at a final DNA concentration of 20 ng/μL. Restriction enzyme buffers were chosen as directed by the manufacturer to ensure optimal enzyme activity. The reaction was incubated at 37 °C for at least 1 hour (at least 0.5 hour for Time-saver qualified enzymes). For double digests with incompatible buffer requirements, single digests were performed sequentially, and PCR purification kit was used

between each digestion step to allow the buffer to be changed. DNA fragments were visualised on an agarose gel after each reaction.

2.1.5. DNA gel electrophoresis

Agarose gels ranging from 0.5% – 1.0% (w/v) were prepared with TBE buffer (90 mM Tris, 90 mM boric acid, 3.2 mM EDTA, pH 8.3), depending on the length of the DNA fragments being analysed. 3 μL of 10 mg/mL ethidium bromide (Sigma) was added to 50 mL agarose gel mixture for gel precasting. DNA samples were diluted with 1/6 volume of 6 × DNA loading dye (NEB) and run against 100 bp or 1kb DNA ladders (NEB). Electrophoresis was carried out at 80 volts for 1 hour in a DNA electrophoresis tank (Bio-Rad). Bands were visualized on a UV transilluminator (Uvitec) and photographed on a gel documentation system (Uvitec). For band excision, gels were visualized on a UV transilluminator, and bands were excised from the gel using a single edge razor blade. The DNA fragment was extracted from the agarose gel slice using a Gel Extraction kit (Qiagen).

2.1.6. DNA ligation

Ligation was performed on complementary sticky end DNA products using the Rapid DNA Ligation Kit (Roche) following the manufacturer's recommended protocol. The ratio of vector DNA to insert DNA ranged from 1:3 to1:6. The total volume of each reaction was 20 μL including 2 μL of 5 × DNA dilution buffer, 10 μL of 2 × ligase buffer and 1 μL of Rapid DNA ligase, and the final volume was adjusted using MilliQ water. The reaction mixture was left at room temperature for 30 minutes, and 5 μL of ligation mix was transformed into 50 μL of NEB5α competent cells (NEB).

2.1.7. Transformation

Plasmids for transformation were gently mixed with 50 μL NEB5α competent cells (NEB), and the mixture was incubated on ice for 30 minutes. After the incubation, competent cells were heat shocked at 42 °C for precisely 30 seconds followed by 5 minutes recovering on ice. 950 μL SOC Outgrowth Medium was added to the competent cell mixture, prior to incubation at 37 °C with shaking at 300 rpm for 30 minutes. 200 μL of the transformation mix was plated onto a 2 × YT agar plate containing appropriate antibiotic selection reagent (100 mg/mL ampicillin or 50 mg/mL kanamycin) and incubated at 37 °C overnight. A single colony was picked using a sterile pipette tip and resuspended by pipetting in 100 mL 2 × YT Broth medium containing 100 mg/mL ampicillin or 50 mg/mL kanamycin at 37 °C, 200 rpm overnight.

2.1.8. Isolation of plasmids and DNA sequencing

Miniprep or Midiprep plasmid extraction kits (Qiagen) were used to extract plasmids from *E. coli* for sequencing according to the manufacturer's suggested protocol. Plasmids were sequenced by Sanger sequencing service provided by Source Bioscience. Samples for DNA sequencing were diluted to a final concentration of 100 ng/mL in MilliQ H_2O in a final volume of 5 mL per sequencing sample. Sequencing traces were read using SnapGene® Viewer 5.2.5.

Plasmids with the correct sequence were transformed into DH5α competent cells for further plasmid expansion if needed. Midiprep or Maxiprep plasmids purification kits (Qiagen) were used to prepare DNA for large-scale transfections.

2.2. Protein purification

Jagged1 proteins were produced in human kidney embryonic 293T (HEK293T) cells (Aricescu et al., 2006), while DLL4 proteins were expressed by HEK293F (FreeStyle™) using a transient transfection system. Human Notch receptors were expressed by S2 stable cell lines. All tissue culture work was carried out in a laminar flow sterile hood.

2.2.1. HEK293T cell maintenance and protein expression

2.2.1.1. HEK293T cell maintenance

HEK293T cells were cultured in complete DMEM medium, consisting of Dulbecco's modified Eagle's Medium (DMEM, Gibco™) supplemented with 10% FBS (Gibco™), 50 U/mL penicillin and 0.05 mg/mL streptomycin (Sigma), and 2 mM L-glutamine (Gibco™), using 175 cm^2 tissue culture flasks (T175 flask, Greiner). They were maintained in a 37 °C humidified incubator with 5% CO_2 and split every 3 to 4 days. Each T175 flask of cells were washed with 10 mL sterile PBS and digested with 2 mL Trypsin (Gibco™) for 1 minute at 37 °C. 8 mL complete medium was added into the flask, and cells were resuspended by pipetting. The cell suspension was transferred into a sterile Falcon tube and centrifuged at 1000 rpm for 3 minutes. After aspirating the supernatant, HEK293T cells were resuspended and split into a new T175 flask containing 25 mL fresh complete medium at a 1:10 ratio.

2.2.1.2. Freeze and thaw HEK293T cells

For freezing, cells were trypsinized (section 2.2.1.1) and resuspend in FBS containing 10% (v/v) DMSO (Sigma). 1 mL cell suspension was aliquoted into each cryotube and put in to a cryofeezer (Corning®). The cryofreezer was kept at -80 °C overnight to freeze cell aliquots, and cryotubes were subsequently transferred into liquid nitrogen for longer term storage.

To thaw cells, cryotubes were taken out of liquid nitrogen storage and placed in a 37 °C water bath with gentle shaking. Immediately after cells had thawed, the cell suspension was transferred into a falcon tube containing 9 mL of complete medium for centrifuge at 1000 rpm for 3 minutes. The supernatant was removed after spinning, and cells were resuspended in 15 mL fresh complete medium and transferred to a T75 flask. The medium was replaced with fresh complete medium on the following day.

2.2.1.3. Large scale transfection of HEK293T

For recombinant protein expression, a Falcon® 875 cm^2 5-layer cell culture flask (each layer is 175 cm^2) was used to culture HEK293T cells, and a T175 flask was seeded at the same cell density as the 5-layer flask to observe confluency of cells. Transient transfection was conducted when HEK293T cells were 90% confluent. Transfection mix (containing 5 mL DMEM, 100 mg polyethyleneimine, 50 mg plasmids per T175 flask) were incubated for 20 minutes at room temperature before transfection to allow formation of complex. Complete medium was carefully removed from T175 flask, and fresh DMEM without additives (20 mL per T175 flask) and transfection mix were then added. HEK293T cells were cultured for 4 days before medium collection.

2.2.1.4. HEK293T culture medium collection

During the collection, medium was transferred to Falcon tubes and centrifuged at 4,400 rpm (JLA-16.250, Beckman Coulter) for 10 minutes at 4 °C, and supernatant was further filtered by a 0.45 mm bottle-top filter (Thermo Scientific). 3 × volume of Tris buffer (50 mM Tris, 200 mM NaCl, pH = 9.0) was added to dilute the collected medium. Samples of cell lysate and media were reserved for Western blotting.

2.2.2. HEK293F cell maintenance and protein expression

2.2.2.1. HEK293F cell maintenance

HEK293F cells were maintained in FreeStyle™ 293 Expression Medium (Thermo Fisher Scientific) in a volume of 40 mL using a 125 mL polycarbonate Erlenmeyer flask with vented cap (Corning®). They were cultured at 37 °C in a shaker rotating at 135 rpm and containing a humidified atmosphere with 8% CO_2. HEK293F cells were counted and split every 2 to 3 days to a cell density of 0.1 - 0.2 $\times$ 10^6 cells/mL each time. 293F cells were split by directly transferring cell suspension into a new flask, containing fresh medium, without centrifugation.

2.2.2.2. Freezing and thawing of HEK293F cells

The freezing and thawing processes for HEK293T cells were as described for HEK293T cells (section 2.2.1.2) with some modifications. Freezing medium for HEK293F cells was 90% FreeStyle™ 293 Expression Medium with 10% DMSO supplied, and the final cell density was around 1 $\times$ 10^7 cells/mL. To thaw, cells were transferred into sterile shaker flasks after thawed in a 37 °C water bath instead of the flasks used for adherent cells.

2.2.2.3. Large scale transfection of HEK293F

24 hours before transfection, cells were split to a density of 0.6 - 0.7 $\times$ 10^6 cells/mL, in a total volume of 80 mL, in a 250 mL polycarbonate Erlenmeyer flask with vented cap (Corning®). On the day of transfection, cells were split again to a density of 1.0 $\times$ 10^6 cells/mL in a volume of 80 mL in a 250 mL flask. Plasmids were filtered by a 0.22 μm syringe filter (Millex®) for sterilisation. For each 250 mL flask of cell suspension, 112

μg of plasmids was diluted in OptiPro™ SFM to a total volume of 1.6 mL and mixed in a 15 mL sterile Falcon tube. In a separate 15 mL Falcon tube, 112 μL of FreeStyle™ MAX Transfection Reagent was diluted in OptiPro™ SFM to a total volume of 1.6 mL and mixed gently. These two mixtures were then gently mixed together and incubated for 10 minutes at room temperature to form DNA complexes. Following the incubation, the 3.2 mL of DNA-lipid mixture was slowly added to the flask of cells, and cells were incubated in a shaker rotating at 135 rpm at 37 °C with 8% CO_2. Culture medium was collected 4 days post-transfection for protein purification.

2.2.2.4. HEK293F culture medium collection

On the day of medium collection, cell suspension was transferred to 50 mL Falcon tubes and centrifuged at 3500 rpm (JLA-16.250, Beckman Coulter) for 10 minutes at 4 °C, and the supernatant was filtered by a 0.45 mm bottle-top filter. After filtering, 2 volumes of MES buffer (20 mM MES, 200 mM NaCl, pH = 6.5) was used to dilute the medium. Samples of the cell lysate and medium were kept for western blotting.

2.2.3. S2 cell maintenance and protein expression

2.2.3.1. S2 cell maintenance

25 mL S2 cells (Expres2ion® Biotechnologies, Denmark) were maintained in Ex-Cell 420 medium (Sigma) supplemented with 10% FBS in a 125 mL polycarbonate Erlenmeyer flask with vented cap (Corning®) at 25 °C, 115 rpm. Every 3 to 4 days, cells were counted by a haemocytometer and split to 5×10^6 cells/mL by direct transfer of cell suspension into new flasks containing fresh culture medium, without centrifugation.

2.2.3.2. S2 cell freezing and thawing

Cells were counted using a haemocytometer before centrifugation at 125 ×g for 3 minutes. After removing the supernatant, S2 cells were resuspend in freeze medium (containing 40% Ex-Cell 420, 50% FBS and 10% DMSO) at 40 - 250 × 10^6 cells/mL. 1mL of cell suspension was transferred to a 1.5 mL cryovial immediately and placed into a cryo-freezer at -80 °C overnight. Frozen cells were transferred into liquid nitrogen for long term storage within one week of freezing in order to maintain cell viability.

S2 cells in cryovials were thawed in a 25 °C water bath and transferred directly into a 125 mL shake flask containing 25 mL Ex-Cell 420 medium supplemented with 10% FBS. After 1 to 2 days of culture at 25 °C, cells were counted and centrifuged at 330 ×g for 5 minutes and resuspended in fresh medium to remove the DMSO from the freezing medium. Cells were resuspended in fresh Ex-Cell 420 medium with 10% FBS at 5 × 10^6 cells/mL. FBS was removed after S2 cells were cultured for two passages in 10% FBS-containing medium, and cells were resuspended at 8 × 10^6 cells/mL in Ex-Cell 420 medium for culture.

2.2.3.3. S2 stable cell lines generation

The day before transfection, S2 cells were split to 5 × 10^6 cells/mL and cultured as for maintenance (section 2.2.3.1). On the day of transfection, cells were centrifuged at 450 ×g for 3 minutes and resuspended to 2 × 10^6 cells/mL in Ex-Cell 420 medium (without FBS). 5 mL cell suspension was aliquot into each 75 cm^2 tissue culture flasks (Greiner) for transfection, and 50 μL ExpreS^2 Insect-TR 5 × transfection reagent was added directly into each flask. 12.5 μg of plasmid DNA (human Notch1$_{EGF11\text{-}13\text{-}BirA\text{-}His}$

and human $Notch2_{EGF11\text{-}13\text{-}BirA\text{-}His}$ cloned into pExS2-2 vector) were subsequently added into each flask. Flasks were mixed gently and incubated at 25 °C. After 2 - 4 hours, 1 mL of FBS were added into each flask. After a further 24 hours, Geneticin (G418) was added into each flask to a final concentration of 4000 μg/mL. 2 days after adding selection agent, 3 mL cell suspension was discarded and replaced with fresh Excell420 supplemented with 10% FBS and 4 mg/mL Geneticin.

1 mL cell suspension in each flask was replaced with 1 mL fresh Excell420 supplemented with 10% FBS and 4000 μg/mL Geneticin twice a week until 26 days after transfection (extra medium changes were carried out if cells began to appear unhealthy). 26 days after transfection, the cell suspension was resuspended into 15 mL fresh Ex-Cell 420 with 10% FBS (without selection reagent) to a 125 mL shaker flask and shaken at 25 °C, 115 rpm. Stable cell lines were further expanded to 50 mL fresh Ex-Cell 420 with 10% FBS in 250 mL shake flask at 5×10^6 cells/mL. Samples of the stable pools of cells were frozen for long term storage, and the remaining cells were cultured for protein production.

2.2.3.4. S2 cell protein expression and medium collection

Cells were resuspended in Ex-Cell 420 medium with 10% FBS at 5×10^6 cells/mL, and FBS was removed after cells were cultured in Ex-Cell 420 with 10% FBS for two passages. Stable S2 cells were further expanded to 500 mL (sometimes to 1 L) in a 2 L tissue culture roller bottle (Greiner) at 8×10^6 cells/mL and cultured 4 days before protein purification. Cell suspensions were centrifuged at 4,400 ×g at 4 °C for 20 minutes, and the supernatant containing recombinantly expressed protein was filtered

and loaded onto a cOmplete His-tag Purification Column (Roche) for purification of Notch constructs.

2.2.4. Affinity and size exclusion chromatography

2.2.4.1. Immobilised metal affinity chromatography (IMAC) using a nickel column

Culture medium (after filtering or diluting) from HEK293T, HEK293F or S2 was loaded to a 1 mL His-Tag Purification Column (Roche) by a peristaltic P-1 pump (GE Healthcare) at a 1 mL/minute. After all the medium had been loaded, the His-Tag purification column was washed with 50 mL of wash buffer at a flow rate 1 mL/minute. Following the washing step, protein in the nickel column was eluted with 20 mL elution buffer at the same speed. Washing buffers and elution buffers of different protein production systems are listed in Table 2-1, Table 2-2 and Table 2-3. Eluted protein solutions were concentrated to around 1 mL on a Vivaspin® protein concentrator spin column at 4 ^{o}C, and proteins were further purified by size-exclusion chromatography (SEC).

(A)

Washing Buffer of HEK293T purification system (pH = 9.0)	
Component	**Concentration (mM)**
Tris	50
NaCl	200
Imidazole	10

(B)

Elution Buffer of HEK293T purification system (pH = 9.0)	
Component	**Concentration (mM)**
Tris	50
NaCl	200
Imidazole	300

Table 2-1. Buffers of HEK293T purification system at the IMAC step

(A)

Washing Buffer of HEK293F purification system (pH = 6.5)	
Component	**Concentration (mM)**
MES	20
NaCl	200
Imidazole	50

(B)

Elution Buffer of HEK293F purification system (pH = 6.5)	
Component	**Concentration (mM)**
MES	20
NaCl	200
Imidazole	300

Table 2-2. Buffers of HEK293F purification system at the IMAC step

(A)

Washing Buffer of S2 purification system (pH = 8.5)	
Component	**Concentration (mM)**
Tris	50
NaCl	200
$CaCl_2$	1
Imidazole	2.5

(B)

Elution Buffer of S2 purification system (pH = 8.5)	
Component	**Concentration (mM)**
Tris	50
NaCl	200
$CaCl_2$	1
Imidazole	250

Table 2-3. Buffers of S2 purification system at the IMAC step

2.2.4.2. Size exclusion chromatography (SEC)

Proteins were further purified using the Superdex^{TM} 20 Increase 30/300 GL column (GE Healthcare). Both MilliQ water and gel filtration buffer were filtered using 0.45 mm bottle-top filters before use. Gel filtration buffers for different protein purification systems are listed in Table 2-4. Initial equilibration was carried out using filtered MilliQ H_2O followed by filtered gel filtration buffer. 500 μL of eluted protein solution was injected into the column and run at a flow rate of 0.7 mL/minute. Fractions within the elution peaks were collected and analysed by SDS-PAGE. Correct fractions were pooled and concentrated using a Vivaspin® protein concentrator spin column at 4 °C. Aliquots of 50 mL to 200 mL protein sample were then frozen in liquid nitrogen and stored at -80 °C.

(A)

Gel filtration Buffer of HEK293T and HEK293F protein purification system (pH = 7.5)	
Component	**Concentration (mM)**
Tris	50
NaCl	200

(B)

Gel filtration Buffer of S2 purification system (pH = 7.5)	
Component	**Concentration (mM)**
Tris	10
NaCl	200
$CaCl_2$	1

Table 2-4. Buffers of various purification system at the SEC step

2.2.5. Protein concentration measurements

Protein concentrations were measured using a nanodrop spectrophotometer. Absorbance was measured at 280 nm (A_{280}), and protein concentrations were calculated according to the following formula:

$$Protein\ concentration = \frac{Dilution\ factor \times A_{280}}{\varepsilon}$$

The theoretical extinction coefficient value for each recombinant construct was obtained from the ExPASy bioinformatics server, using ProtParam.

2.2.6. SDS-PAGE

SDS-PAGE gels were cast in two stages, the separation gel followed by the stacking gel, in a 1.5 mm gel casting system (Bio-Rad). The separating gel (10% - 12% acrylamide depending on size of the protein sample, 0.1% SDS, 0.38 M Tris, 0.15% APS, 0.15% TEMED, pH = 8.8) was cast first and allowed to set under a layer of isopropanol. After the gel had set, the isopropanol layer was removed, and the top of the gel was washed with MilliQ water. The stacking layer (4% acrylamide, 0.1% SDS, 0.25 M Tris, 0.2% APS, 0.2% TEMED, pH = 6.8) was poured, and a gel comb was inserted immediately to create sample lanes.

Protein samples for SDS-PAGE analysis were mixed either with non-reducing loading dye (10% glycerol, 50 mM Tris, 3% SDS, bromophenol blue) or reducing loading dye (non-reducing loading dye with 5% β-mercaptoethanol added) and heated at 100 °C for 2 minutes. Gels were run at 150 V for 70 minutes in electrophoresis buffer (0.1% SDS, 30 mM Tris, 250 mM glycine). Gels were stained using SimplyBlue™ SafeStain according to the manufacturer's instructions (Thermo Fisher Scientific). Gel images were taken using a scanner (Canon LiDE) or Gel Doc XR+ gel documentation system (Bio-Rad).

2.2.7. Western blot

After completion of SDS-PAGE, the proteins were transferred to a nitrocellulose membrane (GE Healthcare Amersham™) using the Mini Trans-Blot Cell electrophoresis system (Bio-Rad) at 100 V for 90 minutes. The Trans-Blot Cell was filled with pre-chilled transfer buffer (25 mM Tris, 192 mM Glycine, 20% Methanol and 0.1% SDS) and left on ice during the electrophoretic transfer process. After the transfer step, nitrocellulose membranes were transferred to fresh blocking buffer (PBS containing 5% Skimmed Milk powder, 0.1% Triton X-100) to block for 1 hour at room temperature or overnight at 4 °C. After blocking, membranes were incubated with the primary antibody (HRP conjugated), diluted to an appropriate concentration in blocking buffer, in a 50 mL Falcon tube and incubated for 1 hour with rotation on a roller mixer. The membrane was subsequently washed 3 times, 10 minutes each time, with fresh PBST buffer (PBS containing 0.1% Triton X-100) to remove unbound antibodies.

The peroxidise signal was detected by chemiluminescent detection system. 2 mL mixed ECL western blotting detection reagents (from GE Healthcare Amersham™, 1 mL of each detection regent in the kit) was added to one nitrocellulose membrane and left for 1 minute. After ECL reagent was removed, membranes were then fixed on a cassette by taped cling film and exposed on chemiluminescence films (GE Healthcare Amersham™). The film was then developed using an OPTIMAX® 2010 X-Ray Automatic Film Processor (PROTEC X-ray technology).

2.3. Notch activation assays

2.3.1. Notch activation assay of HEK mN1-NLuc/CLuc-RBPjk and mN2-NLuc/CLuc-RBPjk reporter cells

2.3.1.1. HEK mN1-NLuc/CLuc-RBPjk and mN2-NLuc/CLuc-RBPjk cell culture

The assay was performed according to Ilagan et al., 2011. MN1-NLuc/CLuc-RBPjk and mN2-NLuc/CLuc-RBPjk reporter cells were maintained in complete DMEM medium supplied with 0.4 μg/mL puromycin and 100 μg/mL hygromycin in T25 flasks and cultured in a 37 °C humidified incubator with 5% CO_2 supplied in an atmosphere. Reporter cells were split 1:5 every 3 to 4 days in as for HEK293T cells (section 2.2.1.1).

Freezing and initiating of HEK reporter cells were performed as for HEK293T cells except that complete DMEM medium was supplemented with 0.4 μg/mL puromycin and 100 μg/mL hygromycin (section 2.2.2.2).

2.3.1.2. Setting up of the activation assay by HEK reporter cells

Before assays were set up, HBS buffer (20 mM HEPES, 150 mM NaCl, 0.9 mM $CaCl_2$, pH = 7.4) was autoclaved for sterilisation. To set up the assay, mN1-NLuc/CLuc-RBPjk or mN2-NLuc/CLuc-RBPjk reporter cells were split 1:3 into complete DMEM culture medium (without selection reagents) one day before plate coating. 50 μL of 10 μg/mL purified proteins in HBS buffer was added into each well of a tissue culture treated 96-well plate (Corning® flat clear bottom black polystyrene TC-treated microplates) and kept at 4 °C overnight. Wells were washed once with 200 μL HBS buffer before addition of reporter cells. Reporter cells were trypsinized and counted by a haemocytometer. MN1-NLuc/CLuc-RBPjk or mN2-NLuc/CLuc-RBPjk reporter cells were then diluted to 2×10^5 cells/mL or 5×10^5 cells/mL in complete DMEM culture medium, respectively. 200 mL cell suspension was added into each well and cultured

at 37 °C for 24 hours. On the day of signal detection, medium was gently aspired, and cells were carefully washed once by 200 μL HBS. 100 μL luciferin substrate solution (150 μg/mL D-luciferin, 1 mM $MgCl_2$, 0.1% Glucose in HBS buffer) was added into each well and pipetted 10 times to ensure thorough mixing before signal detection. Luciferin signal was measured by Tristar LB941 (Berthold Technologies) or PHERAstar FS microplate reader (BMG LABTECH). All data was analysed with Prism 7, and comparisons between two groups were performed with a two-tailed unpaired *t*-test. Values are presented as the mean ± SD.

2.3.2. Notch activation assay of CHO hN1G4^{esn} reporter cells

2.3.2.1. CHO hN1G4^{esn} reporter cells maintenance

CHO hN1G4^{esn} reporter cells were maintained in a T175 tissue culture flask with CHO reporter cell medium, which is complete MEM Alpha medium (Gibco^{TM}) (including 10% FBS, 50 U/mL penicillin and 0.05 mg/mL streptomycin and 2 mM L-Glutamine) supplemented with 400 μg/mL Zeocin, 10 μg/mL Blasticidin, and 600 mg/mL Geneticin. CHO cells were cultured in a 5% CO_2 supplied tissue culture incubator at 37 °C and were split twice a week. The CHO cells in each T175 flask were washed with 10 mL sterile PBS followed by 2 mL trypsin digestion for 2 minutes at 37 °C. After adding 10 mL complete medium, cells were resuspended by pipetting. Cell suspension was centrifuged at 1000 rpm for 3 minutes in a Falcon tube. After supernatant was removed, CHO cells were resuspended and split into a T175 flask containing 25 mL fresh CHO hN1G4^{esn} reporter cell culture medium at a 1:7 ratio.

Freezing and thawing procedure was same as HEK293T cells except CHO reporter cell medium instead of complete DMEM medium was used during these procedures (section 2.2.2.2).

2.3.2.2. Setting up of the activation assay by CHO hN1G4^{esn} reporter cells

Each well of a tissue culture treated 96-well plate (Corning® flat clear bottom black polystyrene microplates) was coated with 50 μL of 10 μg/mL purified proteins in the autoclaved HBS buffer (the same HBS buffer composition as indicated in the HEK luciferase activation assay, section 2.3.1.2) overnight at 4 °C. On the next day, wells were washed once by 200 μL HBS buffer. Reporter cells were trypsinized and diluted to 2×10^5 cells/mL in complete MEM Alpha medium with selection reagents added as indicated before. 200 μL cell suspension was added into each well and cultured at 37°C. After 48 hours, medium was carefully aspirated, and cells were gently washed once with 200 μL PBS. After removing PBS, 30 μL Trypsin was added into each well and incubated at 37 °C for 2 minutes. 200 μL PBS was then added, and the plate was centrifuged at 500 ´g at 4 °C for 10 minutes. After carefully aspirating the supernatant, cells were resuspended in 40 mL PBS and kept on ice before analysing by CyAn ADP compact benchtop flow cytometer (Beckman Coulter) or CytoFLEX LX flow cytometer (Beckman Coulter, excitation at 488 nM, emission at 525 nM) or BD LSRFortessa™ X20 flow cytometer system (excitation 488 nm, emission 530 nm). All FACS data was analysed by FlowJo software.

2.4. Notch binding assays

2.4.1. Notch binding assay using MaxiSorp™ plates

50 μL of 40 ng/μL purified Notch$_{EGF11\text{-}13\text{-}BirA\text{-}His}$ constructs (expressed by S2 cells, see section 2.2.3) diluted in binding assay buffer (20 mM HEPES, 200 mM NaCl, 5 mM $CaCl_2$, pH = 7.5) was added to each well of a Nunc MaxiSorp™ flat-bottom 96-well plate (Thermo Scientific), and incubated at 4 °C overnight. After washing 3 times with

200 μL binding assay buffer, the plate was blocked with a solution containing 1% milk (w/v) and 2% gelatin (w/v) diluted in the binding assay buffer, for 90 minutes at room temperature. After 3 washes with 200 μL of washing buffer (20 mM HEPES, 200 mM NaCl, 5 mM $CaCl_2$, 0.05% Tween-20, pH = 7.5), 50 μL of 200 nM $Jagged1_{N\text{-}EGF3\text{-}Fc\text{-}His}$ solution (purified from HEK293T cells, see section 2.3.1) diluted by binding assay buffer was added and incubated for 90 minutes at room temperature on a shaker with mixing at 40 rpm. Wells were washed as in the previous step with washing buffer and incubated with a 1:2000 dilution of Goat monoclonal anti-human IgG Fc HRP conjugated antibody (Abcam) for 60 minutes. After washing as above, 100 μL fresh ELISA substrate solution (12 mL of 0.1 M citrate acid, 10 μL 30% H_2O_2 and 4 mg ABTS, pH = 4) was added to each well. A PHERAstar FS microplate reader (BMG LABTECH) was used to detect absorbance at a wavelength of 415 nm. When combining data, values from individual experiments was standardised to wild type to take into account the HRP reaction rate variations between different days. Data was analysed and plotted using Prism 7.

2.4.2. Notch binding assay by nickel-coated plates

Pierce™ 96-well clear nickel-coated plates (Thermo Scientific) were coated with 5 μg/mL purified Jagged1 or DLL4 (N-EGF3 constructs with Fc and His tag at C-terminus) in 100 μL binding assay buffer (components are indicated in 2.4.1). After incubating at 4 °C overnight, the plate was washed 3 times with 200 μL binding assay buffer and blocked with 4% (w/v) bovine serum albumin (BSA, Sigma) in the same buffer for 1 hour at room temperature. Notch1 and Notch2 EGF11-13 constructs that had been biotinylated by site-specific biotin ligase (Avidity BirA-500 kit, performed by Dr Pat Whiteman) were mixed at a 4:1 molar ratio to NeutrAvidin-HRP (Life Technologies) in

the binding assay buffer for 1 hour on a rotor (40 rpm speed) at room temperature. After the plate blocking step, three washes with 200 mL binding assay buffer were performed to remove remaining BSA. The pre-clustered Notch constructs at different concentrations in 50 μL binding assay buffer were then added to the ligand-coated plates and incubated for 1.5 hour on a shaker (around 40 rpm) at room temperature. After washing four times with 200 μL washing buffer (indicated in section 2.4.1), followed by two washes with 200 μL binding assay buffer, the plate was developed with 100 μL ELISA substrate solution (see section 2.4.1) per well. Absorbance was measured with a PHERAstar FS microplate reader (BMG LABTECH) at a wavelength of 415 nm. Data from individual repeat was standardised to wild type and was plotted using Prism 7.

2.5. Liposome binding assays

2.5.1. Lipid stock preparation

Chloroform solutions of 1-palmitoyl-2-oleoyl-glycero-3-phosphocholine (POPC), 1,2-dioleoyl-sn-glycero-3-phospho-L-serine (DOPS), brain sphingomyelin (SM), 1,2-dioleoyl-sn-glycero-3-phosphoethanolamine-N-carboxyfluorescein (CF-PE) (Avanti®) were mixed in desired ratios (PC-rich liposome: POPC:DOPS:CF-PE (70:25:5), SM-rich liposome: POPC:SM:DOPS:CF-PE (30:40:25:5)) and dried in a round-bottom glass tube under nitrogen (about 15 minutes). Dried lipids were wrapped with foil and left in the freezer dryer for 1 hour of further drying. Lipid films were resuspended in the liposome assay buffer (20 mM HEPES, 200 mM NaCl, 5 mM $CaCl_2$, pH 7.4) at 2 mM lipid concentration and was left on a shaker (100 rpm) for one hour in the dark at room temperature. 300 μL of 2 mM lipid stock was aliquot into 0.5 mL Eppendorf tubes. Aliquots of lipid stock were frozen in liquid nitrogen and then thawed in 37°C water

bath (around 3 minutes), and this freeze-thaw cycle was repeated 8 times. After the last freezing step, aliquots were stored at -80°C until they were needed.

2.5.2. Liposome extrusion and characterisation

One lipid aliquot was thawed at room temperature and extruded on the day of performing the turbidity assay. A clean mini extruder was assembled according to the recommended manufacturer's instructions. Two filter supports that had been pre-wet with liposome binding assay buffer (see section 2.5.1) were placed over each side orifice, and a 100 nm pore width Nuclepore polycarbonate hydrophilic membrane (Whatman™) was place in the middle of extruder. Lipid stock was transferred into a 1 mL glass polar lipid syringe (Avanti®) and were extruded with 21 passes through a 100 nm pore width Nuclepore polycarbonate hydrophilic membrane (Whatman™). Liposome stock was transferred from a glass syringe to an Eppendorf tube after extrusion. The homogeneity of liposomes was confirmed using dynamic light scattering.

Dynamic light scattering measurements were performed using the Viscotek Model 802 instrument with OminiSIZE 3.0 software. Before each measurement, the cuvette was cleaned with 70% Ethanol and MilliQ water, then dried with nitrogen gas. 2 mM liposome stock was diluted 20-fold with the liposome binding assay buffer before addition to the cuvette. The measurement was performed by 35% transmission scatter light intensity at room temperature.

2.5.3. Protein G bead coating

The day before performing the liposome turbidity assay, protein G beads were mixed with purified $Jagged_{N\text{-}EGF3\text{-}Fc\text{-}His}$ and kept at 4 °C overnight. To do this, fluorescent Protein G coated beads (5.88 μm, PAK blue, SPHERO™) were vortexed, and the desired volume of bead solution (10 μL bead solution needed for each sample) was transferred into an Eppendorf tube. 10 volumes of HBS/BSA buffer (3% fatty-acid free BSA, 20 mM HEPES, 200 mM NaCl, 5 mM $CaCl_2$, pH 7.4) was mixed with bead solution. Beads were then centrifuged at 13,000 rpm for 5 minutes, and supernatant was carefully removed. A further was with 10 volumes of HBS/BSA buffer was performed before beads were resuspended by 5 volumes of HBS/BSA. 50 μL of bead suspension was aliquoted for each sample and 2 μg $Jagged1_{N\text{-}EGF3\text{-}Fc\text{-}His}$ constructs or mouse IgG (a negative control in the turbidity assay, Santa Cruz Biotechnology) was added into each bead aliquot. The bead-protein mixture was kept at 4°C overnight in dark.

2.5.4. FACS-based liposome turbidity assay

Ligands coated protein G beads were washed once with 100 μL HBS/BSA buffer per reaction to wash off any unbound protein and resuspended in 50 μL ice-cold liposome binding assay buffer. 2 μL of coated beads were kept for western blotting checking. 2 mM liposome stock was diluted 400-fold with liposome binding assay buffer, and 48 μL of liposome solution was added into each reaction. After 30 minutes incubation on ice, 200 μL of liposome binding assay buffer was added to each reaction before analysing by flow cytometer.

Immunofluorescent images of beads and liposomes were taken by Amnis® ImageStream®ˣ Mk II flow cytometer at higher speed using a 60´ objective lenses, and

images from channel 01 (bright field channel with 435 - 480 nm filter), channel 02 (excitation at 488 nm, emission 480 - 560 nm), channel 06 (excitation at 561 nm, and emission at 595 - 642 nm), channel 09 (bright field channel with 570 – 595 nm filters), channel 11 (excitation at 642 nm, emission at 642 - 745 nm) were recorded. Data were analysed by Amnis® AI Image Analysis Software.

Liposome aggregation was analysed by BDX-20 (BD Biosciences) flow cytometer, and 10,000 events were recorded each experiment. Data were acquired from both excitation/emission at 488 nm/530nM and 640 nm/670 nm. Aggregation percentages were analysed using FlowJo software and were plotted using Prism 7.

Chapter 3. Study of the C2 domain of human Jagged1 using COSMIC variants

3.1 Introduction

The N-terminal C2 domain of Notch ligands was proved to have both membrane binding and Notch binding properties, and was showed to modulate the Notch signalling pathway in different ways (Chillakuri et al., 2013) (Suckling et al., 2017) (Luca et al., 2017). A series of missense mutations which cause diseases, such as Alagille syndrome and EHBA, are found within the C2 domain of human Jagged1, and affect Notch signalling through loss of function mechanisms (see section 1.2.2.2 and section 1.5.3).

Missense mutations locating within the hydrophobic core of Jagged1-C2 domain are found to cause Alagille syndrome (Figure 3-1). These mutations result in improper folding and trafficking of Jagged1 and lead to haploinsufficiency (Piccoli and Spinner, 2001). In addition, a series of single substitutions at apical loops of Jagged1-C2 domain were found in EHBA patients (Figure 3-1). Interestingly, these EHBA variants were shown to decrease Notch signalling most likely by decreasing the C2 membrane-binding property, since their Notch-binding ability and protein stability were not affected but their liposome-binding capability was (Suckling et al., 2017). Due to the small number of variants tested, the effects of other disease-related Jagged1-C2 domain substitutions on Notch signalling need to be investigated to establish the contribution of lipid and Notch binding surfaces. Whilst protein engineering is a valid approach to probe structure-function relationships, the COSMIC database was used as an alternative source of variants. Cells have been shown to acquire gene mutations in Notch in ageing (Martincorena et al., 2018) and in specific cancers (Loganathan et al., 2020), although ligand contributions are much less well studied.

COSMIC is the largest online database of acquired mutations in cancer across whole genomes, including coding and non-coding mutations, structural rearrangements and gene fusions. A number of previously unscreened ligand variants are present which could provide structure-function information and give insight into Notch ligand contribution to cell survival tumorigenesis. So far, most attention has centred on the mutational status and activity of Notch (Loganathan et al., 2020) (Nowell and Radtke, 2017).

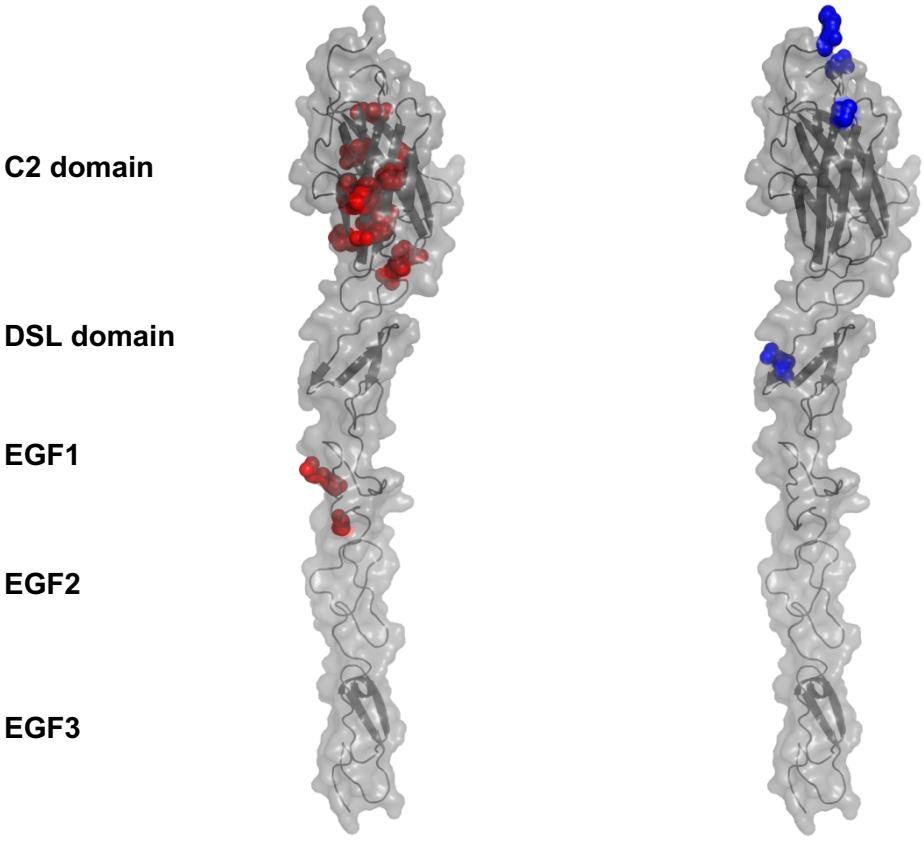


Figure 3-1. Missense mutations associated with Alagille syndrome and EHBA

Alagille syndrome (red spheres) and Extrahepatic biliary atresia (EHBA) (blue spheres) associated missense mutations which affect the N-terminal region are mapped onto the structure of Jagged1$_{N\text{-}EGF3}$ using PyMOL (PBD: 4CBZ, grey cartoon and solid surface). Structure images are adapted (Chillakuri et al., 2013), and the position of each domain is indicated on the left hand side. Note that most C2 domain variants associated with Alagille syndrome map to the hydrophobic core, whilst EHBA variants are present in loops.

The aim of this chapter is to study the functional importance of the C2 domain in human Jagged1 by testing missense mutations obtained from COSMIC cancer database. This was performed using site-directed mutagenesis to produce Jagged1$_{N\text{-}EGF3}$ variants which can be expressed as soluble fragments. A human Jagged1 construct containing C2 domain to EGF3 domain produced by HEK293T was previously used to test its ability to bind to a human Notch1 EGF11-13 construct generated from S2 cells, to bind to liposomes and to test its ability to activate Notch (Suckling et al., 2017). All variants were therefore expressed similarly as Jagged1$_{N\text{-}EGF3}$ constructs using the pHL-sec expression vector in HEK293T cells with Fc and His-tag fusion tags at the C-terminus. The effect of the different amino acid substitutions on expression into 1) extracellular media and 2) Notch activation after purification was tested, followed where appropriate, by binding assays.

3.2 COSMIC missense mutation selection

In the COSMIC database, somatic mutations have been recorded from 38357 tested tumour samples (719 samples among these have mutations at *JAG1*) until August 2020, which includes missense, synonymous, nonsense, insertion and deletion mutations across *JAG1* (Figure 3-2) (Table 3-1). More than half of these mutations are missense mutations (Table 3-1), and the distribution of these missense mutations at Jagged1$_{N\text{-}EGF3}$ is shown in Figure 3-2. Out of all the missense mutations affecting the extracellular domain, 13 of them are obviously loss of function by affecting key cysteine residues responsible for stabilising domain fold through disulphide bond formation. Around 13% of Jagged1 missense mutations were found to affect Jagged1-C2 domain residues located in the loop regions and the hydrophobic core (Table 3-1).

In order to probe the function of these variants in more detail, 13 somatic tumour missense mutations, which were chosen because they are located in both the hydrophobic core and different loop regions of C2 domain and the binding interface of the DSL domain, were chosen for further analysis (Table 3-2). These mutations have different histology, came from various primary tissues and have a pathogenic score associated with them. Most of these tumours were of epithelial origin. The pathogenic scores were acquired by a machine learning approach, FATHMM-MKL, which is used to predict the functional consequences of single nucleotide variants. The functional scores are in the form of a single p-value, ranging from 0 to 1. Scores $\geq$ 0.7 are classified as “Pathogenic” (Forbes et al., 2016).

Six of these missense mutations affect residues on the putative membrane binding loops (loop 1-2 and loop 5-6), and one affects a residue located on loop 3-4 (Figure 1-9, 1-10 and 3-3). Among these apical-loop variants, it was noted that one alters a consensus N-glycosylation site on loop 5-6. For the loop 2-3 which has been shown to interact with Notch (see Figure 1-9 and 1-10), two COSMIC missense mutations have been selected. Other than these loop substitutions, three missense mutations affecting β-strands of the hydrophobic core were investigated (Table 3-2) (Figure 3-3). Moreover, a missense mutation leading to an amino acid change, E228K, located on the DSL domain Notch binding loop was selected (Table 3-2) (Figure 3-3). The position of selected COSMIC variants within the C2 domain are shown in Figure 3-3, mapped onto the Jagged1/Notch receptor complex.

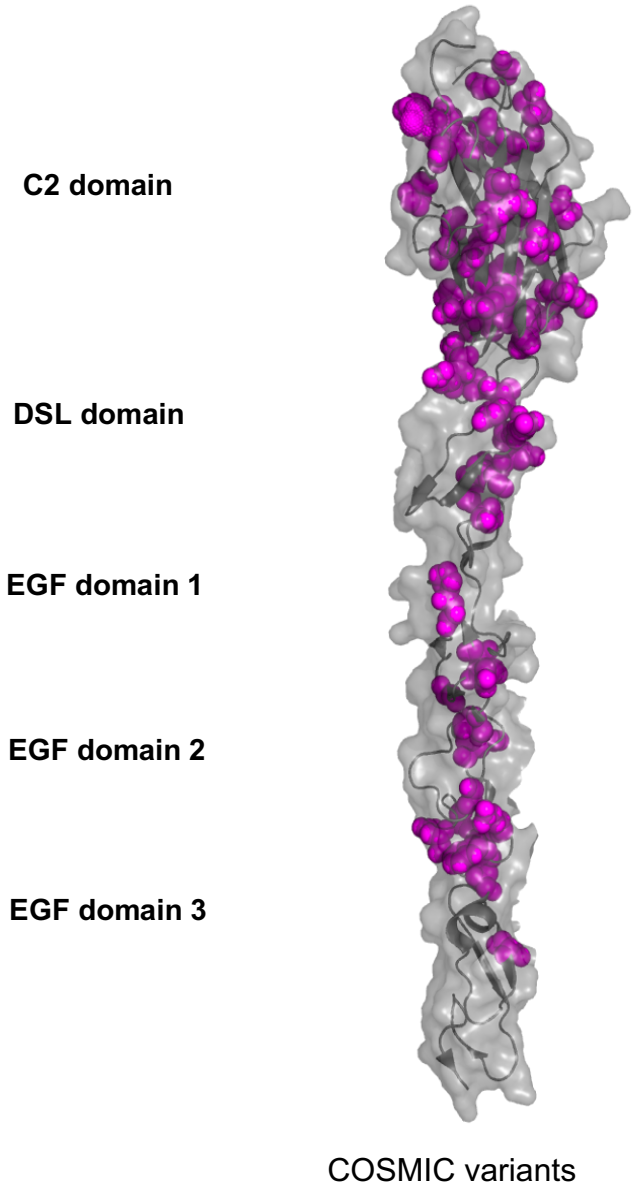


Figure 3-2. Distribution of COSMIC missense mutations in Jagged1$_{N\text{-}EGF3}$

Cancer-associated missense mutations (purple spheres) are mapped onto the structure of Jagged1$_{N\text{-}EGF3}$ (grey cartoon and solid surface). Until August 2020, 80 missense mutations have been recorded in the COSMIC cancer database which affect Jagged1$_{N\text{-}EGF3}$. A subset of these mutations affecting the C2 and DSL domains have been chosen for further study. The Jagged1 model was constructed based on 4CBZ using PyMOL.

Sample type	Number
Samples tested	38357
Jagged1 total mutated samples	669
Jagged1 missense mutation samples	350
Jagged1-extracellular domain missense mutation samples affecting disulphide bonds	13
Jagged1-C2 domain total mutated samples	66
Jagged1-C2 domain missense mutation samples	46

Table 3-1. Mutations in recorded in COSMIC cancer database

Statistical information about Jagged1 cancer-related mutations recorded in COSMIC database. Accurate as of August 2020. Approximately 10% of mutations are located in the Jagged1-C2 domain (66 mutations on C2 versus total 669 mutations found in Jagged1), and most of these Jagged1-C2 mutations are missense mutations (around 70%).

Website URL: https://cancer.sanger.ac.uk/cosmic/gene/analysis?ln=JAG1

Domain	Mutation	Position at C2 domain	Histology	Primary tissue
C2	F35L	beta sheet 1	neoplasm	liver
C2	G47R	loop1-2	carcinoma	breast
C2	A58V	loop1-2	malignant melanoma	skin
C2	D72N	loop1-2	carcinoma	skin
C2	V86F	loop2-3	carcinoma	biliary tract
C2	G89E	loop2-3	glioma	brain
C2	G114D	loop3-4	carcinoma	stomach
C2	T133R	beta sheet 5	carcinoid-endocrine tumour	lung
C2	L135F	beta sheet 5	carcinoma	stomach
C2	S142N	loop5-6	carcinoma	lung
C2	T145N	loop5-6	carcinoid-endocrine tumour	lung
C2	W139S	loop5-6	carcinoma	pancreas
DSL	E228K	n/a	carcinoma	endometrium, large intestine

Table 3-2. Missense mutations in the Jagged1 C2 domain selected from the COSMIC database for study

Most missense mutations in this study were related to epithelial-derived tumours, but the primary tissues differ. Website URL: https://cancer.sanger.ac.uk/cosmic/gene/analysis?ln=JAG1

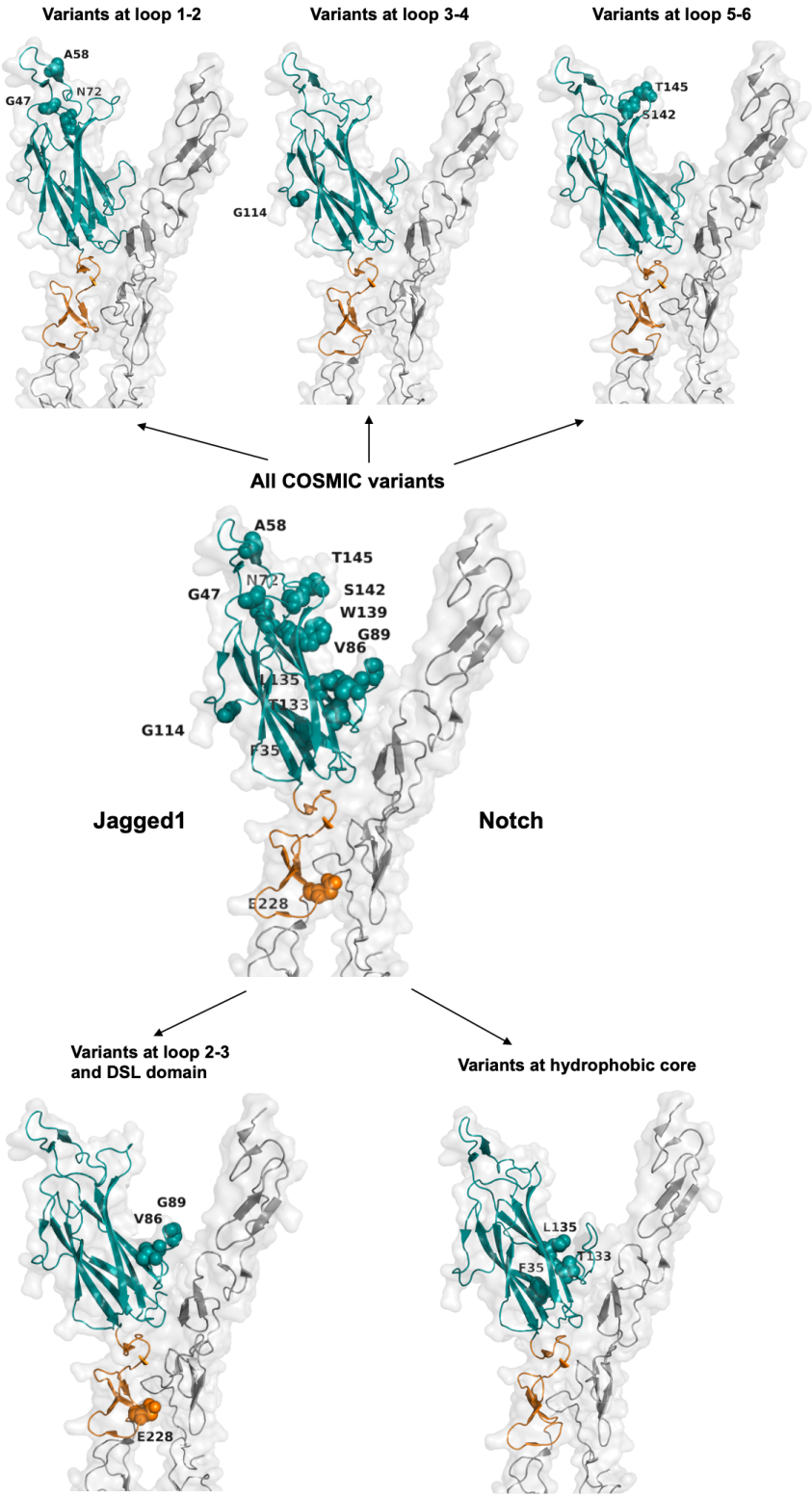


Figure 3-3. Structural location of selected COSMIC Jagged1 variants

C2 domain of Jagged1 showing residues affected in COSMIC variants studied (labelled as teal spheres) in both loop regions and hydrophobic core. The position of E228 in the DSL Notch-binding site is shown. This PyMOL model is produced from the alignment of PDB code 5uk5 (Jagged1 N-EGF3 and Notch1 EGF8-12 complex) and 2vj3 (Notch1 EGF11-13). The C2 domain is in teal, the DSL domain is in orange, and Notch1 EGF domains are in grey.

3.3 Mutagenesis of Jagged1$_{N\text{-}EGF3\text{-}Fc\text{-}His}$ COSMIC variants

A cDNA fragment encoding Jagged1$_{N\text{-}EGF3}$ was cloned into pHL-sec expression vector (see Chapter 2) (Figure 3-4). This construct which lacks the transmembrane domain can be expressed as a soluble fragment in the extracellular medium following transfection of HEK293T cells. An Fc-tag has been inserted into the C-terminus of the construct to produce dimers which aid functional assays through avidity effects, and a His-tag has also been attached at the C-terminus for protein purification and to aid functional assays (Figure 3-4).

Overlap extension PCR was used for site-directed mutagenesis (see Chapter 2, Figure 2-1). Two primers with desired mutations were designed, and the sequence containing the mutation site was achieved through two separate rounds of PCR (see section 2.1.2) (Appendix A). Each PCR product was visualised on an agarose gel to confirm that the correct size of fragment had been produced (Figure 3-5). Two unique restriction sites, *Eco*RI and *Kpn*I, were identified so that the DNA strand generated by PCR could be inserted into the plasmid by restriction enzyme digestion and ligation steps (Figure 3-4). All plasmids with desired sequences were confirmed by Sanger sequencing service provided by Source Bioscience company. F35L, G47R, A58V, D72N, G114D, T133R, S142N, T145N, E228K constructs were created by overlap extension PCR, the remainder, V86F, G89E, L135F, W139S were cloned by Dr Boguslawa Korona, University of Oxford.

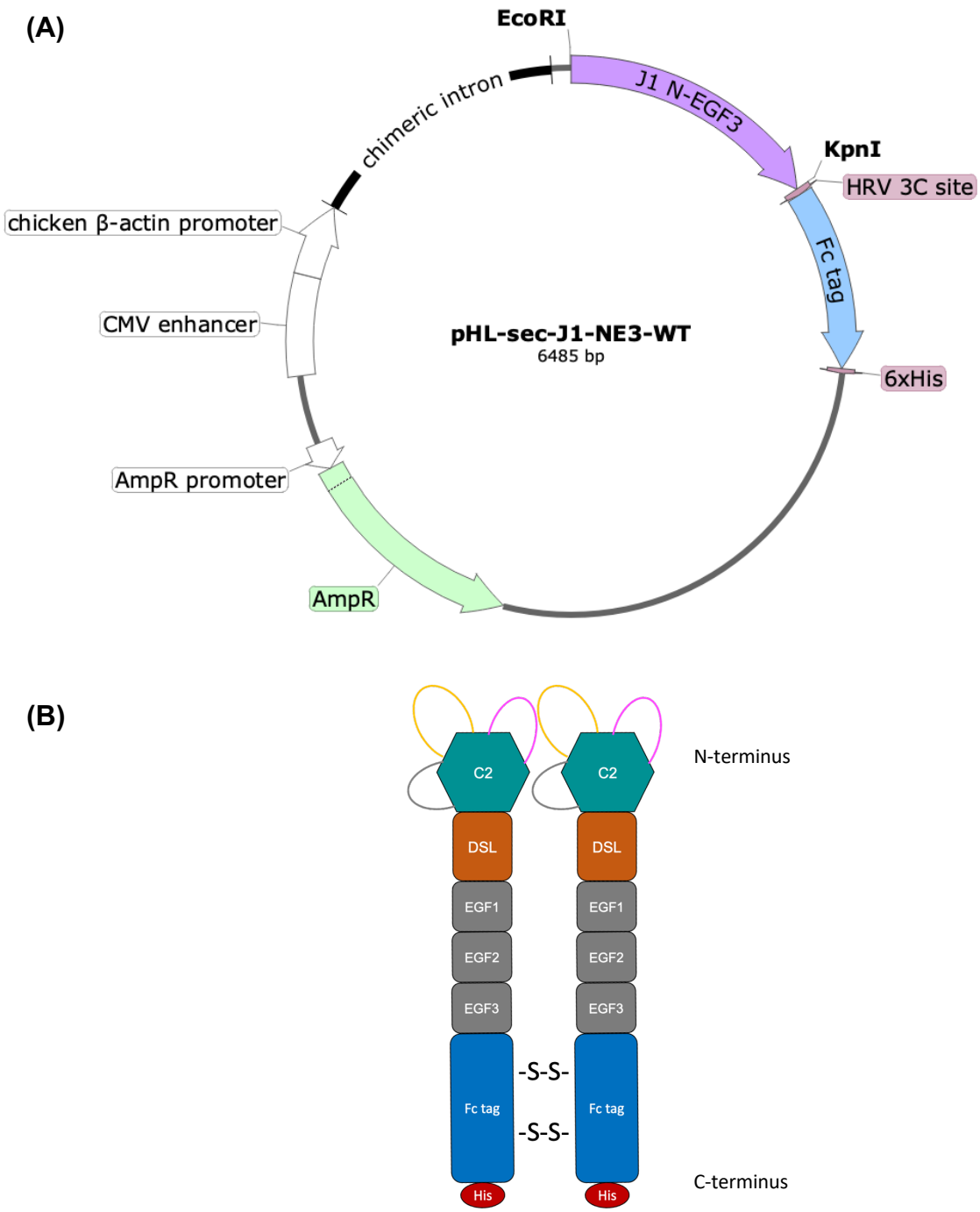


Figure 3-4. pHL-sec-Jagged1$_{N\text{-}EGF3\text{-}Fc\text{-}His6}$ map and domain organisation diagram

(A) The major components of the expression plasmid are indicated in the map (adapted from SnapGene Viewer). The chicken β-actin promoter (white arrow) and CMV enhancer (white block) are used to drive high levels of protein expression in HEK293T cells. cDNA encoding the Jagged1$_{N\text{-}EGF3}$ construct (purple arrow) is inserted into the plasmid via 5' *Eco*RI and 3' *Kpn*I restriction sites. At the 3' of Jagged1$_{N\text{-}EGF3}$ cDNA sequence, an Fc tag (blue arrow) and a 6 × His tag (brick red arrow) is encoded. (B) Domain organisation of recombinant Jagged1 constructs (not to scale). C2 domains are shown in teal with loop1-2 (yellow), loop3-4 (grey), loop 5-6 (purple) indicated.

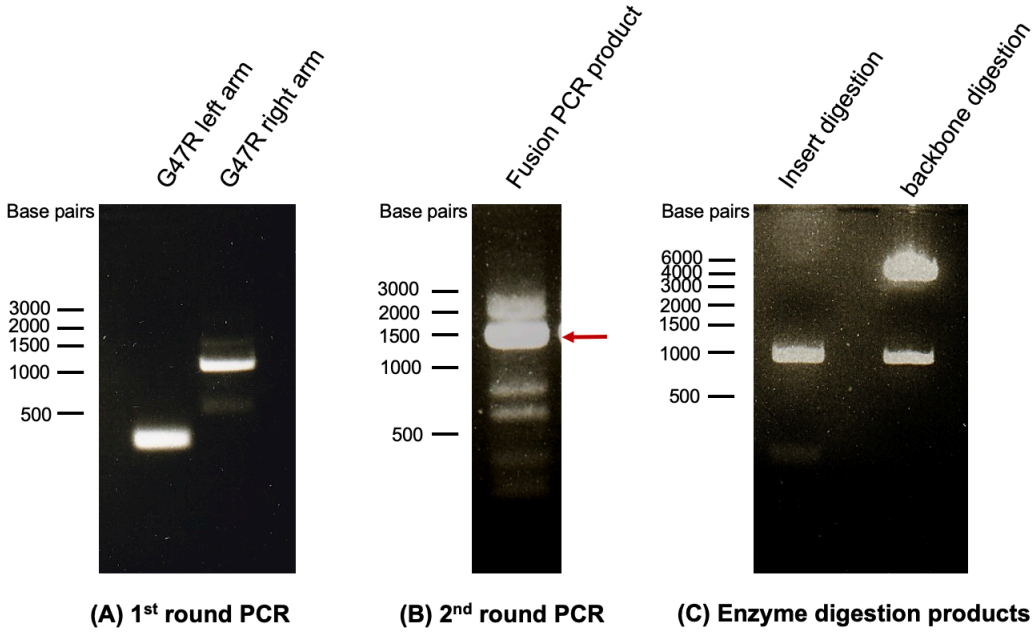


Figure 3-5. Agarose gel electrophoresis to visualise products from overlap PCR mutagenesis

Construction of Jagged1 G47R variant is shown as an example of the mutagenesis procedure used. The size ladder is shown on the left. (A) The products from the first round of PCR reactions, the left arm (276 bp) and right arm (1021 bp) for overlap extension PCR (Figure 2-1), were run on a 1% TBE agarose gel. (B) The products from the second round of PCR reactions (an overlap extension PCR) were visualized on a 1% TBE agarose gel. The red arrow indicates the band with the correct size (1278 bp). (C) DNA fragments after digestion by *Eco*RI and *Kpn*I restriction enzymes were run on a 0.5% TBE agarose gel. The first lane indicates the digestion of the insert from the second round PCR, and the second lane shows the digestion of the pHL-sec-Jagged1$_{N\text{-}EGF3}$-Fc-His$_6$ wild type plasmid to produce the 5475bp vector backbone (upper band).

3.4 Secretion tests of Jagged1 COSMIC mutants

In order to test whether or not the COSMIC substitutions affect the expression, folding and trafficking of Jagged1, secretion tests by western blotting were performed. All the COSMIC variants were expressed in HEK293T cells by small-scale transient transfections (see Materials and Methods), together with a positive control (the pHL-sec-Jagged1$_{N\text{-}EGF3}$-Fc-His$_6$ wild type plasmid) and a negative control (no plasmid was added to the transfection mixture).

Western blot analysis of cell lysate and medium samples, following reducing SDS-PAGE, demonstrated there were bands present for the wild type sample and no bands present for the negative controls detected by anti-His-HRP antibody. As there is no loading control that can be used in analysing extracellular medium samples, equal volumes of medium were analysed and three independent repeats were performed to obtain reliable results. The same approach was taken for cell lysates, although ideally a loading control such as probing for tubulin should have been included to infer changes in expression levels. Immunoreactive bands migrated at the position expected for monomeric/reduced Jagged1$_{N\text{-}EGF3}$ at approximately 61 kDa (Figure 3-6). Signals from all COSMIC variants were detected from cell lysate samples, which suggest that all these variants were expressed by the cells (Figure 3-6). Some heterogeneity was present in lysate samples most likely due to different glycosylated species. However, no signals were detected from medium samples of Jagged1 F35L, T133R and W139S and very low signal detected from G47R, which suggested they were misfolded and retained in the cell (Figure 3-6). In the medium samples of other COSMIC variants (A58V, D72N, V86F, G89E, G114D, L135F, S142N, T145N and E228K), signal levels were similar to wild type Jagged1$_{N\text{-}EGF3}$, which suggested the introduced amino acid substitutions did not affect protein folding significantly (Figure 3-6). These variants were scaled up for protein purification and further study.

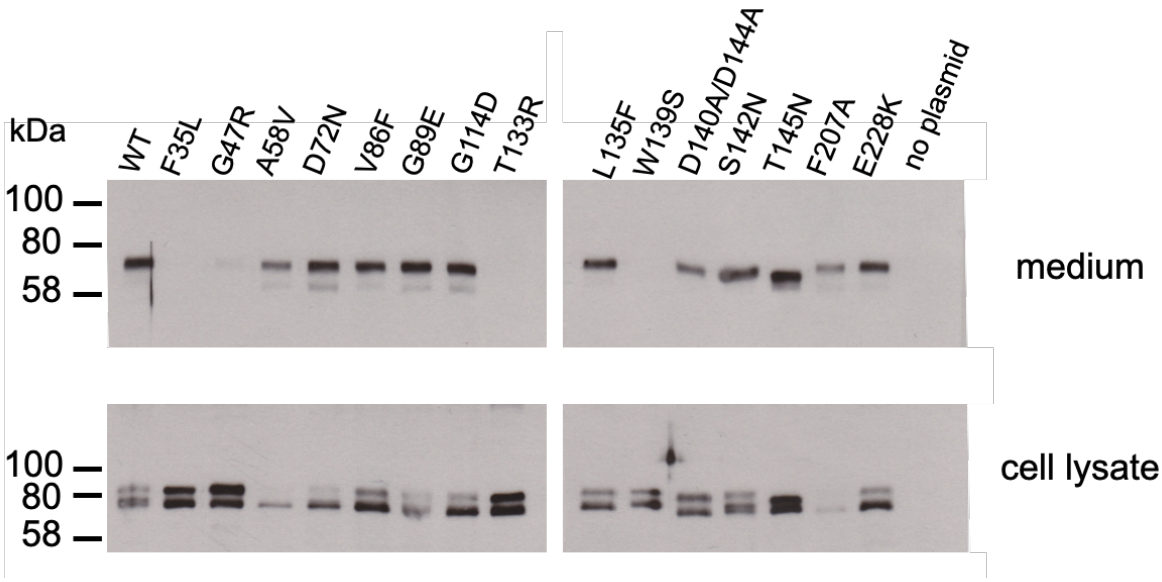


Figure 3-6. Western blot analysis of Jagged1 COSMIC variant expression in cell lysate and medium samples

Western blot shows expression of Jagged1 COSMIC variants compared with Jagged1 wild type and the negative control. Equivalent volume of medium and cell lysate samples were collected and separated by 10% reducing SDS-PAGE. The negative control (no plasmids) is indicated. The molecular weight of monomeric WT Jagged1 construct is 61kDa from the amino acid sequence but migrates higher due to glycosylation. A subset of COSMIC variants are expressed but appear to cause protein misfolding and are retained (F35L, G47R, T133R, W139S). Others are secreted similarly to WT Jagged1$_{N\text{-}EGF3}$. A polyclonal anti-His-HRP rat antibody (1 in 2000 dilution) was used for signal detection. Three independent transfections were performed, and a representative western blot is shown. Molecular weight markers (kDa) are indicated.

3.5 Production and purification of recombinant Jagged1

3.5.1 Overview of the HEK293T expression system

The HEK293T cell line is a fast-growing and highly transfectable human embryonic kidney cell line and is able to grow in serum-free media. It is a useful expression system for studying proteins that require complex-folding machineries, co-factors or post-translational modifications. It can efficiently express protein by a transient transfection approach in a relatively short time, which is useful when comparing many variants. Purified WT Jagged1$_{N\text{-}EGF3}$ construct (with two consensus N-glycosylation

sites and 15 disulphide bonds) obtained from the HEK293T expression system in high yields (~ 800 μg/L of conditioned media) has been shown previously to activate Notch signalling in mN1-NLuc/CLuc-RBPjk reporter cells and this system has enabled a comparison of functional variants (Chillakuri et al., 2013) (Suckling et al., 2017). Thus, the HEK293T expression system was used to express COSMIC Jagged1 variants for investigating the function of the C2 domain.

3.5.2 Protein purification of Jagged1$_{N\text{-}EGF3}$ COSMIC variants

All COSMIC variants shown to secrete similarly to wild type were expressed in HEK293T cells following transient transfection and purified for use in a variety of functional assays (Figure 3-6). Wild type Jagged1$_{N\text{-}EGF3}$ was purified as a positive control, as were three negative controls, F207A, F207A/E228K and D140/144A variants. F207A and E228K are Notch binding deficiency substitutions, which are located at the receptor-ligand binding interface (Cordle et al., 2008) (Luca et al., 2017). The D140/144A double variant reduces Ca^{2+} binding to the Jagged1-C2 domain increasing loop 1-2 and 5-6 flexibility and shows decreased liposome binding (Chillakuri et al., 2013). Medium was collected four days after transfection, and cell debris was removed by centrifugation and filtering. The protein was initially purified utilising its His-tag by immobilised metal affinity chromatography (IMAC) at 4 °C before concentration, and subsequent purification by size exclusion chromatography (SEC) (Figure 3-7). Fractions across the SEC peak were collected and analysed by non-reducing and reducing SDS-PAGE. All Jagged1 variants were purified to a near homogenous (>95%) product, and formed high MW dimers under non-reducing conditions, similar to WT (Figure 3-7). D72N gave a double band, and T145N migrated at a slightly lower MW compared to other variants and WT under reducing conditions.

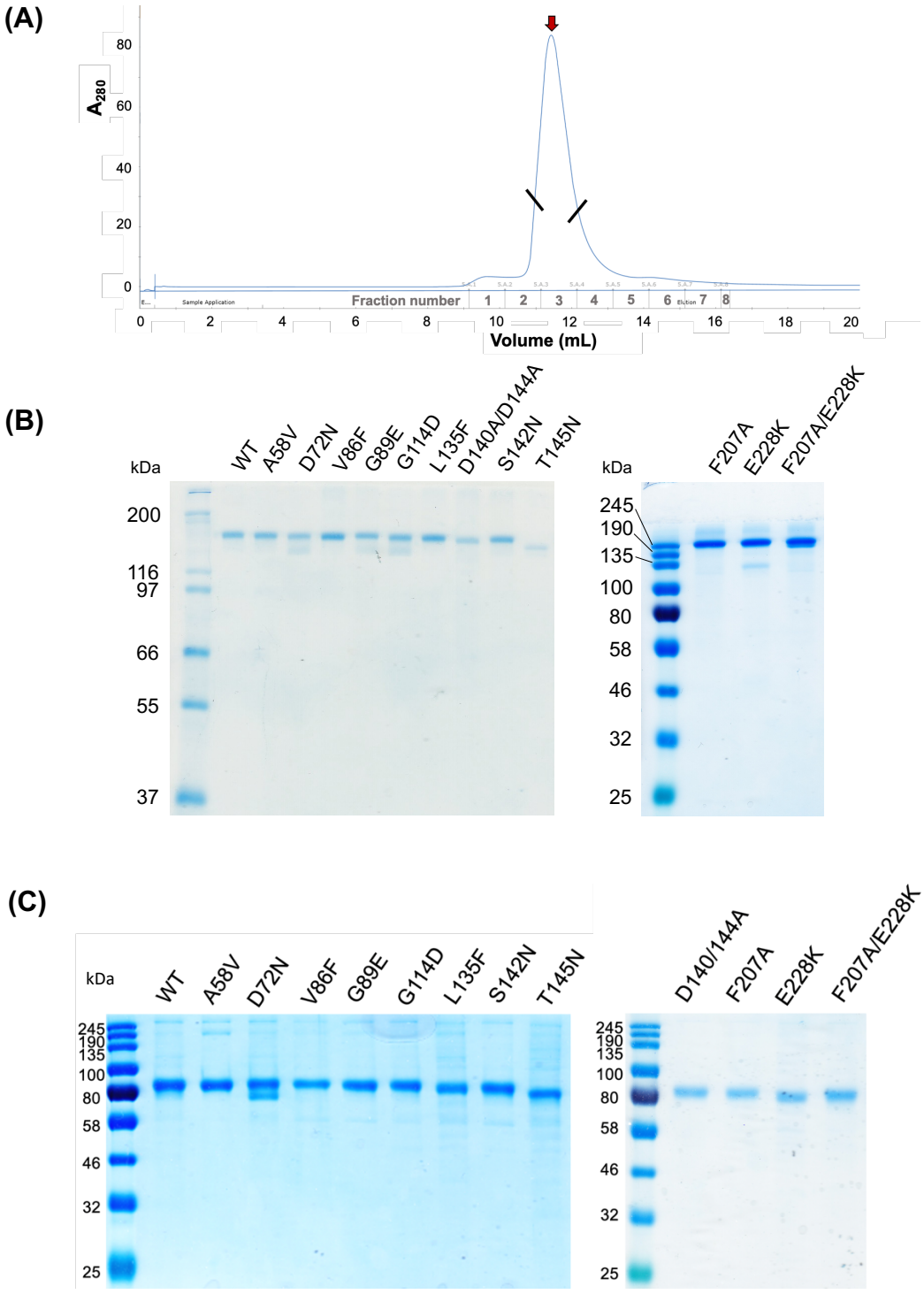


Figure 3-7. Purification of recombinant Jagged1$_{N\text{-}EGF3\text{-}Fc\text{-}His}$

(A) Size exclusion chromatogram of Jagged1$_{N\text{-}EGF3\text{-}Fc\text{-}His}$ WT. The peak (one fraction) collected is indicated by the red arrow and black lines. (B) (C) The final purification products of all Jagged1 variants were analysed by 10% SDS-PAGE to assess the purity. Samples were run under non-reducing (B) and reducing (C) conditions. All show the expected high molecular weight dimer form mediated by the Fc tag under non-reducing conditions, and monomer form under reducing conditions. In each case the dimer (~122 kDa) and monomer (~61 kDa) migrate at a higher molecular weight than expected, most likely due to presence of post-translational modifications e.g. N-glycosylation.

3.6 Testing the effect of Jagged1 COSMIC variants on Notch activation by two different reporter systems

In order to investigate the impact of Jagged1 COSMIC mutations on Notch activation, each purified variant was immobilised on the surface of 96-well tissue culture plates. Two engineered systems, HEK mN1-NLuc/CLuc-RBPjk (Ilagan et al., 2011) and CHO hN1G4^{esn} (Sprinzak et al., 2010) were used as reporter lines for measuring Notch activity. MN1-NLuc/CLuc-RBPjk cells are generated from HEK293 cells and use a luciferase complementary-based reporter quantitative read out, whilst CHO hN1G4^{esn} cells are modified from CHO cells with a YFP transcriptional reporter read out.

3.6.1 Comparison of two Notch activation assays

MN1-NLuc/CLuc-RBPjk reporter cells express mouse full-length chimeric Notch1 receptors which are fused to half of luciferase (NLuc) at the C-terminal end of Notch on the NICD (Figure 3-8) (Table 3-3). After the binding of ligand to receptor and receptor S2 and S3 cleavage events, the NICD translocates to the nucleus and interacts with the Notch transcriptional co-effector RBPjk that has been engineered to contain the other half of luciferase (Chapter1, Section 1.1.3) (Figure 3-8). The interaction of RBPjk and NICD following cleavage brings the two luciferase fragments into close proximity to form enzymatically active luciferase which produces luminescence on addition of substrate luciferin in proportion to the amount of Notch activation (NICD released at the cell membrane). This reporter system can be used to quantitate Notch activation in live cells and in real time, and therefore investigate the molecular mechanisms of Notch activation regulation (Ilagan et al., 2011).

In CHO hN1G4^{esn} reporter cells, the NICD of human Notch1 was replaced with Gal4 which is a transcriptional activator that binds to upstream activating sequence (UAS) promoters to initiate transcription (Figure 3-9). After human Notch1 is activated by ligand binding and cleavage at S2 and S3, Gal4 is released and binds to UAS promoters in the nucleus. The UAS promoter sequence has been fused to a cDNA encoding a fluorescent histone 2B (H2B)-Citrine fusion protein (YFP) (Figure 3-9). Therefore, after activation, expression and translation H2B–Citrine was used for quantification (Figure 3-14). In CHO cells, H2B-Citrine/YFP localizes to the cell nuclei, and the YFP signal was measured by flow cytometry after CHO hN1G4^{esn} reporter cells were cocultured with ligands for 48 hours.

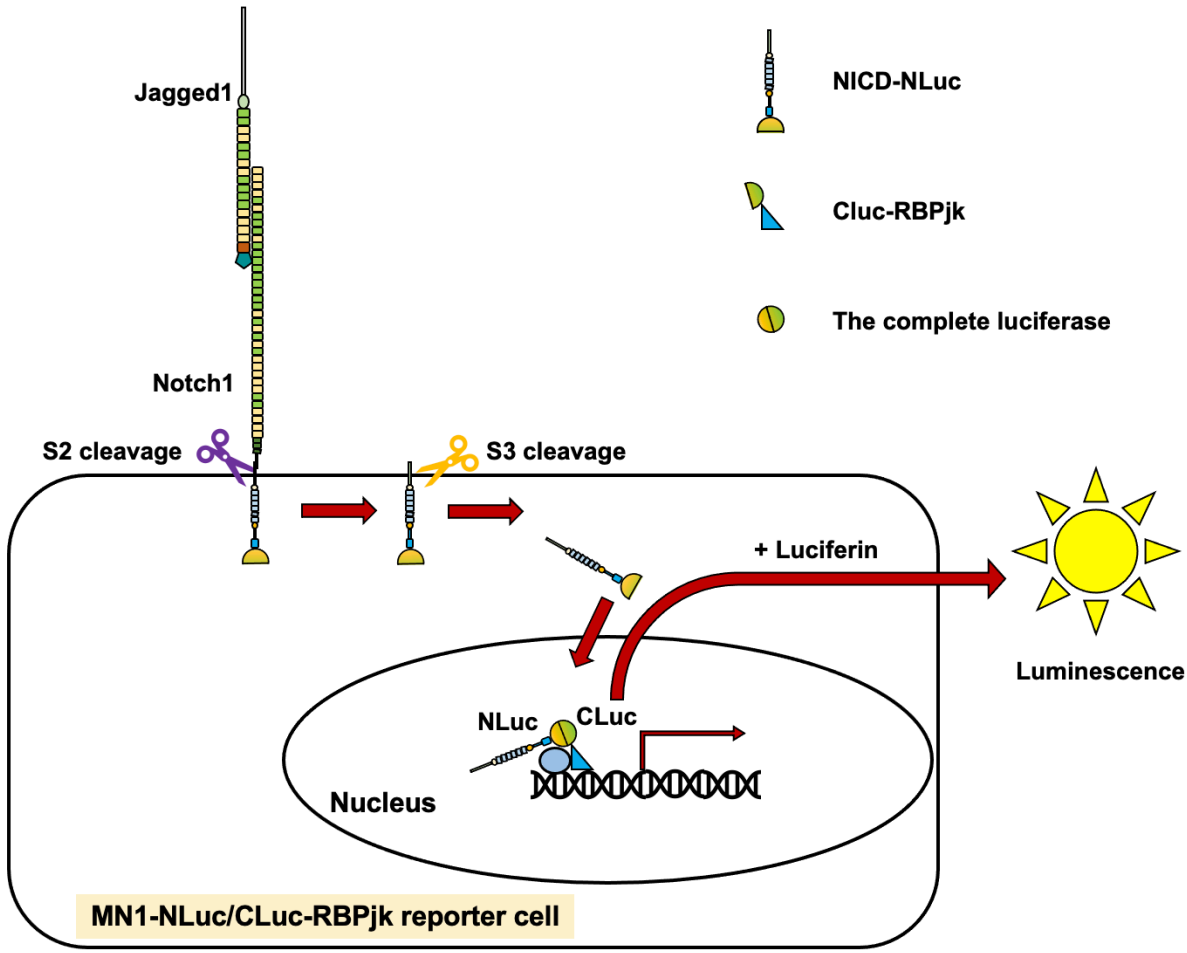


Figure 3-8. Schematic of mN1-NLuc/CLuc-RBPjk HEK reporter cell activation assay

The NICD of mouse Notch1 receptor is fused with N-terminal region of Luciferase (labelled NLuc, yellow semicircle). After ligand binding, S2 and S3 proteolytic cleavages occur, which release the NICD luciferase chimera to the nucleus. The NICD interacts with RBPjk which is fused to the C-terminal region of luciferase (labelled CLuc, green semicircle). This interaction leads to the association of N and C halves to produce a functional luciferase molecule. The HEK reporter cell produces a luminescent signal in the presence of substrate luciferin and ATP. Ligand utilised in this assay is a dimer, immobilised to a plate and comprises N-EGF3 portion, previously shown to activate Notch (Chillakuri et al., 2013) (Suckling et al., 2017).

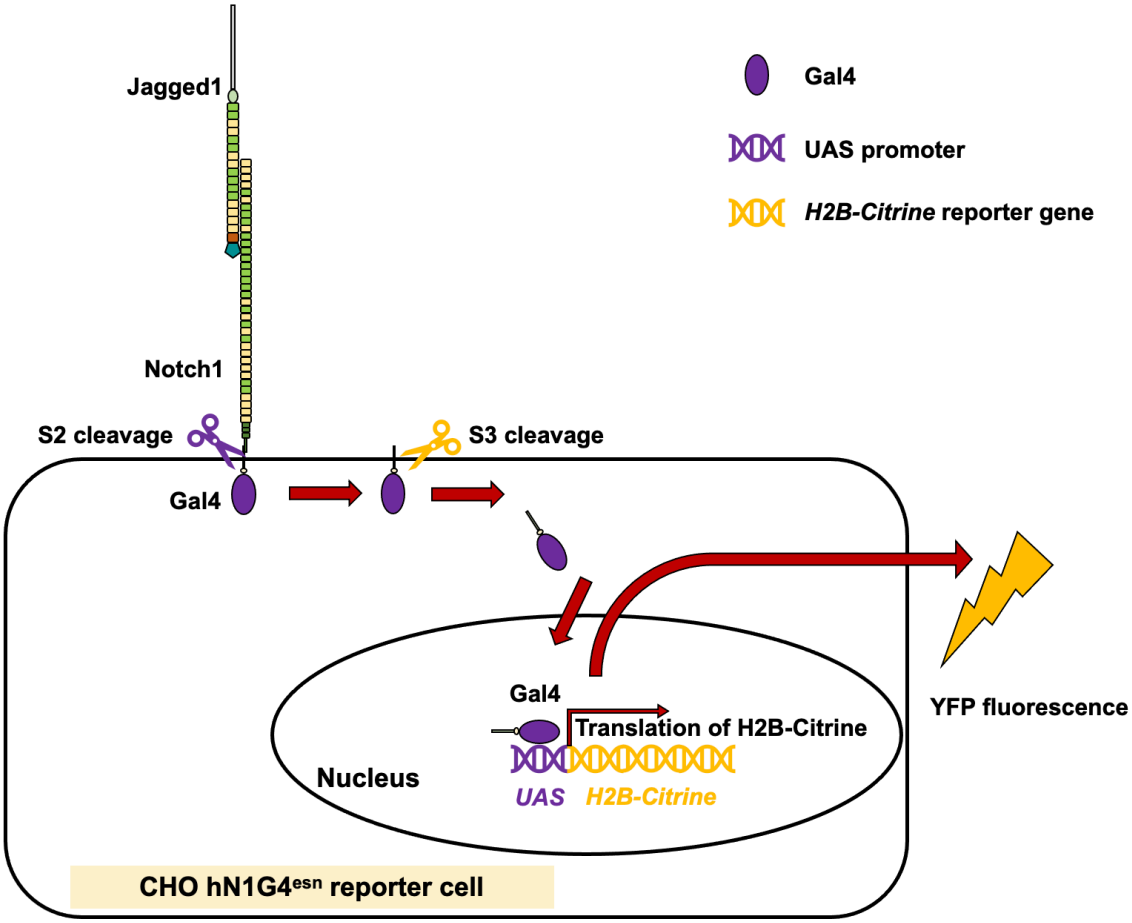


Figure 3-9. Schematic of CHO hN1G4^{esn} reporter cell activation assay

The NICD (from 1742 to 2556 amino acids) of human Notch1 was replaced by Gal4 (purple oval). H2B-Citrine cDNA (genome sequence is labelled in yellow) is stably integrated and linked to the UAS promoter (purple DNA sequence) and when expressed and translated is used as a fluorescent reporter. When human Notch1 is activated, Gal4 is liberated and translocates to the nucleus to initiate H2B-YFP gene expression. YFP signal from a population of cells was quantified using flow cytometry. Ligand utilised in this study is a dimer, immobilised to a plate and comprises N-EGF3 portion, previously shown to active Notch (Chillakuri et al., 2013).

It should be noted that the luciferase reporter system uses mouse Notch1 rather than human Notch1. However, these mammalian Notch1 receptors are identical in terms of domain organisation, each comprising 36 EGF domains in the extracellular domain. Sequence alignment of human and mouse Notch1 EGF11-12 showed that the amino acid sequence is highly conserved including key residues involved in ligand binding

(Figure 3-10). These data suggest that very small differences between human Notch1 and mouse Notch1 are not likely to impact on receptor activation by different mammalian species of ligand.

In addition to species differences between Notch1 receptors of these two reporter systems, they are generated in two different mammalian cell lines which are likely to have varying membrane compositions (Table 3-3). This will allow testing of whether different lipid compositions of cell membrane might affect Notch activation. Finally, two types of readouts, average luminescence versus distribution of YFP fluorescence in a cell population allows different levels of interrogation of the activation process. A summary of the key features of each reporter system is shown in Table 3-3.

	MN1-NLuc/CLuc-RBPjk reporter cells	**CHO hN1G4^{esn} reporter cells**
Cell line	HEK293 cells	CHO cells
Notch1 receptor	full length mouse Notch1 receptor*	human Notch1 receptor without intracellular domains
Reporter	luciferase complementation-based reporter	UAS/Gal4-based citrine (YFP) transcriptional reporter
Readout	luminescence plate reader	flow cytometry (excitation 488 nM, emission 525 nM)

Table 3-3. Comparison of two Notch activation assays

*In addition to mN1, a reporter system based on mN2 constructed similarly is also available.

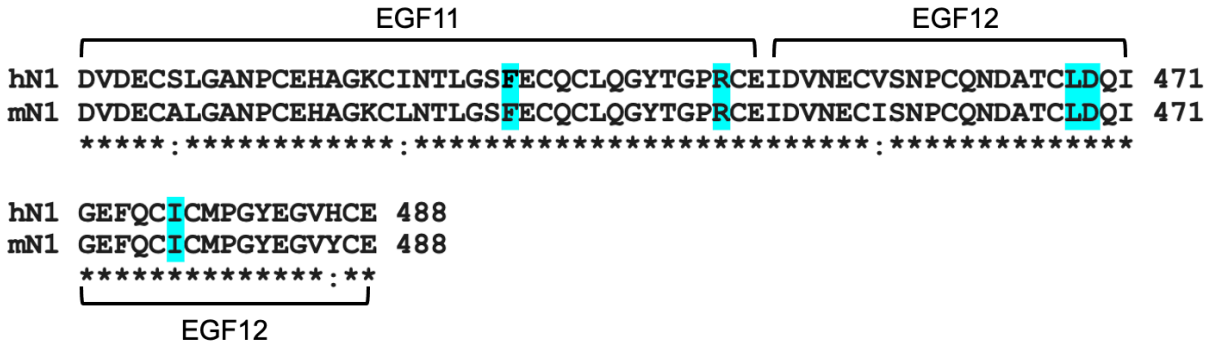


Figure 3-10. Amino acid alignment of human Notch1 and mouse Notch1 EGF11-12

The sequence of the human Notch key binding region, EGF11-12, was aligned with mouse Notch1 using sequence alignment software Clustal Omega 1.2.4. The sequence of EGF11 and EGF12 are indicated (from UniProtKB-P46531 and UniProtKB-Q01705). The key residues involved in ligand binding (Luca et al., 2017) are highlighted in blue. Positions which are absolutely conserved are indicated by "*", highly conserved ":".

3.6.2 Luciferase complementary-based reporter system

In order to establish the activation assay using mN1-NLuc/CLuc-RBPjk reporter cells, a series of controls were analysed first. These included two Notch binding-deficient variants, F207A and F207A/E228K, and a lipid-binding deficient variant, D140/144A (section 3.5.2), as well as wild type Jagged1 positive control (Suckling et al., 2017). Moreover, additional conditions containing no immobilised ligands, and either no ligands or reporter cells were included alongside to check background signal.

Initially purified Jagged1 constructs were immobilised to a 96-well cell culture plate, followed by washing steps and then seeding of reporter cells. In preliminary experiments, different concentrations of protein were added to each well to determine the saturation point (performed by Dr Boguslawa Korona, University of Oxford). In this experiment, all variants appear to have saturated the surface of 96-well plate similarly

(50 μL of 10 ng/μL purified proteins in HBS buffer were used in each well), as judged by signal obtained from using anti-His-HRP detection (data not shown).

Using luciferase reporter cells, three independent repeats demonstrate that all negative controls, F207A, F207A/E228K, D140/144A and empty wells with only reporter cells/only substrate, showed a substantial decrease in Notch activation compare to Jagged1 wild type (Figure 3-11). These data indicate that this assay can be used to test the effect of COSMIC variants on Notch activation.

One out of nine tested COSMIC variants, A58V, showed similar activation to Jagged1 wild type under the conditions of the assay used (Figure 3-11). Except A58V, all other eight COSMIC Jagged1 variants, including one DSL variant (E228K), caused a statistically significant decrease in Notch activation ($P < 0.0001$). Among Jagged1 variants giving lower Notch activation ability, three variants (V86F, T145N and E228K) showed extremely low activity (similar to binding deficient negative control variant F207A) and lower than D140/144A (Figure 3-11). The remainder D72N, G89E, G114D, L135F and S142N showed intermediate levels of activity greater than F207A and D140/144A. However, some of the data were observed to have a large spread (D72N, L135F, S142N).

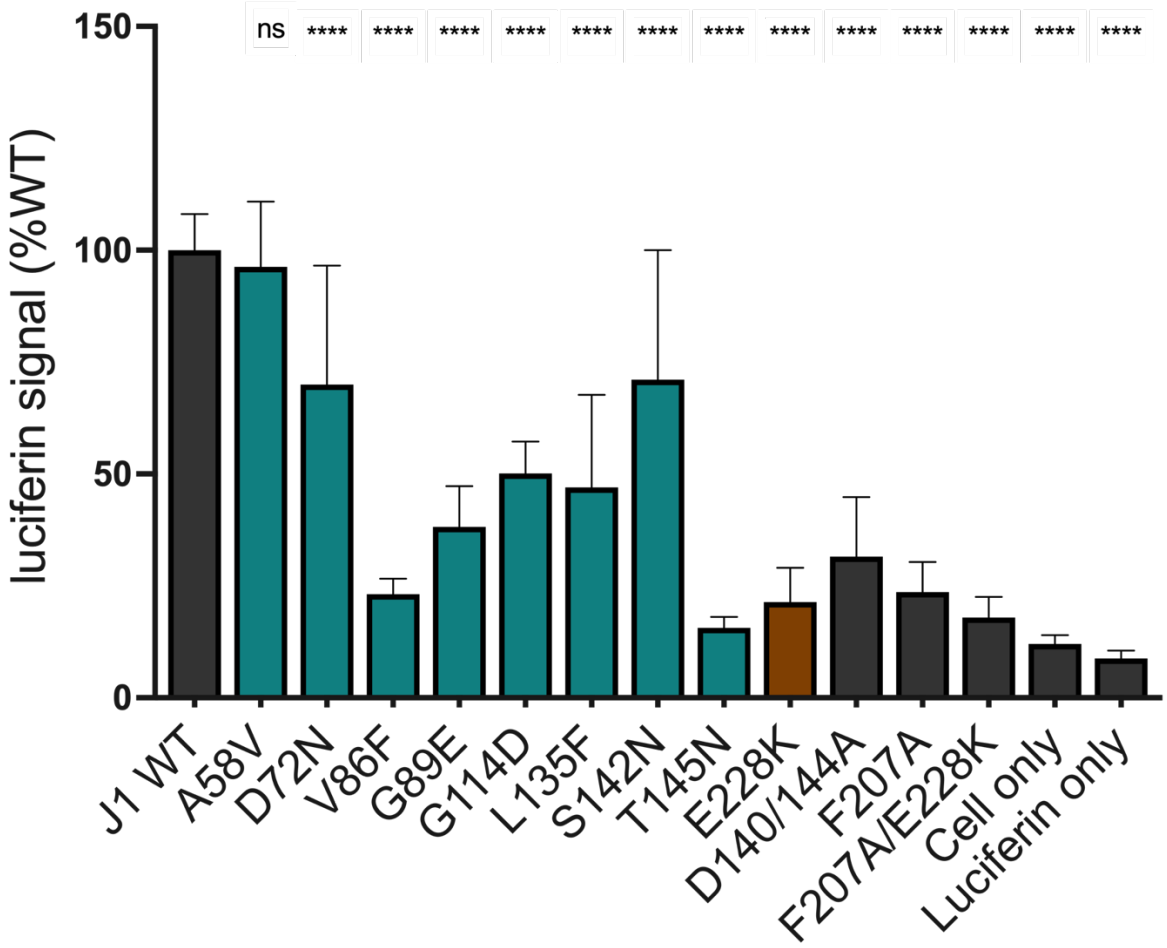


Figure 3-11. Split luciferase Notch activation assay of Jagged1 COSMIC variants by mN1-NLuc/CLuc-RBPjk reporter cells

Three independent experiments (each with 5 replicates) were performed, and data combined. The average value of activation by WT ligand was taken to be 100%. Results were expressed as a percentage of wild type activation and error bars denote the standard deviation for each data set. COSMIC variants showed high, intermediate and low levels of activity. Comparisons between two groups were performed with a two-tailed unpaired *t*-test. ****$P < 0.0001$, ns = no significant difference. Data were analysed with Prism 9 (GraphPad, San Diego, CA, USA). Controls are in dark grey, COSMIC variants in C2 (teal) in DSL (brown).

3.6.3 YFP (Citrine) transcription-based reporter system

A previously published CHO hN1G4^{esn} reporter cell line which uses a YFP fluorescent readout was established. These cells were a kind gift from Professor David Sprinzak. Cells were added to a 96-well tissue culture plate coated with purified Jagged1 variants (see section 3.5.2). Initial experiments were carried out to test whether or not the YFP-histone signal generated by ligand-dependent activation using wild type Jagged1$_{N\text{-}EGF3}$ protein could be observed directly using a fluorescence microscope (excitation 500 nm, emission 535 nm) (Figure 3-12). Jagged1$_{N\text{-}EGF3}$ F207A (section 3.6.2) and BSA coated wells were set up as negative controls. YFP signal in the nuclei of CHO cells was clearly observed in wild type sample wells after 48 hours incubation (Figure 3-12). Negative controls, F207A and BSA showed a lower level of YFP signal intensity compared to wild type Jagged1 under the same experimental conditions (Figure 3-12).

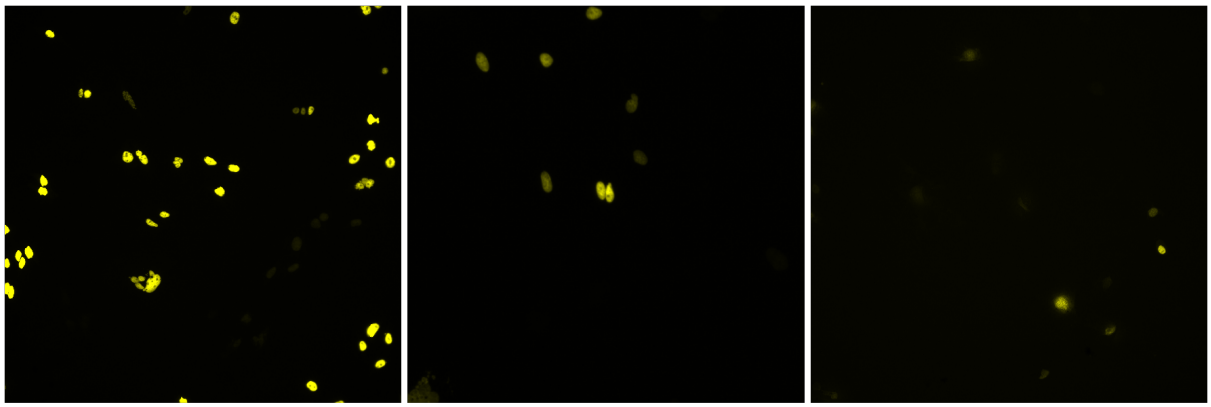


Figure 3-12. CHO hN1G4^{esn} cellular response to purified Jagged1 constructs

CHO hN1G4^{esn} reporter cells were cultured on a protein-coated 96-well plate at 2×10^4 cells/mL. Images were acquired after 24 hours through an DeltaVision Core system, Olympus inverted microscope (excitation 500 nm, emission 535 nm). Fluorescence was clearly enriched in nuclei. More YFP signal was observed in the Jagged1 WT sample than F207A and BSA samples. Images were analysed with Image J (Schindelin et al., 2012).

In order to test Jagged1 COSMIC variants in a high through-put manner and quantify data more precisely, YFP signal intensities from cell populations were detected by flow cytometry. Before testing COSMIC variants, Jagged1 wild type and BSA samples were analysed first to optimise the gating strategy and make sure this method can effectively measure the Notch activation difference (Figure 3-13). CHO cells were first gated through forward scatter versus side scatter to identify single cell population, and single cells were further gated using forward scatter versus pulse width to exclude YFP signal from cell aggregations (Figure 3-13). FACS data was acquired at excitation 488 nm, emission 530/40 nm. From a YFP histogram comparison of BSA and Jagged1 wild type cells, a clear rightward shift of YFP signal distribution was observed, which indicated cells plated on Jagged1 wild type expressed more YFP (Figure 3-13).

Negative controls were then tested prior to COSMIC variant analysis alongside wild type Jagged1. Notch binding deficient variants, F207A and F207A/E228K, that previously showed a decrease in Notch activation by the luciferase complementation-based assay were used, together with the lipid-binding-deficient negative control D140/144A. In addition, BSA was also coated onto the plate to check for any background YFP signal from CHO hN1G4^{esn} reporter cells. As for the luciferase complementation assay, wells were saturated by individual ligands so that each well had an equal amount of protein bound.

Clear differences between wild type and negative controls were observed (data not shown) which allowed subsequent testing of all COSMIC variants. Following three independent assays, among all COSMIC variants, the YFP signal distribution from cell populations plated onto A58V and L135F were similar to wild type (Figure 3-14). Seven

out of nine COSMIC variants (D72N, V86F, G89E, G114D, S142N, T145N and E228K) showed decreased YFP expression indicative of lower levels of Notch activation (Figure 3-14). These variants can be further distinguished into “intermediate “(D72N, G89E, G114D, S142N) and “low” (V86F, T145N, E228K) groups. In the “intermediate” group, the peak/modal value lies between wild type and the lipid binding deficiency negative control, D140/144A, while in the “low” group, the peak of the distribution is similar to the negative controls and lower than signal obtained for D140/144A. In conclusion, the Notch activation results from the YFP reporter system are in agreement with those obtained from the luciferase system except there is no histogram shift obtained for L135F variant.

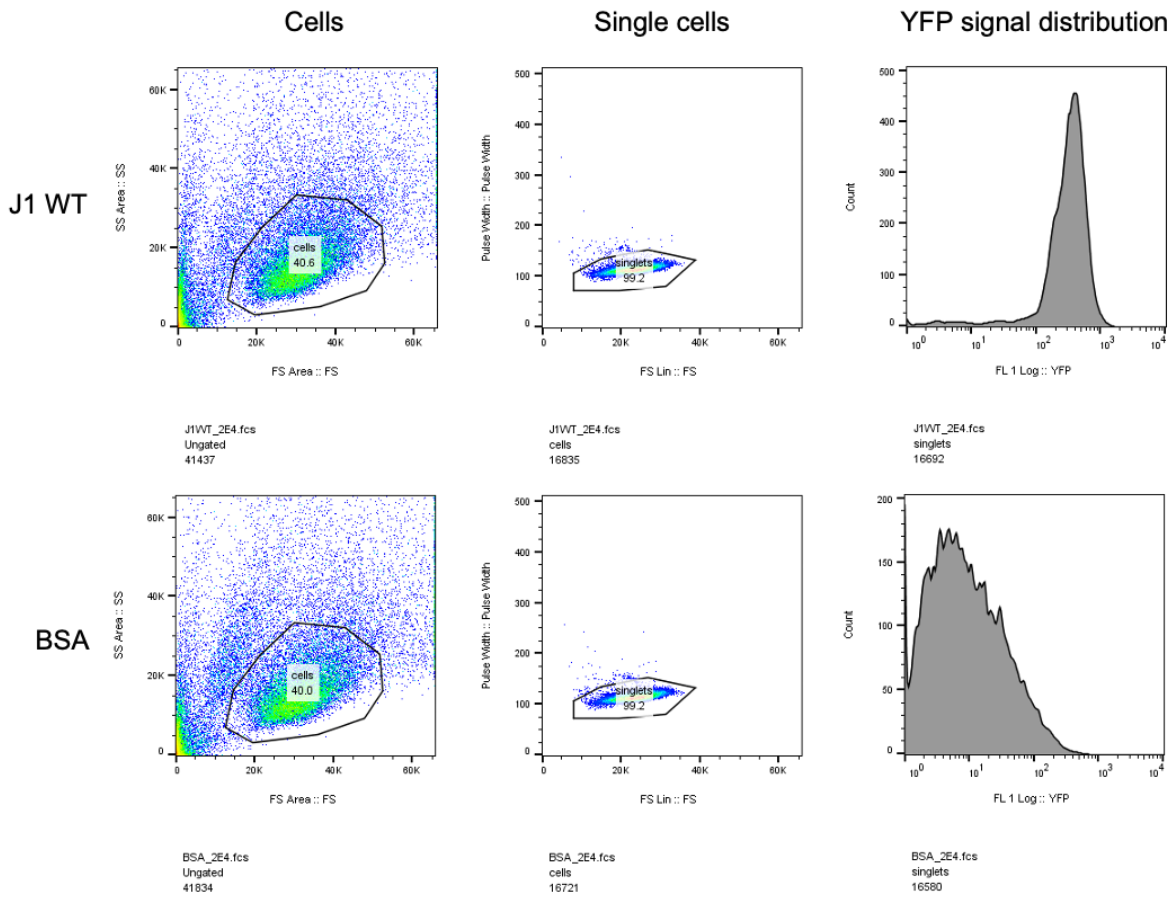


Figure 3-13. CHO hN1G4esn reporter cell Notch activation assay gating strategy

Flow cytometry plots of CHO cells incubated with Jagged1 wild type and the negative control (BSA). Following 48 hours incubation, cells were removed from plate wells. Total cells were first gated on a forward scatter vs side scatter analysis. These cells were then further gated for single cells by forward scatter/pulse width. YFP fluorescence distribution from these cells was indicated by log YFP fluorescence/cell count. The distribution of Jagged1 wild type cells was compared to BSA and showed a rightward shift, indicative of increased YFP fluorescence.

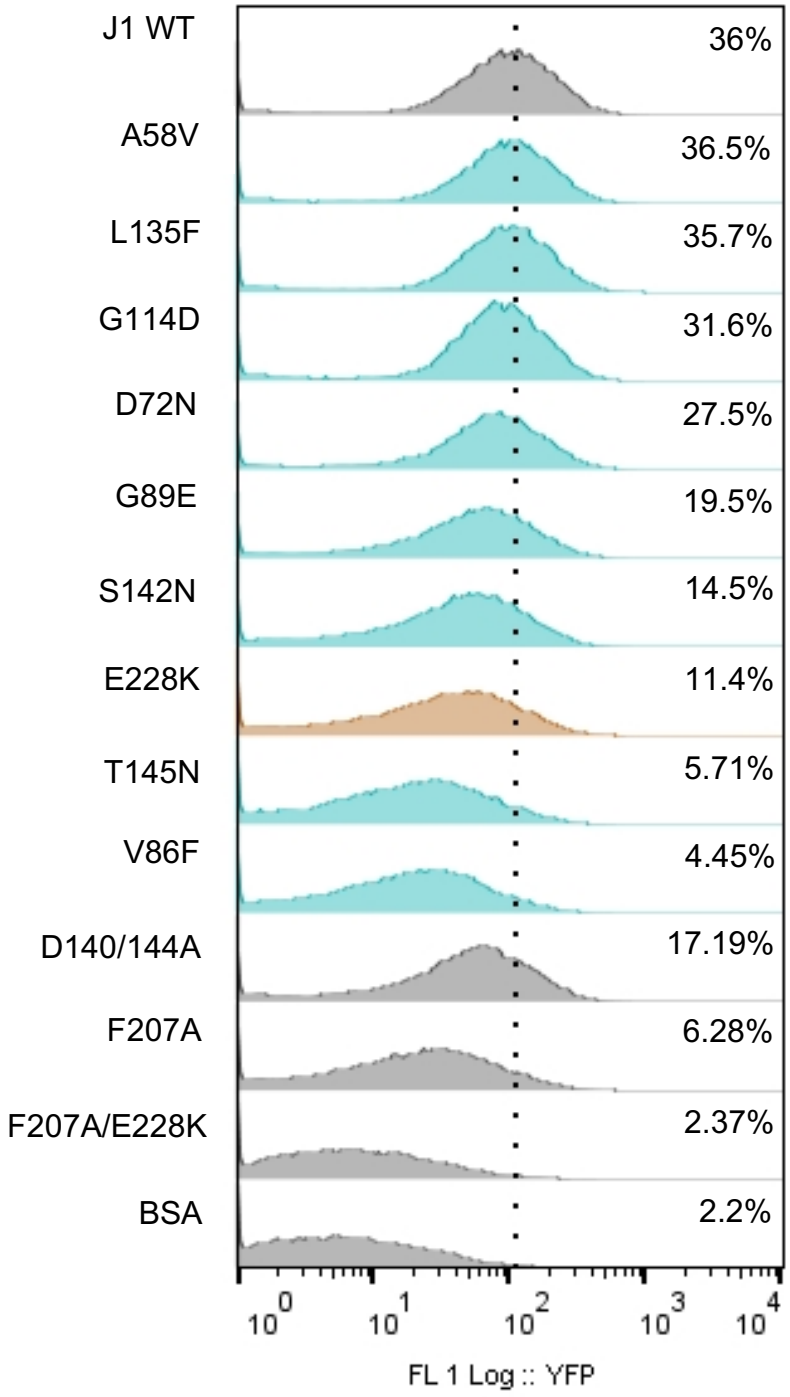


Figure 3-14. Notch activation assay of COSMIC variants using CHO hN1G4esn cells

Flow cytometry histograms of COSMIC variants (C2-teal, DSL-brown) with Jagged wild type and negative controls (grey). The horizontal axis shows the intensity of the YFP signal, and the vertical axis indicates the number of cells. The vertical dotted line indicates the peak max (mode) of a distribution from cells plated on Jagged1 wild type, and the fraction of cells for each sample above this value is shown as percentage. Three independent experiments were performed, and data from 6,000 single cells were recorded for each variant. Data were acquired by CyAn ADP compact benchtop flow cytometer (Beckman Coulter) and analysed by FlowJo®_V10. FACS data were acquired at excitation 488 nm and emission 530/40 nm to identify YFP fluorescence intensity.

3.7 Summary of COSMIC variants (expression and activity)

In this chapter, 13 missense mutations affecting amino acids within the Jagged1-C2 domain were selected from the COSMIC database. 12 of them behaved as loss of function variants (Table 3-4). Four (F35L, G47R, T133R and W139S) out of 13 variants affected Jagged1 ligand folding and resulted in poor or absent secretion into media (Table 3-4). F35L, T133R and W139S are located in the beta sheet of the hydrophobic core of Jagged1-C2, and the other folding deficiency variants, G47R, is at the end of loop sequences and close to the core, and G is a residue which perform key structural roles (Table 3-4) (Figure 3-3). Consistent with observations from Alagille syndrome (section 1.2.2.2 and 3.1), substitutions which affect the hydrophobic core result in misfolding and cellular retention.

After successful purification of all secreted COSMIC variants, activation assays based on two different reporter systems were performed to test whether or not the amino acid substitutions had an effect on Notch activation. All but one (A58V) of the secreted variants showed a decrease in Notch activation, which indicated loops 1-2, 2-3, 3-4 and 5-6 within the C2 domain are all important for Notch signal generation (Figure 3-11) (Figure 3-14) (Table 3-4). In general, there was good agreement between the system used, which gives more reliability in results, except L135F showed a decrease in Notch activation using mN1-NLuc/CLuc-RBPjk reporter cells (HEK cell origin) but not CHO hN1G4esn reporter cells (Figure 3-11) (Figure 3-14) (Table 3-4). This demonstrated Jagged1 might interact differently with HEK293 and CHO cell membranes, although in the absence of detailed knowledge of membrane composition and levels of Notch available for transactivation, this remains unproven. Alternatively, this might suggest the interaction between Jagged1 and mouse Notch1 is slightly

different from its interaction with human Notch1. A58V showed no effects on Notch activation, which demonstrates that some mutations found in cancer cells might not contribute to cancer.

Domain	Missense mutation	Position at C2 domain	Secretion	Luciferase Notch1 activation	CHO-YFP Notch1 activation
C2	F35L	beta sheet 1	X	n/a	n/a
C2	G47R	loop1-2	X	n/a	n/a
C2	A58V	loop1-2	✓	no effect	no effect
C2	D72N	loop1-2	✓	intermediate[1]	intermediate[2]
C2	V86F	loop2-3	✓	low[1]	low[2]
C2	G89E	loop2-3	✓	intermediate[1]	intermediate[2]
C2	G114D	loop3-4	✓	intermediate[1]	intermediate[2]
C2	T133R	beta sheet 5	X	n/a	n/a
C2	L135F	beta sheet 5	✓	intermediate[1]	no effect
C2	S142N	loop5-6	✓	intermediate[1]	intermediate[2]
C2	T145N	loop5-6	✓	low[1]	low[2]
C2	W139S	beta sheet 5	X	n/a	n/a
DSL	E228K	n/a	✓	low[1]	low[2]

Table 3-4. Summary of COSMIC variant effects on secretion and activation

"Intermediate" variant was defined as having an activity (%WT)[1] or a peak maximum[2] which occurs at greater or similar fluorescence intensity compared to D140/144A, but lower than the WT distribution. A "low" variant has activity (%WT)[1] or a peak maximum[2] which occurs at a lower fluorescence intensity than D140/144A. Note that S142N showed a similar distribution as D140/144A in individual repeat experiments and is classed as "intermediate".

Chapter 4. Study of the functional importance of N-glycosylation in the C2 domain of Jagged1

4.1 Introduction

As discussed in Chapter1, the regulation of Notch signalling by O-glycans has emerged as an important post-translational means of signal transduction modulation in both *Drosophila* and mammalian experimental systems (section 1.4). Both Notch ligands and receptors contain many consensus O-glycosylation sites. These post-translational modifications within the Notch receptor are known to modulate signalling by altering ligand binding and receptor activation (Taylor et al., 2014) (Luca et al., 2015) (Luca et al., 2017). Sugar modifications of Notch ligands are less well studied compared to Notch receptors. It was found recently that O-glycosylation of Jagged1 EGF domains contributes to the autosomal dominant peripheral nerve disease, Charcot-Marie-Tooth disease type 2 (Sullivan et al., 2020). For N-glycans, there are several N-glycosylation consensus sequences present in both ligands and receptors (e.g., in humans, 9 in Jagged1, 4 in DLL4 and 6 in Notch1). However, the biological function of N-linked sugars present on Notch ligands and receptors is unclear.

The general roles of N-glycans on extracellular/cell surface proteins are many; they can mediate protein-protein interactions outside the cell, and also facilitate protein quality and folding inside the cell (Varki, 2017). Thus, many biological processes, such as inflammation, extracellular matrix biosynthesis, cell proliferation and differentiation rely on N-glycosylation (Reily et al., 2019) (Li et al., 2021). One COSMIC Jagged1 variant, T145N, was found to destroy an N-glycan motif, NDT to NDN, on loop 5-6 of C2 domain, and was shown to dramatically decrease Notch activation tested in both CHO hN1G4esn and mN1-NLuc/CLuc-RBPjk cells (Chapter 3). The occupancy of this site in the WT ligand is likely since T145N showed a drop in MW on purification compared to WT and an N-glycan on loop 5-6 of Jagged2 is shown by crystallography

using protein expressed by *Drosophila* cells. The α(1,6)-linked fucose on this site packs against a Tryptophan, which may stabilise the loop structure at the apex of C2 domain (Suckling et al., 2017). In addition, an N-linked sugar is seen in a homologous position in the crystal structure of *Drosophila* Delta (Martins et al., 2021a). The aim of this chapter is to confirm the presence of the N-glycan on Jagged1-C2 domain and establish its importance for Notch activation. This was performed using site-directed mutagenesis to change the N-glycan consensus motif directly. Alongside, a DSL-N-glycan site was also mutated as a control. Mass spectrometry glycoproteomic analysis of wild type Jagged1N-EGF3 was performed to confirm the presence and type of N-glycan on loop5-6 or the DSL domain. Subsequently, variants lacking N-glycosylation motifs were purified using the HEK293T expression system. The effect of the different amino acid substitutions on Notch activation was tested using Notch1 and Notch2 HEK-luciferase, Notch1 CHO-YFP reporter cells, and in a primary smooth muscle cell differentiation assay. PNGase F digestion of purified WT protein was also performed and activity was analysed using CHO-YFP reporter cells.

4.2 Conservation of the C2 N-glycosylation site in Jagged ligands

Since conservation of sequence can indicate biological importance, an amino acid alignment of loop 5-6 sequences from both Jagged and Delta like family ligands across diverse species, including human, rat, mouse, chicken, frog, zebrafish, and *Drosophila*, was performed (Figure 4-1). This analysis showed that the N-glycan site in the C2 domain is highly conserved in Jagged (in Jagged1 residue N143) but not Delta-like family ligands across species. However, an exception is *Drosophila*, where the NXT/S sequence exists in both Serrate and Delta ligands (Figure 4-1). Other than the C2

domain, DSL to EGF3 sequences on Notch ligands were also screened for N-glycosylation motifs.

It was noted that another N-glycosylation site exists within the DSL domain of Jagged1. Comparative alignment of DSL amino acid sequences from diverse species was performed (Figure 4-2). It showed that the N-glycan consensus motif incorporating N217 exists in Jagged1, but not Jagged2, of aligned species including human, rat, mouse, and zebrafish. It was also observed in frog and *Drosophila* Serrate, but not chicken. However, the N-glycan motif in *Drosophila* Serrate-DSL is located at a different position (Figure 4-2). In Delta-like ligands, this DSL N-glycan site is only found in human DLL4. Compared to the consensus N-glycosylation site in the C2 domain, the motif in the DSL domain in Notch ligands is less well conserved.

Other than these two N-glycosylation motifs, no other motifs were found within C2 to EGF3 domain sequences. As the COSMIC variant T145N showed a substantial decrease in Notch activation and the N-glycan motif at loop5-6 was highly conserved across various species in the Jagged ligand family, we hypothesized that the N-glycan on the loop5-6 of C2 domain might be important for Notch activation.

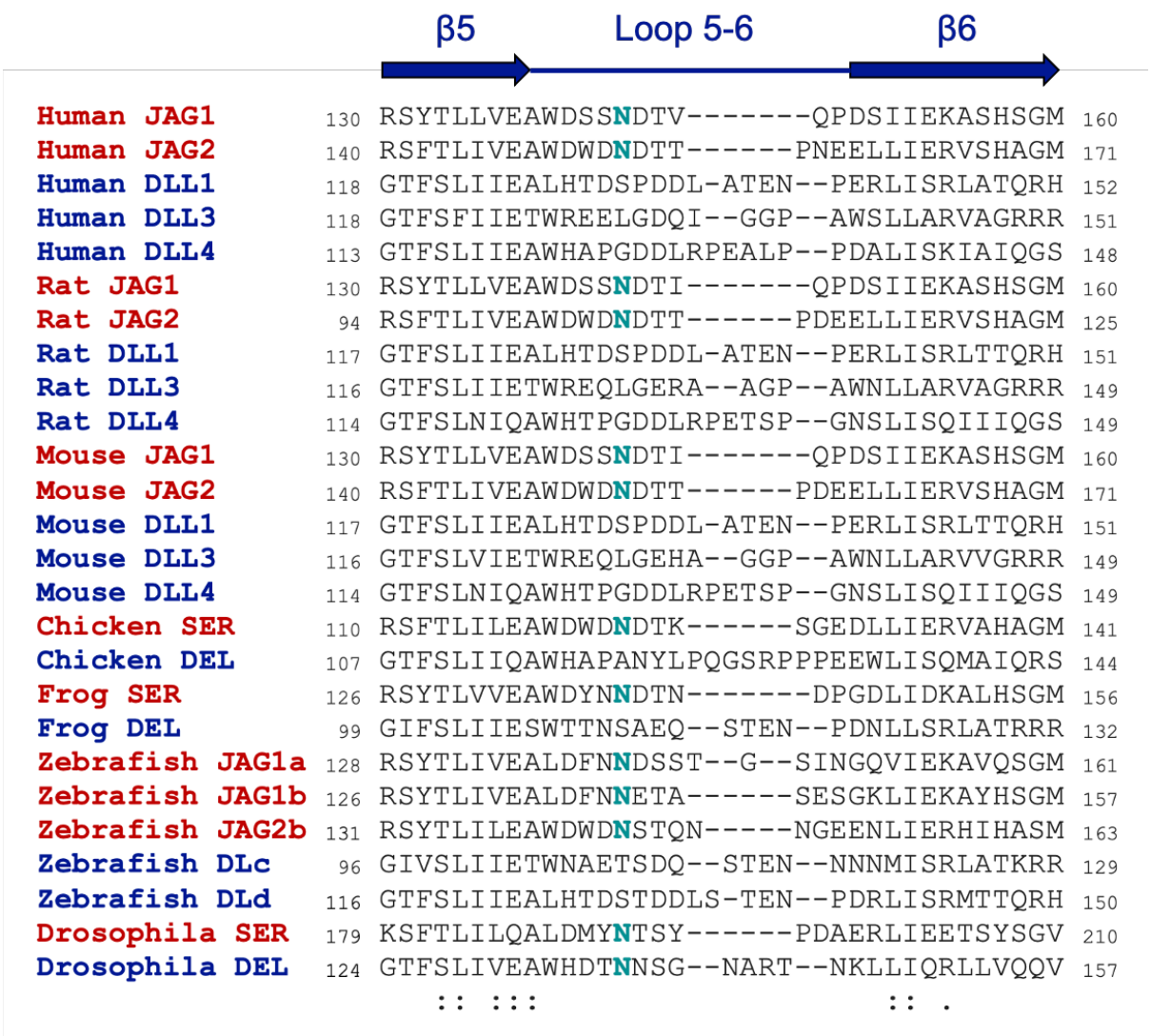


Figure 4-1. The N-glycosylation motif within the C2 domain of Notch ligands is highly conserved in loop 5-6 of Jagged family and *Drosophila* ligands

Amino acid alignment of the loop 5-6 region across various species. Name of species is indicated on the left (Jagged family ligands are in red and Delta-like family ligands are in blue), and numbering of the amino acid sequence is indicated on the left and right. N-glycan sites are highlighted in teal. The position of loop 5-6 and beta strands either side is indicated at the top. (:) indicates residues exhibiting strong similarity (scoring > 0.5 in the Gonnect PAM 250 matrix, Thompson et al., 1994). (.) indicates a site showed weak similarity (corresponds to a score of 0.5 or less in the Gonnect PAM 250 matrix). Note that the N-glycan site at loop 5-6 in C2 domain is absolutely conserved in the Jagged family and both *Drosophila* ligands. Amino acid sequence of each species was provided by UniProt. The alignment was generated with Clustal Omega (1.2.4) multiple sequence alignment programme.



Figure 4-2. The N-glycosylation motif within the DSL domain of Notch ligands is less conserved

Sequence alignment of the DSL region across various species showed less conservation of the N-glycosylation motif. Labelling as in Figure 4-1. N-glycan modification positions are highlighted in teal. Positions fully conserved are labelled by an asterisk (*), weak similarity (.). The N-glycan within the DSL domain exists in human, rat, mouse, zebrafish Jagged1, human DLL4, and frog, *Drosophila* Serrate. Amino acid sequence of each species was obtained from UniProt. The alignment was generated with Clustal Omega (1.2.4) multiple sequence alignment programme.

4.3 Target sites for mutagenesis and secretion tests

Two additional single amino acid substitutions that eliminate the N-glycosylated residue in C2 (N143A) and DSL (N217A) domain of human Jagged1 were introduced within pHL-sec-Jagged1$_{N\text{-}EGF3}$-Fc-His$_6$ construct for further study. Both were generated through overlap extension PCR mutagenesis (see Materials and Methods). Plasmids encoding variants were sequenced (Sanger sequencing service provided by Source Bioscience) to confirm that the desired DNA sequence had been obtained. N143A and N217A were then analysed alongside two COSMIC variants, T145N and S142N, to study the effect of N-glycan on Notch signalling. S142N was included, since this altered a loop 5-6 residue, but retained the N-glycan site (Figure 4-3).

The effects of these protein-engineered substitutions on Jagged1 folding and trafficking were analysed by western blot. After four days post-transient transfection of HEK293T cells, cell lysate and medium samples were collected for reducing SDS-PAGE electrophoresis (Figure 4-4). Jagged1$_{N\text{-}EGF3\text{-}Fc\text{-}His}$ construct expression was detected by anti-His-HRP antibody. Clear bands were present in wild type lysate and medium samples, but not the negative controls (HEK293T cells mock transfected) (Figure 4-4). Same volume of medium samples was analysed, and three independent repeats were performed to obtain reliable results, although no proper loading control could be used to assess extracellular medium samples. Similar intensity of immunoreactive bands can be observed in all N-glycan related variants (S142N, T145N, N143A and N217A) cell lysate and medium samples compared to the wild type (Figure 4-4). This suggests all variants were expressed by cells at equivalent levels to the wild type and were trafficked similarly. Note that WT and S142N samples migrate

at a higher molecular weight compared to T145N, N143A and N217A, suggestive of changes in N-glycosylation (Figure 4-4). This is particularly evident in medium samples.

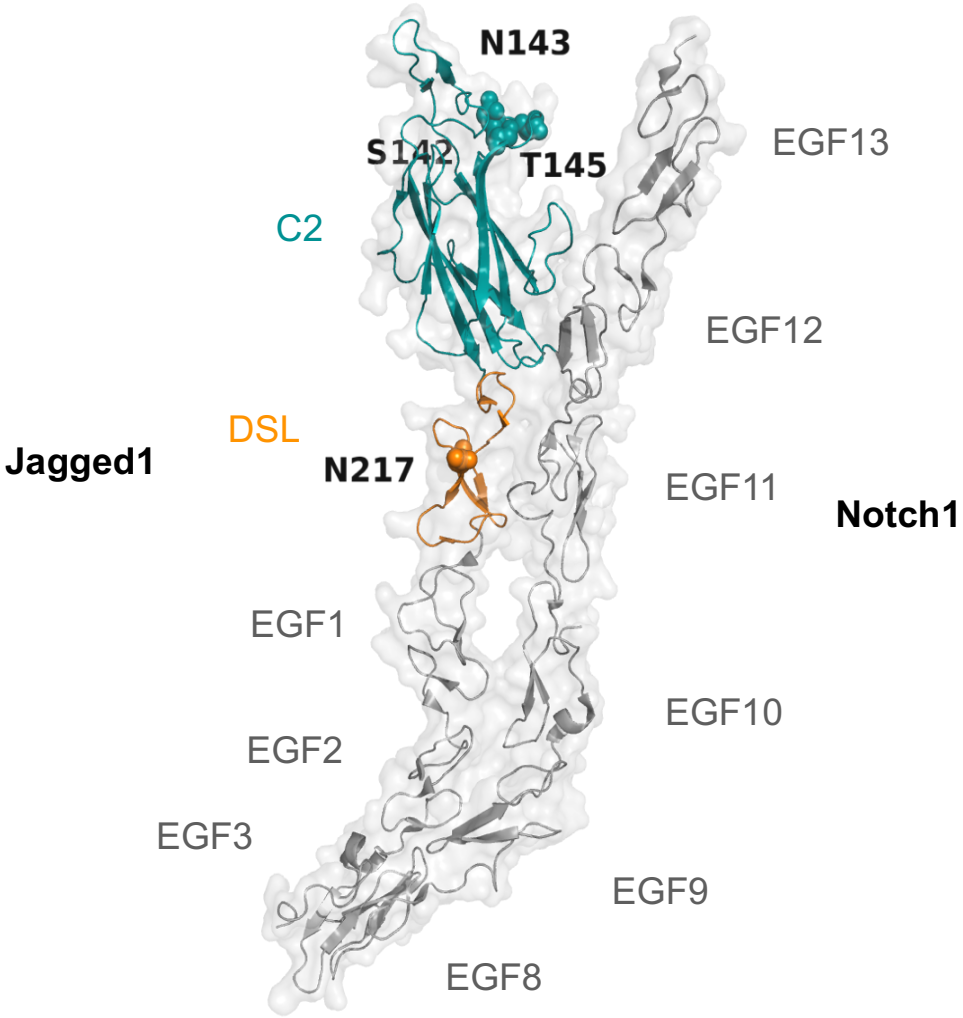


Figure 4-3. Structure of Jagged1 NE3 fragment with selected N-glycan variants labelled

Human Jagged1/Notch1 complex showing position of N-glycan related substitutions (highlighted as spheres). Protein engineered N143 and N217 are shown together with previously described COSMIC S142, T145. This PyMOL model is produced from the alignment of PyMOL code 5uk5 (Human Jagged1 N-EGF3 and Notch1 EGF8-12 complex) and 2vj3 (Notch1 EGF11-13). The C2 domain is in teal, the DSL domain is in orange, and EGF domains are in grey.

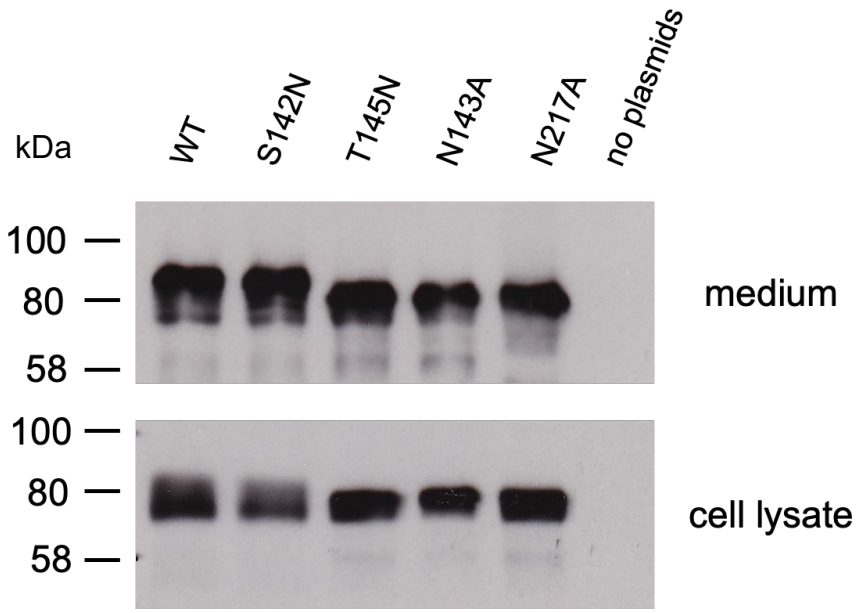


Figure 4-4. Western Blot analysis of cell lysate and medium samples of Jagged1 N-glycan related variants

Expression of protein engineered Jagged1 N-glycan variants N143A and N217A compared with Jagged1 wild type, COSMIC variants S142N and T145N, and the negative control (no plasmid transfected) analysed by Western Blot. Equivalent volumes of medium were collected for reducing 10% SDS-PAGE, and Jagged1 protein expression detected by a monoclonal anti-His-HRP rabbit antibody (1: 2000), although no proper loading control could be used to assess extracellular medium samples. The same approach was taken for cell lysates, although ideally a loading control such as probing for tubulin should have been included to infer changes in expression levels. All Jagged1 N-glycan related variants are secreted similarly to Jagged1$_{\text{N-EGF3-Fc-His}}$ wild type construct. Note the slightly higher molecular weight of WT and S142N. Three independent repeats were performed, and a representative western blot is shown.

4.4 Protein purification and PNGase F digestion of Jagged1 N-glycan variants

4.4.1. Purification of N-glycan variants

Jagged1 N-glycan variants were expressed by HEK293T cells following transient transfection and purified. Conditioned media samples were collected after four days of transfection, and cells were removed by spinning and filtering. Jagged1 glycan variants were purified according to the standard Jagged1 protocol (see materials and

methods and Chapter 3). The final purification products were visualised by 10% SDS-PAGE under both reducing and non-reducing conditions. All N-glycan related variants showed a near homogenous product (Figure 4-5). As suggested by western blotting of extracts, variants with an altered N-glycosylation motif (T145N, N143A and N217A) were found to have a drop in molecular weight, whilst S142N showed a similar mobility to the wild type (Figure 4-5). These changes in molecular weight were more distinct under reducing conditions than non-reducing conditions. To confirm this molecular weight drop was caused by the loss of N-glycan, a PNGase F digestion experiment was further performed.

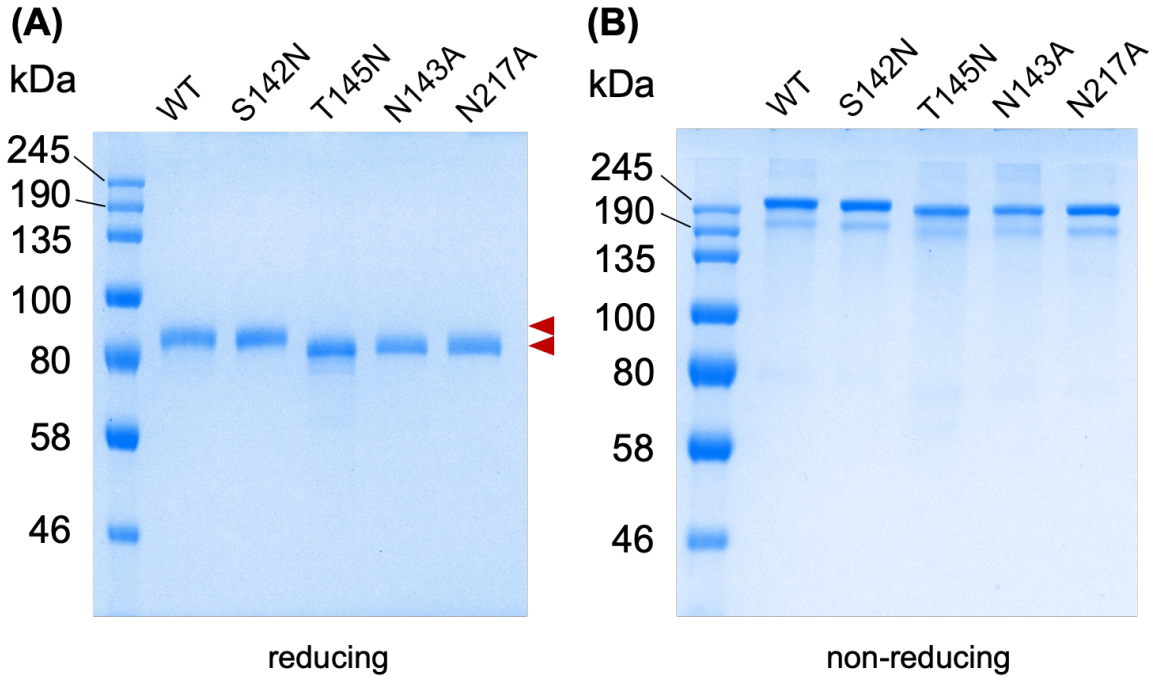


Figure 4-5. Final purification products of Jagged1$_{N\text{-}EGF3\text{-}Fc\text{-}His}$ N-glycan variants

The final purification products of wild type and N-glycan variants after IMAC and SEC analysed by 10% SDS-PAGE under reducing (A) and non-reducing (B) conditions to confirm the purity of the protein. All N-glycan variants showed more than 90% purity. Variants with altered N-glycan motif (T145N, N143A and N217A) showed a reduction in molecular weight compared to the wild type and S142N. The two different bands positions under reducing conditions are indicated by red arrowheads.

4.4.2. PNGase F digestion of Jagged1 N217A monomer

There are three N-glycosylation motifs within the Jagged1$_{N\text{-}EGF3\text{-}Fc\text{-}His}$ fusion construct. In addition to Asn143 site in C2 and Asn217 in DSL, Asn425 on the Fc tag is also a potential N-glycosylation site. To confirm the presence of an N-glycan in the C2 domain and demonstrate that the faster migration of T145N and N143A variant was caused by loss of the sugar modification in C2, a Jagged1$_{N\text{-}EGF3\text{-}Avi\text{-}His}$ N217A monomer construct lacking the Fc-tag was generated for a PNGase F digestion experiment. This N217A monomer construct contains only one N-glycosylation consensus sequence which is located in the C2 domain. PNGase F is the most effective enzyme for removing an N-linked sugar complex. It catalyses cleavage between the innermost GlcNAc and the asparagine residue and converts the asparagine to aspartate thereafter.

Jagged1 $_{N\text{-}EGF3\text{-}Avi\text{-}His}$ wild type construct was previously cloned into the pHL-sec vector by Dr Chandramouli Chillakuri. This plasmid was used as template to produce Jagged1$_{N\text{-}EGF3\text{-}Avi\text{-}His}$ N217A substitution by overlap extension mutagenesis. After confirmation of the correct base change by Sanger sequencing, the N217A monomer variant was then expressed by HEK293T cells and purified from culture medium following a protocol utilized previously for the Jagged1 Fc dimer constructs. The final Jagged1$_{N\text{-}EGF3\text{-}Avi\text{-}His}$ N217A purification product showed an estimated purity of 90% by non-reducing and reducing 12% SDS-PAGE (Figure 4-6).

Jagged1 N217A monomer was incubated with PNGase F enzyme overnight at 37°C (see Chapter 2 - Materials and Methods). A positive control, N217A variant, was set up alongside and treated similarly except without the addition of PNGase F. These

constructs were then analysed by 12% SDS-PAGE under both non-reducing and reducing conditions (Figure 4-6).

The positive control protein migrated to a similar position as the N217A monomer starting material under both conditions indicating no degradation over the course of the digestion (Figure 4-6). Two bands were observed in PNGase F digested samples. The upper protein band (37 kDa) showed an increase in mobility compared to the undigested positive control and N217A starting material under both reducing and non-reducing conditions. In addition, this upper band was less broad than the positive control and the normal sample (Figure 4-6). The molecular weight of the lower band is around 36 kDa, which is the expected molecular weight of PNGase F (Figure 4-6). Since removal of the single N-glycan from monomeric material results in a MW drop, these data suggest that the lower molecular weight observed previously (Figure 4-5) is caused by the loss of the C2 domain N-glycan and not due to any effect of the amino acid substitution.

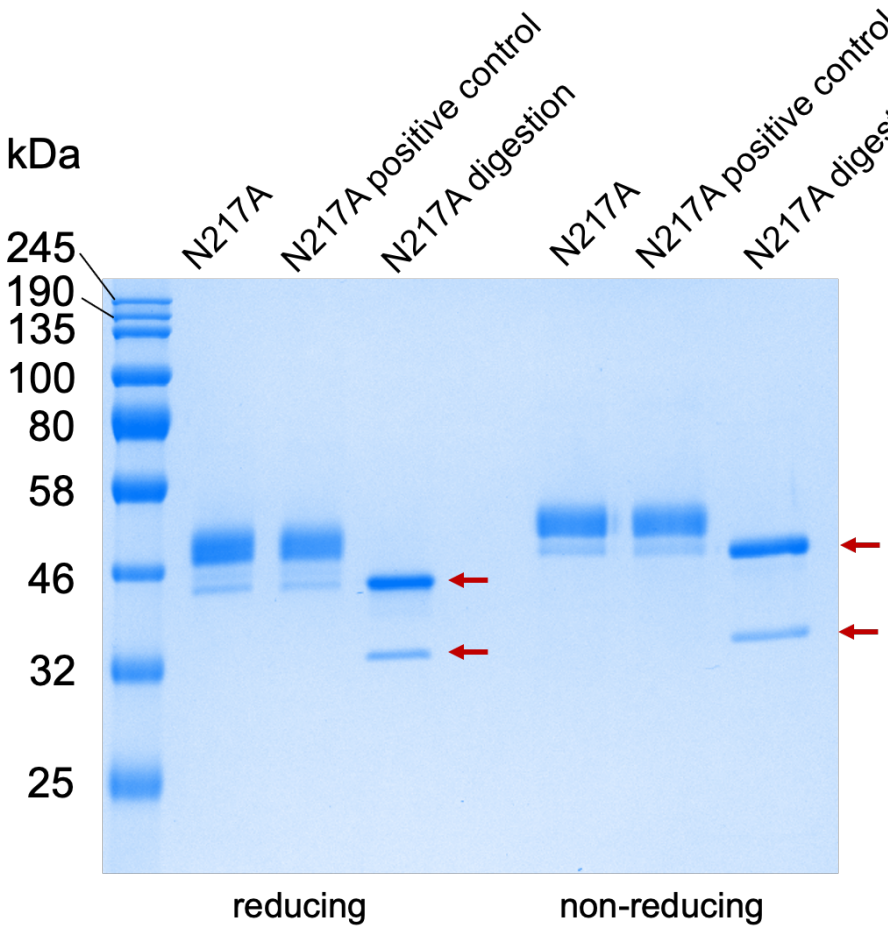


Figure 4-6. PNGase F digestion of N217A monomer showing a reduction in molecular weight

The final purification product of Jagged1$_{\text{N-EGF3-Avi-His}}$ N217A ("N217A") and PNGase F digested samples ("N217A digestion") alongside with the positive control ("N217A positive control") were analysed by 12% SDS-PAGE (reducing and non-reducing) and stained with Coomassie blue. Two bands were present in the PNGase digest samples (arrowed). The upper band showed the N217A monomer expected molecular weight (37 kDa), and the lower band showed an expected size of PNGase F (36 kDa). N217 digestion sample showed a sharper band compared to this construct without digestion, as well as a MW drop, suggesting loss of N-glycosylation. Three independent repeats were performed, and one representative figure is shown.

4.5 Mass spectrometry based glycoproteomic analysis of Jagged1 N-glycan

To investigate the N-glycan composition of human Jagged1 N-EGF3, mass spectrometry was performed. The N-glycan biosynthesis pathway includes consecutive enzymatic steps, which occur in the ER and Golgi complex. All eukaryotic N-glycans share common core sequences containing two GlcNAc residues and three mannose residues (Figure 4-7). N-glycans can be classified into three types: 1) oligomannose, 2) complex and 3) hybrid, dependent upon the types of sugar which extend the core (Figure 4-7). In addition, core fucosylation is a common modification of vertebrate N-glycans (Figure 4-7).

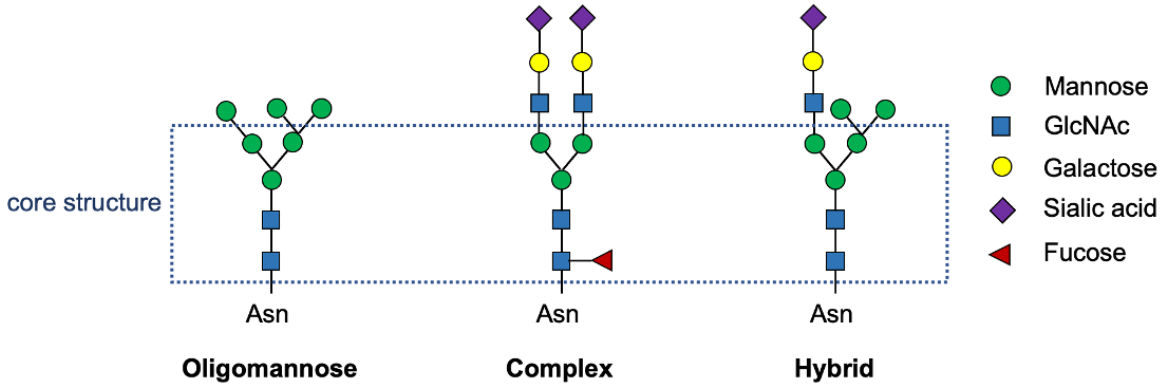


Figure 4-7. Three major types of N-glycan structure

Schematic structures of major types of N-glycans are shown. Oligomannose, complex and hybrid N-glycans share a common core structure that are highlighted in dark blue dotted box. The antennae of N-glycans consist of either all mannose residues (oligomannose), a combination of GlcNAc, galactose, sialic acid (complex), or a mixture of these, with one branch being complex, the other oligomannose (hybrid).

Mass spectrometry-based technology is a powerful tool for analysing components of the proteome. It has the resolution of a single amino acid through peptide-fragment ion spectra when used to study post-translational modifications, such as glycosylation

and phosphorylation. A streamlined protocol, “bottom-up” proteomics, is the most widespread proteomic workflow. It begins with protein extraction and digestion by a sequence-specific enzyme such as trypsin. Several bottom-up techniques, such as data dependent acquisition (DDA), targeted proteomics and data independent acquisition (DIA), have been developed, and each has a specific purpose (Aebersold and Mann, 2016).

In this section, the Jagged1$_{\text{N-EGF3-Fc-His}}$ construct was analysed by DDA methods to achieve unbiased and complete coverage of the glycoproteome by Dr Weston Struwe, University of Oxford. After reducing SDS-PAGE of purified WT Jagged1$_{\text{N-EGF3-Fc-His}}$ protein, a band was excised from the gel. Trypsin digestion of the gel band was performed, and glycopeptides were extracted and pooled. A full spectrum of peptides were separated by reverse-phase chromatography and electrospray ionization (MS^1 level), subsequently peptide ions were fragmented in the gas phase at the vacuum of a mass spectrometer to generate MS^2 level spectra which contain the information of identity and quantity of specific peptide. The resulting data were analysed with Byonic (Protein Metrics).

From mass spectrometry-based glycoproteomic analysis, the N-glycan species at N143 and N217 on the Jagged1$_{\text{N-EGF3-Fc-His}}$ construct can be detected. Both were complex N-glycans with core fucosylation on the innermost GlcNAc residue (Figure 4-8). These complex N-glycans include bi-antennary, tri-antennary and tetra-antennary elements. At the N143 site, the most abundant N-glycan was tetra-antennary, the least bi-antennary, although around 60% of Jagged1$_{\text{N-EGF3-Fc-His}}$ tryptic peptide was not glycosylated at this site (Figure 4-8). At the N217 site, complex glycans with tri-

antennary and tetra-antennary glycosylation were in highest abundance (Figure 4-8). Bi-antennary glycosylation on N217 was less than 5%, and around 10% constructs were not glycosylated on this position (Figure 4-8).

As the tetra-antennary complex was the most common N-glycan at N143, to further study the N-glycan on C2, it was modelled on the receptor/ligand complex structure by Dr Weston Struwe, University of Oxford (Figure 4-8). One of the *Drosophila* ligands, Delta, was crystallised with an N-glycan on loop 5-6 of C2 domain, which allows the complex N-glycan to be positioned (Martins et al., 2021a). Moreover, an overlay of Jagged1-Notch1 (PDB: 5uk5) with *Drosophila* Delta demonstrates the position of the N-glycan in context with Notch1. The N-glycan on loop 5-6 of C2 domain is located away from the Notch binding interface (Figure 4-8). It covers one face of the domain between loop 5-6 and loop 3-4 and extends downwards to beta strand 4 of C2 (Figure 4-8).

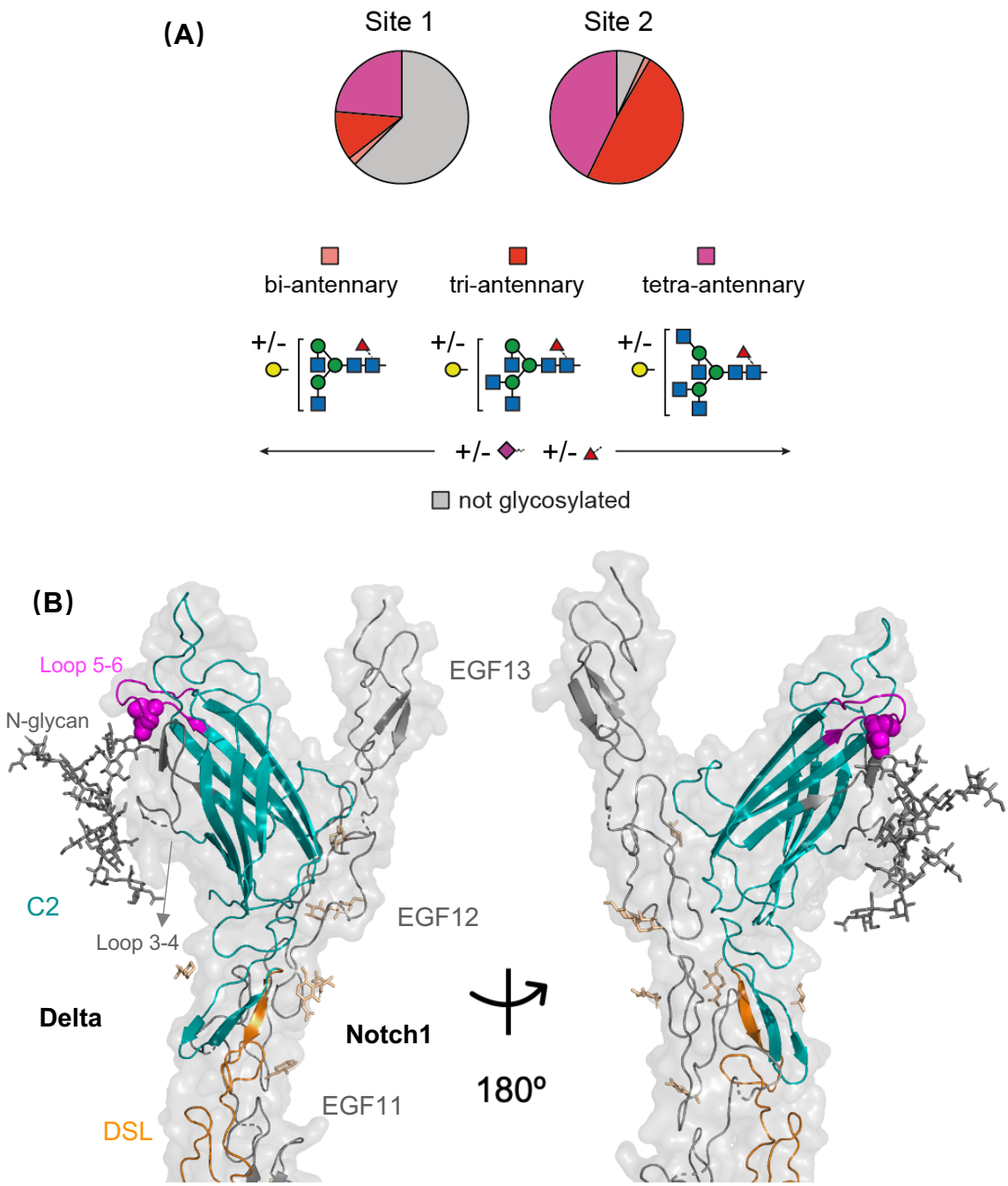


Figure 4-8. Mass spectrometry glycoproteomic analysis and of Jagged1

Complex N-glycans with different branches were observed at C2 loop 5-6 by mass spectrometry analysis. The Asn-linked GlcNAc was modified by fucose at both N143 and N217 sites. (A) Pie graphs show composition of N-glycans on tryptic peptides covering two different sites of Jagged1$_{\text{N-EGF3-Fc-His}}$ construct. Site 1 indicates Asn143, and site 2 indicates Asn217. (B) The structure of the *Drosophila* Delta C2 and DSL domains with tetra-antennary N-glycan complex (dark grey sticks) modelled on loop 5-6 (magenta) in the context of the complex (PDB: 5UK5) with Notch1$_{\text{EGF11-13}}$ (grey). Asn143 shown as magenta spheres. C2 coloured in teal, and DSL in orange.

4.6 Testing the effect of Jagged1 N-glycan related variants on Notch activation

4.6.1. Notch1 activation measurement

To investigate whether or not, as suggested by the T145N COSMIC variant (Chapter 3), removal of the N-glycan on loop 5-6 of Jagged1-C2 affects Notch1 activation, assays with N-glycan variants were undertaken using both mN1-NLuc/CLuc-RBPjk cells and CHO hN1G4^{esn} cells, as described previously (section 3.6).

Compared to Jagged1 wild type, all negative controls showed a significant decrease in Notch1 activation in each independent repeat ($P < 0.0001$) (Figure 4-9). The DSL N-glycan variant, N217A, showed a similar Notch1 activation level as the wild type ($P = 0.4593$). S142N, T145N and N143A substitutions all lead to a statistical decrease in Notch1 activation in the context of this assay ($P < 0.0001$). Compared to S142N, variants without the N-glycan in C2 (T145N and N143A) showed extremely low Notch1 activity, with less than 50% of the wild type signal (Figure 4-9).

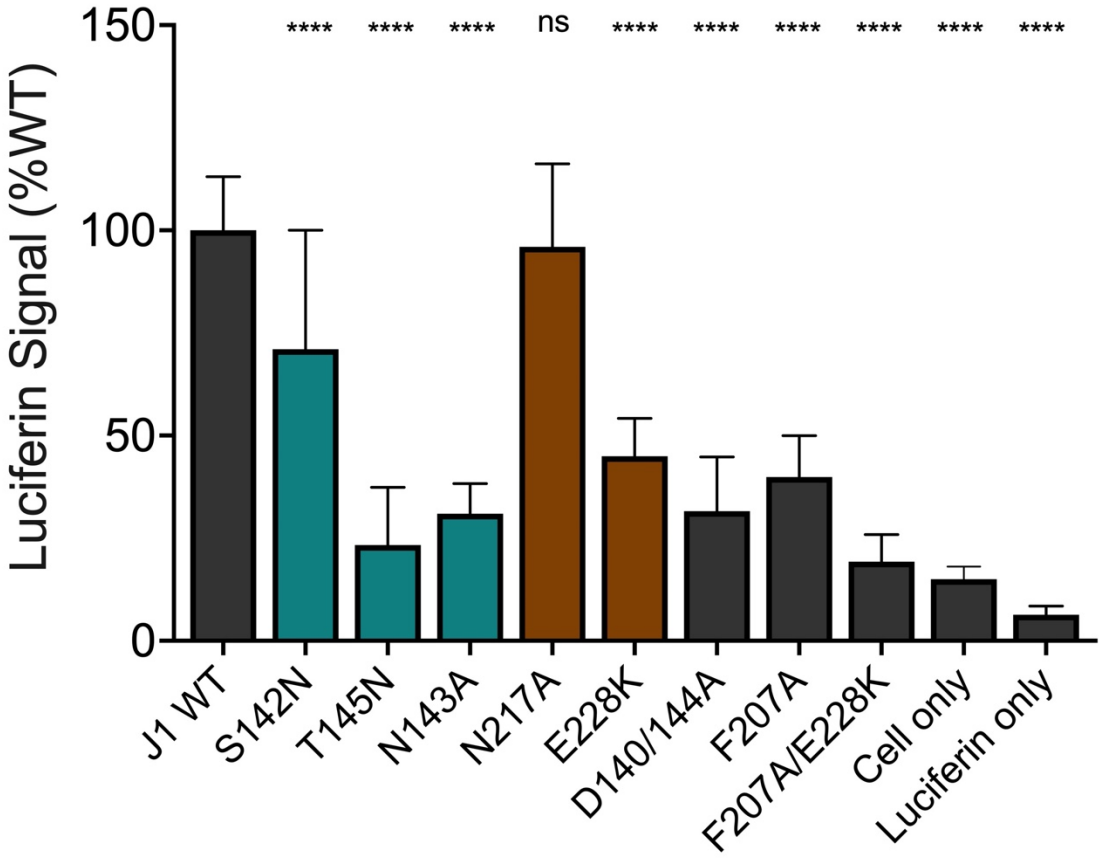


Figure 4-9. Split luciferase Notch1 activation assay of Jagged1 N-glycan variants by mN1-NLuc/CLuc-RBPjk cells

Notch1 activation of N-glycan related variants was assessed by split luciferase Notch1 reporter cells. Combined results of more than four independent experiments, each of 5 repeat wells are shown. Jagged1 wild type and negative controls coloured in dark grey, C2 variants in teal, DSL variants in brown. Luminescence signal acquired is presented relative to Jagged1 wild type. Values are presented with mean ± SD. Comparisons between two groups were analysed with two-tailed unpaired *t*-test using Prism 9. ns = not significant; ****$P < 0.0001$.

The YFP transcriptional-based Notch1 activation assay was also performed on the same set of variants. In addition to Notch binding and lipid binding defective deficiency negative controls, wells coated with IgG and wells with CHO hN1G4^{esn} cells only (without proteins coated) were included.

From three independent repeats, all negative controls, including D140/144A, F207A, F207A/E228K, IgG and CHO hN1G4^{esn} cell only, and a binding defective COSMIC

variant E228K (section 5.3) showed a decrease in YFP positive population percentage (Figure 4-10). Jagged1 N217A showed a similar YFP signal distribution to the wild type (Figure 4-10). S142N, T145N and N143A all showed less signal compared to wild type, although S142N was milder in its effect (Figure 4-10). The results from this YFP transcriptional-based Notch1 activation assay were broadly consistent with the luciferase complementation-based Notch1 activation assay.

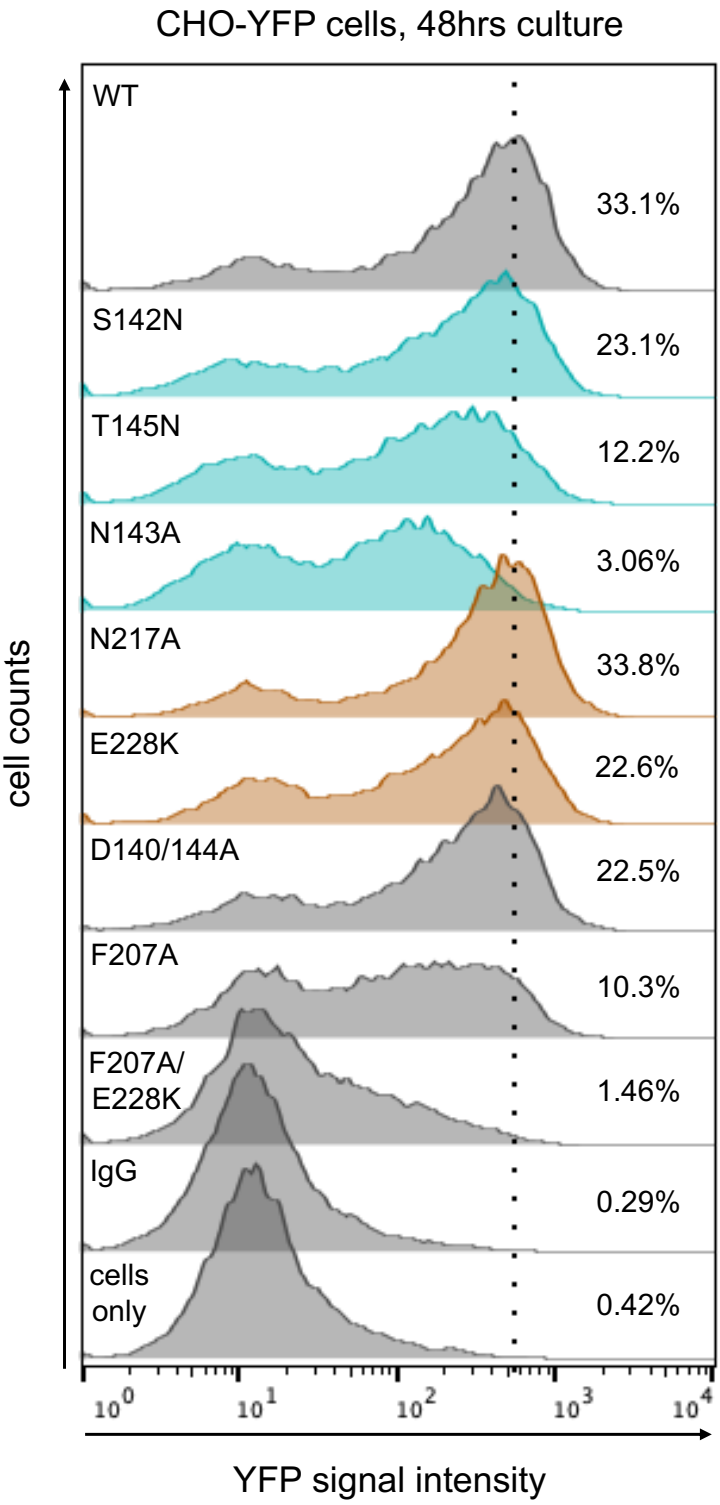


Figure 4-10. Notch activation assay of glycan variants using CHO hN1G4^{esn} cells

FACS analysis of N-glycan variants with Jagged1 wild type and negative controls. CHO hN1G4^{esn} cells were cultured on immobilized protein for 48 hours. Dotted vertical line denotes the modal signal of a Jagged1 wild type population, and for each sample, the fraction of cells above this value is shown as a percentage. Data from 10,000 single cells from each sample were recorded by BD LSRFortessa™ X-20 flow cytometer and analysed by FlowJo®_V10.7.2.

4.6.2. Notch2 activation measurement

Notch2 activation of the N-glycan variant set was also assayed using mN2-NLuc/CLuc-RBPjk cells (Chapter 2). The Notch2 reporter cell is constructed in HEK cells similarly to mN1-NLuc/CLuc-RBPjk cells except the N-terminal region of luciferase is fused with the mouse Notch2 NICD region (see section 3.6.1).

In the Notch2 activation assay, four negative controls, F207A/E228K double mutant, wells added only reporter cells (cells only) and wells with only substrate (luciferin only), and the binding deficiency COSMIC variant E228K showed a statistically significant decreased Notch2 activation ($P < 0.0001$) compared to WT Jagged1 (Figure 4-11). However, two of the negative controls, D140/144A and F207A showed a similar Notch2 activation ability as the Jagged1 wild type ($P = 0.1270$ and $P = 0.1867$ respectively). Variants without a C2 N-glycan (T145N and N143A) lead to a significant decrease in Notch2 activation ability, while the DSL N-glycan variant (N217A) showed no significance difference in signal compared with wild type ($P = 0.0551$) (Figure 4-11). The loop 5-6 variant, S142N, showed a similar Notch2 activity as wild type ($P = 0.0765$) (Figure 4-11). The Notch2 activation results of N-glycan related variants are consistent with Notch1 activation results, with the exception of S142N, which showed a decrease only in Notch1 activation. In addition, all of the negative controls F207A and D140/144A were less inhibitory to Notch2 activation than Notch1.

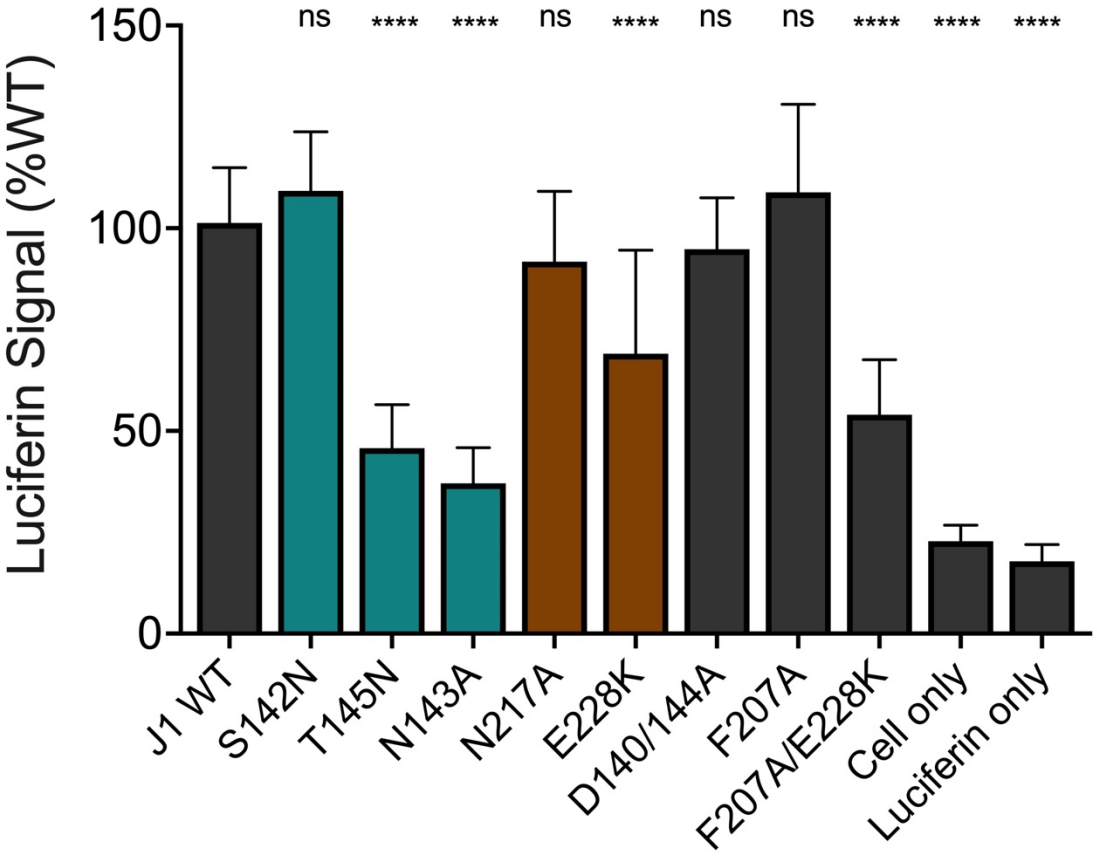


Figure 4-11. Split luciferase Notch2 activation assay of Jagged1 N-glycan variants by mN2-NLuc/CLuc-RBPjk cells

Notch2 luciferase complementation-based reporter cells were used to assess Notch2 activity of N-glycan related variants. Wild type and negative controls are coloured in dark grey, C2 variants in teal, and DSL in brown. Signal is shown relative to Jagged1 wild type. Combined results from 4 independent experiments, each of 5 wells, are shown. Values are presented with mean ± SD. Comparisons were performed with two-tailed unpaired *t*-test using Prism 9. ns = not significant; ****$P < 0.0001$.

4.6.3. Deglycosylated Jagged1$_{N\text{-}EGF3\text{-}Fc\text{-}His}$ Notch activation measurement

To confirm the decrease in Notch activation by T145N and N143A variants was due to a direct loss of N-glycan on the C2 domain rather than any partial misfolding of Jagged1$_{N\text{-}EGF3\text{-}Fc\text{-}His}$, PNGase F digestion of the wild type dimer construct was performed. As mentioned before, three N-glycans exist on this construct, and there is one glycosylation site on the Fc tag (Asn425) in addition to Asn143 and Asn217. The digested constructs were assessed by 10% SDS-PAGE before the CHO hN1G4^{esn}

Notch1 activation measurement. A positive control incubated at 37 °C overnight, without the addition of PNGase F was assessed alongside. In addition, an unrelated protein, BSA, was used to detect the background signal.

The positive control migrated to a similar position as the purified wild type construct under both reducing and non-reducing conditions, suggesting no non-specific degradation had taken place during the long incubation at 37 °C (Figure 4-12). Two bands appeared in PNGase F digested samples. The upper protein band (~ 200 kDa non-reducing, ~ 60 kDa reducing) showed an increase in mobility compared to the positive control. The molecular weight of the faint lower band is around 36 kDa (expected molecular weight of PNGase F). These data suggest successful deglycosylation of the dimer construct. YFP expression from the Jagged1 positive control was similar to Jagged1 WT starting material. The deglycosylated sample however showed a significant reduction in signal (Figure 4-12). Collectively, these data suggest deglycosylation of folded WT ligand abrogates activity rather than any partial misfolding caused by the lack of N-glycan. This is consistent with a critical role for the C2 N-glycan in WT Jagged1 function.

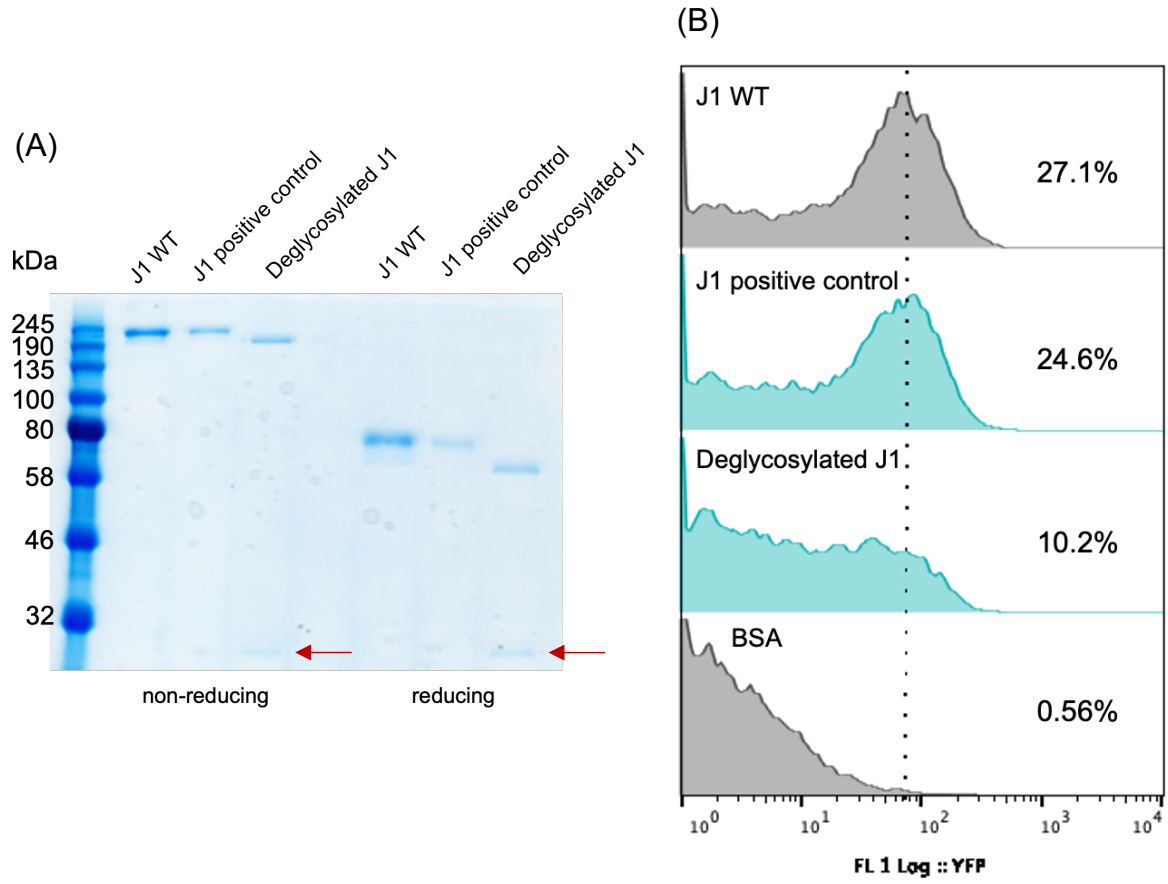


Figure 4-12. Notch activation assay of deglycosylated Jagged1$_{N\text{-}EGF3\text{-}Fc\text{-}His}$

(A) Jagged1$_{N\text{-}EGF3\text{-}Fc\text{-}His}$ (J1 WT), PNGase F digested samples (Deglycosylated J1) and the positive control incubated under similar conditions (J1 positive control) were viewed by 10% reducing/non-reducing SDS-PAGE and stained with Coomassie blue. A faint lower molecular weight band (indicated by red arrows) present in the PNGase F digest samples only, corresponds to added enzyme (36 kDa). (B) CHO hN1G4^{esn} Notch1 activation analysis of PNGase digested Jagged1 wild type with positive and negative controls. Dotted vertical line denotes modal signal from a Jagged1 wild type population, and for each sample, the fraction of cells above this value is shown as a percentage. Data from 10,000 single cells from each sample were recorded by CyAn ADP compact benchtop flow cytometer and analysed by FlowJo®_V10.7.2.

4.7 Physiological importance of the Jagged1-C2 N-glycan complex

Notch signalling plays an important role in the development and homeostasis of the vasculature through control of endothelial cells (ECs) and vascular smooth muscle cells (VSMCs) and their interactions with each other (section 1.2.2.1). Jagged1-Notch

signalling plays a role in VSMC differentiation from mesenchymal cells, which is essential for proper cardiovascular development and homeostasis (Benedito et al., 2009b). Moreover, continuous Jagged1 signalling in VSMC is important to maintain its phenotype (Briot et al., 2014). In addition to Jagged1, Notch2 and Notch3 predominate in VSMCs (Baeten and Lilly, 2017). Aberrant Notch signalling causes many vascular disorders, such as cerebral autosomal dominant arteriopathy (see section 1.2.2.4).

VSMCs exhibit a wide spectrum of phenotypes, ranging from a contractile to a synthetic phenotype, which can be distinguished by morphology, proliferation and migration rates, specific protein marker expression (Figure 4-13). The phenotypic diversity of VSMCs is regulated by innate genetic programmes and environmental cues including biochemical factors, extracellular matrix components and physical factors. Synthetic VSMCs have a cobblestone morphology, and they are characterized by higher proliferation, migration and produce more extracellular matrix proteins, but less contractile proteins (Figure 4-13). In contrast, contractile VSMCs are elongated, spindle-shaped cells. They have low proliferation, migration capacity, and produce less extracellular matrix components (Figure 4-13).

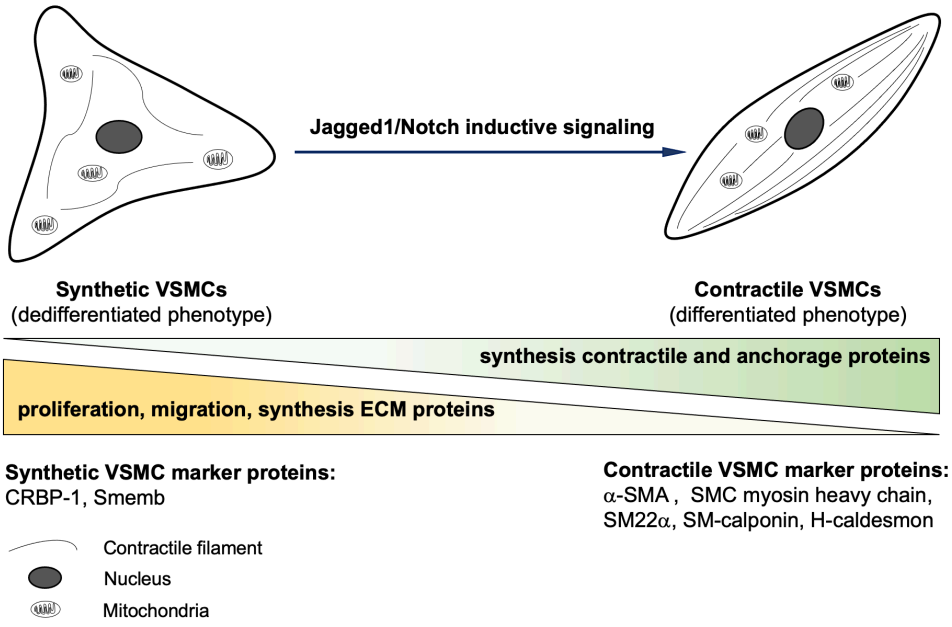


Figure 4-13. Jagged1/Notch induces synthetic to contractile VSMC phenotype

Schematic shows Jagged1 induced changes in VSMC differentiation. Characteristics and marker proteins of synthetic VSMC and contractile VSMC are shown. Synthetic VSMCs show a cobble-stone morphology, while contractile VSMCs have elongated and spindle-shaped morphology in culture with more contractile filaments. α-smooth muscle actin, together with other contractile proteins, can be used to distinguish VSMC phenotype.

Previously experiments showed that Jagged1/Notch signalling directly induces expression of the mesenchymal and smooth muscle cell marker, α-smooth muscle actin (α-SMA), in endothelial and vascular smooth muscle cells during endothelial-to-mesenchymal transformation. This process is carried out via its major effector, CSL, which directly binds a conserved cis element in the α-SMA promoter and induces its expression (Noseda et al., 2006). During the differentiation process, actin filament (F-actin) assembly and disassembly drives the phenotypic and physical structural changes of the VSMC. Actin filament assembly provides the cells with a contractile apparatus, and prepares them for migration and proliferation (Doevendans and Van Eys, 2002).

To investigate the impact of N-glycan variants on a cell-type expressing physiological levels of Notch, a smooth muscle cell differentiation assay was performed using primary human aortic smooth muscle cells (HAoSMCs). Purified ligand variants were used by Sami Sanlidag, in Prof Cecilia Sahlgren's laboratory at Åbo Akademi University, Finland. HAoSMCs were cultured on Jagged1 coated plates for 5 days, and differentiation was assessed by measurement of α-SMA levels. Initial immunoblotting experiments were first carried out to prove α-SMA levels were dependent upon WT Jagged1 using commercially available Jagged1-Fc (R&D) (Figure 4-14. A).

DAPT, a γ-secretase inhibitor which can inhibit Notch signalling, was used to block Jagged1 induced Notch signalling. An unrelated protein to the Notch pathway, immunoglobulin G (IgG), was utilized as a negative control to measure the α-SMA background signal. As DAPT is diluted from stock solutions in dimethylsulfoxide (DMSO), DMSO was added in all samples to exclude its effect on the results of the assay. From the immunoblotting detection, levels of a loading control β-tubulin were similar in all samples (Figure 4-14. A). The α-SMA signal from WT Jagged1 was clearly observed and was much higher than signals obtained from negative controls (IgG and Jagged1/DAPT), which suggested α-SMA expression was induced by Jagged1 (Figure 4-14. A).

The set of N-glycan variants were subsequently assessed by the SMC differentiation assay. Immunofluorescent microscopy was performed first on a subset of samples to observe the SMC differentiation state through α-SMA detection and cytoskeletal labelling. Actin filaments (F-actin) were stained by phalloidin, and nuclei were stained

by DAPI. DAPI signals were clearly seen in all samples (Figure 4-14. B). α-SMA expression was clearly observed in the SMCs cultured on Jagged1 wild type samples, but not in negative controls (F207A/E228K and IgG) (Figure 4-14. B). These data indicate that Jagged1$_{NE3\text{-}Fc\text{-}His}$ WT is similar in activity to the commercial preparation of Jagged1-Fc WT chimera protein which comprises the complete extracellular domain. Strikingly, the N-glycan variant N143A did not induce α-SMA expression.

A complete set of N-glycan variants were further blind tested by immunoblotting of SMC differentiation assay samples (Figure 4-14. C). β-tubulin signal from all variants showed equal loading of cell lysate samples (Figure 4-14. C). Consistent with immunofluorescent microscopy, all negative controls, including F207A, F207A/E228K and IgG, and the binding defective COSMIC variant, E228K, showed a decrease in α-SMA expression compared to WT Jagged1 by α-SMA monoclonal antibody detection (Figure 4-14. C). N217A showed similar α-SMA levels as the wild type (Figure 4-14. C). Variants without the C2 N-glycan, T145N and N143A, showed decreased α-SMA expression levels compared to the wild type, and similar to levels from negative controls (Figure 4-14. C). S142N induced α-SMA expression at levels similar to WT Jagged1, and this resembled Notch2, rather than Notch1 reporter assay results.

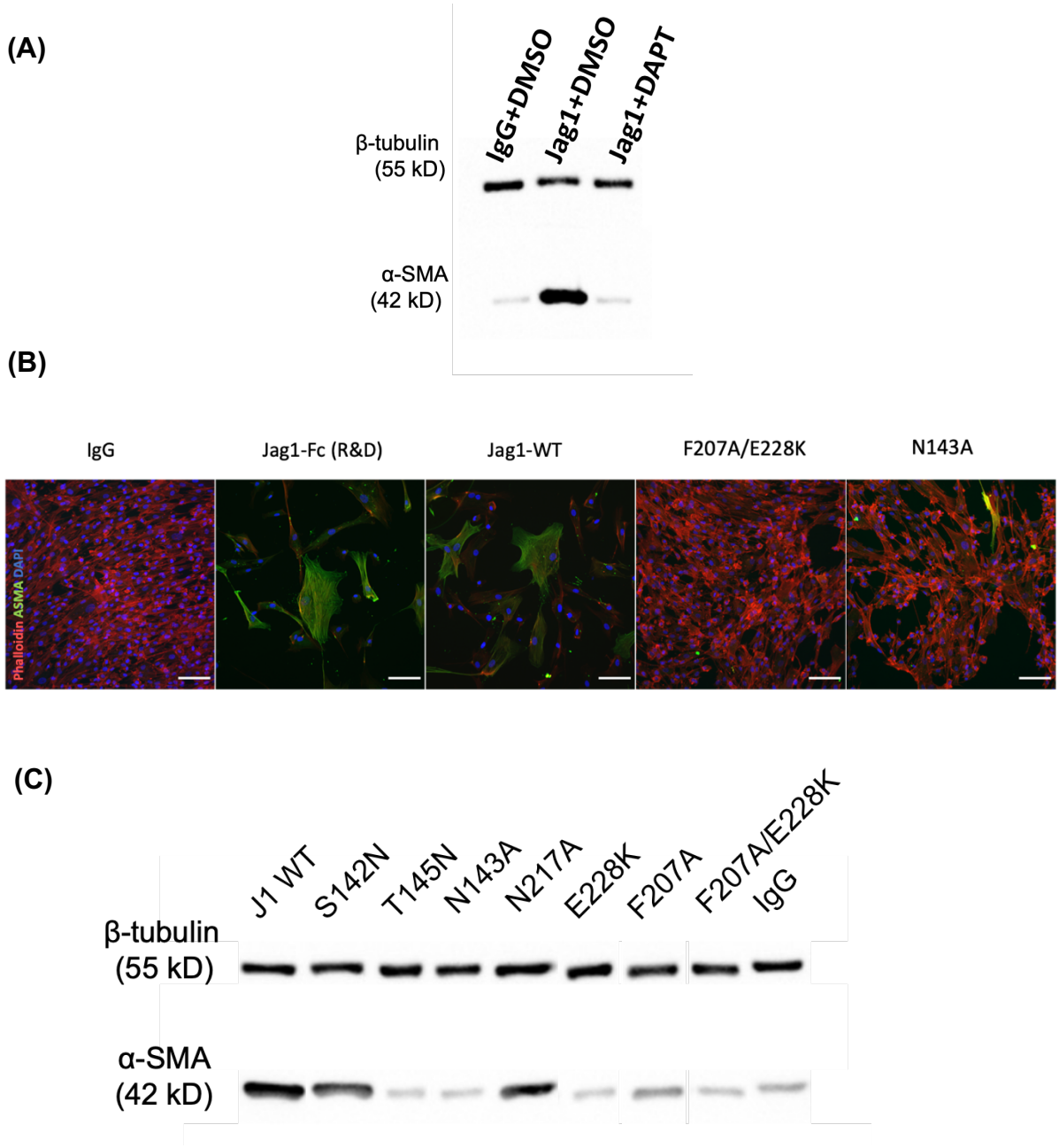


Figure 4-14. Smooth muscle differentiation assay shows loss of N-glycan in C2 domain prevents smooth muscle cell differentiation

HAoSMCs were used to assess the effects of C2 N-glycan variants on VSMC differentiation. β-tubulin (D3U1W) mouse monoclonal antibody and α-SMA (D4K9N)XP rabbit monoclonal antibody were used for signal detection. (A) The DAPT control experiment shows α-SMA level is Jagged1 dependent. (B) Immunofluorescent microscopy shows the N143A variant is similar to negative controls and does not induce smooth muscle cell differentiation. Scale bar is 100μm. phalloidin-AF633 was used to stain actin filaments in smooth muscle cells. (C) Western blot shows α-SMA levels detected from N-glycan related variants and negative controls. β-tubulin levels were used to show equivalent loading. n = 3 independent experiments, and one representative data set is shown.

4.8 Conclusions

This chapter studied the effect of C2 N-glycan variants on Notch activation in reporter cells and VSMCs. The N-glycosylation motif on loop 5-6 of C2 domain was shown to be highly conserved in Jagged family ligands by sequence alignment of seven representative metazoan species. These data suggest the N-glycan on C2 of Jagged family may have a previously unrecognised role in Notch activation (Figure 4-1) (Figure 4-2). Western blotting analysis of a set of glycan variants, S142N, T145N, N143A and N217A after HEK293T transient transfection, showed that loss of the N-glycan modification on both Asn143 and Asn217 sites of human Jagged1 did not have an obvious effect on its proper folding and trafficking, unlike some other N-glycans in extracellular/cell surface proteins (Figure 4-3).

Three variants with substitutions which changed N-glycosylation motif, T145N, N143A and N217A, showed faster migration by reducing SDS-PAGE compared to wild type and a COSMIC loop 5-6 variant (S142N). These data strongly suggest N-glycans are added/present on both glycosylation motifs of Jagged1$_{\text{N-EGF3-Fc-His}}$ (Figure 4-5). N217A monomer, a construct which only has the C2 N-glycan recognition site, showed an increase in mobility by SDS-PAGE analysis after PNGase F digestion (Figure 4-6). These data suggest high occupancy of the N-glycan site on C2 domain, and the observed faster migration of N143A, T145N and N217A is consistent with the loss of N-glycan.

The composition of the N-glycan on both sites were analysed by mass spectrometry. Both Asn143 and Asn217 of human Jagged1 were modified by complex N-glycans with core fucosylation on the inner most GlcNAc (Figure 4-8). Bi-antennary, tri-

antennary and tetra-antennary N-glycans were detected at both sites. The tetra-antennary N-glycan on loop 5-6 of C2 modelled on the observed orientation in *Drosophila* Delta showed that the N-glycan on C2 domain is located away from the Notch binding interface but is close to loop 3-4. If the N-glycan in C2 of Jagged1 is positioned similarly, it might act sterically to occlude a concave lipid binding surface mediated by loop 3-4 (Figure 1-8, Figure 1-11) and/or promote a particular orientation at the cell membrane. It may directly stabilise the loop 5-6, facilitating lipid binding and calcium binding to the apical region. Irrespective of the mechanism, it appears the N-glycan is important for Jagged, but not Delta ligand function.

Two C2 N-glycan variants, T145N and N143A, showed a dramatic decrease in Notch activation detected by all reporter cells tested (Figure 4-9, 4-10, 4-11). In contrast, the DSL N-glycan variant N217A had a similar activity to Jagged1 wild type. These data suggest that the N-glycan on Jagged1-C2, but not Jagged1-DSL, plays an important role in Notch activation. The S142N COSMIC variant, which is located adjacent to the N-glycan residue on loop 5-6, also showed a decrease in Notch1 activation in two of the assays but not Notch2 (Figure 4-9, 4-10, 4-11). The S142N substitution might change the conformation of loop 5-6 due to accommodation of the larger N side chain and this appears more important for Notch1 signal generation than Notch2. In addition, PNGase F digested Jagged1$_{\text{N-EGF3-Fc-His}}$ showed a decrease in Notch activation, which excludes the decrease in Notch activation observed for C2 N-glycan variants being caused by partial misfolding.

The N-glycan on Jagged1 C2 also appears to be essential for smooth muscle differentiation, as decreased levels of α-SMA were observed when HAoSMCs were

cultured on T145N and N143A constructs (Figure 4-14). These data reflect the fact that the N-glycan on C2 plays an important role in Notch activation when physiological level of Notch receptors are expressed. Interestingly, S142N showed a similar ability to induce synthetic HAoSMCs to transition to contractile HAoSMCs as wild type despite showing intermediate activity in its ability to activate Notch1 reporter cells (Figure 4-14). This may be because smooth muscle differentiation is dependent on other Notch paralogues, such as Notch2 (Baeten and Lilly, 2017).

Overall, these data are consistent with a previously unrecognised role for the loop 5-6 N-glycan on Jagged1-C2 in ligand dependent Notch activation and smooth muscle differentiation. The large N-glycan side chain appears to locate along one face of the C2 domain away from Notch binding site. Although the S142N substitution may cause a direct effect on loop 5-6 conformation, it may exert its effect by subtly changing the position of the N-glycan.

Chapter 5. Investigation of Notch- and lipid-binding properties of Jagged1 variants

5.1 Introduction

The C2 domain potentially modulates Notch signalling through its ability to bind to Notch and lipid (see section 1.5.3). Previous studies have investigated the effects of different disease-causing substitutions within the C2 domain on both Notch activation and Notch/lipid binding (Suckling et al., 2017). A number of plate-based *in vitro* techniques were applied to investigate the molecular mechanisms underlying the defects in Notch activation. EHBA disease-causing variants on loop1-2 of Jagged1-C2 showed a decrease in lipid binding in liposome binding assays but no defect in Notch binding using an EGF11-13 ligand binding fragment.

Most of the previously described secreted COSMIC variants and glycan related variants in Chapter 3 and Chapter 4 showed a decrease in Notch activation. However, it is not known whether the decrease of Notch activation of these substitutions on C2 loop structure is caused by changes in their receptor and/or membrane binding capacity. Moreover, the molecular mechanisms underlying the C2 conserved sugar modification effects on Notch signalling have not yet been elucidated.

The aim of this chapter was to analysis whether COSMIC and glycan-related variants affect the receptor and lipid binding capability of Jagged1. The Notch binding ability of COSMIC variants was assessed using a well-established ELISA-type *in vitro* plate assay. Notch1 and Notch2 EGF11-13 receptor constructs were produced using a eukaryotic S2 cell expression system and purified. A modification of the Notch-binding plate assay was performed to assay N-glycan variants, to ensure that the absence of sugar did not affect immobilisation. Moreover, a new method, a flow cytometry-based

assay, was developed to study the lipid-ligand interactions of the COSMIC and glycan variants.

5.2 Production and purification of recombinant Notch receptors

5.2.1 Overview of the S2 expression system

S2 cells are derived from *Drosophila* embryo cells and are known to express high levels of recombinant proteins with post-translational modifications. They have been adapted to high-density suspension culture for large scale protein expression without the requirement of CO_2 (Figure 5-1). Compared to prokaryotic expression systems, these cells can produce properly folded constructs with sugar modifications after simple and fast transient transfections or 3 to 4 weeks of stable line generation. A similar protein production process to that used with the HEK293T system in Chapter 3 can be followed, but with a higher protein yield particularly for Notch constructs. A comparison of the S2 and HEK293T systems is shown in Figure 5-1. The S2 expression system can produce long multiple disulphide-rich domain constructs, for example, Jagged1 and DLL4 N-EGF3 monomers (Suckling et al., 2017), $Notch1_{EGF7-13}$ (unpublished data). The crystal structure of $Notch2_{EGF11-13}$ construct produced from S2 cells has been determined demonstrating native fold and efficient O-glycosylation, and both Notch1 and Notch2 constructs purified from the S2 expression system can bind specifically to purified Jagged1 dimers in ELISA-type assays (Suckling et al., 2017). In this chapter, human Notch1 and Notch2 EGF11-13 receptor fragments were purified using the pEXS2-2 expression vector in S2 cells.

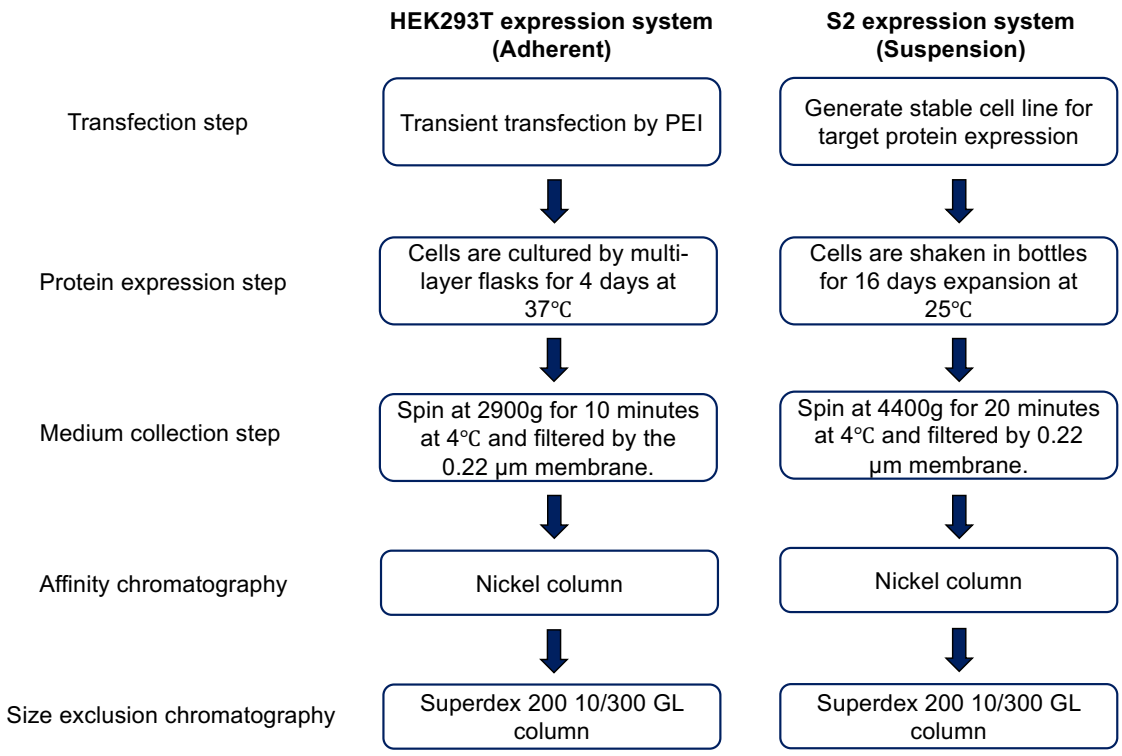


Figure 5-1. A flow diagram for comparison of production and purification of recombinant Notch$_{EGF11-13}$ with Jagged1

Protein yields are higher in S2 cells, most likely due to their ability to grow in suspension. For discrete constructs (e.g., Notch$_{EGF11-13}$), stable cells were established, but transient expression is possible in S2. Transient expression of Jagged variants in HEK293T was used due to the number of variants being tested. The protein purification steps are similar between these two systems, although there are slight differences in buffer used at each step due to different properties of the fragments (Chapter 2).

5.2.2 NotchEGF11-13 protein purification

EGF11 and EGF12 are the core ligand binding regions of Notch (Luca et al., 2015, 2017) (Cordle et al., 2008). Notch1$_{EGF11-13}$ and Notch2$_{EGF11-13}$ structures with glycan modifications have been characterised using X-ray crystallography (Taylor et al., 2014) (Suckling et al., 2017) (Figure 5-2). O-linked sugars (in particular Fringe modifications) on EGF12 increase the affinity of Jagged1 for its receptor, which was demonstrated by both flow cytometry and SPR binding assays (Taylor et al., 2014). Subsequently, crystal structures of Jagged1-Notch1 and DLL4-Notch1 complexes showed that an O-fucose modification in EGF12 is involved in direct inter-molecular interactions with the

C2 domain (Luca et al., 2015) (Luca et al., 2017). After solving the $Notch2_{EGF11-13}$ structure, the modelling of the receptor-binding interface of Notch ligands and Notch1/Notch2 showed that most key residues involved in ligand binding of Notch1 are conserved in Notch2 with the exception of I-477, although this is substituted by L-481, a residue with similar hydrophobic properties (Suckling et al., 2017) (Figure 5-2).

To study the Notch binding capability of ligand constructs, human $Notch1_{EGF11-13}$ and human $Notch2_{EGF11-13}$ constructs were initially cloned into pEXS2-2 plasmids with BirA (biotin ligase) and His-tags at the C-terminus and transfected into S2 cells to generate stable lines by Dr Richard Suckling, University of Oxford. The BirA-tag is widely used in affinity-based biochemical experiments as, following biotinylation, it can tightly bind to avidin and streptavidin, while the His-tag was used for immobilized metal affinity chromatography in this study. $Notch1_{EGF11-13}$ and $Notch2_{EGF11-13}$ fusion proteins were produced from stably transfected cells using an established protocol (Chapter 2). Genomic DNA of each S2 stable line was sequenced before protein purification to verify the line used. 1 L of S2 culture medium was subjected to IMAC and SEC (Figure 5-1) (Chapter 2). SDS-PAGE analysis was used to inspect fractions containing desired proteins of the expected MW which were subsequently pooled together. The purity of each stock was > 95% (Figure 5-3).

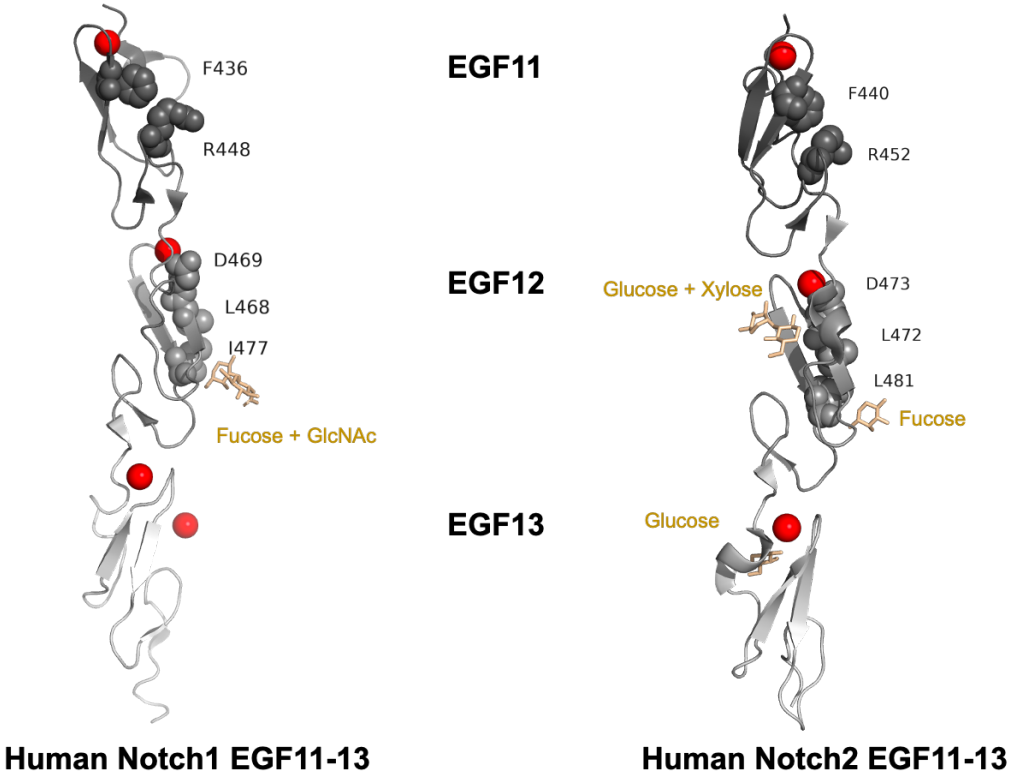


Figure 5-2. Structures of Notch constructs with key binding residues highlighted

The structures of human Notch1$_{EGF11-13}$ (PDB: 4D0E) and human Notch2$_{EGF11-13}$ (PDB: 5MWB) are shown with O-glycan modifications (wheat sticks) and Ca^{2+} ions (red spheres). EGF11 in dark grey, EGF12 in grey and EGF13 in light grey. Key residues in Notch1 and Notch2 structures involved in ligand binding are labelled with grey spheres. Note that Notch1 was crystallised using protein expressed by *E. coli* and refolded (sugar was added enzymatically *in vitro*), and Notch2 was purified directly from S2 cells. PyMOL was used to create images.

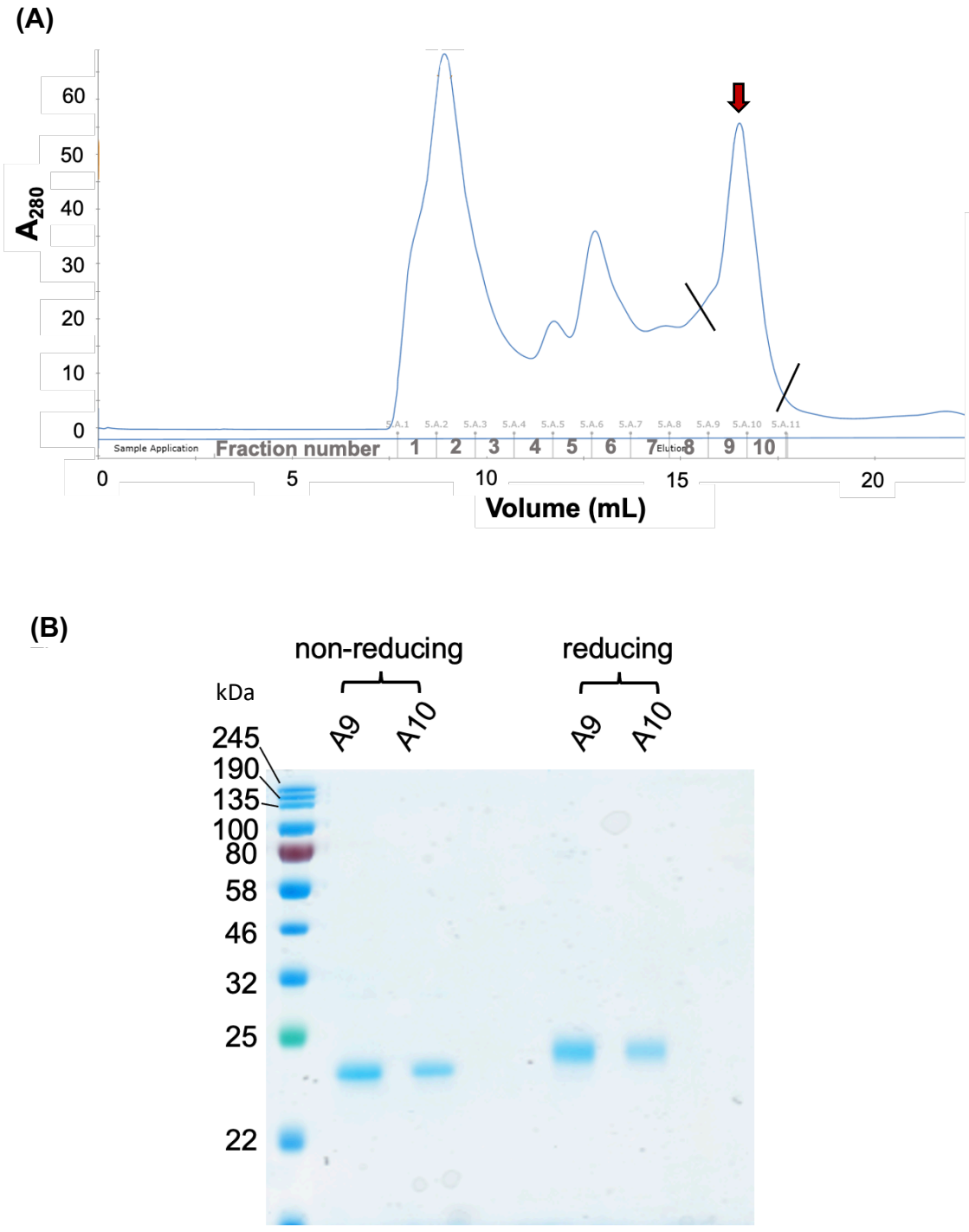


Figure 5-3. Purification of recombinant human Notch2$_{EGF11\text{-}13\text{-}BirA\text{-}His}$

(A) Size exclusion chromatography using S200 Superdex column. The peak collected is indicated by the red arrow and black lines. (B) The A9 and A10 fractions collected after size exclusion chromatography were analysed by 10% SDS-PAGE (reducing and non-reducing) to confirm the purity of the protein. A representative chromatogram and gel are shown. Expected MW of Notch2$_{EGF11\text{-}13\text{-}BirA\text{-}His}$ constructs is 17.2 kDa, and purified constructs run higher than expected most likely due to glycosylation.

5.3 Notch binding ability of COSMIC variants

As most COSMIC variants showed a decrease in Notch activation, an ELISA-type Notch binding assay was performed using both human Notch1 and Notch2 purified from S2 (Suckling et al., 2017). Notch EGF11-13 proteins were immobilized onto a MaxiSorp™ plate surface by adsorption, and soluble Fc-ligand constructs used as analyte (Figure 5-4). After washing steps, the amount of ligand bound was detected by anti-Fc-HRP antibody (Figure 5-4). The HRP (horse radish peroxidase) provides a means of quantitative readout of ligand bound to receptor.

To test the coating efficiency and absorb a maximum amount of receptor protein onto the 96 well plate surface, a saturation curve was produced (Figure 5-5). Solutions which added 400 ng Notch1 and 300 ng Notch2 to each well were required for saturation. An excess of constructs, 500 ng Notch1 and 400 ng Notch2, were therefore used (Figure 5-5). A fixed concentration of Jagged1 variant (200 nM) was subsequently added as analyte according to Suckling et al., 2017 (Figure 3-7).

Previous Mass Spectrometry analysis (performed by Pat Whiteman, University of Oxford) of S2 purified Notch1$_{EGF11-13}$ and Notch2 $_{EGF11-13}$ showed that Notch1 $_{EGF11-13}$ is less efficiently O-glycosylated than Notch2$_{EGF11-13}$ (~ 50% compared to near saturation of Notch2). Moreover, O-glucosylation at EGF13 of Notch1 was ~ 40% compared to Notch2. Thus, in assays, the Notch2 construct binds better (for an equivalent concentration of sample).

In Notch binding assays, binding deficiency negative controls (F207A and F207A/E228K) showed less binding than Jagged1 wild type (the positive control) in independent repeats, which is consistent with previous studies (Figure 5-6, 5-7). Very low signal was observed from HBS only (empty well with neither receptor nor ligand), which indicated antibody detection was specific. Little signal was detected from the J1 WT only sample (no Notch protein coated onto the plate before addition of ligands) again validating specificity (Figure 5-6, 5-7).

Among all the COSMIC variants, V86F, T145N and E228K showed less binding to both Notch1 and Notch2 constructs compared to wild type Jagged1 ($P < 0.0001$). G89E showed less binding to Notch1 ($P < 0.0001$) but not Notch2 ($P = 0.0976$, not significant) (Figure 5-6, 5-7). G114D mutant showed dramatically higher binding to Notch1 and Notch2 than wild type. This was not due to aggregation, as SEC-MALS was used to show predominantly dimer in solution (data not shown). L135F showed higher binding to Notch2 but similar binding to Notch1 when compared to wild type Jagged1. Other COSMIC mutants (A58V, D72N, S142N) showed no change in their binding to Notch1 and Notch2 (Figure 5-6, 5-7). Compared to Notch2 binding assay results, Notch1 binding results are more spread. This is likely because less signal is detected from Jagged1 WT. This may be attributed to the reduced efficiency of O-glycosylation of the Notch1 fragment, resulting in less ligand bound.

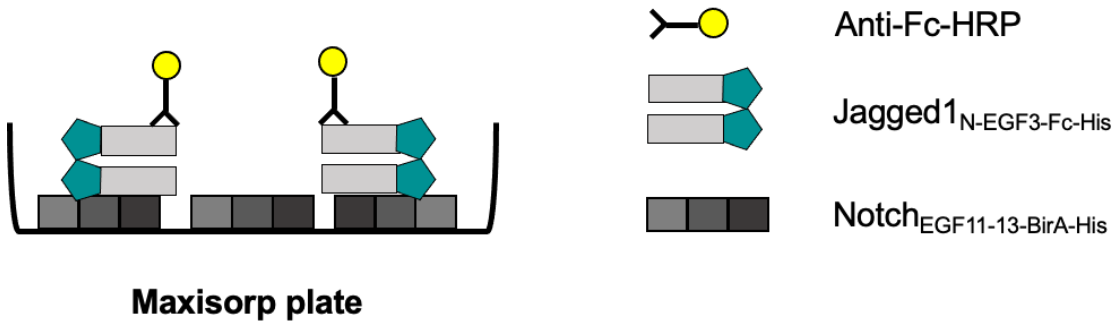


Figure 5-4. Schematic figure of Notch binding assay using Maxisorp plate

The MaxiSorp™ surface wells are coated with $Notch_{EGF11-13}$ (grey rectangles) through passive adsorption. Jagged1 dimers (light grey rectangles with teal pentagon) were added as soluble analyte. Ligands were detected by anti-Fc-HRP (1:2000), and HRP signal is quantified by a plate reader to determine the binding of Jagged1 to Notch receptor constructs in each well.

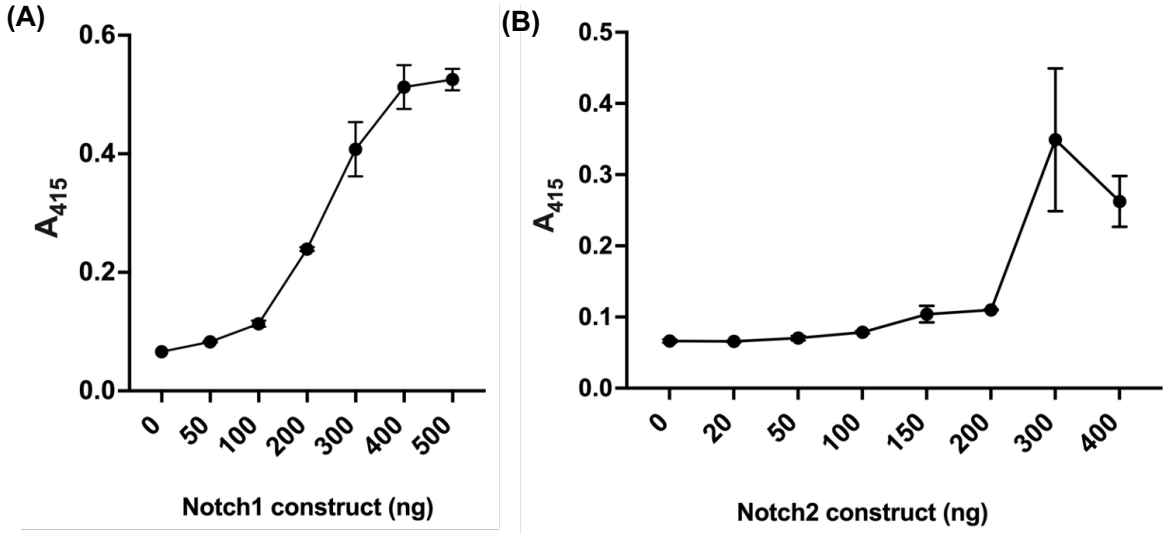


Figure 5-5. Saturation test of Notch1 and Notch2 constructs on Maxisorp plates

Saturation curves of Notch1 (A) and Notch2 (B) receptors on MaxiSorp™ plate surface are shown. $Notch_{EGF11-13}$ binding was probed by an anti-His-HRP antibody (1:2000) (Chapter 2 - Materials and Methods). A series of Notch solutions were made up and added at 50 mL/ well. The amount of Notch shown is that added to each well. Three repeat samples were measured, and mean ± SD were shown.

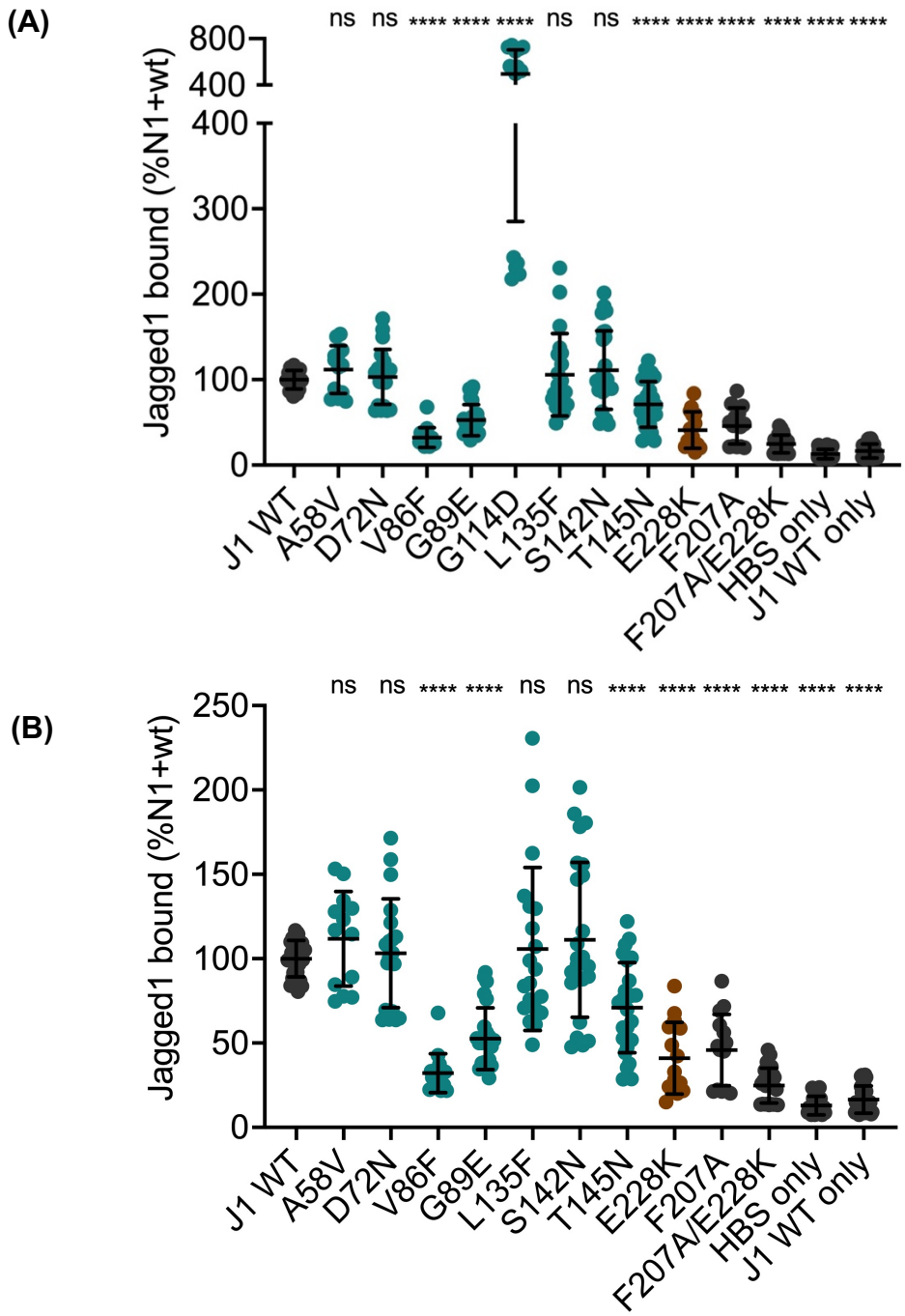


Figure 5-6. Notch 1 binding assay of COSMIC variants

Binding assays of human Notch1 were performed in HBS with 5 mM Ca^{2+} at pH 7.5. Data are displayed with (A) and without G114D (B) using two different y-axis scales. The measured concentrations of ligands were checked by running SDS-PAGE gels in parallel. n ≥ 3 independent experiments, each with 5 replicates, were carried out for each substitution. 1:2000 anti-Fc-HRP antibody was used for signal detection. Absorbance was measured with a PHERAstar FS microplate reader (BMG LABTECH). Data were plotted using GraphPad Prism 9 (GraphPad, San Diego, CA, USA). Two-tailed unpaired *t*-test was applied for comparisons, and values were presented as mean ± SD. ns = no significant difference, ****P < 0.0001.

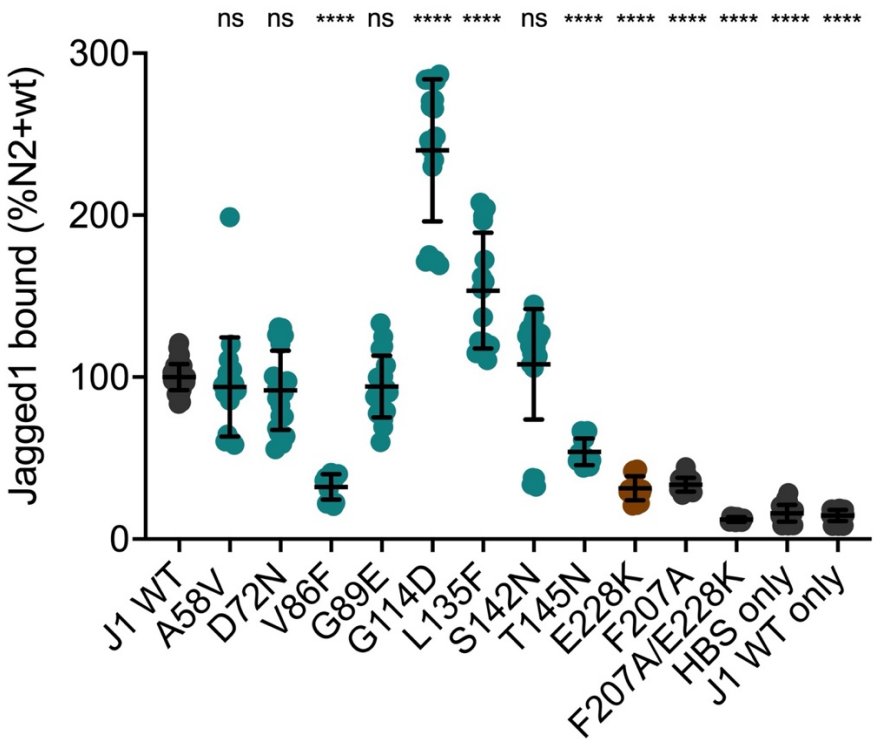


Figure 5-7. Notch2 binding assay of COSMIC variants

Experimental conditions were identical to those used for Notch1. Ligand concentrations were checked by SDS-PAGE. n ≥ 3 independent experiments, each with 5 replicates, were carried out for each variant. Signal of anti-His-HRP was measured with a PHERAstar FS microplate reader (BMG LABTECH). Data were analysed using two-tailed unpaired *t*-test by Prism 9 (GraphPad, San Diego, CA, USA), and values were presented as mean ± SD. ns = no significant difference, ****$P < 0.0001$.

5.4 Notch binding ability of N-glycan variants

5.4.1 Establishing the nickel plate-based Notch binding assay

The role of the N-glycan modification on loop 5-6 of Jagged1-C2 on Notch activation and smooth muscle differentiation has been investigated in Chapter 4. However, it is necessary to consider whether the N-glycan on C2 can affect the Notch binding capacity of Jagged1. As shown in the previous section, T145N showed a decrease in both Notch1 and Notch2 binding, but not the S142N variant located on the same loop 5-6. This suggests loss of the N-glycan on C2 might affect Notch binding. To probe the interaction further, a second plate binding assay was developed using nickel coated plates which allowed immobilisation of ligands via their C-terminal His-tag. This assay is therefore performed in the opposite orientation to the original. All glycan variants, N143A, T145N and N217A were assessed together with S142N. Neutravidin-HRP attached biotinylated $Notch_{EGF11\text{-}13}$ constructs were added as analyte in solution (Figure 5-8).

A saturation curve of Jagged1 immobilisation was first constructed (Figure 5-9). Wells were shown to saturate on addition of 100 ng Jagged1 in 100 μL of HBS, and therefore an excess (300 ng ligand in 100 μL HBS) was added to each well for coating (see Chapter2 – Materials and Methods). $Notch_{EGF11\text{-}13}$ analyte was pre-clustered onto neutravidin-HRP to increase the avidity of the receptor/ligand interaction and enable detection. Purified $Notch1_{EGF11\text{-}13\text{-}BirA\text{-}His}$ and $Notch2_{EGF11\text{-}13\text{-}BirA\text{-}His}$ receptor were biotinylated by adding a mixture of biotin ligase and biotin, followed by reverse phase HPLC purification (performed by Dr Pat Whiteman, University of Oxford).

Saturation curves of Notch1 and Notch2 binding were constructed to optimise their concentrations used in this binding assay (Figure 5-11). Jagged1 WT and the Notch binding negative control, F207A/E228K, were immobilised on the nickel plate well surface respectively. Clustered Notch1 and Notch2 constructs were subsequently added into wells at a range of concentrations, from 0 nM to 600 nM (Figure 5-11). All negative controls showed lower signal than wild type under each concentration. Two Notch concentrations were utilised to assess binding based on this curve, low concentration (40 nM Notch1 and 20 nM Notch2) and high concentration (400 nM Notch1 and 250 nM Notch2) (Figure 5-11).

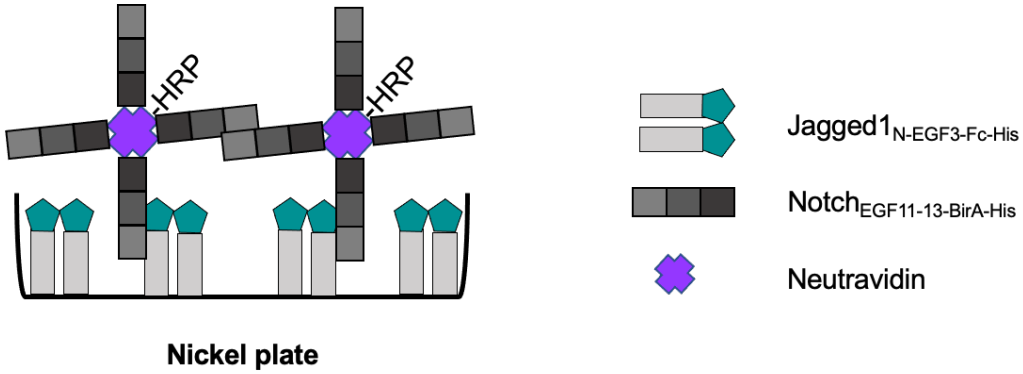


Figure 5-8. Schematic figure of Notch binding assay using nickel plates

His-tagged Jagged1 constructs (teal pentagons with light grey rectangles) were immobilised on nickel coated plates. Biotinylated Notch$_{EGF11-13}$ (grey rectangles) clustered on neutravidin-HRP (purple) was added as analyte. HRP signal was quantified by a PHERAstar FS microplate reader (BMG LABTECH).

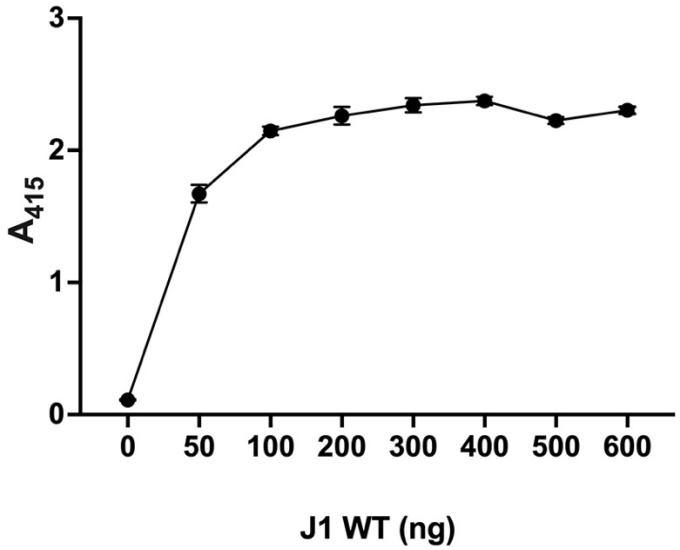


Figure 5-9. Saturation curve of Jagged1$_{N-EGF3-Fc-His}$ immobilisation on nickel plates

Saturation curve generated for Jagged1$_{N-EGF3-Fc-His}$ using anti-Fc-HRP mAb for quantification. After addition of substrate, absorbance at 415 nm was recorded and plotted. Wells were saturated following addition of 100 ng Jagged1 per well in 100 μL HBS, 5 mM Ca^{2+}, pH 7.5. Triplicate samples of ligand were immobilised and mean ± SD are shown.

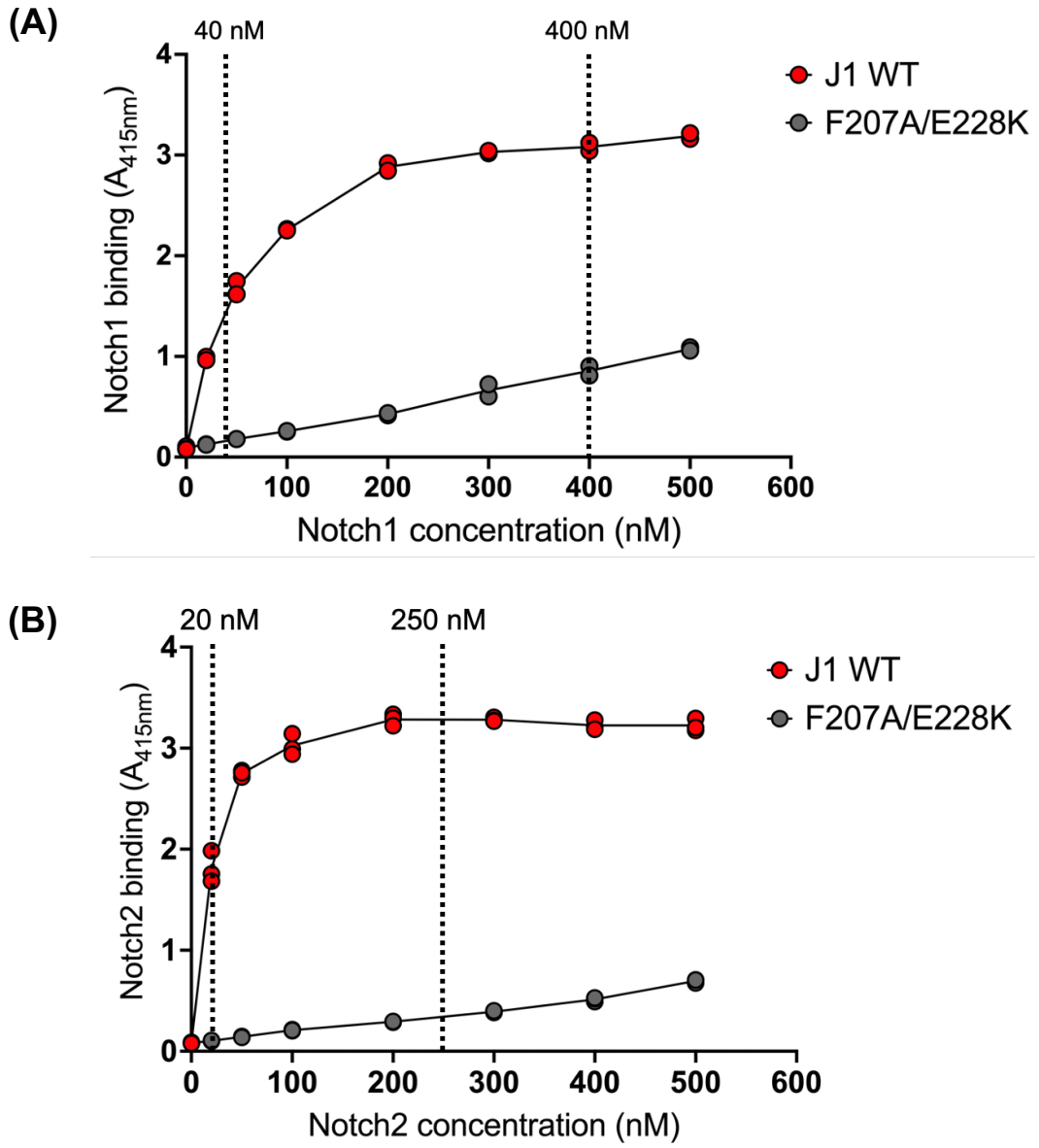


Figure 5-10. Notch$_{EGF11-13}$ saturation curves of immobilised ligands

Human Notch1(A) and Notch2 (B) binding curves were acquired. Jagged1 wild type (red dots) and F207A/E228K (negative control, dark gey dots) samples were attached to the nickel plate via His-tag, and Notch EGF11-13 added at a range of concentrations (0 nM – 500 nM), each of three repeat wells (Figure 5-9). Two concentrations were selected (indicated by dotted vertical lines) for glycan variant testing. Data were plotted using GraphPad Prism 9 (GraphPad, San Diego, CA, USA).

5.4.2 Notch1 and Notch2 binding of glycan variants

After optimisation, Notch binding was assessed. Binding of each variant was expressed as a percentage of Jagged1 WT signal obtained at the high concentration of Notch.

In both Notch1 and Notch2 binding assays, two binding deficiency negative controls (F207A and F207A/E228K) and a binding defective COSMIC variant shown in the previous section (E228K) (section 5.3) gave a lower signal than wild type when both high and low concentrations of Notch were used (Figure 5-11, 5-12). S142N and N217A variants showed no effect on both Notch1 (P = 0.0983 and P = 0.3453 (high Notch), P = 0.5928 and P = 0.0976 (low Notch)) and Notch2 (P = 0.3338 and P = 0.3052 (high Notch), P = 0.2166 and P = 0.2104 (low Notch)) binding capacity (Figure 5-11, 5-12). These data indicate that neither an amino acid substitution on loop 5-6, which retains the N-glycan, nor loss of an N-glycan in the DSL domain affects Notch binding. However, T145N and N143A both showed a decrease in both Notch1 and Notch2 binding at both concentrations (P < 0.0001) suggesting some impact of loss of loop 5-6 N-glycan on binding, although less than that seen with variants (F207A, E228K) which had direct changes to the ligand/receptor binding interface. Results acquired from this Notch1 and Notch2 binding assay were consistent, although negative controls had higher signals in Notch1 binding assay than Notch2 (Figure 5-11, 5-12). This is most likely due to the higher levels of O-glycosylation observed in Notch2 fragment producing less signal to noise.

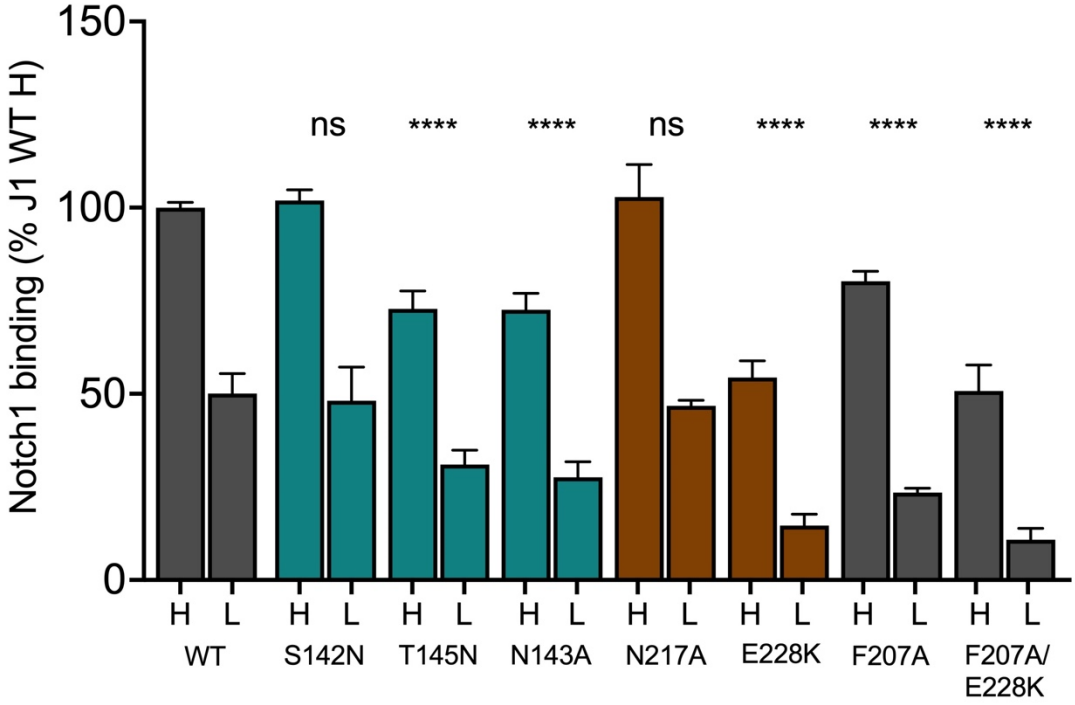


Figure 5-11. Notch1 binding of N-glycan variants

All N-glycan variants were bound to the nickel coated plate alongside wild type Jagged1 and negative controls. Pre-clustered $Notch1_{EGF11\text{-}13}$ was added to wells at high (H, 400 nM) and low (L, 40 nM) concentrations. Three independent experiments were performed with all points in triplicate. Binding was expressed as a percentage of WT signal obtained at the high concentration of Notch. Values from each variant were compared with wild type Jagged1 at high and low concentrations of Notch using a two-tailed unpaired *t*-test. Data were presented together as mean ± SD by Prism9. ****$P < 0.0001$, ns = no significant difference.

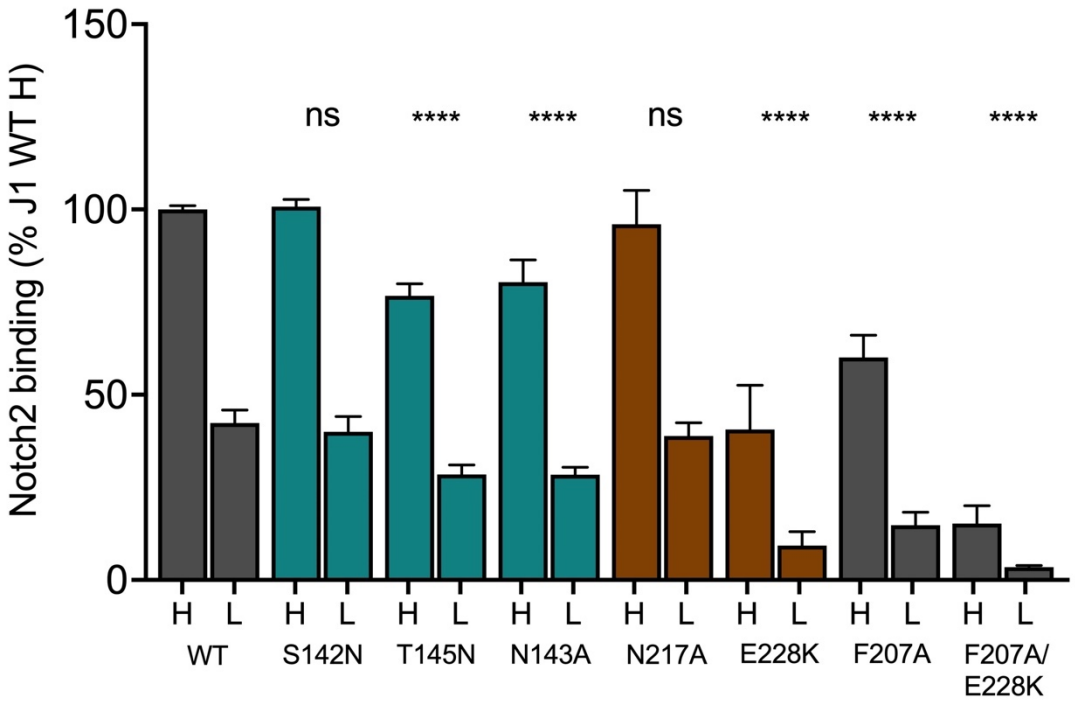


Figure 5-12. Notch2 binding of N-glycan variants

All glycan variants were tested using the same experimental procedure as for Notch1. High (H, 250 nM) and low (L, 20 nM) concentrations of pre-clustered Notch2 constructs were added into wells subsequently. Three independent experiments were performed with all points in triplicate. Data were analysed as for Notch1 and presented as mean ± SD by Prism9. ****P <0.0001, ns = no significant difference.

5.5 Development of a novel lipid binding assay

Notch ligand C2 domains have a lipid-binding property, although they are unlikely to be deeply buried within the cell membrane due to the moderate hydrophobic character of loop regions (section 1.5.3). Apical loops (loop 1-2 and loop 5-6) of C2 comprise the main lipid-binding site and are ordered upon calcium binding in both human Jagged1 and Jagged2 (section 1.5.3). In other C2 domains, loop 3-4 may contribute to lipid-binding. To further investigate the lipid-binding property of both COSMIC and N-glycan variants, a novel liposome binding assay was established.

In previous studies, a plate-based liposome binding assay was used (Suckling et al., 2017) (Figure 5-21). This method involves a combination of immobilizing purified Notch ligands onto a plate surface, incubating the ligand-coated plate with fluorescent liposomes and washing off excess liposomes. From this, the amount bound to ligand in each well can be obtained by the fluorescence intensity readout. However, since Jagged1-C2 domain shows a weak interaction with lipids compared to other intracellular C2 domains, such as that from synaptotagmin1, many repeats are required to obtain sufficient data to demonstrate statistically significant differences (Suckling et al., 2017). Development of an assay is required which avoids washing steps if possible.

Flow cytometry has been used for investigating lipid interactions in previous studies and it can analyse particles in a high throughput manner (Moreno et al., 2009). In an independent C2 phospholipid binding study, it was found that mixing GST-tagged dimer recombinant protein with liposomes in solution increases the solution turbidity (liposome aggregation) due to the association of liposomes with lipid-binding domains (Connell et al., 2008). Thus, a FACS-based liposome aggregation assay was developed in this project utilising the Fc tag of hJagged1.

5.5.1 Liposome binding observed by an imaging flow cytometer

To assess Jagged1-C2 and liposome interactions, a mixture of WT Jagged1$_{\text{N-EGF3-Fc-His}}$ coated protein G fluorescent beads ($\lambda_{excitation}$ = 620 nm, $\lambda_{emission}$ = 650 nm, red fluorescence) and fluorescent-labelled liposomes ($\lambda_{excitation}$ = 490 nm, $\lambda_{emission}$ = 515 nm, green fluorescence) in HEPES buffer, 5 mM Ca^{2+}, pH 7.5 (“Jagged1 WT”) was initially assessed by an imaging flow cytometer, Amnis® ImageStream®^{x} Mk II, and compared with a bead only sample without addition of liposomes (“beads only”). The

saturation point of beads by Jagged1$_{N\text{-}EGF3\text{-}Fc\text{-}His}$ was determined first by western blotting to ensure a maximum and equal amount of ligand was attached to the protein G beads via the Fc-tag.

A dilution series of Jagged1$_{N\text{-}EGF3\text{-}Fc\text{-}His}$ were incubated with 50 μL washed protein G beads, and 2 μL samples of coated beads were analysed by reducing SDS-PAGE followed by immunoblotting using anti-His-HRP detection (see Chapter 2). 50 μL beads were saturated by addition of 1 μg Jagged1. An excess of protein (2 μg) was therefore used in the following liposome binding assessments (Figure 5-13). Buffer conditions used were HBS, 5 mM Ca^{2+}, pH 7.5.

Phosphatidylcholine-rich (PC-rich) liposomes consisting of a mixture of phosphatidylcholine (PC), phosphatidylserine (PS), phosphatidylethanolamine-carboxyfluorescein (PE-CF) (PC:PS:PE-CF = 70:25:5) prepared by Dr Shruti Mittal (University of Oxford), were extruded by a 100 nm filter. Liposome size was assessed by dynamic light scattering, which showed more than 90% homogenous particles with a diameter 70.5 nm (Figure 5-13). Diluted liposomes were then added to the Jagged1-coated bead solution to observe liposome binding (see Chapter 2 - Materials and Methods). In both beads only and Jagged1 WT with addition of liposomes, the red-fluorescent beads can be seen. Green-fluorescent particles were clearly observed on the surface of the Jagged1-coated beads in immunofluorescent images, but were largely absent in the beads only images, taken by the imaging flow cytometer (Figure 5-14). In addition to single beads, aggregation was observed in both samples, corresponding to dimeric and trimeric beads (Figure 5-14). To quantify this

aggregation precisely, further analysis was performed by flow cytometry using a non-imaging conventional machine.

The imaging flow cytometer, which combines traditional flow cytometry with fluorescence microscopy, allows observation of individual events in a population. However, it takes much more time to analyse samples than a conventional flow cytometer, and this will increase incubation time variations (incubation of coated beads with liposomes in solution) when a set of variants and control samples are analysed at one time. To assess more events in each sample and decrease the potential error caused by incubation time variation, a conventional flow cytometer was used to analyse liposome/bead aggregation in individual samples.

5.5.2 Liposome aggregation analysis by FACS

The aggregation gating strategy and liposome incubation time were tested and optimised using a conventional flow cytometer to ensure reproducibility and specificity of the assay. Protein G beads coated by Jagged1$_{N\text{-}EGF3\text{-}Fc\text{-}His}$ were set up initially for a solution turbidity analysis, alongside an IgG (unrelated protein which binds to protein G) sample as a negative control. PC-rich liposomes were added to the Jagged1$_{N\text{-}EGF3\text{-}Fc\text{-}His}$ and IgG beads samples respectively and incubated for 0.5 hour on ice (see Chapter 2). Protein G beads, without any protein coated on the surface, and without any liposomes added, were also tested to observe their background aggregation behaviour.

5.5.2.1. The gating strategy of the aggregation assay

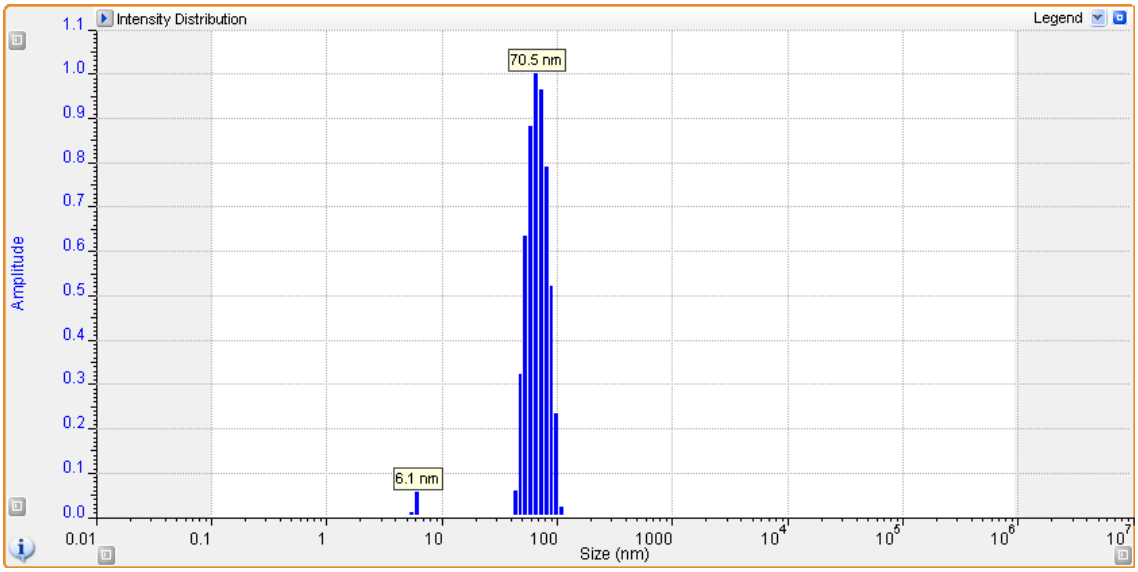
The gating strategy is shown in Figure 5-15. The first step in gating was to distinguish the protein G bead population (including monomers and aggregates) based on forward scatter (FSC, discrimination of events by size) versus side scatter (SSC, identification of events by complexity). The bead population, selected through size and complexity, was further confirmed to be red-fluorescent positive as expected by plotting green-fluorescent intensity (x-axis) versus red-fluorescent intensity (y-axis). More than 99% of the selected population are red-fluorescent positive, which confirms the correct gating of the bead population (Figure 5-15). Furthermore, in the Jagged1 WT sample, more events spread to the green-fluorescent positive side, which suggested more liposomes were bound to the Jagged1 WT coated beads than the negative IgG control (Figure 5-15). Red-fluorescent positive populations were replotted by FSC versus SSC, and the aggregates shown as a percentage of the total bead population. Jagged1 WT showed a ~ 4-fold increase in percentage aggregation than IgG coated beads and beads only sample. These data suggest this aggregation assay can be used to assess liposome binding to Jagged1 variants (Figure 5-15).

5.5.2.2. Optimising incubation time

In a previous synaptotagmin1 C2A domain turbidity assay study, the maximum value of liposome aggregation was observed after around 100 seconds (Connell et al., 2008). Before any variants were tested, a time-dependent aggregation test was set up to optimise incubation time and observe any changes. The aggregate percentage of the Jagged1 WT sample and the negative control, IgG sample, was recorded every 15 minutes (Figure 5-16). From the acquired curve, the liposome/bead aggregation happened in solution almost immediately and was stable for 1.5 hours, the duration of the test (Figure 5-16). Thus, a 0.5-hour incubation time was selected and utilised for

all samples. The rapid aggregation observed in the assay might be due to binding many copies of the ligand to bead via Fc-tag/Protein G interactions which produces a large avidity component.

(A)



(B)

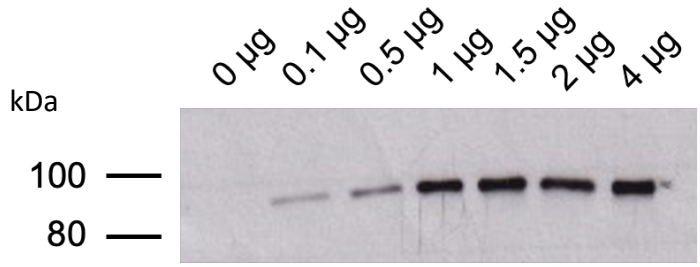


Figure 5-13. Analysis of PC-rich liposomes and saturation of Protein G beads

(A) PC-rich liposomes with a composition of PC/PS/PE-CF (70:25:5) were analysed by dynamic light scattering measurement after 100 nm polycarbonate filter extrusion. (B) Saturation of Protein G beads by Jagged1$_{N\text{-}EGF3\text{-}Fc\text{-}His}$ was determined by western blotting. A dilution series of Jagged1, ranging from 0 µg – 4 µg, was used for bead coating, and 2 µL of coated beads were assessed. 1:2000 anti-His-HRP was used for signal detection. Protein G beads showed saturation when ~ 1 µg Jagged1$_{N\text{-}EGF3\text{-}Fc\text{-}His}$ was added.

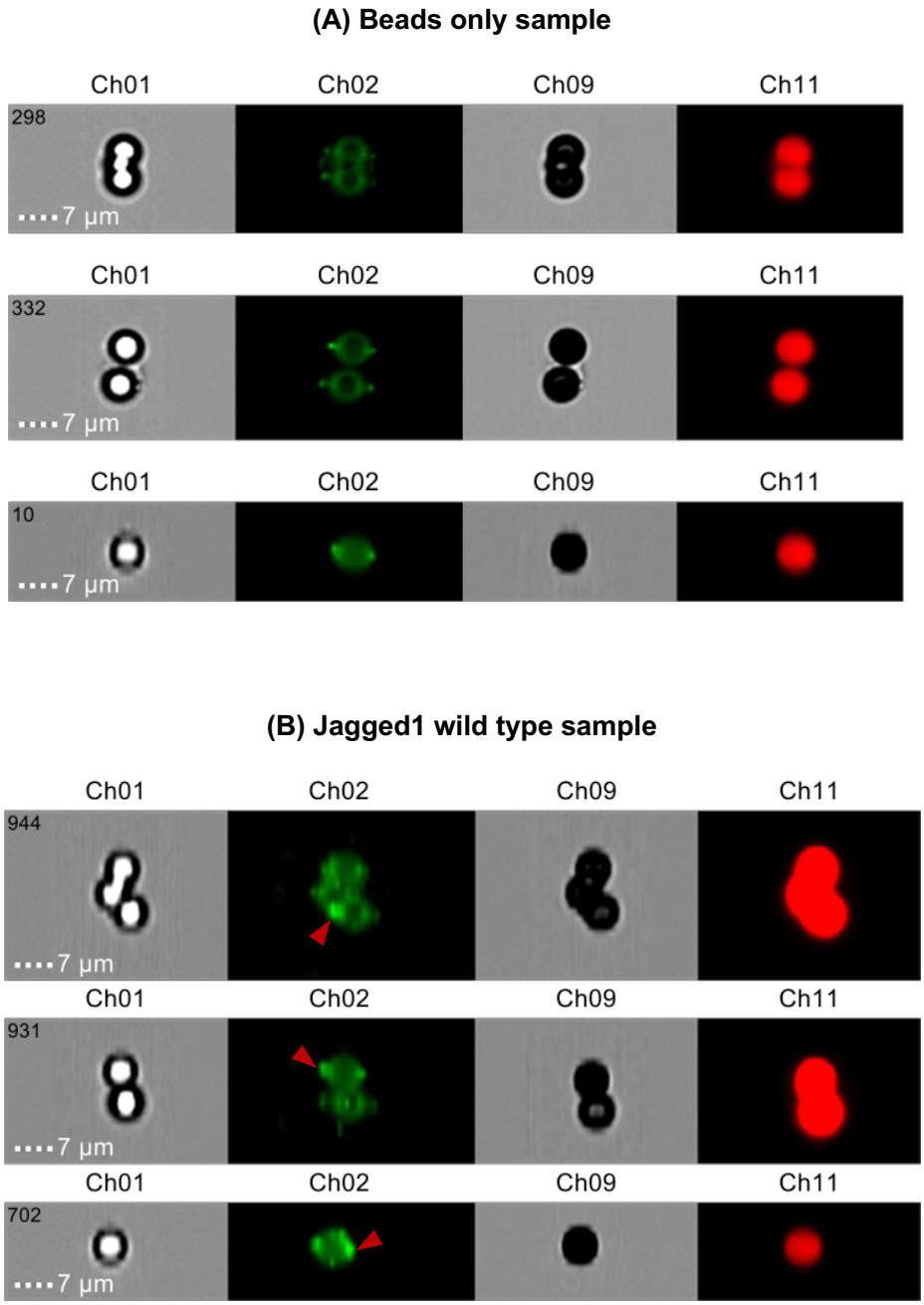


Figure 5-14. Immunofluorescent images of liposome binding to protein G immobilised ligands

Beads only sample (A) and a mixture of Jagged1 coated beads with liposomes (B) were analysed by an imaging flow cytometer, Amnis® ImageStream®^{x} Mk II. Ch01 and Ch09 are brightfield channels, illuminating samples using white light, from two different cameras. Ch02 detects green-fluorescent signal (excitation laser at 488 nm, and emission at 480 - 560 nm), and Ch11 detects red-fluorescent signal (excitation at 642 nm, emission at 642 - 745 nm). Green-fluorescent particles corresponding to liposomes (indicated by red arrow heads) can be observed on the Jagged1 coated beads surface (B) but not on the beads only surface (A) in Ch02. Most events in each sample were single, dimer and trimer beads, and representative figures are shown.

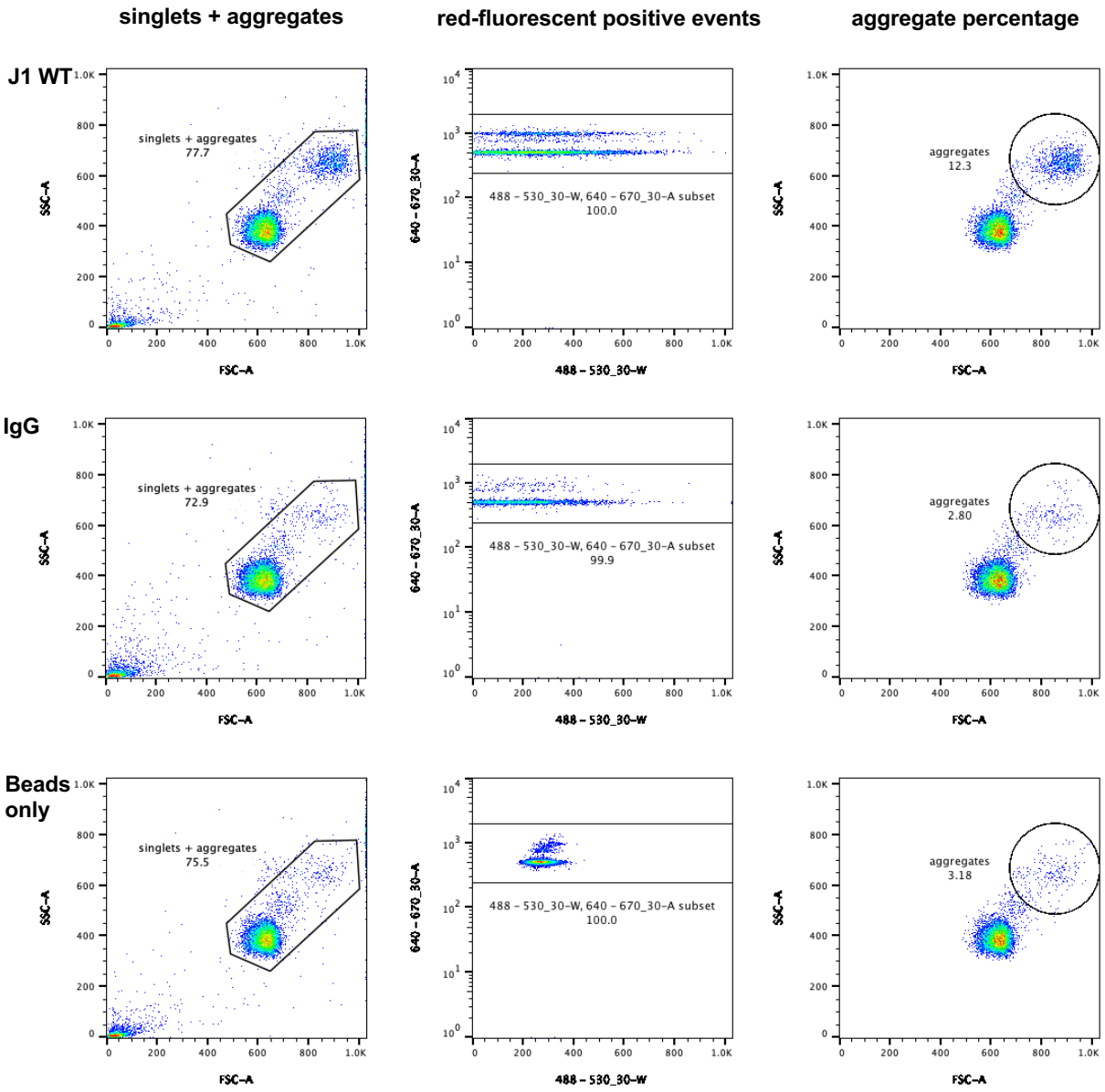


Figure 5-15. Gating strategy for aggregation analysis by a conventional flow cytometer

Jagged1 and IgG protein were immobilised on the surface of protein G fluorescent beads followed by the addition of PC-rich liposomes. Bead population was gated by size and complexity using FSC versus SSC ("singlets + aggregates"). The selected bead population was further confirmed to be red-fluorescent positive by plotting green-fluorescent signal on x-axis (excitation 488 nm/ emission 530 nm) versus red-fluorescent signal on y-axis (excitation 640 nm/ emission 670 nm) ("red-fluorescent positive events"). Confirmed bead population was replotted as FSC versus SSC, and the percentage of aggregated beads was shown as a percentage of the total bead population ("aggregation percentage"). There is a higher aggregate population in the Jagged1 WT sample (12.3%) compared to IgG (2.8%) and beads only (3.18%) sample, which corresponds to an increase in liposome attachment to the Jagged1 coated beads. 10,000 events were recorded for each sample. Data were acquired by BDX-20 (BD Biosciences) flow cytometer and analysed using FlowJo software.

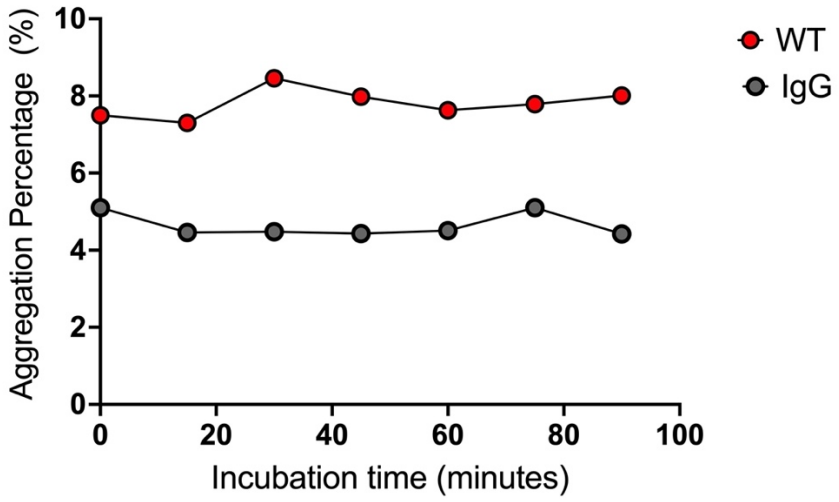


Figure 5-16. Liposome aggregation percentage curve of Jagged1 WT compared to IgG
A time dependent assessment of Jagged1 WT (red circles) and IgG negative control samples (grey circles) showed aggregation of coated Protein G beads happens rapidly on addition of liposomes in HBS with 5 mM Ca^{2+} at pH 7.5. The aggregation percentage did not show an obvious change over 1.5 hours. Aggregation percentage was acquired by BDX-20 (BD Biosciences) flow cytometer and analysed using FlowJo software. The graph was plotted by Prism 9. Individual samples of WT and IgG were tested and monitored, with 10,000 events recorded at each time point.

5.6 Lipid binding property of COSMIC variants

All but one of the secreted COSMIC variants showed a decrease in Notch activation in Chapter 3, and binding to Notch1 and Notch2 were tested using plate-based binding assay in section 5.3. In this section, the effect of COSMIC substitutions on liposome binding was tested using the newly developed FACS-based aggregation assay.

The PC-rich lipid aliquot was thawed and extruded using a 100 nm filter before use and dynamic light scattering performed to check homogeneity of liposomes (Chapter 2) (Figure 5-13, A). In addition to IgG and beads only, Jagged1 D140/144A, a lipid-binding deficient construct (section 3.6.2) and Jagged1 DE3, a Jagged1 construct comprising DSL to EGF3 domains without C2, were also used as negative controls. To be certain that any changes seen in aggregation percentage were not due to

differences in the number of beads used or different amounts of protein loaded, a small volume of resuspended protein coated beads was taken before incubation with liposomes, and equivalent loading of protein on beads was confirmed by immunoblotting (Figure 5-17, B).

Five independent repeats for each variant were measured, and aggregation percentages analysed in each case. All negative controls, including D140/144A, DE3, IgG and beads only, showed a statistically significant reduction in aggregation percentage (Figure 5-17). The data show that two variants, G114D and T145N, in the panel of COSMIC variants showed a statistically significant decrease in PC-rich liposome binding ($P < 0.01$), whilst all other COSMIC substitutions had no statistically significant effect on PC-rich liposome binding, although there was some variation in the level of aggregation observed (Figure 5-17).

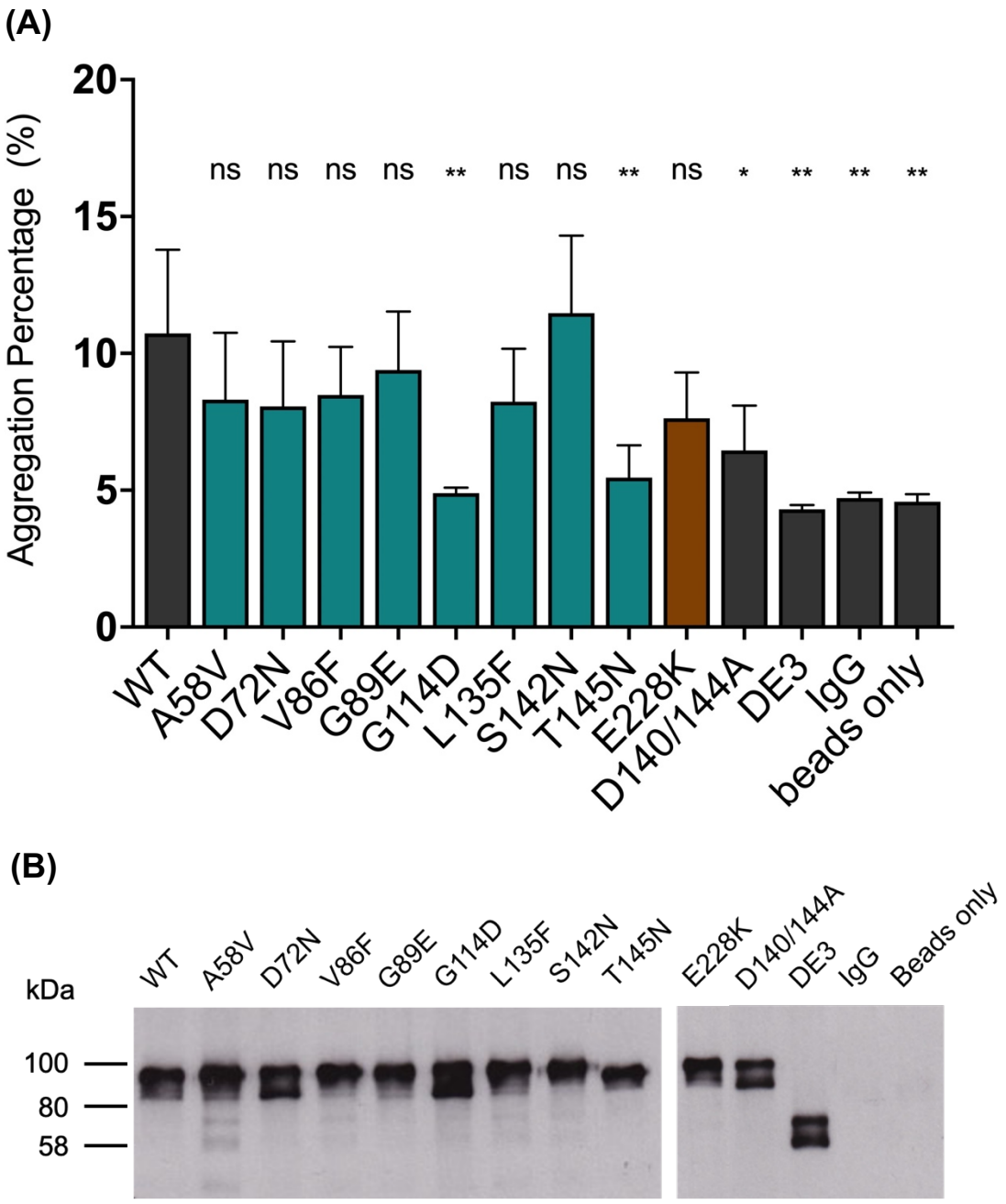


Figure 5-17. Liposome binding of COSMIC variants

(A) The liposome aggregation assay of COSMIC variants using PC-rich liposomes is shown. 5 individual repeats were performed, and the aggregation percentages were presented as mean ± SD. Comparison between each variant and wild type was performed with a two-tailed unpaired *t*-test. ns = no significant difference, **P* < 0.05; ***P* < 0.01. (B) A representative western blot following reducing SDS-PAGE showed equal loading of wild type Jagged1 and variants. Signal was detected by anti-His-HRP (1:2000). No signal is detected in IgG coated beads and the beads only sample, as expected (both lack the His-tag).

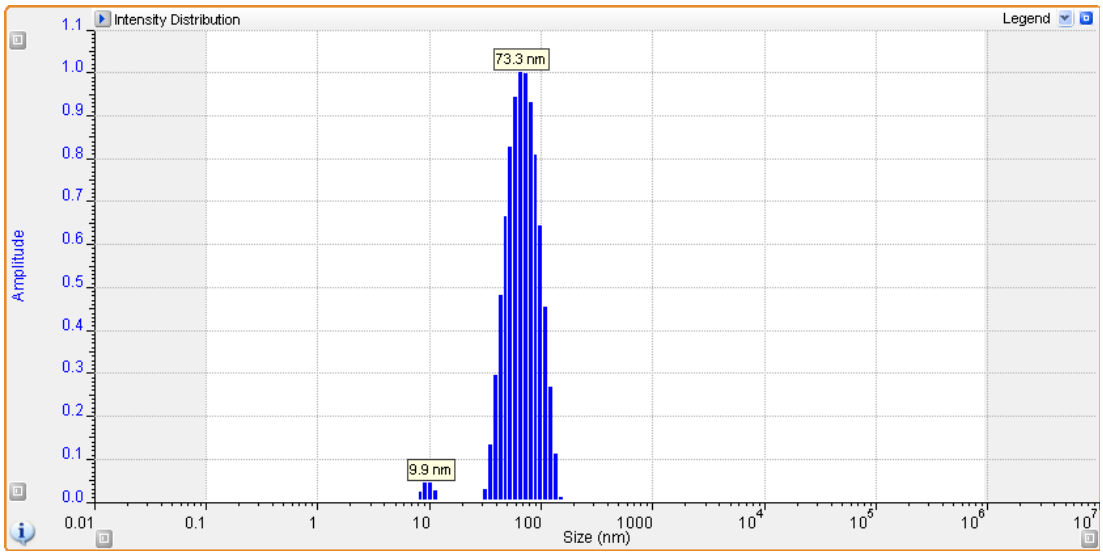
5.7 Lipid binding property of N-glycan variants

The effects of the N-glycan-related substitutions on PC-rich liposome binding were subsequently tested, and the same data analysis was performed. In addition to PC-rich liposomes, an outer-membrane leaflet lipid, sphingomyelin (SM), was incorporated into liposomes for comparison. The SM-rich lipid stock (SM:PC:PS:PE-CF = 40:30:25:5) was made by Dr Shruti Mittal, University of Oxford. The homogeneity of extruded SM-rich liposomes was measured by dynamic light scattering before incubating with ligand coated beads (Figure 5-18). Prior to assay, the coating efficiency of N-glycan variants on Protein G beads was assessed and shown to be equivalent (Figure 5-18).

Using PC-rich liposomes, all negative controls (D140/144A (DDAA), DE3 and IgG and beads only) showed a statistically significant decrease in liposome aggregation (Figure 5-19). Both N-glycan variants, T145N and N143A, also showed a statistically significantly reduction in liposome binding compared to the WT ($P < 0.01$) (Figure 5-19). In contrast, S142N and N217A variants had a similar liposome binding capacity to the WT samples (Figure 5-19).

The N-glycan variants were tested subsequently using SM-rich liposomes and showed a similar trend seen using PC-rich liposomes (Figure 5-20). The T145N and N143A substitutions showed statistically significant decreased binding to SM-rich liposomes ($P < 0.0001$), while S142N and N217A showed no obvious difference in binding compared to WT (Figure 5-20).

(A)



(B)

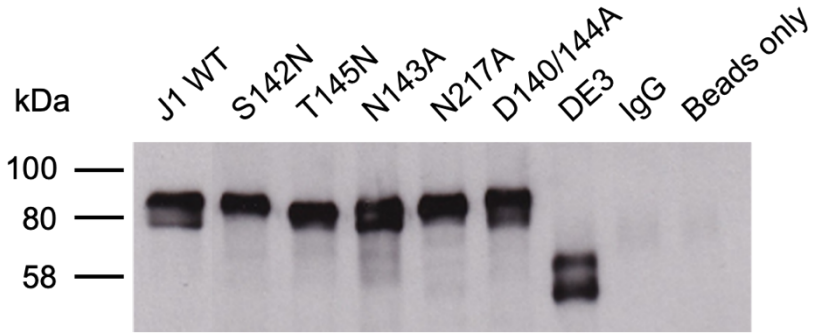


Figure 5-18. Assessment of SM-rich liposomes and coating of beads by N-glycan variants

(A) SM-rich liposomes with a composition of PC/SM/PS/PE-CF (30:40:25:5) were assessed by dynamic light scattering after 100 nm pore width membrane extrusion. Liposomes were 90% homogeneous with 73.3 nm diameter. (B) A representative western blot showed equal loading of N-glycan-related variants. Anti-His-HRP (1:2000) was used for signal detection. No signal was detected in IgG coated beads and the beads only sample, as expected.

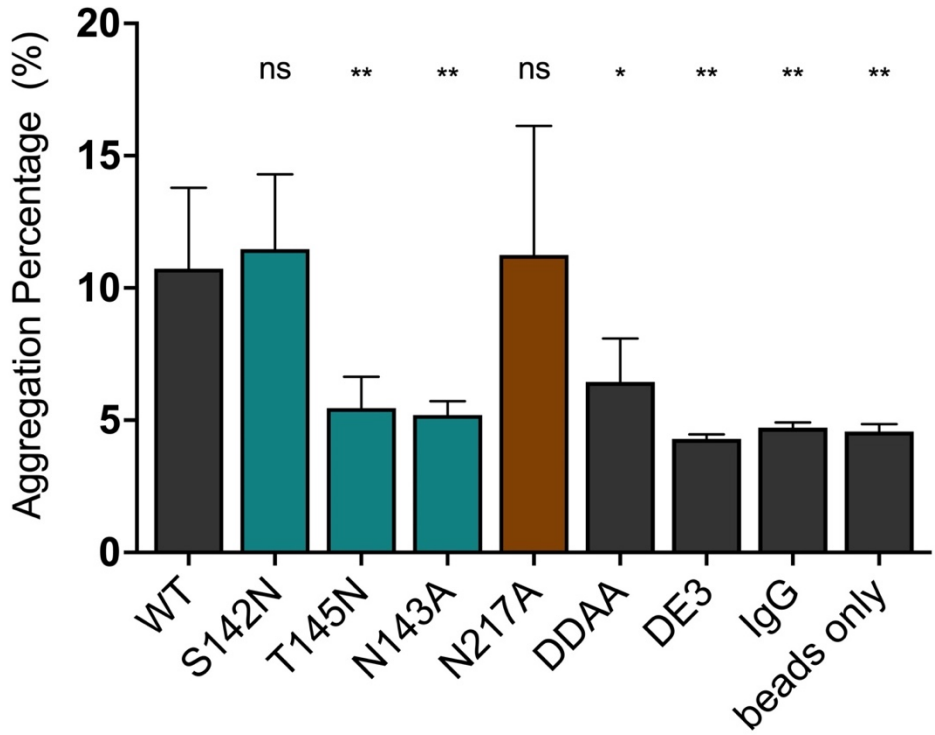


Figure 5-19. PC-rich liposome binding of N-glycan variants

PC-rich liposome aggregation percentages of N-glycan variants are shown. The graph shows the combined results of five independent repeats and data are presented as mean ± SD. More than one preparation of protein stock was used for each variant. DDAA = D140/144A lipid binding defective variant. Statistical comparisons between WT and variants were performed with two-tailed unpaired *t*-test using Prism 9. ns = no significant difference, **P* < 0.05, ***P* < 0.01.

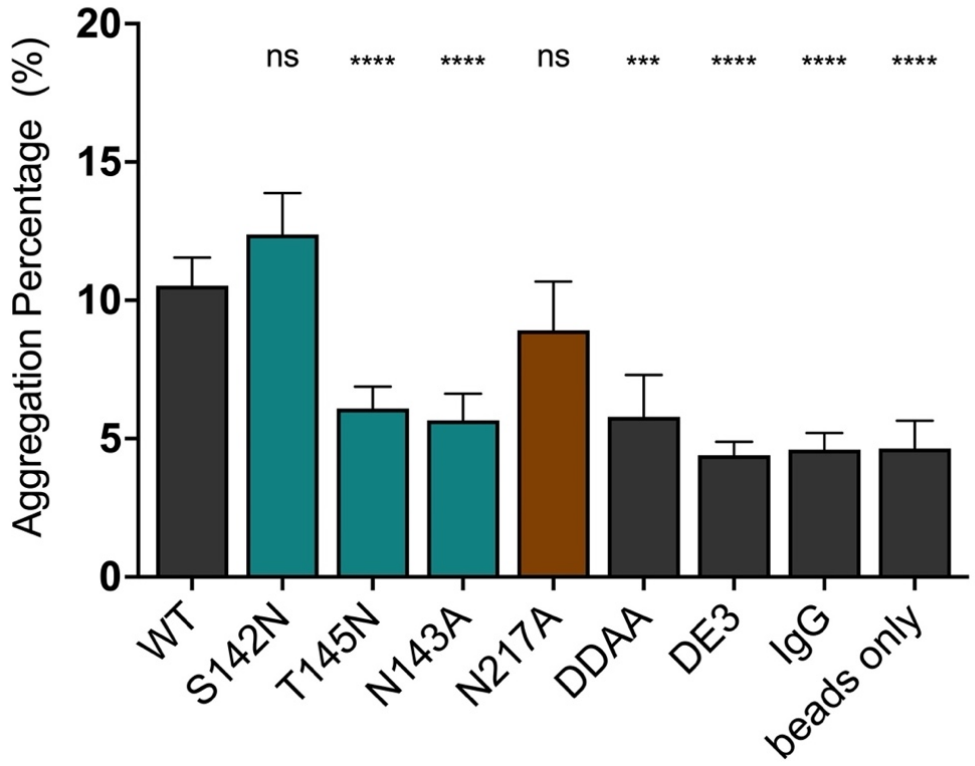


Figure 5-20. SM-rich liposome binding of N-glycan variants

SM-rich liposome aggregation assay was performed to assess N-glycan variants. Five independent repeats were performed using separate batches of protein stocks for each variant. DDAA = D140/144A. Combined data are shown as mean ± SD. Statistical comparisons between WT and variants were analysed by two-tailed unpaired *t*-test using Prism 9. ns = no significant difference, ***$P < 0.001$, ****$P < 0.0001$.

5.8 Conclusion

In this chapter, a novel FACS-based liposome binding assay was developed, and a summary comparing methods as well as the advantages and disadvantages of previously used plate-based assay and this FACS-based assay are described in Figure 5-21. Notch-binding and liposome-binding ability of Jagged1 variants was assessed by a series of molecular assays, and the effects are summarized in Table 5-1 and 5-2.

Firstly, a plate-based Notch binding assay was used for all secreted COSMIC variants. Four of the variants showing reduced activation also showed a decrease in Notch binding. Two of these variants (V86F and G89E) are located at the bottom loop, loop 2-3, of the Jagged1-C2 domain, which is located at the C2-EGF12 binding interface (Figure 5-6, 5-7) (Table 5-1). This reflects that loop 2-3 of Jagged1-C2 has an important role in Notch binding ability. E228 is located in the DSL-EGF11 binding interface and as expected the K substitution greatly reduced Notch binding (Figure 5-6, 5-7). G89E showed low binding to Notch1 but not Notch2 suggesting differences in the way Notch paralogues interact with Jagged1. A variant locating on loop 3-4 of Jagged1-C2, G114D, showed extremely higher Notch binding ability in both Notch1 and Notch2 binding assay. This suggest that mutations on the loop structure of C2 can increase Notch binding ability indirectly. T145N, which removed an N-glycan on the loop 5-6 showed a decrease in both Notch1 and Notch2 binding assays, suggesting that this N-glycan might play an indirect role in Notch binding (Figure 5-6, 5-7) (Table 5-1). Since this result was unexpected, T145N was tested together with other N-glycan related variants using a nickel-plate-based Notch1 and Notch2 binding assays looking at binding in the opposite orientation.

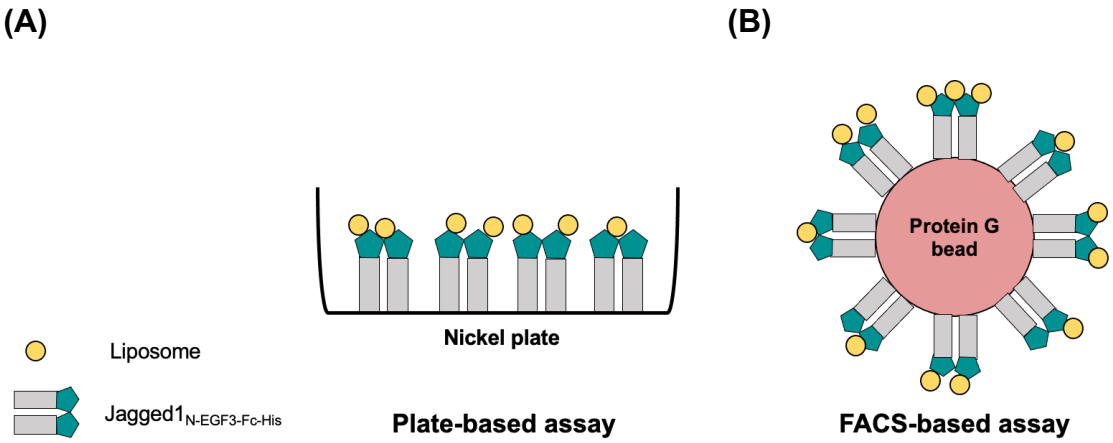
In the nickel plate binding assay, T145N and N143A showed a statistically significant reduction in Notch binding, which suggests the N-glycan on C2 has a role in Notch binding (Figure 5-11, 5-12) (Table 5-2). As it is located on a loop far from the ligand-receptor binding interface (Figure 4-8), the N-glycan on C2 most likely influences Notch binding indirectly, possibly through stabilising a face of the C2 domain. Removing the N-glycan on the DSL domain did not influence Notch1 or Notch2 binding indicating loss of an N-glycan per se does not explain altered binding by loop 5-6

glycan variants (Figure 5-11, 5-12) (Table 5-2). In addition, consistent with Notch binding data collected using maxisorp immobilisation of ligand, S142N did not have an obvious effect on Notch1 and Notch2 binding. This suggests that substitutions of loop 5-6 residues alone, which do not result in N-glycan removal, do not affect the Notch binding capacity of Jagged1 (Figure 5-11, 5-12) (Table 5-2).

Loss of Notch activation by four COSMIC variants, D72N, G114D, L135F and S142N cannot be explained obviously by Notch1,2 binding deficiency. Thus, whether the decrease in activity resulted from altered membrane interaction or membrane/Notch interplay was further investigated.

A new FACS-based aggregation assay was developed and applied. This FACS-based assay avoided washing steps, which facilitated the study of weak lipid-protein interactions. All secreted COSMIC variants showed a similar PC-rich liposome binding ability as wild type, except G114D and T145N (Figure 5-17) (Table 5-1). G114D, located on loop 3-4 of Jagged1-C2, showed a statistically significant decrease in PC-rich liposome binding (Figure 5-17) (Table 5-1). It has been noted that loop 3-4 of the C2 domain forms a β-cationic lipid binding groove in some proteins (section 1.5.1). Liposome data suggest residue G114 is important for membrane binding, either directly or indirectly. As G114D did not show a deficiency in Notch binding, its lipid binding ability might mean that it acts as a dominant negative in Notch activation regulation. Moreover, T145N also showed a decrease in PC-rich lipid binding, which suggests the N-glycan might have an important role in the lipid binding property of Jagged1-C2 (Figure 5-17). Neither liposome-binding nor Notch-binding assays provide an explanation for reduced Notch activation by D72N and L135F variants.

Subsequently, the N-glycan variants were further analysed for liposome binding using two different liposome compositions, PC-rich and SM-rich. Data obtained from both were consistent (Figure 5-19, 5-20) (Table 5-2). T145N and N143A both showed a statistically significant decrease in lipid binding, which indicates loss of the N-glycan on the loop 5-6 influences the lipid binding property of Jagged1-C2 (Figure 5-19, 5-20) (Table 5-2). As the N-glycan on C2 is located very close to loop 3-4 (Chapter 4) and a potential cationic groove site, the N-glycan might stabilise a conformation required for lipid binding. S142N on the loop 5-6 did not have a detectable effect on lipid binding using either lipid compositions, which suggests the N-glycan has a more major role in conferring lipid binding. However, more subtle effects may not be detected in this assay due to the avidity effect of using a ligand coated bead.



(C)

Assay type	Plate-based	FACS-based
Advantages	• Less experimental cost. • Easier to control equal amount of tested protein (by saturating the plate surface).	• High-through output. • Less protein sample needed for each assay. • No washing steps are involved, which reduces losses. • Dimer proteins localized on the bead surface increased the avidity of interaction.
Disadvantages	• Washing steps involved. • More protein sample required.	• High experimental cost. • Needs more attention when resuspending beads to control equal amount of tested sample.

Figure 5-21. Comparison of plate-based and FACS-based liposome binding assays

Schematic figure showing a well-established plate-based method (A) and a FACS-based approach (B) for investigating weak lipid binding properties of ligands (not to scale). Ligands in the plate-based assay are coated onto the plate surface, whilst they are immobilized on the protein G bead surface via an Fc tag in the FACS based assay. After incubating with fluorescent liposomes, the signal from liposomes is acquired by a plate reader (plate-based method) or a flow cytometer (FACS-based method) respectively. (C) Comparison of the advantages and disadvantages of the techniques.

Domain	Mutation	Position at C2 domain	Notch1 binding	Notch2 binding	Lipid binding
C2	A58V	loop 1-2	no effect	no effect	no effect
C2	D72N	loop 1-2	no effect	no effect	no effect
C2	V86F	loop 2-3	low	low	no effect
C2	G89E	loop 2-3	low	no effect	no effect
C2	G114D	loop 3-4	high	high	low
C2	L135F	beta sheet 5	no effect	high	no effect
C2	S142N	loop 5-6	no effect	no effect	no effect
C2	T145N	loop 5-6	low	low	low
DSL	E228K	/	low	low	no effect

Table 5-1. Summary of binding of COSMIC variants to Notch and liposomes

In addition to the DSL variant (E228K), the variant without N-glycan on C2 (T145N) and two variants on loop 2-3, V86F and G89E, showed a decrease in Notch binding, although G89E only showed lower binding to Notch1. Two out of nine variants showed a reduction in the liposome binding assay. One lacks the N-glycan on C2 (T145N), and the other one has a substitution on loop 3-4, which can form a β-cationic groove in some proteins.

Domain	Mutation	Position at C2 domain	Presence of N-glycan on C2	Notch1 binding	Notch2 binding	Lipid binding
C2	S142N	loop 5-6	✓	no effect	no effect	no effect
C2	T145N	loop 5-6	X	low	low	low
C2	N143A	loop 5-6	X	low	low	low
DSL	N217A	/	✓	no effect	no effect	no effect

Table 5-2. Summary of effects of N-glycan variants

T145N and N143A but not S142N and N217A lose the N-glycan on C2. S142N substitutes the residue next to the N-glycan linked residue, N143. N217A changes the N-glycan motif on the DSL domain. Variants without N-glycan on C2 showed loss of function on Notch-binding and lipid-binding property.

Chapter 6. Study of the C2 domain of human DLL4 using cancer databases

6.1. Introduction

Human canonical Delta-like family ligands, DLL1 and DLL4, play important roles in several physiological processes, such as angiogenesis and HSC differentiation (see section 1.2.1). Like Jagged family ligands, the C2 domains of DLL1 and DLL4 in the context of N-EGF3 fragments were shown to have both Notch binding and lipid binding properties using a series of *in vitro* assays in previous studies, and the DLL4-Notch1 binding interface was revealed in the DLL4-Notch1 structural complex (Suckling et al., 2017) (Luca et al., 2015). Loops on the C2 domain differ in length, sequence, and conformation in the Delta-like ligand family. Furthermore, none of the Delta ligands for which structures are available have a calcium binding site within the C2 domain (Luca et al., 2015) (Suckling et al., 2017) (Martins et al., 2021a). With the exception of *Drosophila* Delta, they lack the N-glycan consensus sequence found on the loop 5-6 (Figure 4-1). The replacement of the DLL4 C2 domain with the equivalent from DLL1 affected the function of DLL4, which failed to induce T cell development and inhibit B cell development (Hirano et al., 2020). Recently, CRISPR engineering a loop 1-2 deletion in the C2 domain of *Drosophila* Delta was shown to result in reduced Notch activity in several physiological processes, such as photoreceptor fate decisions (Martins et al., 2021a). These *in vivo* data combined with *in vitro* results, suggests that the reduced Notch activity of the loop 1-2 variant was caused by a decrease in the membrane binding property of the Delta-C2 domain (Martins et al., 2021a). Two whole organism studies, including EHBA and *Drosophila* studies, now demonstrate the membrane binding property of the C2 domain is important for generation of the Notch signal (Suckling et al., 2017) (Martins et al., 2021a).

Previous chapters showed that introduction of certain missense mutations, found in the COSMIC database, into the loop structure of the Jagged1-C2 domain resulted in decreased Notch activation by affecting its Notch/lipid binding properties, which is consistent with observations from EHBA variants (Suckling et al., 2017). To investigate whether substitutions within the human DLL4-C2 affect Notch activation in the same way, DLL4 C2 variants recorded in cancer databases were selected and assayed.

The aim of this chapter is to clone and express human $DLL4_{N\text{-}EGF3\text{-}Fc\text{-}His}$ variants establish a human cell line expression system to acquire sufficient purified DLL4 constructs for functional assays. Previous expression studies had demonstrated low yields of DLL4 from HEK293T cells, therefore a new HEK293F cell expression system was trialled and shown to produce sufficient DLL4. Subsequently, a series of DLL4 variants from cancer databases were selected, expressed and assayed by complementary Notch1 luciferase reporter cells.

6.2. Designing constructs for production of $DLL4_{N\text{-}EGF3\text{-}Fc\text{-}His}$

The DLL4 constructs used for previous structural, Notch binding and liposome binding assays were $DLL4_{N\text{-}EGF3}$ monomers produced from S2 cells (Suckling et al., 2017). To acquire protein suitable for activation studies and allow comparison with Jagged1 variants, a plasmid containing the $DLL4_{N\text{-}EGF3}$ Fc-tagged dimer DNA sequence was cloned for HEK cell expression systems. As with the Jagged1 construct used previously, $DLL4_{N\text{-}EGF3\text{-}Fc\text{-}His}$ contains the core Notch binding region and should express as a soluble dimeric fragment in the extracellular medium with a MW of 61 kDa.

The pHL-sec-Jagged1$_{N\text{-}EGF3\text{-}Fc\text{-}His}$ plasmid was digested by *Eco*RI and *Acc*65I to generate a pHL-sec backbone with Fc and His tag sequences (Figure 6-1). The cDNA of full-length human DLL4 (a kind gift from Prof Adrian Harris, University of Oxford) was used to obtain the desired DLL4 cDNA fragment encoding N-terminus to EGF3 (residue 1 to 325) by PCR. As an *Acc*65I restriction site exists within the DLL4$_{N\text{-}EGF3}$ cDNA sequence, another restriction enzyme digestion site, *Bsi*WI, was used to generate a compatible cohesive end within DLL4 cDNA to allow cloning. The DLL4$_{N\text{-}EGF3}$ insert was amplified by PCR with the full-length DLL4 cDNA as a template, and primers containing restriction enzymes (*Eco*RI and *Bsi*WI) sequences were used for DLL4$_{N\text{-}EGF3}$ amplification (Figure 6-1) (Appendix A). PCR products were digested by *Eco*RI and *Bsi*WI and ligated with *Eco*RI/*Acc*65I digested pHL-sec backbone (Figure 6-1). Putative plasmids containing DLL4 were sequenced, and positive samples selected. The map of pHL-sec-DLL4$_{N\text{-}EGF3\text{-}Fc\text{-}His}$ is shown in Figure 6-2.

Alongside expression trials in HEK293F, a mammalian expression vector, pcDNA3.1(+), with a Geneticin selectable marker (conferred by the Neomycin resistance gene sequence) was used as another vector to create a stable line of DLL4$_{N\text{-}EGF3\text{-}Fc\text{-}His}$ in HEK293. The pcDNA3.1(+) vector has a CMV promoter rather than the chicken β actin promoter in pHL-sec backbone (Figure 6-2, 6-3). Both CMV and chicken β actin promoters are frequently used to drive high levels of expression of recombinant protein in mammalian cells. *Eco*RI and *Xho*I digestion of both pHL-sec-DLL4$_{N\text{-}EGF3\text{-}Fc\text{-}His}$ and pcDNA3.1(+) vectors allowed preparation of cDNA insert and backbone (Figure 6-3, A). The sequence of pcDNA3.1(+)-DLL4$_{N\text{-}EGF3\text{-}Fc\text{-}His}$ obtained after ligation was confirmed by the Sanger sequencing service (Source Bioscience). The plasmid map is shown in Figure 6-3, B.

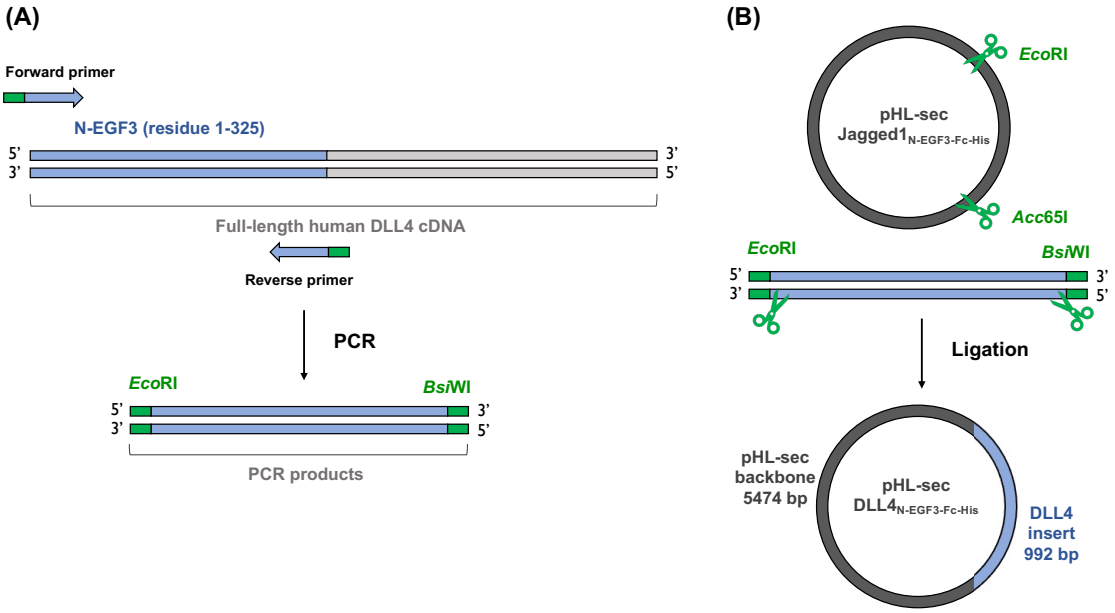


Figure 6-1. Cloning strategy for expression of DLL4$_{N\text{-}EGF3\text{-}Fc\text{-}His}$

(A) hDLL4$_{N\text{-}EGF3}$ insert DNA (blue) was amplified from full length DLL4 cDNA. Both forward and reverse primers (indicated by arrows) have desired unmatched restriction enzyme recognition sequences (highlighted in green). (B) pHL-sec-Jagged1$_{N\text{-}EGF3\text{-}Fc\text{-}His}$ was cut by *Eco*RI and *Acc*65I to acquire the pHL-sec backbone containing Fc and His tag DNA sequence, while the DLL4 cDNA PCR product was digested by *Eco*RI and *Bsi*WI. *Acc*65I and *Bsi*WI generate compatible cohesive ends for ligation.

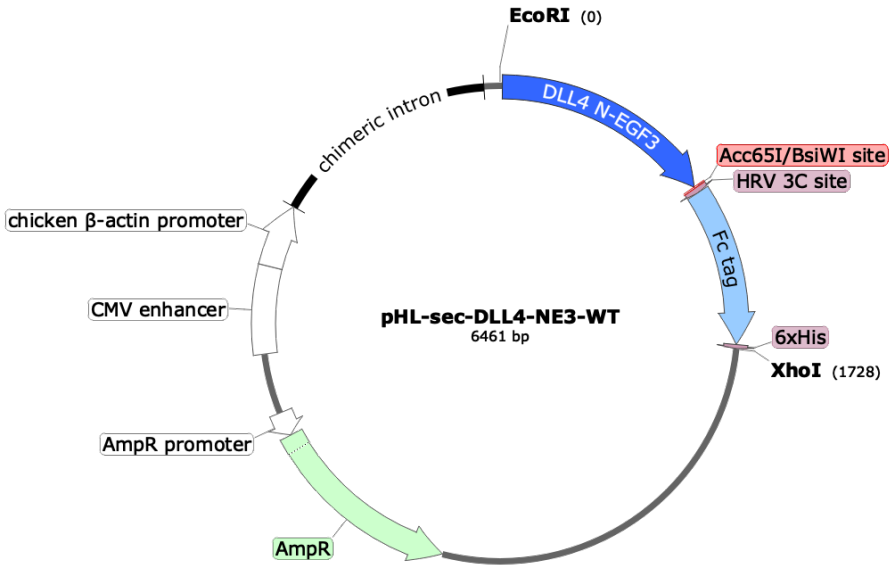


Figure 6-2. pHL-sec- DLL4$_{N\text{-}EGF3\text{-}Fc\text{-}His}$ expression plasmid

Major elements of the pHL-sec-DLL4$_{N\text{-}EGF3\text{-}Fc\text{-}His}$ are shown in the map adapted from SnapGene Viewer. The cDNA sequence encoding DLL4 $_{N\text{-}EGF3\text{-}Fc\text{-}His}$ (cobalt blue arrow) was inserted into pHL-sec backbone through 5' *Eco*RI and 3' *Bsi*WI (*Acc*65I site on backbone, labelled in red) restriction enzyme sites. DNA sequences encoding an Fc tag (light blue arrow) and 6 × His tag (light red arrow) are located at the 3' end of the DLL4 cDNA sequence.

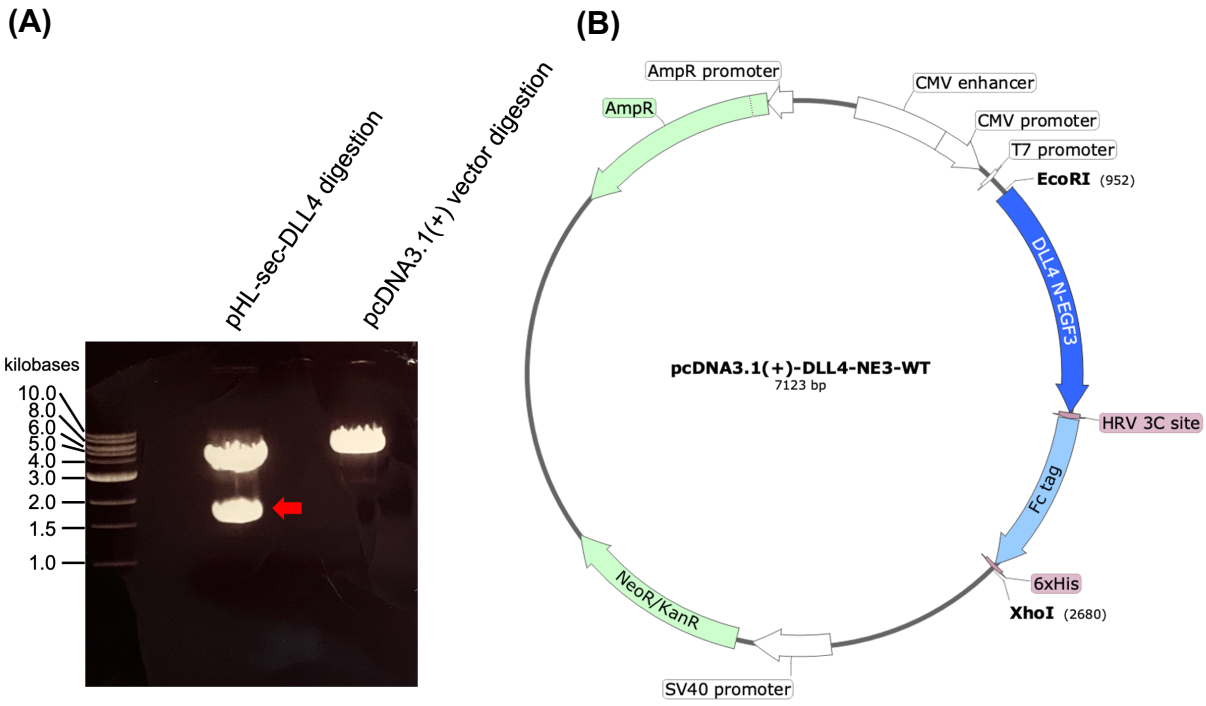


Figure 6-3. pcDNA3.1(+)-DLL4$_{N\text{-}EGF3\text{-}Fc\text{-}His}$ plasmid generation

(A) Insert and vector digestion products were analysed on a 0.5% TBE agarose gel. The insert encoding the recombinant DLL4 (indicated by a red arrow) is 1728 bp, while the size of pcDNA3.1(+) vector is 5395 bp after digestion. (B) pcDNA3.1(+)-DLL4$_{N\text{-}EGF3\text{-}Fc\text{-}His}$ is shown in the map with key components labelled. DLL4$_{N\text{-}EGF3\text{-}Fc\text{-}His}$ cDNA sequence (cobalt blue arrow) with an Fc tag (light blue arrow) and 6 × His tag (light red arrow) at the 3' end was inserted into the pcDNA3.1(+) backbone through 5' *Eco*RI and 3' *Xho*I restriction enzyme sites. This map is adapted from SnapGene Viewer.

6.3. Production and purification of DLL4$_{N\text{-}EGF3\text{-}Fc\text{-}His}$

6.3.1. Preliminary expression trials of DLL4 constructs

The transient expression of DLL4$_{N\text{-}EGF3\text{-}Fc\text{-}His}$ using pHL-sec and pcDNA3.1(+) plasmids was first analysed by western blotting of medium and lysate samples to test for efficient secretion before protein purification (Figure 6-4). The DLL4 secretion test was performed in the same way to the Jagged1 variants secretion analysis (Chapter 3). Four days after transfection, same volumes of the medium and cell lysate were taken and analysed by western blotting after reducing SDS-PAGE, although no loading control can be used in extracellular medium assessments (Figure 6-4). The

same approach was taken for cell lysates, although ideally a loading control such as probing for tubulin should have been included to infer changes in expression levels. pHL-sec-Jagged1$_{N\text{-}EGF3\text{-}Fc\text{-}His}$ was transfected as a positive control, along with a negative control (no plasmid added). Expression was detected using an anti-His-HRP antibody.

Immunoreactive bands were present in the pHL-sec-Jagged1$_{N\text{-}EGF3\text{-}Fc\text{-}His}$ transfected HEK293T medium and cell lysate samples, but not the negative control (Figure 6-4). A similar intensity of immunoreactive signal was detected in both pHL-sec-DLL4$_{N\text{-}EGF3\text{-}Fc\text{-}His}$ and pcDNA3.1(+)-DLL4$_{N\text{-}EGF3\text{-}Fc\text{-}His}$ transfected HEK293T medium and cell lysate samples compared to the Jagged1 WT (Figure 6-4). These data suggest that both pHL-sec and pcDNA3.1(+) backbone can express DLL4$_{N\text{-}EGF3\text{-}Fc\text{-}His}$ constructs, and both of the vectors express DLL4 into media at equivalent levels to the Jagged1 WT. HEK293 stable lines using pcDNA3.1(+)-DLL4$_{N\text{-}EGF3\text{-}Fc\text{-}His}$ were also generated with Geneticin selection, but no obvious increase of DLL4 recombinant protein expression levels in the media were observed (data not shown).

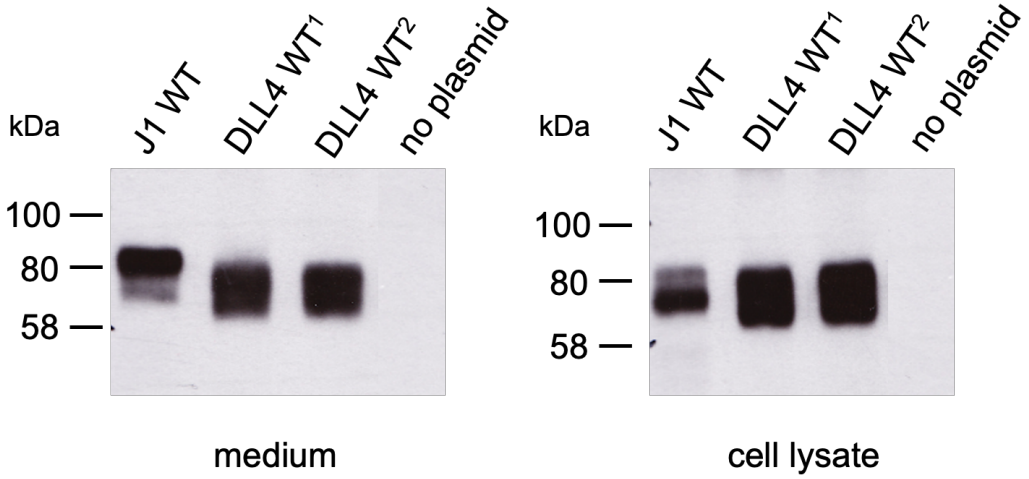


Figure 6-4. Western Blot analysis of transient DLL4 WT expression in cell lysate and medium samples of HEK293T cells

Expression of $DLL4_{N\text{-}EGF3\text{-}Fc\text{-}His}$ compared with $Jagged1_{N\text{-}EGF3\text{-}Fc\text{-}His}$ and the negative control (HEK293T cells were mock transfected). DLL4 WT^1 = HEK293T cells transfected by pHL-sec-$DLL4_{N\text{-}EGF3\text{-}Fc\text{-}His}$, DLL4 WT^2 = HEK293T cells transfected by pcDNA3.1(+)-$DLL4_{N\text{-}EGF3\text{-}Fc\text{-}His}$. Equivalent volumes of medium and cell lysate samples were analysed by reducing 10% SDS-PAGE followed by anti-His-HRP mAb detection (1:2000). $DLL4_{N\text{-}EGF3\text{-}Fc\text{-}His}$ expressed by both vectors was observed at similar levels to the $Jagged1_{N\text{-}EGF3\text{-}Fc\text{-}His}$ in both medium and cell lysate samples. Note that the DLL4 sample migrates with a lower MW to Jagged1 in medium samples.

6.3.2. Protein purification of recombinant DLL4

Based on preliminary trials, large scale recombinant DLL4 protein purification was attempted using HEK293T cells and conditions similar to those used for $Jagged_{N\text{-}EGF3\text{-}Fc\text{-}His}$. However, the final protein purification product had a lower purity (Figure 6-5, A). This might be due to the different intrinsic properties of $DLL4_{N\text{-}EGF3}$, such as the isoelectric point (pI, 6.18 for Jagged1, 6.29 for DLL4), which might affect solubility and separation using chromatography. Thus, more conditions were trialled for optimisation of the purification process.

6.3.2.1. Optimisation of buffer conditions

Firstly, a series of dilution buffers at different pH (buffer added into collected cell culture medium before IMAC) were tested (Chapter 2). The pH of dilution buffers ranged from

5.0 to 9.0, and more homogenous final products were acquired at pH 6.5 (comparison of pH 9.0 and pH 6.5 is shown in Figure 6-5, pH 9.0 was used in Jagged1 purification). There were still some impurities observed after IMAC and SEC steps. Thus, further optimisation was performed on the nickel column washing step.

Use of buffers with higher imidazole concentration can help with elimination of non-specific binding to the nickel column. Thus, the imidazole concentration of washing buffer was increased from 10 mM to 50 mM. Buffer containing 50 mM imidazole at pH 6.5 improved the purity without reducing DLL4 yield (Figure 6-6).

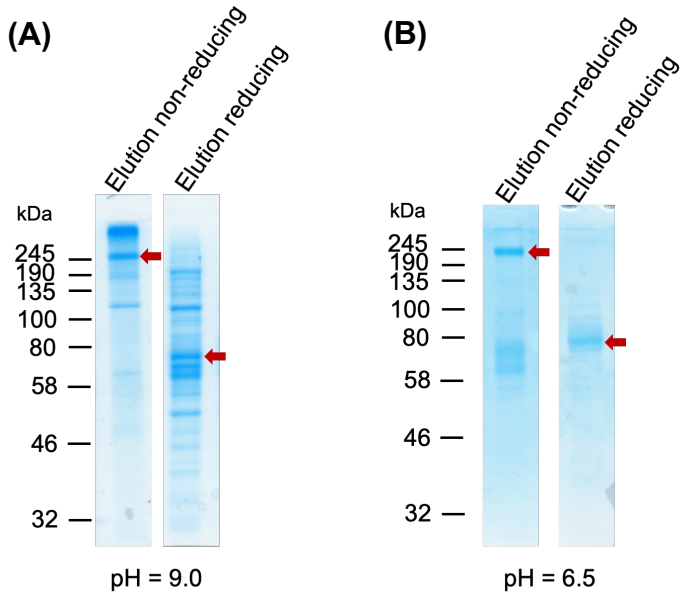


Figure 6-5. SDS-PAGE of elution samples following use of pH 9.0 and 6.5 dilution buffer

Elution samples (eluted protein in elution buffer after the IMAC procedure) were analysed by 10% reducing and non-reducing SDS-PAGE. Bands corresponding to the expected MW of DLL4$_{\text{N-EGF3-Fc-His}}$ are indicated by red arrows. Less impurities were observed under pH 6.5 dilution buffer (B) than pH = 9.0 (A, the condition applied in Jagged1 purification).

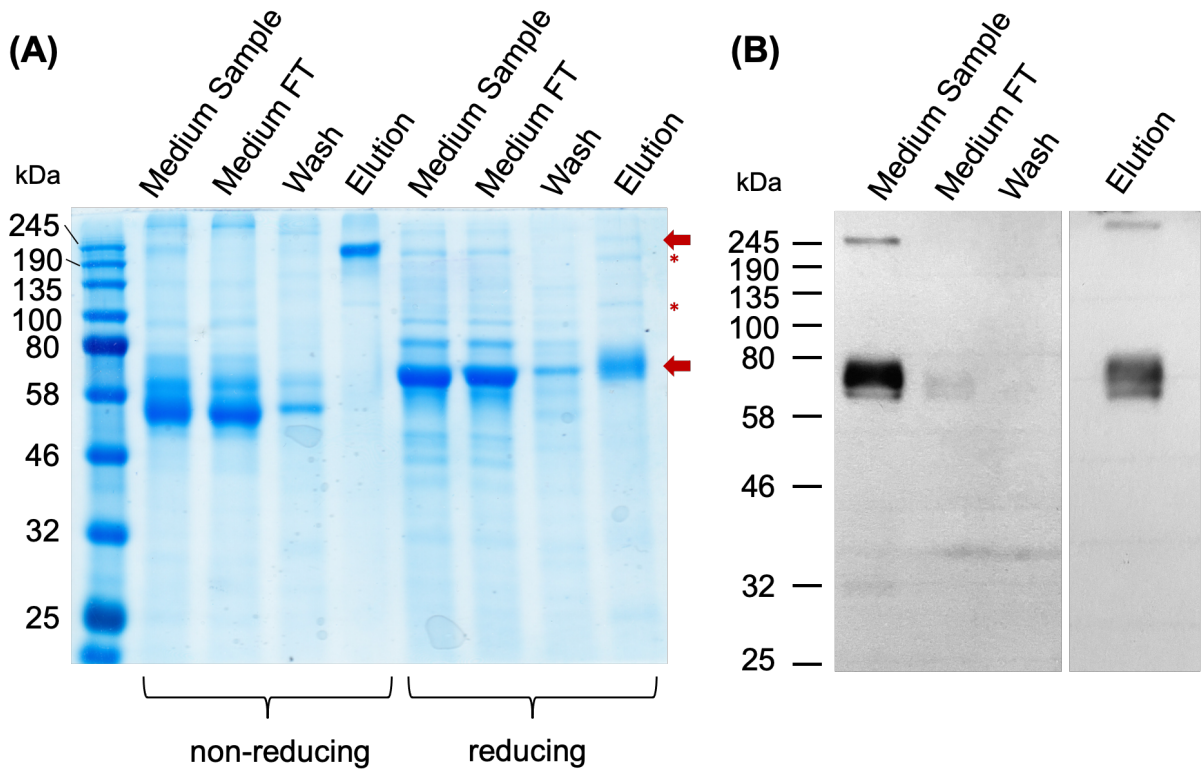


Figure 6-6. SDS-PAGE and Western Blot of HEK293T raw medium and protein purification intermediates following optimisation

Medium sample (HEK293T culture medium before protein purification) following dilution in buffer at pH 6.5, Medium FT (medium flow-through, culture medium after passing through the nickel column), wash (washing buffer collected after passing through nickel column) and elution (eluted protein after IMAC in elution buffer) were analysed by 10% reducing and non-reducing SDS-PAGE (A) and reducing western blot (B) detected by anti-His-HRP. Elution products after IMAC under reducing and non-reducing conditions identify a band of correct MW (arrowed) and few impurities (asterisked). Little signal was detected from medium flow-through by western blot, which suggests efficient binding of His-tagged DLL4 to the nickel column. No signal was detected from the wash sample by western blot, although several protein bands were visible by SDS-PAGE, which suggests the bands observed in SDS-PAGE were impurities. Use of 50 mM imidazole in elution buffer aids removal of non-specific binding proteins.

6.3.2.2. Expression of $DLL4_{N\text{-}EGF3\text{-}Fc\text{-}His}$ using HEK293F cells

To attempt a better yield of DLL4 recombinant constructs for functional assays, HEK293F cells were trialled as an alternative expression system. HEK293F cells, also named as FreeStyle™ 293F cells, are derived from the HEK293 cell line and are adapted to high-density, serum-free suspension culture. Similar to HEK293T cells,

HEK293F cells can produce properly folded constructs with mammalian sugar modifications after fast and simple transient transfections. No cell seeding step is required as for HEK293T cells in advance of transfection, although a specific cell concentration of 1.2×10^6 to 1.5×10^6 cells/mL was required on the day of transfection (Chapter 2).

After the transient transfection of HEK293F cells using pcDNA3.1(+)-$DLL4_{N\text{-}EGF3\text{-}Fc\text{-}His}$ followed by protein purification with optimised buffer conditions established for expression in HEK293T cells (section 6.3.2.1), a high level of recombinant WT DLL4 purity was achieved (> 90%) (Figure 6-7). 160 mL HEK293F culture medium produced a similar yield of purified DLL4 (~ 0.2 mg) to 250 mL culture medium by HEK293T cells, and the final product was of high purity. Thus, HEK293F cells are an effective expression system for $DLL4_{N\text{-}EGF3\text{-}Fc\text{-}His}$ in future studies. It should be noted there are two bands observed by reduced SDS-PAGE. This may reflect heterogeneity of N-glycosylation. Although hDLL4 lacks the C2 loop 5-6 N-glycan seen in Jagged1, it contains N-glycans in the C2 loop 4-5, DSL domain and the Fc-tag.

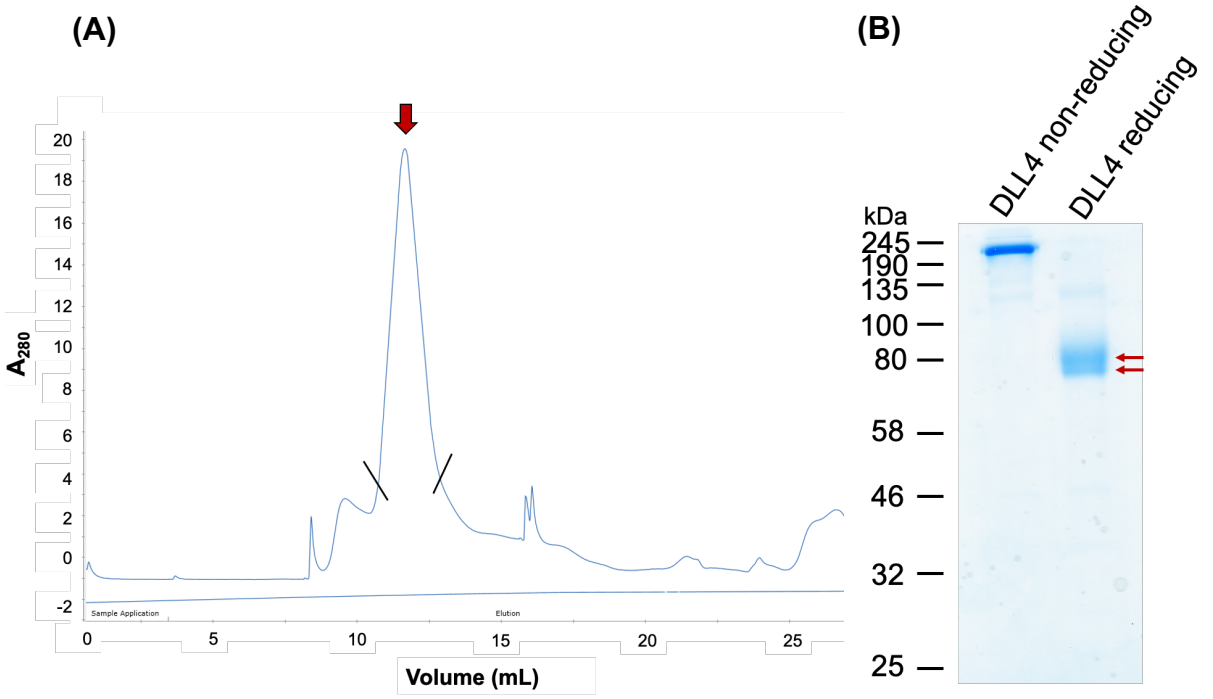


Figure 6-7. Size exclusion chromatogram of DLL4$_{N\text{-}EGF3\text{-}Fc\text{-}His}$ WT and the final purification product obtained from the HEK293F system

Fractions which correspond to SEC protein elution peaks (indicated by a red arrow and black lines in (A)) were collected and analysed by reducing and non-reducing SDS-PAGE (B). The expected MW of the monomeric DLL4 construct is ~ 64 kDa, and final purification products migrate to a higher position more likely due to N-glycosylation. Final products showed more than 90% homogeneity. Note there are two bands in the reduced sample which might indicate heterogeneity of glycosylation.

6.4. Testing Notch activation of DLL4 cancer variants

6.4.1. Selection and expression of DLL4 cancer variants

After optimisation of the protein purification process for DLL4, six of DLL4-C2 missense mutations recorded in cancer databases were selected and constructed by Oliver Webb, University of Oxford, using the pcDNA3.1(+)-DLL4$_{N\text{-}EGF3\text{-}Fc\text{-}His}$ WT vector as template. A summary of these is shown in Table 6-1, and the position of each substitution within C2 domain structure is shown in Figure 6-8. Four substitutions are located on loop 1-2, whilst two others affect residues on the other apical loop of C2, loop 5-6. These missense mutations were identified in different primary tissues and

have various histologies (Table 6-1). Moreover, all of these cancers were epithelial-derived.

A secretion test was performed for each DLL4 variant using HEK293T cells by Oliver Webb. All these apical loop variants showed no obvious effect on DLL4 folding and trafficking, with similar levels of expression into media to WT (Appendix C). All DLL4 variants were subsequent expressed in HEK293F and purified together with WT DLL4 and a negative control which was negative for Notch binding (F195A/Y216A) for further functional assays. One of the cancer variants, G47W, failed to express in HEK293F, although it showed secretion at a similar level to WT in HEK293T cells, and was not taken further. All variants showed > 90% purity except E40K which showed additional minor impurities (~ 85%) (Figure 6-9, A).

Domain	Missense mutation	Position at C2 domain	Histology	Histology subtype	Primary tissue	Tissue subtype
C2	E40K[1]	loop1-2	carcinoma	n/a	urinary tract	bladder
C2	R41S[1]	loop1-2	other	neoplasm	liver	n/a
C2	G47W[1]	loop1-2	other	neoplasm	liver	n/a
C2	P49S[1]	loop1-2	carcinoma	endometrioid carcinoma	endometrium	n/a
C2	D128N[2]	Loop5-6	melanoma	cutaneous melanoma	skin	n/a
C2	P135A[2]	Loop5-6	carcinoma	neoplasm	ovary	n/a

Table 6-1. Summary information of DLL4 missense mutations

[1]Variants selected from COSMIC cancer database. https://cancer.sanger.ac.uk/cosmic/gene/analysis?ln=DLL4,
[2]Variants selected from National Cancer Institute GDC Portal database. https://portal.gdc.cancer.gov/genes/ENSG00000128917

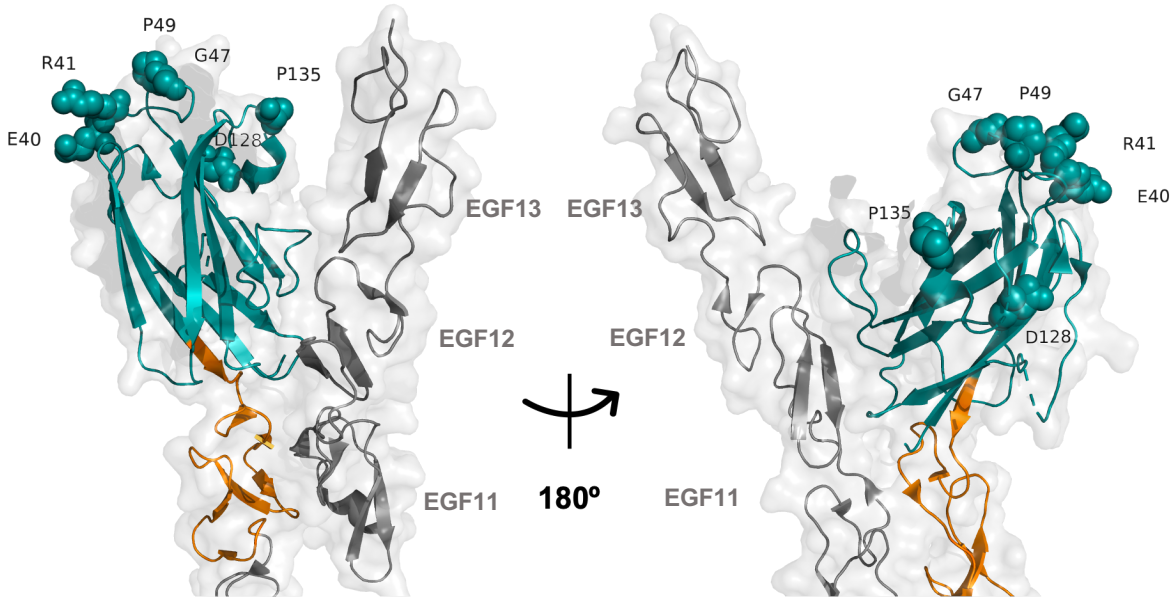


Figure 6-8. Location of selected DLL4 cancer substitutions within C2 domain

Residues which are found substituted in cancer cells (teal spheres) in apical loop regions of DLL4-C2 domain (E40K, R41S, G47W, P49S – loop 1-2; D128N, P135A – loop 5-6). Images were produced using PyMOL (PDB 4XL1) with two orientations showed. The C2 domain is in teal, the DSL domain is orange, and Notch EGF domains are grey.

6.4.2. Testing the effect of DLL4 cancer variants on Notch1 activation

To study whether these variants in apical loops of DLL4-C2 affected Notch activation, mN1-NLuc/CLuc-RBPjk cells were used following previously established protocols. Purified DLL4 variants, alongside DLL4 WT and a Notch binding-deficient negative control (F195A/Y216A), were immobilised on a 96-well tissue culture plate surface followed by the culturing of mN1-NLuc/CLuc-RBPjk cells for 24 hours on the coated plate. After addition of luciferin, luciferase activity was measured and quantified (Chapter 2). Wells with mN1-NLuc/CLuc-RBPjk cells only, and substrate only, were also set up as negative controls to detect the background signal.

All negative controls, including F195A/Y216A, cells only and luciferin substrate only, showed a statistically significant decrease in Notch1 activation ($P < 0.0001$) (Figure 6-

9). Two variants with loop 1-2 substitutions, R41S and P49S, and two variants with loop 5-6 substitutions, D128N and P135A, lead to a small, but statistically significant, increase in Notch1 activation (P = 0.0024, 0.005, 0.0045 and 0.0114 respectively) (Figure 6-9). One variant (loop 1-2, E40K) showed a similar Notch1 activation to the WT (P = 0.8941).

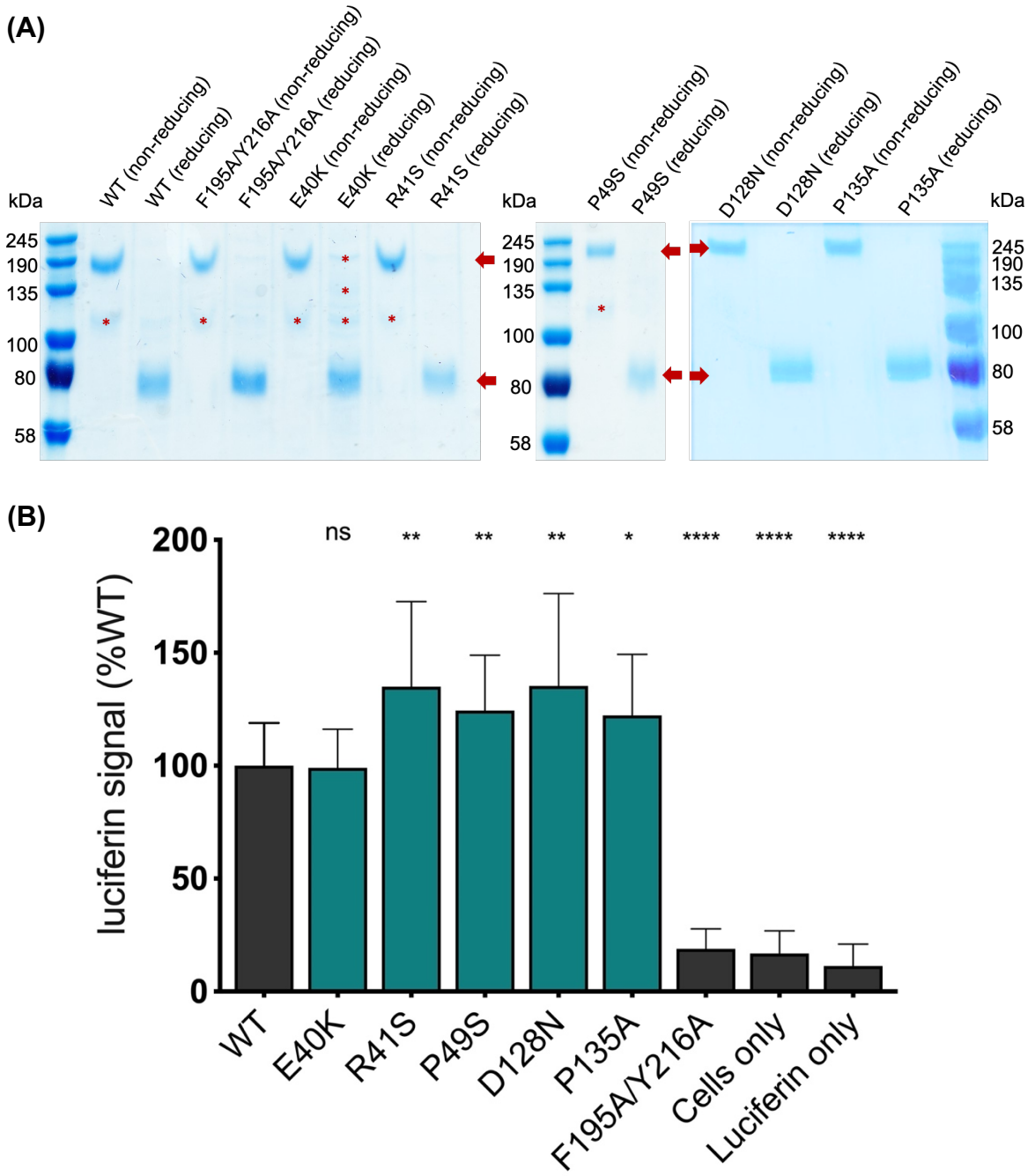


Figure 6-9. SDS-PAGE analysis and split luciferase Notch1 activation assay of DLL4 cancer variants

(A) Purified DLL4 cancer variants were analysed by 10% reducing and non-reducing SDS-PAGE. All variants showed > 90% homogeneity with expected MW band (arrowed, ~ 64 kDa in reducing and ~ 128 kDa in the non-reducing condition) except E40K which showed minor impurities. Impurities labelled by asterisks. (B) Notch1 activation by DLL4 cancer variants was assayed using mN1-NLuc/CLuc-RBPjk cells. n ≥ 3 independent experiments, each of 5 repeat wells, were performed. Luminescence signal from WT was taken to be 100% activation, and signal from variants was expressed as a percentage of WT. WT and negative controls are coloured in dark grey, C2 variants in teal. Data were analysed using Prism 9 and presented as mean ± SD. ns = not significant, **P* < 0.05, ***P* < 0.01, *****P* < 0.0001.

6.5. Conclusion

In a previous DLL4-C2 domain study, $DLL4_{N\text{-}EGF3}$ monomers were purified from insect cells for molecular and structure studies (Suckling et al., 2017). However, in activation assays, DLL4 monomers did not work efficiently (unpublished data). To study DLL4-C2 domain variants using various activation assays and to allow a comparative study with Jagged1, a $DLL4_{N\text{-}EGF3\text{-}Fc\text{-}His}$ protein purification procedure using a human cell line was established and optimised. A dilution buffer, pH of 6.5 (compared to pH of 9.0 used in Jagged1) was shown to facilitate DLL4 recombinant protein separation from other proteins using IMAC, and inclusion of 50 mM imidazole (rather than 10 mM for Jagged1) improved purity of eluted product without having a detrimental effect on the final yield (Figure 6-6). Moreover, transient transfection of HEK293F cells for large-scale purification increased the yield of protein compared to that obtained from HEK293T cells. This is most likely due to adaptation of HEK293F cells for growth in high-density suspension culture compared to adherent HEK293T cells. Overall, this optimised protein purification process allows production of at least 85% pure recombinant DLL4, and the higher yield enables protein to be used in functional assays.

Six missense mutations affecting loop 1-2 and 5-6 in DLL4-C2 from two cancer databases, COSMIC and National Cancer Institute GDC Portal database, were selected for study. In the HEK293T secretion assay, all six variants secreted at wild type levels. Thus, consistent with data from Jagged1, substituting single residues on the loop structure of C2 did not have an obvious effect on DLL4 folding and trafficking except for the variant G47W which expressed poorly in the HEK293F system.

All secreted DLL4 cancer variants were tested in the split luciferase Notch1 activation assay following purification as Fc dimers. Introduction of missense mutations into Jagged1-C2 loops showed predominantly a decrease in Notch1 and Notch2 activation. However, a small increase in activation of Notch1 was observed from all DLL4 variants except E40K (Figure 6-9). Note that the purified E40K construct was shown to have a number of impurities compared to other purified DLL4 constructs which might have affected the activation result. It would be interesting to investigate whether the increase in Notch1 activation can be also observed in the CHO-YFP activation assay.

Chapter 7. Discussion and future work

7.1. Thesis objective

As was articulated in the introduction, the C2 domain of Notch ligands is thought to fine-tune Notch activation through its membrane-binding property and also contribute to the core Notch binding interface. The aim of this thesis was to gain a better understanding of the Notch ligand C2 domain's contribution to Notch activation modulation. Therefore, a series of missense mutations were selected from the COSMIC cancer database that are located in both loop structures and the hydrophobic core of C2.

The role of these substitutions in protein stability was tested in a HEK293T cell-based secretion assay. By expressing secreted variants as Fc-tagged extracellular constructs, it was possible to examine their Notch activation, Notch-binding and liposome-binding properties in molecular and cellular assays, ultimately probing the role of these loops further. The physiological importance of the sugar modification in the Jagged1-C2 domain was studied further in primary vascular smooth muscle cells.

7.2. Expression and secretion of cancer-associated variants

13 missense mutations in Jagged1 identified in tumours, obtained from the COSMIC cancer database, were first studied in this project (Chapter 3). 12 selected mutations affect different regions of Jagged1-C2 domain including apical loops (loop 1-2 and 5-6), a loop in the hinge region next to the DSL domain (loop 2-3), a loop on the opposite face of the Notch binding surface (loop 3-4) and beta sheets contributing to the hydrophobic core of C2, whilst one mutation, E228K, locates at the Notch binding interface of the DSL domain (Figure 3-3).

4 out of 13 variants were shown to misfold and were retained in cells, and 9 variants were expressed and secreted at wildtype levels (Figure 3-6). Three substitutions associated with misfolding are located in the hydrophobic core of Jagged1-C2 (beta strands 1 and 5), while the other substitution, G47R, is located at end of the loop 1-2 sequence prior to the β strand with the larger arginine side chain most likely perturbing domain structure at this position.

6 DLL4 cancer-associated substitutions located on the apical loops of the C2 (loop 1-2 and loop 5-6) were selected, cloned, expressed and examined subsequently for secretion as for Jagged1 variants (Chapter 6). All of these variants secreted at a similar level to wildtype protein in HEK293T, as shown by western blotting (Appendix C). DLL4 constructs were then purified for further study. After optimising a series of buffer conditions and trialling expression in different cell types, for the first time in the research group, DLL4 Fc-tagged dimer constructs were successfully purified from HEK293F cells with more than 90% purity and a high yield. The higher yield obtained from HEK293F cells compared to HEK293T is most likely due to the higher culture density of HEK293F cells in suspension. One variant, G47W, homologous to Jagged1 G47, was shown to secrete similarly to wild type in the HEK293T cell-based assay but failed to secrete in HEK293F cells.

These results suggest that substituting residues in the C2 hydrophobic core or close to the core of Jagged1-C2 significantly affect proper folding of the protein, which is consistent with observations from Alagille syndrome substitutions which mainly cause disease by haploinsufficiency mechanisms (section 1.2.2.2). In most cases, however,

substitution of individual residues in the loops of C2 of either Jagged1 or DLL4 did not affect folding and trafficking.

7.3. The effect of cancer-associated variants on Notch activation

All secreted cancer variants were purified from HEK293T/HEK293F cells and assessed for Notch activation using two different reporter cell lines. The HEK split-luciferase reporter cells are able measure Notch activation in live cells in real time due to lack of requirement for a downstream reporter for readout. The luciferase complementation-based reporter is highly specific and sensitive as no intrinsic bioluminescence or luciferase activity is detected in HEK cells, and luciferase confers inherent sensitivity resulting from signal amplification. However, since the HEK split-luciferase activation assay is carried out in a 96-well plate format and read by a plate reader, signals from single cells in each well are combined to give an average, and less information can be acquired from individual cells in each population. This makes it more challenging to distinguish small changes in activation levels. Thus, a FACS-based activation assay using a fluorescent protein readout (YFP) was established alongside in this project.

The CHO-YFP activation assay is useful as it can use flow cytometry to record the signal in individual cells in a high throughput manner. Fusion of a heterologous protein (Gal4), which binds specifically to the UAS promoter, to the Notch receptor helps with boosting sensitivity of the CHO-YFP reporter cells as no endogenous Notch activity is detected. Since little cellular autofluorescence is detected in individual experiments, YFP reporter cells can be used to accurate quantify Notch activation. Using CHO cell-derived reporter cells also provides information about Notch activation in a different

cell type. Overall, applying two different reporters, HEK split-luciferase and CHO-YFP cells, allowed more detailed examination of activation.

All secreted Jagged1 COSMIC variants were purified and assayed using the two reporter systems. In HEK split-luciferase activation assay, all but one (A58V) showed low Notch1 activation capability (Figure 3-11). Similar results were observed in CHO-YFP reporter cells except L135F which showed lower activity only in HEK-luciferase reporter cells (Figure 3-14). In all these Jagged1 COSMIC variants, those showing the largest effects on activation were V86F and E228K located in the Notch binding interface and T145N affecting an N-linked glycosylation sequence in loop 5-6 of C2.

In the comparative study of DLL4, 5 cancer variants, affecting the loop1-2 and loop 5-6 of the C2, have also been assessed using HEK-luciferase reporter cells (Chapter 6). Interestingly, all but one (E40K) showed an unexpected increased ability to activate Notch. However, E40K showed less purity (~ 85%) than other purified DLL4 protein (~ 90%) which might underestimate its activity (Figure 6-9). Due to time limitations, DLL4 variants were not assessed by CHO-YFP reporter cells.

Most single substitutions in Jagged1 affecting the apical loops (loop 1-2 and 5-6), the loop in the opposite of the Notch binding surface (loop 3-4) of C2 and the loop in the hinge region next to the DSL domain (loop 2-3) lead to decreased Notch activation, which was confirmed by two different activation assays. Only one variant, L135F, behaved differently in two assays. It is interesting to speculate this might be due to different cell membrane compositions (lipid and/or protein) between the HEK and CHO. In the comparative study of DLL4, 5 cancer variants in apical loops (loop 1-2 and 5-6)

caused the opposite effect on Notch activation to that seen with Jagged1 variants, a statistically significant increase in activity assessed by HEK-luciferase cells. The CHO-YFP assay needs to be performed on the DLL4 cancer variants in the future to confirm the results obtained.

7.4. Significance of opposing effects on Notch activation by Jagged1 and DLL4 cancer substitutions

The different effects associated with Jagged1 variants (loss of function) and DLL4 variants (mild gain of function) are interesting. It has been previously observed that normal oesophageal cells on aging accrue loss of function Notch mutations to gain a selective advantage (Martincorena et al., 2018). The fact that DLL4 variants, at least in the C2 loop regions, do not show loss of function might suggest that cancer cells in which these mutations arise may gain an advantage losing Jagged1 function, but gaining DLL4 function. More detailed analysis of normal as well as cancer cells is required, and further investigation is required to confirm enhanced Notch activation by DLL4 variants in the YFP system. It is worth noting that the process of angiogenesis is regulated by the balance of Jagged1/DLL4 ligands. Should DLL4 activity of variants be confirmed, it will be interesting to examine their effects on endothelial cell fate in HUVEC cells which express physiological levels of Notch (Tiemeijer et al., 2018).

7.5. Functional assessment of Jagged1 cancer-associated variants in lipid-binding and Notch-binding

As most of secreted Jagged1 COSMIC variants showed a reduction in Notch activation in cellular assays, to interpret the molecular mechanisms leading to this reduction, their lipid-binding capability was next examined. In this project, a novel FACS-based aggregation assay was developed to reduce variations caused by washing steps in a previously used plate binding assay and obtain reproducible liposome-binding data with less protein sample consumed.

The assessment of Notch binding of Jagged1 COSMIC variants used a previously established Maxisorp plate-based Notch binding assay. Both Notch1 and Notch2 binding were examined using purified $Notch_{EGF11\text{-}13}$ fragments produced from S2 cells. As purified Notch2 constructs were more efficiently O-glycosylated than Notch1, higher binding to Jagged1 was observed with Notch2 compared to Notch1 (section 5.3).

In the FACS-based aggregation assay of Jagged1 COSMIC variants, two variants, G114D and T145N showed significantly reduced liposome binding using PC-rich liposomes (Figure 5-17). Seven other secreted variants did not have a distinguishable difference in this liposome-binding assay compared to WT (Figure 5-17). In Notch binding assays, V86F, T145N and E228K showed a statistically significant decrease in Notch1 and Notch2 binding, while G89E significantly reduced Notch1 binding, but not Notch2 (Figure 5-6, 5-7). All other variants (A58V, D72N, G114D, L135F, S142N) did not have an obvious decrease in Notch1 or Notch2 binding (Figure 5-6, 5-7). Interestingly, G114D showed a dramatically increase in Notch1 and Notch2 binding ability. The summary of effects of Jagged1 COSMIC variants are shown in Table 7-1.

7.6. Implications of Jagged1 COSMIC variants in Notch signalling

Overall, most Jagged1 COSMIC variants, expressed as Fc-NE3 extracellular constructs, were loss of function with respect to Notch activation, either due to the effect of the substitution on C2 domain folding resulting in lack of secretion, or due to effects on activity. For the latter group, most of decreased Notch activation can be explained by effects on lipid/Notch binding except D72N, L135F and S142N. Three variants locating at the binding interface of Notch, including two in loop 2-3 of C2 domain (V86F and G89E) and one in DSL domain (E228K), showed a decrease in Notch-binding but not lipid-binding. This underscores the importance of the C2 domain loop 2-3 at site 1 together with the DSL domain (site 2) for Notch binding. The Notch activation reduction associated with G114D which substituted a residue in loop 3-4 could be caused by its reduced lipid-binding capability. As introduced in section 1.5.1, in many other C2 domains, loop 3-4 is associated with a β-groove that can bind to lipid through electrostatic interactions. One variant, T145N, altering an N-glycosylation motif showed a dramatic decrease in Notch activation, and reduced lipid-binding and Notch-binding, which unexpectedly implicated an N-glycan in loop 5-6 of Jagged1-C2 as having an important functional role.

Domain	Mutation	Position at C2 domain	Secretion	Luciferase Notch1 activation	CHO-YFP Notch1 activation	Notch1 binding	Notch2 binding	Lipid binding	mechanism
C2	F35L	beta sheet 1	X	n/a	n/a	n/a	n/a	n/a	affects Jagged1 folding and secretion
C2	G47R	loop1-2	X	n/a	n/a	n/a	n/a	n/a	affects Jagged1 folding and secretion
C2	A58V	loop1-2	✓	no effect	no effect	no effect	no effect	no effect	no effect
C2	D72N	loop1-2	✓	intermediate	intermediate	no effect	no effect	no effect	not clear
C2	V86F	loop2-3	✓	low	low	low	low	no effect	disruption of Notch binding interface
C2	G89E	loop2-3	✓	intermediate	intermediate	low	no effect	no effect	disruption of Notch binding interface
C2	G114D	loop3-4	✓	intermediate	intermediate	high	high	low	reduced lipid binding capability
C2	T133R	beta sheet 5	X	n/a	n/a	n/a	n/a	n/a	affects Jagged1 folding and secretion
C2	L135F	beta sheet 5	✓	intermediate	no effect	no effect	high	no effect	not clear
C2	W139S	beta sheet 5	X	n/a	n/a	n/a	n/a	n/a	affects Jagged1 folding and secretion
C2	S142N	loop5-6	✓	intermediate	intermediate	no effect	no effect	no effect	not clear
C2	T145N	loop5-6	✓	low	low	low	low	low	reduced lipid and Notch binding capability
DSL	E228K	/	✓	low	low	low	low	no effect	disruption of Notch binding interface

Table 7-1. Summary of effects of Jagged1 COSMIC variants

Molecular mechanisms explaining loss of function for all variants except those indicated in red. These variants may have mild effect on membrane binding or ligand-receptor interplay, which cannot be distinguished by *in vitro* plate-based assays at the concentrations used.

7.7. The role of Jagged1-C2 highly conserved N-glycan in Notch signalling

7.7.1. Conservation and the presence of the N-glycan in Jagged1-C2

Amino acid alignment of loop 5-6 of the C2 domain across representative metazoan species, including human, rat, mouse, chicken, frog, zebrafish and *Drosophil*a, showed that an N-glycosylation motif is evolutionarily conserved in Jagged ligands but not Delta-like ligands, with the exception of *Drosophila* that has the motif in both Serrate and Delta (Figure 4-1). However, an N-glycan consensus sequence found in the Jagged1 DSL domain is less conserved across species and the ligand families (Figure 4-2). Sequence conservation, together with functional data from the T145N COSMIC variant, suggested that the N-glycan in Jagged1-C2 may have a previously unrecognised role in Notch activation.

Two site-directed variants that eliminated the N-glycosylated residue in C2 (N143A) and DSL (N217A) were generated for further study, alongside two COSMIC variants that eliminated the N-glycosylation motif (T145N) and altered a loop 5-6 residue next to the N-glycan (S142N). From reducing and non-reducing SDS-PAGE and reducing western blotting analysis, variants which altered a N-glycosylation motif, either directly or indirectly (N143A, T145N and N217A), showed a molecular weight drop compared to WT and S142N (Figure 4-4) (Figure 4-5). Moreover, this molecular weight drop was also observed in a PNGase F digested N217A monomer that only contains the N-glycosylation motif in the C2 domain (Figure 4-6). These data suggest high occupancy of an N-glycan in WT Jagged1$_{\text{N-EGF3-Fc-His}}$ produced from HEK293T cells, which allowed analysis of N-glycan composition using mass spectrometry.

From mass spectrometry-based glycoproteomic analysis, the N-linked sugar in both C2 and DSL domains was shown to be a core-fucosylated complex N-glycan with different levels of branching, including bi-antennary, tri-antennary and tetra-antennary N-glycans (Figure 4-8). The tetra-antennary N-glycan was modelled on the C2 domain of *Drosophila* Delta according to the observed orientation of the N-glycan in this structure (Figure 4-8) (Martins et al., 2021b). The tetra-antennary complex N-glycan is located away from Notch-binding region and occupies the area between loop 5-6 and 3-4 and extends towards the end of beta strand 4. As illustrated previously, loop 3-4 might be the potential position of a cationic β-groove (section 1.5.1), and the presence of the N-glycan on this surface might alter the lipid-binding potential of this site. Mass spectrometry glycoproteomic analysis observed relatively low occupancy of the N143 site despite SDS-PAGE analysis showing an expected MW drop. This may be due to difficulties in digesting this region with trypsin. It would be worth trying to digest Jagged1 constructs with different enzymes and analyse more than one protein preparation. It would be also valuable to crystallise Jagged1 material from HEK293T line and directly demonstrate the presence and position of the N-glycan. Additional substitutions could be made in loop 3-4 to see if their lipid-binding properties and activity are affected. In addition, it was noted that no direct interactions were observed between the N-glycan and the Notch-binding interface.

7.7.2. Regulation of Notch activation by the N-glycan in Jagged1-C2

Two different Notch1 activation assays, together with a Notch2 HEK-luciferase activation assay, showed that both variants lacking the N-glycan in the C2 domain (T145N and N143A) led to a substantial decrease in Notch activation (Figure 4-9, 4-10, 4-11). The S142N substitution reduced activation in two Notch1 activation assays

to an intermediate level, while it had a similar Notch activation to WT in the HEK-luciferase Notch2 activation assay suggesting substitution of a residue in this loop has less impact than loss of the sugar (Figure 4-9, 4-10, 4-11). The variant without the N-glycan in DSL (N217A) showed no obvious effect on Notch activation in all three activation assays. This further supports a specific role for the Jagged1 C2 N-glycan in ligand-dependent activation.

In FACS-based liposome aggregation assays using two different compositions of liposomes (PC-rich and SM-rich liposomes), two variants lacking the N-glycan in C2 showed decreased binding to both, whilst S142N and N217A did not have detectable changes in liposome binding assays (Figure 5-19, 5-20). In Notch1 and Notch 2 binding assays, there was a good agreement between two sets of data acquired. Variants without the N-glycan in C2 showed a reduction in both Notch1 and Notch2 binding abilities, while S142N and N217A left Notch-binding unaltered (Figure 5-11, 5-12).

Overall, these studies suggest the presence of the N-glycan in C2, but not DSL, together with the native conformation of loop 5-6 are essential for the ability of Jagged1 to activate Notch at the cell. Liposome-binding and Notch-binding assays provide some insight into the molecular mechanism behind the modulatory effects of the Jagged1-C2 N-glycan in mediating the interactions of Jagged1 to lipid and the Notch receptor. Similar results in liposome-binding were obtained when PC-rich and SM-rich lipid compositions were used suggesting that loss of the loop 5-6 N-glycan significantly decreased the lipid-binding property of C2 when an outer leaflet lipid (SM) was included.

7.7.3. Physiological importance of the N-glycan in Jagged1

In order to investigate whether the N-glycan variants affected receptor activation in primary cells with a physiological level of Notch signalling, a vascular smooth muscle differentiation assay was carried out in collaboration with the Sahlgen group. Immunofluorescent microscopy and western blot analysis showed that variants lacking the N-glycan in C2 failed to promote differentiation of VSMC, similarly to DSL Notch binding negative variants, in contrast to wildtype Jagged1 (Figure 4-14). However, S142N and N217A did not have a detectable effect on VSMC differentiation (Figure 4-14).

The activity effects observed in Notch reporter cells were thus recapitulated in VSMC primary cells that undergo differentiation in a Jagged1-dependent manner and suggest a physiological role of the C2 N-glycan in modulating smooth muscle differentiation.

7.7.4. Possible implications of the effect of the N-glycan

The summary of effects of N-glycan variants are shown in Table 5-2. Activation effects seen in three reporter lines and primary VSMC cells imply that the evolutionarily conserved N-glycan site in the C2 domain of Jagged family ligands has an essential role in modulating Notch activation. Interestingly, this N-glycan is absent in Delta-ligand family except *Drosophila* Delta, which might contribute to their specific roles in different tissues. Liposome binding capability of C2 was decreased in assays, which suggests that the presence of the N-glycan is important for the lipid-binding property of Jagged1-C2. The N-glycan possibly exhibits its role in promoting lipid-binding through the apical loops, loop 1-2 and 5-6 of C2. One possible mechanism might

involve the N-glycan sterically blocking the β-groove (loop 3-4) subsequently affecting the specific orientation of Jagged1-C2 on the cell surface. Different modes of binding have been observed in molecular dynamics studies with C2 domains from other proteins (Larsen and Sansom, 2021). If the N-glycan does act sterically, then the effect of the COSMIC variant G114D might be to repel the N-glycan. Alternatively, it might act directly to disrupt lipid binding via the loop 3-4 (Figure 7-1).

Loss of N-glycan in C2 lead to a decrease in Notch1 and Notch2 binding although the N-glycan is located away from human Notch binding sites. The mechanism for this is unknown – the sugar may rigidify part of the C2 domain, promoting Notch binding indirectly, through entropic effects (Luca et al., 2017). Recently interactions have been proposed between the C2 domain of Jagged1 and NRR of Notch1 (Zeronian et al., 2021). Although not proven using functional assays, it might suggest the C2/membrane interaction is critical for facilitating formation of receptor/ligand complex, optimal for proteolytic cleavage. However, in this study, soluble fragments were used to show the interactions in the absence of membrane, so more detailed examination of this interaction is required.

Domain	Mutation	Position at C2 domain	N-glycan in C2	Normal VSMC differentiation	Notch activation	Notch1 binding	Notch2 binding	Lipid binding
C2	S142N	loop 5-6 sheet 1	✓	✓	med	no effect	no effect	no effect
C2	T145N	loop 5-6	X	X	low	low	low	low
C2	N143A	loop 5-6	X	X	low	low	low	low
DSL	N217A	/	✓	✓	no effect	no effect	no effect	no effect

Table 7-2. Summary of effects of N-glycan variants

T145N and N143A, but not S142N and N217A, lose the N-glycan on C2. S142N substitutes the residue next to the N-glycan linked residue, N143. N217A changes the N-glycan motif on the DSL domain. Variants without N-glycan on C2 showed loss of function in Notch activation, Notch binding and lipid binding assays.

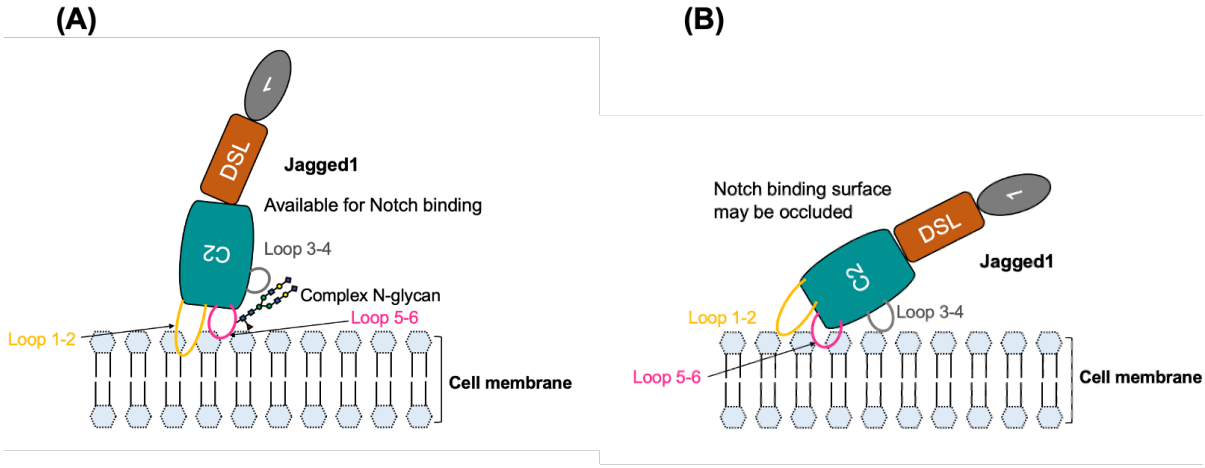


Figure 7-1. The C2 N-glycan might influence Jagged1 orientation at the cell membrane

Possible effects of the C2 N-glycan on ligand orientation at the cell membrane. (A) N-glycan interacts along one face of the hydrophobic core as shown in human Jagged2, *Drosophila* Delta crystal structures, occluding loop 3-4, and favouring Jagged1-C2 binding in a more perpendicular orientation through 1-2 and 5-6 loops. This may facilitate formation of Notch/ligand complex. (B) Lack of N-glycan allows Jagged1 to adopt a "flatter" interaction, utilising 1-2, 5-6 and 3-4 loops which is less favourable for Notch/ligand complex formation.

7.8. Future directions

The results of the experiments performed in this project have revealed several findings regarding the molecular mechanisms and the biological importance of the C2 domain of Jagged1 and DLL4 in activation of Notch. However, more work is needed to gain

an understanding of the Notch activation modulation of C2 in DLL4 and other Notch ligands. It would also be of interest to study Notch ligands using additional methods. Moreover, further studies are required to characterise the physiological importance of the C2 domain in Notch ligands.

As Notch activation of DLL4 cancer variants was only assessed by HEK-luciferase cells in this project, further validation is required using the CHO-YFP reporter line. Should enhanced activation be observed, Notch/lipid binding assays could be carried out to understand the molecular mechanisms of DLL4-C2 in Notch activation modulation and further explore the significance of the opposing effects of Jagged1 and DLL4 in cancer cells. Moreover, as a low Notch activation Jagged1 variant on loop 3-4, G114D, showed extremely higher Notch binding but lower lipid binding ability, it would be worth to select mutations on loop 3-4 of DLL4 for a comparison study. To better understand whether the lipid binding ability play a dominant negative in Notch activation regulation of G114D, it would be interesting to test the Notch activation ability of the high affinity variant used for Jagged-Notch complex crystallisation (Luca et al., 2017).

Changes in shapes of FACS profile were observed in individual repeat of the CHO-YFP activation assay. To better understand the changes, it would be useful to use FACS to sort different populations of CHO-YFP reporter cells for further analysis, such us expression levels of Notch ligands/receptors. To complement activation assays, a co-culture type experiment where full-length Notch ligand expressed on cells is mixed with reporter cells would also be of interest since Notch signalling is a juxtacrine pathway. Moreover, it would be worth using a co-culture type experiment to study

whether the N-glycan on Jagged1-C2 affects the preference of which ligand is bound by Notch receptors when cells express similar levels of Jagged and Delta family ligands. In addition, to better understand Notch binding capability of ligands, longer Notch fragments, such as EGF11-17, could be used to confirm the observations in Chapter 5, and assess other ligands. Further investigation of the C2/NRR interaction proposed by Zeronian et al. (2021) and identification of the specific region binding to Notch (in addition to the known interface) would also clarify complex formation at the cell membrane. For membrane-binding assessment, more liposome compositions relevant to the outer leaflet of the cell membrane could be further tested, and cellular assays replacing lipids of the outer leaflet could be performed (Li et al., 2016). In protein purification, an increased yield of DLL4 recombinant protein was acquired by using HEK 293F compared to HEK293T (Chapter 6). Therefore, the protein purification of Jagged1 and other ligands using HEK293F could be tested in future experiments to improve the protein yield and facilitate experimentation.

The investigation of the role of C2 N-glycan could extend to other Jagged-family ligands, such as human Jagged2 or *Drosophila* Serrate, to have a better understanding of the N-glycan in Notch activation regulation. Since a structure of Jagged2 with the N-glycan is available, mutagenesis of the NXS/T site and testing this variant alongside WT protein would validate findings in this thesis. It would also be worth to test the effect of swapping loop 5-6 of Jagged1 to DLL4, which would provide insights into roles of two family ligands in Notch activation modulation. Furthermore, it would be interesting to explore the role of the β-groove in Jagged-family and Delta-family ligands, which would provide evidence to support different orientations at the cell membrane.

Finally, examining the effects of ligand amino acid substitutions using *ex vivo* or *in vivo* techniques would complement *in vitro* assays. For Jagged1, the use of a liver organoid model may be possible, utilising CRISPR genome editing to introduce the N-glycan substitutions into Jagged, e.g. (Campana et al., 2021). In addition, the *Drosophila* system could be used, as has recently been demonstrated by study of the loop 1-2 (Martins et al., 2021).

References

Acar, M., Jafar-Nejad, H., Takeuchi, H., Rajan, A., Ibrani, D., Rana, N.A., Pan, H., Haltiwanger, R.S., and Bellen, H.J. (2008). Rumi Is a CAP10 Domain Glycosyltransferase that Modifies Notch and Is Required for Notch Signaling. Cell *132*, 247–258.

Adams, F.H., and Oliver, C.P. (1945). Hereditary deformities in man. J. Hered. *36*, 3–7.

Aebersold, R., and Mann, M. (2016). Mass-spectrometric exploration of proteome structure and function. Nature *537*, 347–355.

Agrawal, N., Frederick, M.J., Pickering, C.R., Bettegowda, C., Chang, K., Li, R.J., Fakhry, C., Xie, T.-X., Zhang, J., Wang, J., et al. (2011). Exome sequencing of head and neck squamous cell carcinoma reveals inactivating mutations in NOTCH1. Science *333*, 1154–1157.

Del Amo, F.F., Smith, D.E., Swiatek, P.J., Gendron-Maguire, M., Greenspan, R.J., McMahon, A.P., and Gridley, T. (1992). Expression pattern of Motch, a mouse homolog of Drosophila Notch, suggests an important role in early postimplantation mouse development. Development 737–744.

Aricescu, A.R., Lu, W., and Jones, E.Y. (2006). A time- and cost-efficient system for high-level protein production in mammalian cells. Acta Crystallogr. Sect. D Biol. Crystallogr. *62*, 1243–1250.

Artavanis-Tsakonas, S. (1999). Notch Signaling: Cell Fate Control and Signal Integration in Development. Science (80-.). *284*, 770–776.

Artavanis-Tsakonas, S., Matsuno, K., and 1Fortini, M.E. (1995). Notch Signaling. Science (80-.). *268*, 225–232.

Artavanis-Tsakonas, S., Rand, M.D., and Lake, R.J. (1999). Notch Signaling: Cell Fate Control and Signal Integration in Development.

Austin, J., and Kimble, J. (1989). Transcript analysis of glp-1 and lin-12, homologous genes required for cell interactions during development of C. elegans. Cell.

Baeten, J.T., and Lilly, B. (2017). Notch Signaling in Vascular Smooth Muscle Cells. Adv. Pharmacol. *78*, 351–382.

Becam, I., Fiuza, U.-M., Arias, A.M., and Milán, M. (2010). A Role of Receptor Notch in Ligand cis-Inhibition in Drosophila. Curr. Biol. *20*, 554–560.

Benedito, R., Roca, C., Sörensen, I., Adams, S., Gossler, A., Fruttiger, M., and Adams, R.H. (2009a). The Notch Ligands Dll4 and Jagged1 Have Opposing Effects on Angiogenesis. Cell *137*, 1124–1135.

Benedito, R., Roca, C., Sörensen, I., Adams, S., Gossler, A., Fruttiger, M., and Adams, R.H. (2009b). The Notch Ligands Dll4 and Jagged1 Have Opposing Effects on Angiogenesis. Cell.

Bierkamp, C., and Campos-Ortega, J.A. (1993). A zebrafish homologue of the Drosophila neurogenic gene Notch and its pattern of transcription during early embryogenesis. Mech. Dev.

Bogaart, G. van den, Meyenberg, K., Diederichsen, U., and Jahn, R. (2012). Phosphatidylinositol 4,5-Bisphosphate Increases Ca2+ Affinity of Synaptotagmin-1 by 40-fold. J. Biol. Chem. *287*, 16447–16453.

Le Borgne, R., Remaud, S., Hamel, S., and Schweisguth, F. (2005). Two Distinct E3 Ubiquitin Ligases Have Complementary Functions in the Regulation of Delta and Serrate Signaling in Drosophila. PLoS Biol. *3*, e96.

Bray, S.J., Takada, S., Harrison, E., Shen, S.-C., and Ferguson-Smith, A.C. (2008). The atypical mammalian ligand Delta-like homologue 1 (Dlk1) can regulate Notch signalling in Drosophila. BMC Dev. Biol. *8*, 11.

Brennan, A.J., Law, R.H.P., Conroy, P.J., Noori, T., Lukoyanova, N., Saibil, H., Yagita, H., Ciccone, A., Verschoor, S., Whisstock, J.C., et al. (2018). Perforin proteostasis is regulated through its C2 domain: supra-physiological cell death mediated by T431D-perforin. Cell Death Differ. *25*, 1517–1529.

Briot, A., Jaroszewicz, A., Warren, C.M., Lu, J., Touma, M., Rudat, C., Hofmann, J.J., Airik, R., Weinmaster, G., Lyons, K., et al. (2014). Repression of Sox9 by Jag1 is continuously required to suppress the default chondrogenic fate of vascular smooth muscle cell.

Bulman, M.P., Kusumi, K., Frayling, T.M., McKeown, C., Garrett, C., Lander, E.S., Krumlauf, R., Hattersley, A.T., Ellard, S., and Turnpenny, P.D. (2000). Mutations in the human Delta homologue, DLL3, cause axial skeletal defects in spondylocostal dysostosis. Nat. Genet. *24*, 438–441.

Campana, L., Esser, H., Huch, M., and Forbes, S. (2021). Liver regeneration and inflammation: from fundamental science to clinical applications. Nat. Rev. Mol. Cell Biol. *22*, 608–624.

Cao, Z., Ding, B.-S., Guo, P., Lee, S.B., Butler, J.M., Casey, S.C., Simons, M., Tam,

W., Felsher, D.W., Shido, K., et al. (2014). Angiocrine Factors Deployed by Tumor Vascular Niche Induce B-Cell Lymphoma Invasiveness and Chemoresistance.
Carrieri, F.A., Murray, P.J., Ditsova, D., Ferris, M.A., Davies, P., and Dale, J.K. (2019). CDK1 and CDK2 regulate NICD1 turnover and the periodicity of the segmentation clock. EMBO Rep. *20*, e46436.
de Celis, J.F., and Bray, S. (1997). Feed-back mechanisms affecting Notch activation at the dorsoventral boundary in the Drosophila wing. Development *124*, 3241–3251.
de Celis, J.F., and Bray, S.J. (2000). The Abruptex domain of Notch regulates negative interactions between Notch, its ligands and Fringe. Development *127*, 1291–1302.
Chastagner, P., Israël, A., and Brou, C. (2008). AIP4/Itch Regulates Notch Receptor Degradation in the Absence of Ligand. PLoS One *3*, e2735.
Chen, N., and Greenwald, I. (2004). The lateral signal for LIN-12/Notch in C. elegans vulval development comprises redundant secreted and transmembrane DSL proteins. Dev. Cell *6*, 183–192.
Chen, J., Moloney, D.J., and Stanley, P. (2001). Fringe modulation of Jagged1-induced Notch signaling requires the action of β4galactosyltransferase-1. Proc. Natl. Acad. Sci. *98*, 13716–13721.
Chillakuri, C.R., Sheppard, D., Xenia, M., Ilagan, G., Holt, L.R., Abbott, F., Liang, S., Kopan, R., Handford, P.A., and Lea, S.M. (2013). Structural Analysis Uncovers Lipid-Binding Properties of Notch Ligands. CellReports *5*, 861–867.
Cho, W., and Stahelin, R. V. (2006). Membrane binding and subcellular targeting of C2 domains. Biochim. Biophys. Acta - Mol. Cell Biol. Lipids.
Coffman, C., Harris, W., and Kintner, C. (1990). Xotch, the Xenopus homolog of Drosophila notch. Sci. *249*, 1438–1441.
Connell, E., Scott, P., and Davletov, B. (2008). Real-time assay for monitoring membrane association of lipid-binding domains. Anal. Biochem. *377*, 83–88.
Corbalan-Garcia, S., and Gómez-Fernández, J.C. (2014). Signaling through C2 domains: More than one lipid target. Biochim. Biophys. Acta - Biomembr. *1838*, 1536–1547.
Cordle, J., Redfield, C., Stacey, M., Van Der Merwe, P.A., Willis, A.C., Champion, B.R., Hambleton, S., and Handford, P.A. (2008a). Localization of the delta-like-1-binding site in human Notch-1 and its modulation by calcium affinity. J. Biol. Chem.
Cordle, J., Redfieldz, C., Stacey, M., van der Merwe, P.A., Willis, A.C., Champion, B.R., Hambleton, S., and Handford, P.A. (2008b). Localization of the delta-like-1-

binding site in human Notch-1 and its modulation by calcium affinity. J. Biol. Chem. *283*, 11785–11793.

D'souza, B., Miyamoto, A., and Weinmaster, G. (2008). The many facets of Notch ligands. Oncogene.

D'souza, B., Meloty-Kapella, L., and Weinmaster, G. (2010). Canonical and non-canonical Notch ligands. Curr. Top. Dev. Biol. 73–129.

Davletov, B.A., and Sudhof, T.C. (1993). A single C2domain from synaptotagmin I is sufficient for high affinity Ca2+/phospholipid binding. J. Biol. Chem. *268*, 26386–26390.

Dexter, J.S. (1914). The Analysis of a Case of Continuous Variation in Drosophila by a Study of Its Linkage.

Diaz-Cuadros, M., Wagner, D.E., Budjan, C., Hubaud, A., Tarazona, O.A., Donelly, S., Michaut, A., Al Tanoury, Z., Yoshioka-Kobayashi, K., Niino, Y., et al. (2020). In vitro characterization of the human segmentation clock. Nature *580*, 113–118.

Doevendans, P.A., and Van Eys, G. (2002). Smooth muscle cells on the move: the battle for actin.

Doi, H., Iso, T., Sato, H., Yamazaki, M., Matsui, H., Tanaka, T., Manabe, I., Arai, M., Nagai, R., and Kurabayashi, M. (2006). Jagged1-selective Notch Signaling Induces Smooth Muscle Differentiation via a RBP-J-dependent Pathway *.

Dorsch, M., Zheng, G., Yowe, D., Rao, P., Wang, Y., Shen, Q., Murphy, C., Xiong, X., Shi, Q., Gutierrez-Ramos, J.-C., et al. (2002). Ectopic expression of Delta4 impairs hematopoietic development and leads to lymphoproliferative disease. Blood *100*, 2046–2055.

Duchatelet, S., Clerc, H., Machet, L., Gaboriaud, P., Miskinyte, S., Kervarrec, T., and Hovnanian, A. (2018). A new nonsense mutation in the *POGLUT1* gene in two sisters with Dowling-Degos disease. J. Eur. Acad. Dermatology Venereol. *32*, e440–e442.

Earles, C.A., Bai, J., Wang, P., and Chapman, E.R. (2001). The tandem C2 domains of synaptotagmin contain redundant Ca2+ binding sites that cooperate to engage t-SNAREs and trigger exocytosis. J. Cell Biol. *154*, 1117–1124.

Eiraku, M., Tohgo, A., Ono, K., Kaneko, M., Fujishima, K., Hirano, T., and Kengaku, M. (2005). DNER acts as a neuron-specific Notch ligand during Bergmann glial development. Nat. Neurosci. *8*, 873–880.

Ellisen, L.W., Bird, J., West, D.C., Soreng, A.L., Reynolds, T.C., Smith, S.D., and Sklar, J. (1991a). TAN-1, the human homolog of the Drosophila Notch gene, is broken by chromosomal translocations in T lymphoblastic neoplasms. Cell *66*, 649–661.

Ellisen, L.W., Bird, J., West, D.C., Soreng, A.L., Reynolds, T.C., Smith, S.D., and Sklar, J. (1991b). TAN-1, the human homolog of the Drosophila Notch gene, is broken by chromosomal translocations in T lymphoblastic neoplasms. Cell.

Evans, J.H., Murray, D., Leslie, C.C., and Falke, J.J. (2006). Specific translocation of protein kinase Ca to the plasma membrane requires both Ca2+ and PIP2 recognition by its C2 domain. Mol. Biol. Cell *17*, 56–66.

Fabris, L., Cadamuro, M., Guido, M., Spirli, C., Fiorotto, R., Colledan, M., Torre, G., Alberti, D., Sonzogni, A., Okolicsanyi, L., et al. (2007). Analysis of Liver Repair Mechanisms in Alagille Syndrome and Biliary Atresia Reveals a Role for Notch Signaling. Am J Pathol *171*, 641–653.

Fabris, L., Fiorotto, R., Spirli, C., Cadamuro, M., Mariotti, V., Perugorria, M.J., Banales, J.M., and Strazzabosco, M. (2019). Pathobiology of inherited biliary diseases: a roadmap to understand acquired liver diseases. Nat. Rev. Gastroenterol. Hepatol. *16*, 497–511.

Fernandez-Valdivia, R., Takeuchi, H., Samarghandi, A., Lopez, M., Leonardi, J., Haltiwanger, R.S., and Jafar-Nejad, H. (2011). Regulation of mammalian Notch signaling and embryonic development by the protein O-glucosyltransferase Rumi. Development *138*, 1925.

Fiuza, U.-M., Klein, T., Martinez Arias, A., and Hayward, P. (2010). Mechanisms of ligand-mediated inhibition in Notch signaling activity in *Drosophila*. Dev. Dyn. *239*, 798–805.

Fleming, R.J., Gu, Y., and Hukriede, N.A. (1997). Serrate-mediated activation of Notch is specifically blocked by the product of the gene fringe in the dorsal compartment of the Drosophila wing imaginal disc. Dev. *124*, 2973–2981.

Forbes, S.A., Beare, D., Boutselakis, H., Bamford, S., Bindal, N., Tate, J., Cole, C.G., Ward, S., Dawson, E., Ponting, L., et al. (2016). COSMIC: somatic cancer genetics at high-resolution. Nucleic Acids Res. *45*, 777–783.

Le Friec, G., Sheppard, D., Whiteman, P., Karsten, C.M., Shamoun, S.A.-T., Laing, A., Bugeon, L., Dallman, M.J., Melchionna, T., Chillakuri, C., et al. (2012). The CD46-Jagged1 interaction is critical for human TH1 immunity. Nat. Immunol. *13*, 1213–1221.

Fu, R., Lv, W.-C., Xu, Y., Gong, M.-Y., Chen, X.-J., Jiang, N., Xu, Y., Yao, Q.-Q., Di, L., Lu, T., et al. (2020). Endothelial ZEB1 promotes angiogenesis-dependent bone formation and reverses osteoporosis. Nat. Commun. *11*, 460.

Furukawa, T., Mukherjee, S., Bao, Z.Z., Morrow, E.M., and Cepko, C.L. (2000). rax,

Hes1, and notch1 promote the formation of Muller glia by postnatal retinal progenitor cells. Neuron.

Gale, N.W., Dominguez, M.G., Noguera, I., Pan, L., Hughes, V., Valenzuela, D.M., Murphy, A.J., Adams, N.C., Lin, H.C., Holash, J., et al. (2004). Haploinsufficiency of delta-like 4 ligand results in embryonic lethality due to major defects in arterial and vascular development. Proc. Natl. Acad. Sci. U. S. A. *101*, 15949–15954.

Le Gall, M., and Giniger, E. (2004). Identification of Two Binding Regions for the Suppressor of Hairless Protein within the Intracellular Domain of Drosophila Notch*.

Garcia, J., Gerber, S.H., Sugita, S., Südhof, T.C., and Rizo, J. (2004). A conformational switch in the Piccolo C2A domain regulated by alternative splicing. Nat. Struct. Mol. Biol. *11*, 45–53.

Garg, V., Muth, A.N., Ransom, J.F., Schluterman, M.K., Barnes, R., King, I.N., Grossfeld, P.D., and Srivastava, D. (2005). Mutations in NOTCH1 cause aortic valve disease. Nature *437*, 270–274.

Gibb, S., Maroto, M., and Dale, J.K. (2010). The segmentation clock mechanism moves up a notch. Trends Cell Biol. *20*, 593–600.

Glittenberg, M., Pitsouli, C., Garvey, C., Delidakis, C., and Bray, S. (2006). Role of conserved intracellular motifs in Serrate signalling, cis-inhibition and endocytosis. EMBO J. *25*, 4697–4706.

Gordon, W.R., Vardar-Ulu, D., Histen, G., Sanchez-Irizarry, C., Aster, J.C., and Blacklow, S.C. (2007). Structural basis for autoinhibition of Notch.

Grynfeld, A., Påhlman, S., and Axelson, H. (2000). Induced neuroblastoma cell differentiation, associated with transient HES-1 activity and reducedHASH-1 expression, is inhibited by Notch1. Int. J. Cancer *88*, 401–410.

Guerrero-Valero, M., Ferrer-Orta, C., Querol-Audí, J., Marin-Vicente, C., Fita, I., Gómez-Fernández, J.C., Verdaguer, N., and Corbalán-García, S. (2009). Structural and mechanistic insights into the association of PKCalpha-C2 domain to PtdIns(4,5)P2. Proc. Natl. Acad. Sci. U. S. A. *106*, 6603–6607.

Guo, B., McMillan, B.J., and Blacklow, S.C. (2016). Structure and function of the Mind bomb E3 ligase in the context of Notch signal transduction. Curr. Opin. Struct. Biol.

Guo, M., Jan, L.Y., and Jan, Y.N. (1996). Control of daughter cell fates during asymmetric division: Interaction of Numb and Notch. Neuron.

Gupta-Rossi, N., Six, E., LeBail, O., Logeat, F., Chastagner, P., Olry, A., Israël, A., and Brou, C. (2004). Monoubiquitination and endocytosis direct γ-secretase cleavage

of activated Notch receptor. J. Cell Biol. *166*, 73–83.
Haines, N., and Irvine, K.D. (2003). Glycosylation regulates Notch signalling. Nat. Rev. Mol. Cell Biol. *4*, 786–797.
Hambleton, S., Valeyev, N. V., Muranyi, A., Knott, V., Werner, J.M., McMichael, A.J., Handford, P.A., and Downing, A.K. (2004). Structural and functional properties of the human Notch-1 ligand binding region. Structure.
Hamel, S., Fantini, J., and Schweisguth, F. (2010). Notch ligand activity is modulated by glycosphingolipid membrane composition in Drosophila melanogaster. J. Cell Biol. *188*, 581–594.
Harrison, O.J., Visan, A.C., Moorjani, N., Modi, A., Salhiyyah, K., Torrens, C., Ohri, S., and Cagampang, F.R. (2019). Defective NOTCH signaling drives increased vascular smooth muscle cell apoptosis and contractile differentiation in bicuspid aortic valve aortopathy: A review of the evidence and future directions. Trends Cardiovasc. Med. *29*, 61–68.
Harvey, B.M., Rana, N.A., Moss, H., Leonardi, J., Jafar-Nejad, H., and Haltiwanger, R.S. (2016). Mapping Sites of O-Glycosylation and Fringe Elongation on Drosophila Notch. J. Biol. Chem. *291*, 16348–16360.
Hasan, S.S., Jabs, M., Taylor, J., Wiedmann, L., Leibing, T., Nordström, V., Federico, G., Roma, L.P., Carlein, C., Wolff, G., et al. (2020). Endothelial Notch signaling controls insulin transport in muscle. EMBO Mol. Med. *12*.
Hellström, M., Phng, L.-K., Hofmann, J.J., Wallgard, E., Coultas, L., Lindblom, P., Alva, J., Nilsson, A.-K., Karlsson, L., Gaiano, N., et al. (2007). Dll4 signalling through Notch1 regulates formation of tip cells during angiogenesis. Nature *445*, 776–780.
Henderson, S.T., Gao, D., Christensen, S., Kimble, J., and ¶#§ (1997). Functional Domains of LAG-2, a Putative Signaling Ligand for LIN-12 and GLP-1 Receptors in Caenorhabditis elegans.
Heuss, S.F., Ndiaye-Lobry, D., Six, E.M., Israë, A., and Dé Rique Logeat, F. (2008). The intracellular region of Notch ligands Dll1 and Dll3 regulates their trafficking and signaling activity.
Hicks, C., Ladi, E., Lindsell, C., Hsieh, J.J.D., Hayward, S.D., Collazo, A., and Weinmaster, G. (2002). A secreted Delta1-Fc fusion protein functions both as an activator and inhibitor of Notch1 signaling. J. Neurosci. Res. *68*, 655–667.
High, F.A., Lu, M.M., Pear, W.S., Loomes, K.M., Kaestner, K.H., and Epstein, J.A. (2008). Endothelial expression of the Notch ligand Jagged1 is required for vascular

smooth muscle development. Proc. Natl. Acad. Sci. U. S. A. *105*, 1955–1959.

Hirano, K., Suganami, A., Tamura, Y., Yagita, H., Habu, S., Kitagawa, M., Sato, T., and Hozumi, K. (2020). Delta-like 1 and Delta-like 4 differently require their extracellular domains for triggering Notch signaling in mice. Elife *9*.

Hirano, Y., Gao, Y.G., Stephenson, D.J., Vu, N.T., Malinina, L., Simanshu, D.K., Chalfant, C.E., Patel, D.J., and Brown, R.E. (2019a). Structural basis of phosphatidylcholine recognition by the C2-domain of cytosolic phospholipase A2α. Elife *8*.

Hirano, Y., Gao, Y.G., Stephenson, D.J., Vu, N.T., Malinina, L., Simanshu, D.K., Chalfant, C.E., Patel, D.J., and Brown, R.E. (2019b). Structural basis of phosphatidylcholine recognition by the C2-domain of cytosolic phospholipase A2α. Elife *8*.

Hu, Q.-D., Ang, B.-T., Karsak, M., Hu, W.-P., Cui, X.-Y., Duka, T., Takeda, Y., Chia, W., Sankar, N., Ng, Y.-K., et al. (2003). F3/Contactin Acts as a Functional Ligand for Notch during Oligodendrocyte Maturation. Cell *115*, 163–175.

Hubbard, E.J.A., Wu, G., Kitajewski, J., and Greenwald, I. (1997). sel-10, a negative regulator of lin-12 activity in Caenorhabditis elegans, encodes a member of the CDC4 family of proteins. Genes Dev. *11*, 3182.

Hurlbut, G.D., Kankel, M.W., Lake, R.J., and Artavanis-Tsakonas, S. (2007). Crossing paths with Notch in the hyper-network. Curr. Opin. Cell Biol.

Ilagan, M.X.G., Lim, S., Fulbright, M., Piwnica-Worms, D., and Kopan, R. (2011). Real-time imaging of Notch activation with a luciferase complementation-based reporter. Sci. Signal. *4*.

Irvine, K.D., and Wieschaus, E. (1994). fringe, a boundary-specific signaling molecule, mediates interactions between dorsal and ventral cells during Drosophila wing development. Cell *79*, 595–606.

Iso, T., Kedes, L., and Hamamori, Y. (2003). HES and HERP families: Multiple effectors of the Notch signaling pathway. J. Cell. Physiol. *194*, 237–255.

Iso, T., Maeno, T., Oike, Y., Yamazaki, M., Doi, H., Arai, M., and Kurabayashi, M. (2006). Dll4-selective Notch signaling induces ephrinB2 gene expression in endothelial cells. Biochem. Biophys. Res. Commun.

De Joussineau, C., Soulé, J., Martin, M., Anguille, C., Montcourrier, P., and Alexandre, D. (2003). Delta-promoted filopodia mediate long-range lateral inhibition in Drosophila. Nature *426*, 555–559.

Joutel, A., Corpechot, C., Ducros, A., Vahedi, K., Chabriat, H., Mouton, P., Alamowitch, S., Domenga, V., Cécillion, M., Maréchal, E., et al. (1996). Notch3 mutations in CADASIL, a hereditary adult-onset condition causing stroke and dementia. Nature *383*, 707–710.

Joutel, A., Andreux, F., Gaulis, S., Domenga, V., Cecillon, M., Battail, N., Piga, N., Chapon, F., Godfrain, C., and Tournier-Lasserve, E. (2000). The ectodomain of the Notch3 receptor accumulates within the cerebrovasculature of CADASIL patients. J. Clin. Invest. *105*, 597–605.

Kakuda, S., and Haltiwanger, R.S. (2017). Deciphering the Fringe-Mediated Notch Code: Identification of Activating and Inhibiting Sites Allowing Discrimination between Ligands. Dev. Cell *40*, 193–201.

Kamath, B.M., Spinner, N.B., and Rosenblum, N.D. (2013). Renal involvement and the role of Notch signalling in Alagille syndrome. Nat. Publ. Gr. *9*, 409–418.

Kang, K., Lee, D., Hong, S., Park, S.-G., and Song, M.-R. (2012). The E3 Ligase Mind Bomb-1 (Mib1) Modulates Delta-Notch Signaling to Control Neurogenesis and Gliogenesis in the Developing Spinal Cord *.

Kang, T.-Y., Bocci, F., Jolly, M.K., Levine, H., Onuchic, J.N., and Levchenko, A. (2019). Pericytes enable effective angiogenesis in the presence of proinflammatory signals. Proc. Natl. Acad. Sci. U. S. A. *116*, 23551–23561.

Katic, I., Vallier, L.G., and Greenwald, I. (2005). New Positive Regulators of lin-12 Activity in Caenorhabditis elegans Include the BRE-5/Brainiac Glycosphingolipid Biosynthesis Enzyme. Genetics *171*, 1605–1615.

Kim, A.D., Melick, C.H., Clements, W.K., Stachura, D.L., Distel, M., Panáková, D., MacRae, C., Mork, L.A., Crump, J.G., and Traver, D. (2014). Discrete Notch signaling requirements in the specification of hematopoietic stem cells. EMBO J. *33*, 2363–2373.

Kim, J., Irvine, K.D., and Carroll, S.B. (1995). Cell recognition, signal induction, and symmetrical gene activation at the dorsal-ventral boundary of the developing drosophila wing. Cell.

Koch, U., Lacombe, T.A., Holland, D., Bowman, J.L., Cohen, B.L., Egan, S.E., and Guidos, C.J. (2001). Subversion of the T/B lineage decision in the thymus by Lunatic Fringe-mediated inhibition of Notch-1. Immunity.

Kohsaka, T., Yuan, Z., Guo, S., Tagawa, M., Nakamura, A., Nakano, M., Kawasasaki, H., Inomata, Y., Tanaka, K., and Miyauchi, J. (2002). The significance of human jagged 1 mutations detected in severe cases of extrahepatic biliary atresia.

Hepatology *36*, 904–912.

Kopan, R., and Ilagan, M.X.G. (2009). The Canonical Notch Signaling Pathway: Unfolding the Activation Mechanism. Cell.

Kumano, K., Chiba, S., Kunisato, A., Sata, M., Saito, T., Nakagami-Yamaguchi, E., Yamaguchi, T., Masuda, S., Shimizu, K., Takahashi, T., et al. (2003). Notch1 but Not Notch2 Is Essential for Generating Hematopoietic Stem Cells from Endothelial Cells. Immunity *18*, 699–711.

Labban, D. Al, Jo, S.-H., Ostano, P., Saglietti, C., Bongiovanni, M., Panizzon, R., and Dotto, G.P. (2018). Notch-effector CSL promotes squamous cell carcinoma by repressing histone demethylase KDM6B. J. Clin. Invest. *128*, 2581–2599.

Ladi, E., Nichols, J.T., Ge, W., Miyamoto, A., Yao, C., Yang, L.-T., Boulter, J., Sun, Y.E., Kintner, C., and Weinmaster, G. (2005a). The divergent DSL ligand Dll3 does not activate Notch signaling but cell autonomously attenuates signaling induced by other DSL ligands. J. Cell Biol. *170*, 983–992.

Ladi, E., Nichols, J.T., Ge, W., Miyamoto, A., Yao, C., Yang, L.-T., Boulter, J., Sun, Y.E., Kintner, C., and Weinmaster, G. (2005b). The divergent DSL ligand Dll3 does not activate Notch signaling but cell autonomously attenuates signaling induced by other DSL ligands. J. Cell Biol. *170*, 983–992.

Lardelli, M., Williams, R., and Lendahl, U. (1995). Notch-related genes in animal development. Int. J. Dev. Biol. *39*, 769–780.

Larsen, A.H., and Sansom, M.S.P. (2021). Binding of Ca2+-independent C2 domains to lipid membranes: A multi-scale molecular dynamics study. Structure.

Lavado, A., and Oliver, G. (2014). Jagged1 is necessary for postnatal and adult neurogenesis in the dentate gyrus. Dev. Biol.

Lee, C.Y., Vogeli, K.M., Kim, S.-H., Chong, S.-W., Jiang, Y.-J., Stainier, D.Y.R., and Jin, S.-W. (2009). Notch Signaling Functions as a Cell-Fate Switch between the Endothelial and Hematopoietic Lineages. Curr. Biol. *19*, 1616–1622.

Lee, J.S., Cella, M., Mcdonald, K.G., Garlanda, C., Kennedy, G.D., Nukaya, M., Mantovani, A., Kopan, R., Bradfield, C.A., Newberry, R.D., et al. (2012). AHR drives the development of gut ILC22 cells and postnatal lymphoid tissues via pathways dependent on and independent of Notch. Nat. Immunol. *13*.

Lehmann, R., Jim~nez, F., Dietrich, U., and Campos-Ortega, J.A. (1983). On the Phenotype and Development of Mutants of Early Neurogenesis in Drosophila melanogaster.

Li, G., Kim, J., Huang, Z., St. Clair, J.R., Brown, D.A., and London, E. (2016). Efficient replacement of plasma membrane outer leaflet phospholipids and sphingolipids in cells with exogenous lipids. Proc. Natl. Acad. Sci. *113*, 14025–14030.

Li, J., Pauley, A., Wolf, E., Gurney, M., and Lendahl, U. (2001). The Notch Intracellular Domain Is Ubiquitinated and Negatively Regulated by the Mammalian Sel-10 Homolog*.

Li, R.C., Wong, M.Y., DiChiara, A.S., Hosseini, A.S., and Shoulders, M.D. (2021). Collagen's enigmatic, highly conserved N-glycan has an essential proteostatic function. Proc. Natl. Acad. Sci. U. S. A. *118*.

Lin, S., Negulescu, A., Bulusu, S., Gibert, B., Delcros, J.-G., Ducarouge, B., Rama, N., Gadot, N., Treilleux, I., Saintigny, P., et al. (2017). Non-canonical NOTCH3 signalling limits tumour angiogenesis. Nat. Commun.

Loganathan, S.K., Schleicher, K., Malik, A., Quevedo, R., Langille, E., Teng, K., Oh, R.H., Rathod, B., Tsai, R., Samavarchi-Tehrani, P., et al. (2020). Rare driver mutations in head and neck squamous cell carcinomas converge on NOTCH signaling. Science *367*, 1264–1269.

Lombardi, F., Nakamura, K.J., Chen, T., Sobrera, E.R., Tobin, N.H., and Aldrovandi, G.M. (2015). A Conserved Glycan in the C2 Domain of HIV-1 Envelope Acts as a Molecular Switch to Control X4 Utilization by Clonal Variants with Identical V3 Loops. PLoS One *10*, e0128116.

Lowell, S., Jones, P., Le Roux, I., Dunne, J., and Watt, F.M. (2000). Stimulation of human epidermal differentiation by Delta-Notch signalling at the boundaries of stem-cell clusters. Curr. Biol.

Lu, J., Ye, X., Fan, F., Xia, L., Bhattacharya, R., Bellister, S., Tozzi, F., Sceusi, E., Zhou, Y., Tachibana, I., et al. (2013). Endothelial Cells Promote the Colorectal Cancer Stem Cell Phenotype through a Soluble Form of Jagged-1. Cancer Cell.

Luca, V.C., Jude, K.M., Pierce, N.W., Nachury, M. V., Fischer, S., and Garcia, K.C. (2015). Structural basis for Notch1 engagement of Delta-like 4. Science (80-.). *347*, 847–853.

Luca, V.C., Kim, B.C., Ge, C., Kakuda, S., Wu, D., Roein-Peikar, M., Haltiwanger, R.S., Zhu, C., Ha, T., and Garcia, K.C. (2017). Notch-Jagged complex structure implicates a catch bond in tuning ligand sensitivity. Science (80-.). *355*, 1320–1324.

Ma, W., Du, J., Chu, Q., Wang, Y., Liu, L., Song, M., and Wang, W. (2011). hCLP46 regulates U937 cell proliferation via Notch signaling pathway. Biochem. Biophys. Res.

Commun. *408*, 84–88.

Major, R.J., and Irvine, K.D. (2005). Influence of Notch on dorsoventral compartmentalization and actin organization in the Drosophila wing. Development *132*, 3823–3833.

Malecki, M.J., Sanchez-Irizarry, C., Mitchell, J.L., Histen, G., Xu, M.L., Aster, J.C., and Blacklow, S.C. (2006). Leukemia-Associated Mutations within the NOTCH1 Heterodimerization Domain Fall into at Least Two Distinct Mechanistic Classes †. Mol. Cell. Biol. *26*, 4642–4651.

Martincorena, I., Fowler, J.C., Wabik, A., Lawson, A.R.J., Abascal, F., Hall, M.W.J., Cagan, A., Murai, K., Mahbubani, K., Stratton, M.R., et al. (2018). Somatic mutant clones colonize the human esophagus with age. Science *362*, 911–917.

Martins, T., Meng, Y., Korona, B., Suckling, R., Johnson, S., Handford, P., Lea, S.M., and Bray, S. (2021a). Delta C2 Domain β1-2 loop contributes to robust Notch signalling. BioRxiv 2021.02.16.431397.

Martins, T., Meng, Y., Korona, B., Suckling, R., Johnson, S., Handford, P.A., Lea, S.M., and Bray, S.J. (2021b). The conserved C2 phospholipid-binding domain in Delta contributes to robust Notch signalling. EMBO Rep. e52729.

Maš, J., and Andersson, E.R. (2017). The developmental biology of genetic Notch disorders.

Matsumoto, K., Ayukawa, T., Ishio, A., Sasamura, T., Yamakawa, T., and Matsuno, K. (2016). Dual Roles of O-Glucose Glycans Redundant with Monosaccharide O-Fucose on Notch in Notch Trafficking *.

Matsuno, K., Diederich, R.J., Go, M.J., Blaumueller, C.M., and Artavanis-Tsakonas, S. (1995). Deltex acts as a positive regulator of Notch signaling through interactions with the Notch ankyrin repeats. Development *121*, 2633–2644.

Maya Kamath, B., Bauer, R.C., Loomes, K.M., Chao, G., Gerfen, J., Hutchinson, A., Hardikar, W., Hirschfield, G., Jara, P., Krantz, I.D., et al. (2012). NOTCH2 mutations in Alagille syndrome. 138–144.

McGill, M.A., Dho, S.E., Weinmaster, G., and McGlade, C.J. (2009). Numb Regulates Post-endocytic Trafficking and Degradation of Notch1. J. Biol. Chem. *284*, 26427–26438.

McKellar, S.H., Tester, D.J., Yagubyan, M., Majumdar, R., Ackerman, M.J., and Sundt, T.M. (2007). Novel NOTCH1 mutations in patients with bicuspid aortic valve disease and thoracic aortic aneurysms. J. Thorac. Cardiovasc. Surg. *134*, 290–296.

Meester, J.A.N., Southgate, L., Stittrich, A.B., Venselaar, H., Beekmans, S.J.A., Den Hollander, N., Bijlsma, E.K., Helderman-Van Den Enden, A., Verheij, J.B.G.M., Glusman, G., et al. (2015). Heterozygous Loss-of-Function Mutations in DLL4 Cause Adams-Oliver Syndrome. Am. J. Hum. Genet.

Meester, J.A.N., Verstraeten, A., Alaerts, M., Schepers, D., Van Laer, L., and Loeys, B.L. (2019). Overlapping but distinct roles for NOTCH receptors in human cardiovascular disease. Clin. Genet. *95*, 85–94.

Miller, A.C., Lyons, E.L., Herman, T.G., and Herman, T. (2009). Cis-inhibition of Notch by endogenous Delta biases the outcome of lateral inhibition. Curr Biol *19*, 1378–1383.

Miyamoto, A., Lau, R., Hein, P.W., Shipley, J.M., and Weinmaster, G. (2006). Microfibrillar Proteins MAGP-1 and MAGP-2 Induce Notch1 Extracellular Domain Dissociation and Receptor Activation. J. Biol. Chem. *281*, 10089–10097.

MK, S., FF, B., VB, K., H, T., NE, N., RS, H., R, G.-S., and H, B. (2009). Identification of glycosyltransferase 8 family members as xylosyltransferases acting on O-glucosylated notch epidermal growth factor repeats. J. Biol. Chem. *285*, 1582–1586.

Moloney, D.J., Panin, V.M., Johnston, S.H., Chen, J., Shao, L., Wilson, R., Wang, Y., Stanley, P., Irvine, K.D., Haltiwanger, R.S., et al. (2000a). Fringe is a glycosyltransferase that modifies Notch. Nature *406*, 369–375.

Moloney, D.J., Shair, L.H., Lu, F.M., Xia, J., Locke, R., Matta, K.L., and Haltiwanger, R.S. (2000b). Mammalian Notch1 Is Modified with Two Unusual Forms of O-Linked Glycosylation Found on Epidermal Growth Factor-like Modules*.

Monet-Leprêtre, M., Haddad, I., Baron-Menguy, C., Fouillot-Panchal, M., Riani, M., Domenga-Denier, V., Dussaule, C., Cognat, E., Vinh, J., and Joutel, A. (2013). Abnormal recruitment of extracellular matrix proteins by excess Notch3ECD: a new pathomechanism in CADASIL. Brain *136*, 1830–1845.

Moreno, R.U., Gil, J., Rodriguez-Sainz, C., Cela, E., Lafay, V., Oloizia, B., Herr, A.B., Sumegi, J., Jordan, M.B., and Risma, K.A. (2009). Functional assessment of perforin C2 domain mutations illustrates the critical role for calcium-dependent lipid binding in perforin cytotoxic function.

Moretti, J., and Brou, C. (2013). Ubiquitinations in the Notch Signaling Pathway. Int. J. Mol. Sci. *14*, 6359–6381.

Morgan, T.H. (1917). The Theory of the Gene.

Müller, J., Rana, N.A., Serth, K., Kakuda, S., Haltiwanger, R.S., and Gossler, A. (2014). O-fucosylation of the Notch Ligand mDLL1 by POFUT1 Is Dispensable for Ligand

Function. PLoS One *9*, e88571.
Müller, R., Jenny, A., and Stanley, P. (2013). The EGF Repeat-Specific O-GlcNAc-Transferase Eogt Interacts with Notch Signaling and Pyrimidine Metabolism Pathways in Drosophila. PLoS One *8*, e62835.
Nandagopal, N., Santat, L.A., and Elowitz, M.B. (2019). Cis-activation in the Notch signaling pathway. Elife *8*.
Nichols, J.T., Miyamoto, A., and Weinmaster, G. (2007). Notch Signaling - Constantly on the Move. Traffic *8*, 959–969.
Noguera-Troise, I., Daly, C., Papadopoulos, N.J., Coetzee, S., Boland, P., Gale, N.W., Chieh Lin, H., Yancopoulos, G.D., and Thurston, G. (2006). Blockade of Dll4 inhibits tumour growth by promoting non-productive angiogenesis. Nature *444*, 1032–1037.
Noseda, M., Fu, Y., Niessen, K., Wong, F., Chang, L., McLean, G., and Karsan, A. (2006). Smooth Muscle alpha-actin is a direct target of Notch/CSL. Circ. Res. *98*, 1468–1470.
Nowell, C.S., and Radtke, F. (2017). Notch as a tumour suppressor. Nat. Rev. Cancer *17*, 145–159.
Ogawa, M., Sawaguchi, S., Kawai, T., Nadano, D., Matsuda, T., Yagi, H., Kato, K., Furukawa, K., and Okajima, T. (2015). Impaired O-Linked N-Acetylglucosaminylation in the Endoplasmic Reticulum by Mutated Epidermal Growth Factor (EGF) Domain-specific O-Linked N-Acetylglucosamine Transferase Found in Adams-Oliver Syndrome. J. Biol. Chem. *290*, 2137–2149.
Okajima, T., and Irvine, K.D. (2002). Regulation of Notch Signaling by O-Linked Fucose. Cell *111*, 893–904.
Okajima, T., Xu, A., and Irvine, K.D. (2003). Modulation of Notch-Ligand Binding by Protein O-Fucosyltransferase 1 and Fringe. J. Biol. Chem. *278*, 42340–42345.
Okajima, T., Reddy, B., Matsuda, T., and Irvine, K.D. (2008). Contributions of chaperone and glycosyltransferase activities of O-fucosyltransferase 1 to Notch signaling. BMC Biol. *6*, 1.
Okamura, Y., and Saga, Y. (2008). Pofut1 is required for the proper localization of the Notch receptor during mouse development. Mech. Dev. *125*, 663–673.
Pagliaro, L., Sorrentino, C., and Roti, G. (2020). Targeting Notch Trafficking and Processing in Cancers. Cells *9*, 2212.
Pajcini, K. V, Speck, N.A., and Pear, W.S. (2011). Notch signaling in mammalian hematopoietic stem cells. Leukemia *25*, 1525–1532.

Pandey, A., Harvey, B.M., Lopez, M.F., Ito, A., Haltiwanger, R.S., and Jafar-Nejad, H. (2019). Glycosylation of Specific Notch EGF Repeats by O-Fut1 and Fringe Regulates Notch Signaling in Drosophila. Cell Rep. *29*, 2054-2066.e6.

Panin, V.M., Papayannopoulos, V., Wilson, R., and Irvine, K.D. (1997). Fringe modulates Notch–ligand interactions. Nature *387*, 908–912.

Panin, V.M., Shao, L., Lei, L., Moloney, D.J., Irvine, K.D., and Haltiwanger, R.S. (2002). Notch Ligands Are Substrates for ProteinO-Fucosyltransferase-1 and Fringe. J. Biol. Chem. *277*, 29945–29952.

Papayannopoulos, V., Tomlinson, A., Panin, V.M., Rauskolb, C., and Irvine, K.D. (1998). Dorsal-ventral signaling in the Drosophila eye. Science *281*, 2031–2034.

Parker, L.H., Schmidt, M., Jin, S.-W., Gray, A.M., Beis, D., Pham, T., Frantz, G., Palmieri, S., Hillan, K., Stainier, D.Y.R., et al. (2004). The endothelial-cell-derived secreted factor Egfl7 regulates vascular tube formation. Nature *428*, 754–758.

Patel, M.S., Taylor, G.P., Bharya, S., Al-Sanna'a, N., Adatia, I., Chitayat, D., Suzanne Lewis, M.E., and Human, D.G. (2004). Abnormal pericyte recruitment as a cause for pulmonary hypertension in Adams-Oliver syndrome. Am. J. Med. Genet. *129A*, 294–299.

Pear, W.S., Aster, J.C., Scott, M.L., Hasserjian, R.E., Softer, B., Sklar, J., and Baltimore, D. (1996). Exclusive Development of T cell Neoplasms in Mice Transplanted with Bone Marrow Expressing Activated Notch Alleles. J. Exp. Med. *183*, 2283–2291.

Penton, A.L., Leonard, L.D., and Spinner, N.B. (2012). Notch signaling in human development and disease. Semin. Cell Dev. Biol. *23*, 450–457.

Piccoli, D.A., and Spinner, N.B. (2001). Alagille Syndrome and the Jagged1 Gene. Semin. Liver Dis. *21*, 525–534.

Pintar, A., De Biasio, A., Popovic, M., Ivanova, N., and Pongor, S. (2007). Biology Direct The intracellular region of Notch ligands: does the tail make the difference? Background.

Poodry, C.A. (1990). shibire, a neurogenic mutant of Drosophila. Dev. Biol. *138*, 464–472.

Potente, M., Gerhardt, H., and Carmeliet, P. (2011). Basic and therapeutic aspects of angiogenesis. Cell *146*, 873–887.

Poulson, D.F. (1937). Chromosomal Deficiencies and the Embryonic Development of Drosophila Melanogaster.

Poulson, D.F. (1940). The effects of certain X-chromosome deficiencies on the embryonic development of Drosophila melanogaster. J. Exp. Zool. *83*, 271–325.

Radtke, F., Wilson, A., Stark, G., Bauer, M., van Meerwijk, J., MacDonald, H.R., and Aguet, M. (1999). Deficient T Cell Fate Specification in Mice with an Induced Inactivation of Notch1. Immunity *10*, 547–558.

Rakheja, D., Maitra, A., Kapur, P., and Weinberg, A.G. (2006). Extrahepatic Biliary Atresia Demonstrates Abnormal Persistence of HES1 Protein in Neonatal Biliary Epithelium: An Immunohistochemical Study. Pediatr. Dev. Pathol. *9*, 98–102.

Rana, N.A., Nita-Lazar, A., Takeuchi, H., Kakuda, S., Luther, K.B., and Haltiwanger, R.S. (2011). O-Glucose Trisaccharide Is Present at High but Variable Stoichiometry at Multiple Sites on Mouse Notch1. J. Biol. Chem. *286*, 31623–31637.

Rao, Z., Handford, P., Mayhew, M., Knott, V., Brownlee, G.G., and Stuart, D. (1995). The structure of a Ca(2+)-binding epidermal growth factor-like domain: its role in protein-protein interactions. Cell *82*, 131–141.

Rebay, I., Fleming, R.J., Fehon, R.G., Cherbas, L., Cherbas, P., and Artavanis-Tsakonas, S. (1991). Specific EGF repeats of Notch mediate interactions with Delta and serrate: Implications for notch as a multifunctional receptor. Cell.

Reily, C., Stewart, T.J., Renfrow, M.B., and Novak, J. (2019). Glycosylation in health and disease. Nat. Rev. Nephrol. *15*, 346–366.

Reyna, M.A., Haan, D., Paczkowska, M., Verbeke, L.P.C., Vazquez, M., Kahraman, A., Pulido-Tamayo, S., Barenboim, J., Wadi, L., Dhingra, P., et al. (2020). Pathway and network analysis of more than 2500 whole cancer genomes. Nat. Commun. *11*, 16.

Robert-Moreno, À., Espinosa, L., Sanchez, M.J., de la Pompa, J.L., and Bigas, A. (2007). The notch pathway positively regulates programmed cell death during erythroid differentiation. Leukemia *21*, 1496–1503.

Robert-Moreno, À., Guiu, J., Ruiz-Herguido, C., López, M.E., Inglés-Esteve, J., Riera, L., Tipping, A., Enver, T., Dzierzak, E., Gridley, T., et al. (2008). Impaired embryonic haematopoiesis yet normal arterial development in the absence of the Notch ligand Jagged1. EMBO J. *27*, 1886–1895.

Rodilla, V., Villanueva, A., Obrador-Hevia, A., Robert-Moreno, A., Fernández-Majada, V., Grilli, A., López-Bigas, N., Bellora, N., Albà, M.M., Torres, F., et al. (2009). Jagged1 is the pathological link between Wnt and Notch pathways in colorectal cancer. Proc. Natl. Acad. Sci. U. S. A. *106*, 6315–6320.

Rodriguez-Esteban, C., Schwabe, J.W.R., Peña, J.D. La, Foys, B., Eshelman, B., and Belmonte, J.C.I. (1997). Radical fringe positions the apical ectodermal ridge at the dorsoventral boundary of the vertebrate limb. Nature *386*, 360–366.

Sainson, R.C.A., Aoto, J., Nakatsu, M.N., Holderfield, M., Conn, E., Koller, E., and Hughes, C.C.W. (2005). Cell-autonomous notch signaling regulates endothelial cell branching and proliferation during vascular tubulogenesis. FASEB J. *17*.

Saito, T., Chiba, S., Ichikawa, M., Kunisato, A., Asai, T., Shimizu, K., Yamaguchi, T., Yamamoto, G., Seo, S., Kumano, K., et al. (2003). Notch2 Is Preferentially Expressed in Mature B Cells and Indispensable for Marginal Zone B Lineage Development. Immunity *18*, 675–685.

Sakaidani, Y., Nomura, T., Matsuura, A., Ito, M., Suzuki, E., Murakami, K., Nadano, D., Matsuda, T., Furukawa, K., and Okajima, T. (2011). O-Linked-N-acetylglucosamine on extracellular protein domains mediates epithelial cell–matrix interactions. Nat. Commun. *2*, 583.

Sakaidani, Y., Ichiyanagi, N., Saito, C., Nomura, T., Ito, M., Nishio, Y., Nadano, D., Matsuda, T., Furukawa, K., and Okajima, T. (2012). O-linked-N-acetylglucosamine modification of mammalian Notch receptors by an atypical O-GlcNAc transferase Eogt1. Biochem. Biophys. Res. Commun. *419*, 14–19.

Sakamoto, K., Ohara, O., Takagi, M., Takeda, I., and Katsube, K. (2001). Intracellular Cell-Autonomous Association of Notch and Its Ligands: A Novel Mechanism of Notch Signal Modification. Dev. Biol.

Santopolo, G., Magnusson, J.P., Lindvall, O., Kokaia, Z., and Frisén, J. (2020). Blocking Notch-Signaling Increases Neurogenesis in the Striatum after Stroke. Cells *9*, 1732.

Sapir, A., Assa-Kunik, E., Tsruya, R., Schejter, E., and Shilo, B.-Z. (2005). Unidirectional Notch signaling depends on continuous cleavage of Delta. Development *132*, 123–132.

Sawaguchi, S., Varshney, S., Ogawa, M., Sakaidani, Y., Yagi, H., Takeshita, K., Murohara, T., Kato, K., Sundaram, S., Stanley, P., et al. (2017). O-GlcNAc on NOTCH1 EGF repeats regulates ligand-induced Notch signaling and vascular development in mammals. Elife *6*.

Scheer, N., Groth, A., Hans, S., and Campos-Ortega, J.A. (2001). An instructive function for Notch in promoting gliogenesis in the zebrafish retina. Development *128*, 1099–1107.

Schindelin, J., Arganda-Carreras, I., Frise, E., Kaynig, V., Longair, M., Pietzsch, T., Preibisch, S., Rueden, C., Saalfeld, S., Schmid, B., et al. (2012). Fiji: an open-source platform for biological-image analysis. Nat. Methods *9*, 676–682.

Schmidt, M.H.H., Bicker, F., Nikolic, I., Meister, J., Babuke, T., Picuric, S., Müller-Esterl, W., Plate, K.H., and Dikic, I. (2009). Epidermal growth factor-like domain 7 (EGFL7) modulates Notch signalling and affects neural stem cell renewal. Nat. Cell Biol. *11*, 873–880.

Sciacca, S., Pilato, M., Mazzoccoli, G., Pazienza, V., and Vinciguerra, M. (2013). Anti-correlation between longevity gene SirT1 and Notch signaling in ascending aorta biopsies from patients with bicuspid aortic valve disease. Heart Vessels *28*, 268–275.

Serth, K., Schuster-Gossler, K., Kremmer, E., Hansen, B., Marohn-Köhn, B., and Gossler, A. (2015). O-Fucosylation of DLL3 Is Required for Its Function during Somitogenesis. PLoS One *10*, e0123776.

Servián-Morilla, E., Takeuchi, H., Lee, T. V, Clarimon, J., Mavillard, F., Area-Gómez, E., Rivas, E., Nieto-González, J.L., Rivero, M.C., Cabrera-Serrano, M., et al. (2016). A *POGLUT1* mutation causes a muscular dystrophy with reduced Notch signaling and satellite cell loss. EMBO Mol. Med. *8*, 1289–1309.

Sethi, M.K., Buettner, F.F.R., Ashikov, A., Krylov, V.B., Takeuchi, H., Nifantiev, N.E., Haltiwanger, R.S., Gerardy-Schahn, R., and Bakker, H. (2012). Molecular Cloning of a Xylosyltransferase That Transfers the Second Xylose to O-Glucosylated Epidermal Growth Factor Repeats of Notch. J. Biol. Chem. *287*, 2739–2748.

Shaheen, R., Aglan, M., Keppler-Noreuil, K., Faqeih, E., Ansari, S., Horton, K., Ashour, A., Zaki, M.S., Al-Zahrani, F., Cueto-González, A.M., et al. (2013). Mutations in EOGT Confirm the Genetic Heterogeneity of Autosomal-Recessive Adams-Oliver Syndrome. Am. J. Hum. Genet. *92*, 598–604.

Shao, X., Li, C., Fernandez, I., Zhang, X., Südhof, T.C., and Rizo, J. (1997). Synaptotagmin-syntaxin interaction: The C2 domain as a Ca2+-dependent electrostatic switch. Neuron.

Sherwood, D.R., and McClay, D.R. (1997). Identification and Localization of a Sea Urchin Notch Homologue: Insights into Vegetal Plate Regionalization and Notch Receptor Regulation. Development.

Shi, S., and Stanley, P. (2003). Protein O-fucosyltransferase 1 is an essential component of Notch signaling pathways. Proc. Natl. Acad. Sci. U. S. A. *100*, 5234–5239.

Shimizu, K., Chiba, S., Saito, T., Takahashi, T., Kumano, K., Hamada, Y., and Hirai, H. (2002). Integrity of intracellular domain of Notch ligand is indispensable for cleavage required for release of the Notch2 intracellular domain. EMBO J. *21*, 294.

Shimojo, H., Isomura, A., Ohtsuka, T., Kori, H., Miyachi, H., and Kageyama, R. (2016). Oscillatory control of Delta-like1 in cell interactions regulates dynamic gene expression and tissue morphogenesis. Genes Dev. *30*, 102–116.

Shin, O.-H., Lu, J., Rhee, J.-S., Tomchick, D.R., Pang, Z.P., Wojcik, S.M., Camacho-Perez, M., Brose, N., Machius, M., Rizo, J., et al. (2010). Munc13 C2B domain is an activity-dependent Ca2+ regulator of synaptic exocytosis. Nat. Publ. Gr. *17*.

Simpson, P. (1997). Notch signalling in development: On equivalence groups and asymmetric developmental potential. Curr. Opin. Genet. Dev.

Smas, C.M., and Sul, H.S. (1993). Pref-1, a protein containing EGF-like repeats, inhibits adipocyte differentiation. Cell *73*, 725–734.

Sprinzak, D., Lakhanpal, A., Lebon, L., Santat, L.A., Fontes, M.E., Anderson, G.A., Garcia-Ojalvo, J., and Elowitz, M.B. (2010). Cis-interactions between Notch and Delta generate mutually exclusive signalling states. Nature *465*, 86–90.

Sriuranpong, V., Borges, M.W., Ravi, R.K., Arnold, D.R., Nelkin, B.D., Baylin, S.B., and Ball, D.W. (2001). Notch Signaling Induces Cell Cycle Arrest in Small Cell Lung Cancer Cells 1.

Stahelin, R. V (2009). Lipid binding domains: more than simple lipid effectors.

Stahelin, R. V, Rafter, J.D., Das, S., and Cho, W. (2003). The molecular basis of differential subcellular localization of C2 domains of protein kinase C-alpha and group IVa cytosolic phospholipase A2. J. Biol. Chem. *278*, 12452–12460.

Stahl, M., Uemura, K., Ge, C., Shi, S., Tashima, Y., and Stanley, P. (2008). Roles of Pofut1 and O-Fucose in Mammalian Notch Signaling. J. Biol. Chem. *283*, 13638–13651.

Stier, S., Cheng, T., Dombkowski, D., Carlesso, N., and Scadden, D.T. (2002). Notch1 activation increases hematopoietic stem cell self-renewal in vivo and favors lymphoid over myeloid lineage outcome. Blood *99*, 2369–2378.

Stittrich, A.B., Lehman, A., Bodian, D.L., Ashworth, J., Zong, Z., Li, H., Lam, P., Khromykh, A., Iyer, R.K., Vockley, J.G., et al. (2014). Mutations in NOTCH1 Cause Adams-Oliver Syndrome. Am. J. Hum. Genet.

Suckling, R.J., Korona, B., Whiteman, P., Chillakuri, C., Holt, L., Handford, P.A., and Lea, S.M. (2017). Structural and functional dissection of the interplay between lipid

and Notch binding by human Notch ligands. EMBO J. *36*, 2204–2215.

Sullivan, J.M., Motley, W.W., Johnson, J.O., Aisenberg, W.H., Marshall, K.L., Barwick, K.E.S., Kong, L., Huh, J.S., Saavedra-Rivera, P.C., McEntagart, M.M., et al. (2020). Dominant mutations of the Notch ligand Jagged1 cause peripheral neuropathy. J. Clin. Invest. *130*, 1506–1512.

Sun, D., Li, H., and Zolkiewska, A. (2008). The Role of Delta-like 1 Shedding in Muscle Cell Self-Renewal and Differentiation. J. Cell Sci. *121*, 3815.

Sun, W., Gaykalova, D.A., Ochs, M.F., Mambo, E., Arnaoutakis, D., Liu, Y., Loyo, M., Agrawal, N., Howard, J., Li, R., et al. (2014). Activation of the NOTCH pathway in head and neck cancer. Cancer Res. *74*, 1091–1104.

Takeuchi, H., Schneider, M., Williamson, D.B., Ito, A., Takeuchi, M., Handford, P.A., and Haltiwanger, R.S. (2018). Two novel protein O-glucosyltransferases that modify sites distinct from POGLUT1 and affect Notch trafficking and signaling. Proc. Natl. Acad. Sci. U. S. A. *115*, E8395–E8402.

Tamura, K., Taniguchi, Y., Minoguchi, S., Sakai, T., Tun, T., Furukawa, T., and Honjo, T. (1995). Physical interaction between a novel domain of the receptor Notch and the transcription factor RBP-Jκ/Su(H). Curr. Biol. *5*, 1416–1423.

Tanigaki, K., Han, H., Yamamoto, N., Tashiro, K., Ikegawa, M., Kuroda, K., Suzuki, A., Nakano, T., and Honjo, T. (2002). Notch–RBP-J signaling is involved in cell fate determination of marginal zone B cells. Nat. Immunol. *3*, 443–450.

Taylor, P., Takeuchi, H., Sheppard, D., Chillakuri, C., Lea, S.M., Haltiwanger, R.S., and Handford, P.A. (2014). Fringe-mediated extension of O-linked fucose in the ligand-binding region of Notch1 increases binding to mammalian Notch ligands. Proc. Natl. Acad. Sci. U. S. A. *111*, 7290–7295.

Tetzlaff, F., Adam, M.G., Feldner, A., Moll, I., Menuchin, A., Rodriguez-Vita, J., Sprinzak, D., and Fischer, A. (2018). MPDZ promotes DLL4-induced Notch signaling during angiogenesis. Elife *7*.

Thompson, J.D., Higgins, D.G., and Gibson, T.J. (1994). CLUSTAL W: improving the sensitivity of progressive multiple sequence alignment through sequence weighting, position-specific gap penalties and weight matrix choice.

Tiemeijer, L.A., Frimat, J.-P., Stassen, O.M.J.A., Bouten, C.V.C., and Sahlgren, C.M. (2018). Spatial patterning of the Notch ligand Dll4 controls endothelial sprouting in vitro. Sci. Rep. *8*, 6392.

Varki, A. (2017). Biological roles of glycans. Glycobiology *27*, 3–49.

Verdaguer, N., Corbalan-Garcia, S., Ochoa, W.F., Fita, I., and Gómez-Fernández, J.C. (1999). Ca2+ bridges the C2 membrane-binding domain of protein kinase Cα directly to phosphatidylserine. EMBO J. *18*, 6329–6338.

W. J. Welshons, E.S.V.H. (1962). Pseudoallelism at the Noth locus in Drosophila.

Wang, N.J., Sanborn, Z., Arnett, K.L., Bayston, L.J., Liao, W., Proby, C.M., Leigh, I.M., Collisson, E.A., Gordon, P.B., Jakkula, L., et al. (2011). Loss-of-function mutations in Notch receptors in cutaneous and lung squamous cell carcinoma. Proc. Natl. Acad. Sci. U. S. A. *108*, 17761–17766.

Wang, S., Sdrulla, A.D., DiSibio, G., Bush, G., Nofziger, D., Hicks, C., Weinmaster, G., and Barres, B.A. (1998). Notch receptor activation inhibits oligodendrocyte differentiation. Neuron.

Wang, Y., Chan, S.L., Miele, L., Yao, P.J., Mackes, J., Ingram, D.K., Mattson, M.P., and Furukawa, K. (2004). Involvement of Notch signaling in hippocampal synaptic plasticity.

Wang, Y., Wu, B., Lu, P., Zhang, D., Wu, B., Varshney, S., del Monte-Nieto, G., Zhuang, Z., Charafeddine, R., Kramer, A.H., et al. (2017). Uncontrolled angiogenic precursor expansion causes coronary artery anomalies in mice lacking Pofut1. Nat. Commun. *8*, 578.

Weinmaster, G., and Roberts, V.J. (1991). A homolog of Drosophila Notch expressed during mammalian development.

Wharton, K.A., Johansen, K.M., Xu, T., and Artavanis-Tsakonas, S. (1985). Nucleotide sequence from the neurogenic locus Notch implies a gene product that shares homology with proteins containing EGF-like repeats. Cell *43*, 567–581.

Wilkinson, H.A., Fitzgerald, K., and Greenwald, I. (1994). Reciprocal changes in expression of the receptor lin-12 and its ligand lag-2 prior to commitment in a C. elegans cell fate decision. Cell *79*, 1187–1198.

Wong, S.H., Walker, J.A., Jolin, H.E., Drynan, L.F., Hams, E., Camelo, A., Barlow, J.L., Neill, D.R., Panova, V., Koch, U., et al. (2012). Transcription factor RORα is critical for nuocyte development. Nat. Immunol. *13*, 229–236.

Xu, A., Haines, N., Dlugosz, M., Rana, N.A., Takeuchi, H., Haltiwanger, R.S., and Irvine, K.D. (2007). In Vitro Reconstitution of the Modulation of Drosophila Notch-Ligand Binding by Fringe. J. Biol. Chem. *282*, 35153–35162.

Xu, T., Rebay, I., Fleming, R.J., Scottgale, T.N., and Artavanis-Tsakonas, S. (1990). The Notch locus and the genetic circuitry involved in early Drosophila neurogenesis.

Xue, Y., Gao, X., Lindsell, C.E., Norton, C.R., Chang, B., Hicks, C., Gendron-Maguire, M., Rand, E.B., Weinmaster, G., and Gridley, T. (1999). Embryonic Lethality and Vascular Defects in Mice Lacking the Notch Ligand Jagged1. Hum. Mol. Genet. *8*, 723–730.

Yamamoto, N., Yamamoto, S., Inagaki, F., Kawaichi, M., Fukamizu, A., Kishi, N., Matsuno, K., Nakamura, K., Weinmaster, G., Okano, H., et al. (2001). Role of Deltex-1 as a transcriptional regulator downstream of the Notch receptor. J. Biol. Chem. *276*, 45031–45040.

Yao, D., Huang, Y., Huang, X., Wang, W., Yan, Q., Wei, L., Xin, W., Gerson, S., Stanley, P., Lowe, J.B., et al. (2011). Protein O-fucosyltransferase 1 (Pofut1) regulates lymphoid and myeloid homeostasis through modulation of Notch receptor ligand interactions. Blood *117*, 5652–5662.

Yochem, J., Weston, K., and Greenwald, I. (1988). Caenorhabditis elegans lin-12 gene encodes a transmembrane protein with overall similarity to Drosophila Notch.

Yoon, B.-K., Yoon, M.-J., Im, K.-J., and Kim, S.-K. (2007). An Obligatory Role of Mind Bomb-1 in Notch Signaling of Mammalian Development. PLoS One *2*, 1221.

Zeltser, L.M., Larsen, C.W., and Lumsden, A. (2001). A new developmental compartment in the forebrain regulated by Lunatic fringe. Nat. Neurosci. *4*, 683–684.

Zeronian, M.R., Klykov, O., Portell I de Montserrat, J., Konijnenberg, M.J., Gaur, A., Scheltema, R.A., and Janssen, B.J.C. (2021). Notch-Jagged signaling complex defined by an interaction mosaic. Proc. Natl. Acad. Sci. U. S. A. *118*.

Zhang, D., and Aravind, L. (2010). Identification of novel families and classification of the C2 domain superfamily elucidate the origin and evolution of membrane targeting activities in eukaryotes. Gene *469*, 18–30.

Appendix A – Primers

Primers for mutagenesis of Jagged1

pHL Forward	5’ GGCGGCTCTAGAGCCTCTGC 3’
pHL Reverse	5’ CCGGGAGATCATGAGGGTGTC 3’
F35L Forward	5’ GGGTCAGTTAGAGTTGGAGATCCTGTCCATGCAGAACGTG 3’
F35L Reverse	5’ CTCCAACTCTAACTGACCCGAGGCCCCACACACCTTGGC 3’
G47R Forward	5’ GAACGTGAACCGGGAGCTGCAGAACGGG 3’
G47R Reverse	5’ CAGCTCCCGGTTCACGTTCTGCATGGAC 3’
A58V Forward	5’ GCGGCGTCCGGAACCCGGGAGACC 3’
A58V Reverse	5’ CGGGTTCCGGACGCCGCCGCAGCAGTTC 3’
D72N Forward	5’ CGCGACGAGTGTAACACATACTTCAAAGTGTGCC 3’
D72N Reverse	5’ GTATGTGTTACACTCGTCGCGGGTGC 3’
G114D Forward	5’ GCCAGCCGCGACAACGACCGCAACCGCATCGTGCTGC 3’
G114D Reverse	5’ GTCGTTGTCGCGGCTGGCCTTGAGGTTGAAGGTGTTGC 3’
T133R Forward	5’ GTCCTATAGGTTGCTTGTGGAGGCGTGGGATTCCAGTAATG 3’
T133R Reverse	5’ CACAAGCAACCTATAGGACCTCGGCCAGGCGAAACTGAAAG 3’
S142N Forward	5’ GTGGAGGCGTGGGATTCCAATAATGACACCGTTC 3’
S142N Reverse	5’ GAACGGTGTCATTATTGGAATCCCACGCCTCCAC 3’
T145N Forward	5’ GTAATGACAACGTTCAACCTGACAGTATTATTG 3’
T145N Reverse	5’ CAGGTTGAACGTTGTCATTACTGGAATCCCACG 3’
E228K Forward	5’ GGGCCCCAAATGTAACAGAGCTATTTGCCG 3’
E228K Reverse	5’ CTCTGTTACATTTGGGGCCCATCCAGCCTTC 3’
N143A Forward	5’ GATTCCAGTGCTGACACCGTTCAACCTGACAG 3’
N143A Reverse	5’ GAACGGTGTCAGCACTGGAATCCCACGCCTCC 3’
N217A Forward	5’ AGAATGGCGCCAAAACTTGCATGGAAGGCT 3’
N217A Reverse	5’ ATGCAAGTTTTGGCGCCATTCTGGTCACAGGC 3’

Primers for mutagenesis of DLL4

pHL *Eco*RI Forward	5’ TAGTAGGAATTCGCCACCATGGCGGC 3’
pHL *Bsi*WI Reverse	5’ TAGTAGCGTACGGAGCTCCAGCTCAC 3’
pc3.1 Forward	5’ GCGGTTTTGGCAGTACATCAAT 3’
pc3.1 Reverse	5’ TAGAGCCCCAGCTGGTTCTTT 3’
F195A Forward	5’ CAATGACCACGCCGGCCACTATGTGTGCCAG 3’
F195A Reverse	5’ GTGGCCGGCGTGGTCATTGCGCTTCTTGC 3’
Y216A Forward	5’ CTGGGGAAGCTTGCCAACAGCCTATCTGTC 3’
Y216A Reverse	5’ CTGTTGGCAAGCTTCCCCAGTCCAACCGGG 3’

Primers for sequencing of S2 lines

pExS2-2 Forward	5’ GGTAAAAGTTTTGAACGCG 3’
pExS2-2 Reverse	5’ CGCGCTTGAAAGGAGTGTG 3’

Red nucleotides are mis-matched nucleotides required for introduction of mutations through PCR mutagenesis.

Blue nucleotides are overhangs containing restriction enzyme recognition sequences to facilitate cloning.

Appendix B – Peptide sequences

Human Jagged1$_{N\text{-}EGF3\text{-}Fc\text{-}His}$

QFELEILSMQNVNGELQNGNCCGGARNPGDRKCTRDECDTYFKVCLKEYQSRVT
AGGPCSFGSGSTPVIGGNTFNLKASRGNDRNRIVLPFSFAWPRSYTLLVEAWDSS
NDTVQPDSIIEKASHSGMINPSRQWQTLKQNTGVAHFEYQIRVTCDDYYYGFGCNK
FCRPRDDFFGHYACDQNGNKTCMEGWMGPECNRAICRQGCSPKHGSCKLPGDC
RCQYGWQGLYCDKCIPHPGCVHGICNEPWQCLCETNWGGQLCDKDLNYCGTHQ
PCLNGGTCSNTGPDKYQCSCPEGYSGPNCEIGTLEVLFQGPKSCDKTHTCPPCPA
PELLGGPSVFLFPPKPKDTLMISRTPEVTCVVVDVSHEDPEVKFNWYVDGVEVHNA
KTKPREEQYNSTYRVVSVLTVLHQDWLNGKEYKCKVSNKALPAPIEKTISKAKGQP
REPQVYTLPPSRDELTKNQVSLTCLVKGFYPSDIAVEWESNGQPENNYKATPPVLD
SDGSFFLYSKLTVDKSRWQQGNVFSCSVMHEALHNHYTQKSLSLSPGKHHHHHH

Human Jagged1$_{N\text{-}EGF3\text{-}BirA\text{-}His}$

QFELEILSMQNVNGELQNGNCCGGARNPGDRKCTRDECDTYFKVCLKEYQSRVT
AGGPCSFGSGSTPVIGGNTFNLKASRGNDRNRIVLPFSFAWPRSYTLLVEAWDSS
NDTVQPDSIIEKASHSGMINPSRQWQTLKQNTGVAHFEYQIRVTCDDYYYGFGCNK
FCRPRDDFFGHYACDQNGNKTCMEGWMGPECNRAICRQGCSPKHGSCKLPGDC
RCQYGWQGLYCDKCIPHPGCVHGICNEPWQCLCETNWGGQLCDKDLNYCGTHQ
PCLNGGTCSNTGPDKYQCSCPEGYSGPNCEIGTGGSGGLNDIFEAQKIEWHEGKH
HHHHH

Human DLL4$_{N\text{-}EGF3\text{-}Fc\text{-}His}$

SGVFQLQLQEFINERGVLASGRPCEPGCRTFFRVCLKHFQAVVSPGPCTFGTVST

PVLGTNSFAVRDDSSGGGRNPLQLPFNFTWPGTFSLIIEAWHAPGDDLRPEALPPD

ALISKIAIQGSLAVGQNWLLDEQTSTLTRLRYSYRVICSDNYYGDNCSRLCKKRNDH

FGHYVCQPDGNLSCLPGWTGEYCQQPICLSGCHEQNGYCSKPAECLCRPGWQG

RLCNECIPHNGCRHGTCSTPWQCTCDEGWGGLFCDQDLNYCTHHSPCKNGATC

SNSGQRSYTCTCRPGYTGVDCELELRTLEVLFQGPKSCDKTHTCPPCPAPELLGG

PSVFLFPPKPKDTLMISRTPEVTCVVVDVSHEDPEVKFNWYVDGVEVHNAKTKPRE

EQYNSTYRVVSVLTVLHQDWLNGKEYKCKVSNKALPAPIEKTISKAKGQPREPQVY

TLPPSRDELTKNQVSLTCLVKGFYPSDIAVEWESNGQPENNYKATPPVLDSDGSFF

LYSKLTVDKSRWQQGNVFSCSVMHEALHNHYTQKSLSLSPGKHHHHHH

Human Notch1$_{\text{EGF11-13-BirA-His}}$

QDVDECSLGANPCEHAGKCINTLGSFECQCLQGYTGPRCEIDVNECVSNPCQNDA

TCLDQIGEFQCICMPGYEGVHCEVNTDECASSPCLHNGRCLDKINEFQCECPTGFT

GHLCQYDGSGLEVLFQGPGSLHHILDAQKMVWNHRGHHHHHHHHH

Human Notch2$_{\text{EGF11-13-BirA-His}}$

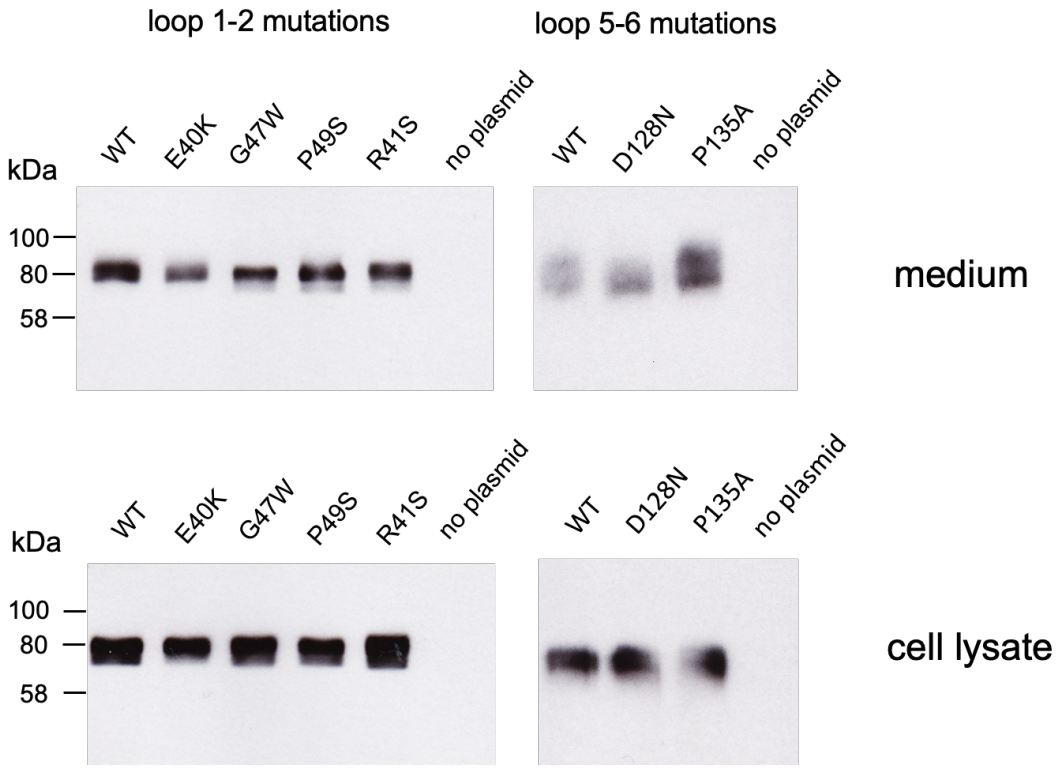
EDVDECAMANSNPCEHAGKCVNTDGAFHCECLKGYAGPRCEMDINECHSDPCQN

DATCLDKIGGFTCLCMPGFKGVHCELEINECQSNPCVNNGQCVDKVNRFQCLCPP

GFTGPVCQIDGSGLEVLFQGPGSLHHILDAQKMVWNHRGHHHHHHHH

Red amino acids are His-tag sequences, blue are Fc-tag sequences, green are Avi-tag sequences, purple are BirA-tag sequences.

Appendix C – DLL4 cancer variants expression



Western blot analysis of DLL4 cancer variants expression in HEK293T cell lysate and medium samples

Western blot shows expression of DLL4 cancer variants compared with Jagged1 wild type and the negative control. Equivalent volumes of medium samples were collected and separated by 10% reducing SDS-PAGE gel, although no proper loading control could be used to assess extracellular medium samples. The same approach was taken for cell lysates, although ideally a loading control such as probing for tubulin should have been used to infer differences in expression levels. The negative control (no plasmids) is indicated. All variants are secreted similarly to WT $DLL4_{N\text{-}EGF3}$. The anti-His-HRP rat antibody (1 in 2000 dilution) was used for signal detection. Three independent transfections were performed by Oliver Webb (University of Oxford) to obtain reliable results, and a representative western blot is shown. Molecular weight markers (kDa) are indicated.